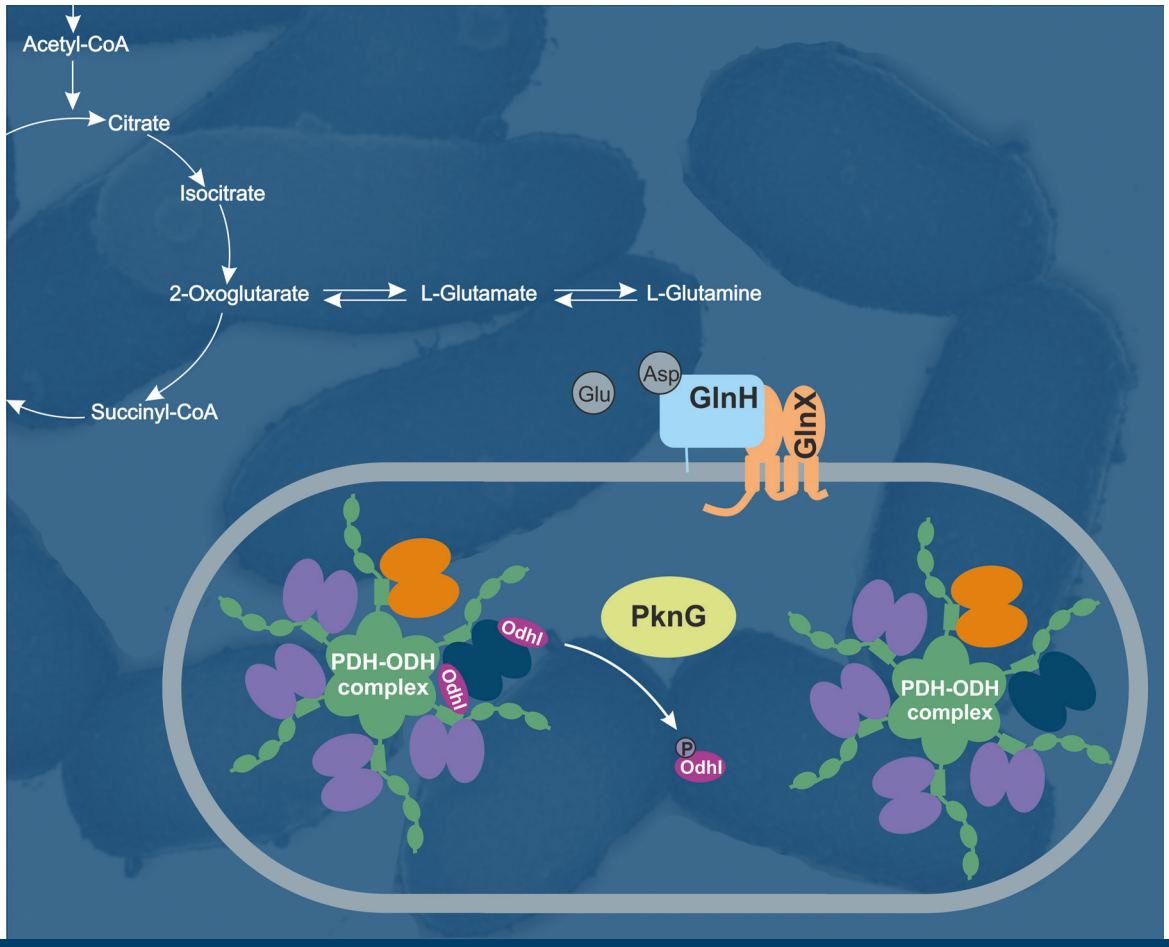

Analysis of the signal transduction cascade tuning the 2-oxoglutarate dehydrogenase activity in *Corynebacterium glutamicum*

Lea Sundermeyer

Schlüsseltechnologien / Key Technologies
Band / Volume 273
ISBN 978-3-95806-722-6

Mitglied der Helmholtz-Gemeinschaft

JÜLICH
Forschungszentrum

Schriften des Forschungszentrums Jülich
Reihe Schlüsseltechnologien / Key Technologies Band / Volume 273

Forschungszentrum Jülich GmbH
Institut für Bio-und Geowissenschaften
Biotechnologie (IBG-1)

Analysis of the signal transduction cascade tuning the 2-oxoglutarate dehydrogenase activity in *Corynebacterium glutamicum*

Lea Sundermeyer

Schriften des Forschungszentrums Jülich
Reihe Schlüsseltechnologien / Key Technologies Band / Volume 273

ISSN 1866-1807 ISBN 978-3-95806-722-6

Bibliografische Information der Deutschen Nationalbibliothek.
Die Deutsche Nationalbibliothek verzeichnet diese Publikation in der
Deutschen Nationalbibliografie; detaillierte Bibliografische Daten
sind im Internet über http://dnb.d-nb.de abrufbar.

Herausgeber und Vertrieb:	Forschungszentrum Jülich GmbH Zentralbibliothek, Verlag 52425 Jülich Tel.: +49 2461 61-5368 Fax: +49 2461 61-6103 zb-publikation@fz-juelich.de www.fz-juelich.de/zb
Umschlaggestaltung:	Grafische Medien, Forschungszentrum Jülich GmbH
Druck:	Grafische Medien, Forschungszentrum Jülich GmbH
Copyright:	Forschungszentrum Jülich 2023

Schriften des Forschungszentrums Jülich
Reihe Schlüsseltechnologien / Key Technologies, Band / Volume 273

D 61 (Diss. Düsseldorf, Univ., 2022)

ISSN 1866-1807
ISBN 978-3-95806-722-6

Vollständig frei verfügbar über das Publikationsportal des Forschungszentrums Jülich (JuSER)
unter www.fz-juelich.de/zb/openaccess.

The thesis in hand has been performed at the Institute of Bio- and Geoscience – IBG-1: Biotechnology, Forschungszentrum Jülich GmbH from April 2019 until September 2022 under the supervision of Prof. Dr. Michael Bott and Dr. Meike Baumgart.

Printed with the permission of
the Faculty of Mathematics and Natural Sciences
at Heinrich Heine University Düsseldorf

Examiner Prof. Dr. Michael Bott
Institute of Bio- and Geosciences - IBG-1: Biotechnology
Forschungszentrum Jülich GmbH

Co-examiner Prof. Dr. Lutz Schmitt
Institute of Biochemistry I
Heinrich-Heine-Universität Düsseldorf

Date of the oral examination: 19.12.2022

The results described in this dissertation have been published in the following original publications or are summarized in manuscripts which will be submitted soon:

Lea Sundermeyer*, Graziella Bosco*, Srushti Gujar, Melanie Brocker, Meike Baumgart, Dieter Willbold, Oliver H. Weiergräber, Marco Bellinzoni, and Michael Bott (2022). Characteristics of the GlnH and GlnX signal transduction proteins controlling PknG-mediated phosphorylation of OdhI and 2-oxoglutarate dehydrogenase activity in *Corynebacterium glutamicum* – Microbiology Spectrum 10(6):e0267722. (doi: 10.1128/spectrum.02677-22)
*shared first author

Lea Sundermeyer, Jan-Gerrit Folkerts, Benita Lückel, Bastian Wollenhaupt, Christina Mack, Meike Baumgart, Dietrich Kohlheyer, and Michael Bott (2022). Polar localization of regulatory proteins and TCA cycle components in an actinobacterium – to be submitted

Additional publication not discussed in this thesis:

Alina Spielmann, Yannik Brack, Hugo van Beek, Lion Flachbart, Lea Sundermeyer, Meike Baumgart and Michael Bott (2020). NADPH biosensor-based identification of an alcohol dehydrogenase variant with improved catalytic properties caused by a single charge reversal at the protein surface – AMB Express 10(1):14 (doi:10.1186/s13568-020-0946-7)

Content

Summary

In *Corynebacterium glutamicum* and many other actinobacteria, the 2-oxoglutarate dehydrogenase complex (ODH), a key enzyme of the tricarboxylic acid cycle, differs from well-known representatives by an unusual E1 subunit (OdhA), which is fused with the succinyltransferase domain usually present in a separate E2o subunit. Therefore, OdhA requires the lipoyl groups of the E2p protein (AceF) of the pyruvate dehydrogenase complex (PDH) for transferring the succinyl group to coenzyme A. As a consequence, ODH forms a hybrid complex with PDH, composed of the four proteins OdhA, AceE (E1p), AceF, and Lpd (E3). Another unusual feature of ODH in *C. glutamicum* and other actinobacteria is its regulation by the 15-kDa protein OdhI, which contains a forkhead-associated (FHA) domain known to bind phospho-threonine epitopes. In its unphosphorylated state, OdhI binds to OdhA with nM affinity and inhibits ODH activity. Phosphorylation of OdhI by the soluble serine/threonine protein kinase PknG triggers a conformational change of OdhI that prevents its interaction with OdhA and thereby abolishes the inhibition of ODH activity. Dephosphorylation of phosphorylated OdhI is catalyzed by the phospho-serine/threonine protein phosphatase Ppp. Previous studies suggested that PknG activity is controlled by the periplasmic binding protein GlnH and the transmembrane protein GlnX, whose genes form an operon with *pknG*.

The major part of this thesis focused on the characterization of GlnH and GlnX. Isothermal titration calorimetry (ITC) with purified GlnH protein identified L-aspartate and L-glutamate as ligands bound with high µM to low mM affinity. For the GlnH homolog of *Mycobacterium tuberculosis*, much higher affinities in the low µM range were reported, triggering the question of the reason for this large difference. Comparison of a *C. glutamicum* GlnH structural model with the crystal structure of *M. tuberculosis* GlnH enabled the identification of differences in the ligand binding site. The relevance of two of the identified amino acid residues for the ligand binding affinity was confirmed by showing that their exchange in *C. glutamicum* GlnH to the corresponding residues in *M. tuberculosis* GlnH caused an up to a 6-fold increase in the binding affinity for L-aspartate and L-glutamate. In this case, the affinities were determined by measuring changes in the intrinsic tryptophan fluorescence. The topology of the membrane protein GlnX was analyzed using several GlnX variants fused with either alkaline phosphatase or β-galactosidase as markers for periplasmic and cytoplasmic localization. The results confirmed the predicted topology with N- and C-terminus located in the cytoplasm, four transmembrane helices, and two large periplasmic domains. Together with a GlnX structural model created by cooperation partners, these results suggested that PknG gets activated when GlnH senses external L-aspartate or L-glutamate and transmits this information to PknG via GlnX, which is assumed to interact in the periplasm with GlnH and in the cytoplasm with PknG. Active PknG relieves the inhibition of ODH activity by OdhI by phosphorylating OdhI. In

this way, carbon flux at the 2-oxoglutarate node is adapted to the presence of the external amino donors L-aspartate and L-glutamate.

In addition to characterizing the GlnH and GlnX proteins, the intracellular localization of OdhI was analyzed by fluorescence microscopy of an OdhI-mVenus fusion protein, which showed that OdhI in the wild type is localized in its unphosphorylated form at the poles of the cell or the cell division site. In contrast, OdhI-mVenus was almost homogeneously distributed in the cytoplasm in a strain lacking the phosphatase Ppp. In this strain, OdhI is almost completely phosphorylated. Additional analyses confirmed the localization results for OdhI. Furthermore, the composition and activity of the hybrid PDH-ODH complex were analyzed by co-purification experiments and *in vivo* interaction tests of OdhA variants.

Zusammenfassung

In *Corynebacterium glutamicum* und vielen anderen Actinobakterien unterscheidet sich der 2-Oxoglutarat-Dehydrogenase-Komplex (ODH), ein Schlüsselenzym des Tricarbonsäurezyklus, von bekannten Vertretern durch eine ungewöhnliche E1-Untereinheit (OdhA), die mit der normalerweise in einer separaten E2o-Untereinheit vorliegenden Succinyltransferase-Domäne fusioniert ist. Daher benötigt OdhA die Lipoylgruppen des E2p-Proteins (AceF) des Pyruvat-Dehydrogenase-Komplexes (PDH) für die Übertragung der Succinylgruppe auf Coenzym A. Infolgedessen bildet ODH einen Hybridkomplex mit PDH, der aus den vier Proteinen OdhA, AceE (E1p), AceF und Lpd (E3) besteht. Eine weitere Besonderheit der ODH in *C. glutamicum* und anderen Actinobakterien ist ihre Regulierung durch das 15-kDa-Protein OdhI, das eine FHA-Domäne (forkhead-associated) enthält, von der bekannt ist, dass sie Phosphothreonin-Epitope bindet. In seinem unphosphorylierten Zustand bindet OdhI mit nM Affinität an OdhA und hemmt die ODH-Aktivität. Die Phosphorylierung von OdhI durch die lösliche Serin/Threonin-Proteinkinase PknG löst eine Konformationsänderung von OdhI aus, die seine Interaktion mit OdhA verhindert und dadurch die Hemmung der ODH-Aktivität aufhebt. Die Dephosphorylierung von phosphoryliertem OdhI wird durch die Phospho-Serin/Threonin-Proteinphosphatase Ppp katalysiert. Frühere Studien legten nahe, dass die Aktivität von PknG durch das periplasmatische Bindeprotein GlnH und das Transmembranprotein GlnX kontrolliert wird, deren Gene ein Opreon mit *pknG* bilden.

Der Hauptteil dieser Arbeit konzentrierte sich auf die Charakterisierung von GlnH und GlnX. Durch isothermale Titrationskalorimetrie (ITC) mit gereinigtem GlnH-Protein wurden L-Aspartat und L-Glutamat als Liganden identifiziert, die mit hoher µM- bis niedriger mM-Affinität gebunden werden. Für das GlnH-Homolog von *Mycobacterium tuberculosis* wurden wesentlich höhere Affinitäten im niedrigen µM-Bereich berichtet, was die Frage nach dem Grund für diesen großen Unterschied aufkommen ließ. Der Vergleich eines Strukturmodells von C. *glutamicum* GlnH mit der Kristallstruktur von *M. tuberculosis* GlnH ermöglichte die

Identifizierung von Unterschieden in der Ligandenbindungsstelle. Die Bedeutung von zwei der identifizierten Aminosäurereste für die Bindungsaffinität wurde bestätigt, indem gezeigt wurde, dass ihr Austausch in *C. glutamicum* GlnH gegen die entsprechenden Reste von *M. tuberculosis* GlnH eine bis zu 6-fache Erhöhung der Bindungsaffinität für L-Aspartat und L-Glutamat bewirkt. In diesem Fall wurden Affinitäten durch Veränderungen der intrinsischen Tryptophanfluoreszenz bestimmt. Die Topologie des Membranproteins GlnX wurde mittels mehrerer GlnX-Varianten analysiert, die entweder mit alkalischer Phosphatase oder β-Galactosidase als Marker für eine periplasmatische bzw. cytoplasmatische Lokalisation fusioniert waren. Die Ergebnisse bestätigten die vorhergesagte Topologie mit N- und C-Terminus im Zytoplasma, vier Transmembranhelices und zwei großen periplasmatischen Domänen. Zusammen mit einem von Kooperationspartnern erstellten GlnX-Strukturmodell deuten die Ergebnisse darauf hin, dass PknG aktiviert wird, wenn GlnH externes L-Aspartat oder L-Glutamat detektiert und diese Information über GlnX an PknG weitergibt. GlnX sollte dabei im Periplasma mit GlnH und im Zytoplasma mit PknG interagieren. Aktives PknG hebt die Hemmung der ODH-Aktivität durch Phosphorylierung von OdhI auf. Auf diese Weise kann der Kohlenstoffffluss am 2-Oxoglutarat-Knotenpunkt an die Anwesenheit der externen Amino-donatoren L-Aspartat und L-Glutamat angepasst werden.

Neben der Charakterisierung der Proteine GlnH und GlnX wurde auch die intrazelluläre Lokalisation von OdhI durch fluoreszenzmikroskopische Untersuchungen eines OdhI-mVenus-Fusionsproteins analysiert. Dabei zeigte sich, dass OdhI im Wildtyp in seiner unphosphorylierten Form an den Polen der Zelle bzw. in der Zellteilungsebene lokalisiert ist. Dagegen war das OdhI-mVenus-Protein in einem Stamm ohne die Phosphatase Ppp annähernd homogen im Cytoplasma verteilt. In diesem Stamm liegt OdhI nahezu vollständig phosphoryliert vor. Die Lokalisierungsergebnisse für OdhI wurden durch weitere Analysen bestätigt. Weiterhin wurde die Zusammensetzung und Aktivität des hybriden PDH-ODH-Komplexes durch Co-Reinigungsversuche und *in vivo*-Interaktionstests von OdhA-Varianten analysiert.

Abbreviations

2D	two-dimensional
Δ	deletion
a.u.	arbitrary units
ATCC	american type culture collection
ATP	adenosine triphosphate
bp	base pairs
BHI(S)	brain heart infusion (with sorbitol)
CGXII	*C. glutamicum* bufferd defined salt medium
C-terminus	carboxy-terminal end of a peptide/protein
CoA	coenzyme A
cryo-EM	cryogenic electron microscopy
Da	Dalton
DNA	desoxyribonucleic acid
DCPIP	2,6-dichlorophenolindophenol
DSP	di-thiobis(succinimidyl propionate)
et al.	*et alii*
FAD	flavin adenine dinucleotide
FHA	forkhead-associated
GDH	glutamate dehydrogenase
GOGAT	glutamate 2-oxoglutarate aminotransferase
GST	glutathione-S-transferase
HEPES	4-(2-Hydroxyethyl)piperazine-1-ethane-sulfonic acid
IPTG	isopropyl-β-D-thiogalactopyranoside
ITC	isothermal titration calorimetry
Kan^R	kanamycin resistance
K_D; K_i; K_m	dissociation constant; inhibitor constant; Michaelis-Menten constant
L	*laevus*, L-configuration (amino acid)
LB	lysogeny broth
LBD	lipoyl binding domain
N-terminus	amino-terminal end of a peptide/protein
NAD^+/NADH	nicotinamide adenine dinucleotide, oxidized/reduced
$NADP^+$/NADPH	nicotinamide adenine dinucleotide phosphate, oxidized/reduced
NMR	nuclear magnetic resonance
MBP	maltose binding protein
mRNA	messenger RNA
MST	microscale thermophoresis
OD_{600}	optical density at 600 nm
ODH	2-oxoglutarate dehydrogenase complex
PASTA	penicillin-binding protein and serine/threonine kinase-associated
PCR	polymerase chain reaction
PBS	phosphate-buffered saline
PDH	pyruvate dehydrogenase complex
PSBD	peripheral subunit binding domain
PTM	post-translational modification
RBS	ribosome binding site
RNA	ribonucleic acid
SDS-PAGE	sodium dodecyl sulfate poly acrylamide gel electrophoresis
SPR	surface plasmon resonance
STPK	serine/threonine protein kinase
SUMO	small ubiquitin-related modifier
TCA	tricarboxylic acid
TCS	two-component system
TEV	Tabaco etch virus
TMAE	tris(2-maleimidoethyl)amine
TPR	tetratricopeptide repeat
TMD	transmembrane domain
TPP	thiamine pyrophosphate
U	Unit (µmol/min)
wt	wild type
w/v; v/v	weight per volume; volume per volume

1. Introduction

1.1. The actinobacterium *Corynebacterium glutamicum*

Actinobacteria are one of the largest and diverse bacterial phyla, containing the six classes *Actinobacteria*, *Acidimicrobiia*, *Coriobacteriia*, *Nitriliruptoria*, *Rubrobacteria*, and *Thermoleophilia*, whereby over 80 % of the more than 50 families are grouped in the class *Actinobacteria* (Barka et al., 2016, Gao and Gupta, 2012). This class includes human pathogens like *Mycobacterium tuberculosis* and *Corynebacterium diphtheriae* as well as inhabitants of the gastrointestinal tract like *Bifidobacterium* species (Ventura et al., 2007). Furthermore, many biotechnologically relevant strains like *Streptomyces* species, known as an original source of most antibiotics and other secondary metabolites (de Lima Procópio et al., 2012, Lacey and Rutledge, 2022), and *Corynebacterium glutamicum*, used for large-scale production of amino acids (Eggeling and Bott, 2005), belong to this class.

C. glutamicum is a non-pathogenic, facultative anaerobic, biotin-auxotrophic, Gram-positive soil bacterium first isolated in Japan in 1956 as a natural glutamate producer (Kinoshita et al., 1957, Abe et al., 1967). Today it is used for the industrial production of glutamate and lysine, used as food and feed additives, respectively (Wendisch et al., 2016, Eggeling and Bott, 2015). Besides this, *C. glutamicum* evolved into an industrial-relevant production strain for more than 70 different compounds (Becker et al., 2018). The product spectrum ranges from bulk chemicals such as lactate or succinate (Tsuge et al., 2015, Kogure and Inui, 2018) and biofuels such as isobutanol (Blombach et al., 2011, Smith et al., 2010) to high-value compounds such as the food flavor raspberry ketone or *scyllo*-inositol, a drug-candidate in Alzheimer's disease (Milke et al., 2020, Ramp et al., 2021, Wolf et al., 2021). The wide expansion of its biotechnological use was supported by the high robustness of *C. glutamicum* towards toxic compounds, which is at least partially enabled by the special composition of the corynebacterial cell envelope. Besides the cytoplasmic membrane, the corynebacterial cell envelope is formed by a thick arabinogalactan–peptidoglycan polymer, which is covalently linked to an outer lipid layer, mainly consisting of mycolic acids and derivatives thereof. This results in an outer membrane-like structure similar to the cell envelope of Gram-negative bacteria (Bayan et al., 2003). Furthermore, the availability of the entire genome sequence (Ikeda and Nakagawa, 2003, Kalinowski et al., 2003) and its GRAS (generally recognized as safe) status enabled an extensive investigation of the metabolism and the regulatory functions and made *C. glutamicum* not only interesting as a production host, but also as a model organism for the related human pathogens *M. tuberculosis* and *C. diphtheria*, which all belong to the order *Corynebacteriales*. To further improve biotechnological applications as well as knowledge of actinobacterial specificities as potential targets for pharmaceutical treatment and drug design, detailed knowledge of metabolic pathways and the underlying regulatory mechanisms is still an important field in corynebacterial research.

1.2. Unique features of the corynebacterial hybrid PDH-ODH complex

2-oxoglutarate dehydrogenase (ODH) and pyruvate dehydrogenase (PDH) are key enzymes of central carbon metabolism and belong to the group of α-ketoacid dehydrogenases, which are known to form large complexes and generate the high-energy compounds succinyl-CoA and acetyl-CoA by oxidative decarboxylation of their substrates, with concomitant reduction of NAD^+ to NADH (nicotinamide adenine dinucleotide) (Perham, 2000, Patel et al., 2014). PDH and ODH typically consist of three different subunits E1, E2, and E3. E1p and E1o catalyze the TPP (thiamine pyrophosphate)-dependent oxidative decarboxylation of pyruvate or 2-oxoglutarate, respectively, and the corresponding acyl groups are transferred by the dihydrolipoyl acyltransferases E2p and E2o to its lipoyl group, which is attached to lysine residues of the E2 subunits. The third subunit, E3 is a dihydrolipoyl dehydrogenase that generates NADH by catalyzing the FAD (flavin adenine dinucleotide)-dependent reoxidation of the E2 dihydrolipoamide group to lipoamide (Bott and Eikmanns, 2013).
These α-ketoacid dehydrogenases build very large complexes (~10 MDa) with a common molecular architecture, where the E2 subunit, consisting of the N-terminal lipoyl binding domains (LBD), followed by a peripheral subunit binding domain (PSBD) and the C-terminal acyltransferase domain, builds a core connecting the three different subunits by the interaction of E1 and E3 with E2 PSBD or the E2 acyltransferase domain (Perham, 1991, Perham, 2000). While E1 and E3 form homodimers, the catalytically active state of E2 is a homotrimer. This homotrimer builds higher oligomeric states by intermolecular trimer-trimer interactions leading to an assembly of up to 60 E2 molecules, which was first observed for the crystal structure of the *Azotobacter vinelandii* E2 protein, and whereby the number of subunits depends on the complex as well as on the species (Mattevi et al., 1992, Perham, 2000, Izard et al., 1999).

In most organisms the E1 and E2 subunits of ODH and PDH are independent enzymes, while the E3 subunit is often shared between ODH and PDH (Schwinde et al., 2001). In *C. glutamicum*, however, the ODH E1 subunit (E1o), OdhA, was found to be fused to the succinyltransferase domain of E2, while an independent E2o subunit is missing (Fig. 1A) (Usuda et al., 1996). In this case, E1o possesses 2-oxoglutarate decarboxylase and transsuccinylase activity, while AceE (E1p) shows only pyruvate decarboxylase activity, and AceF (E2p) conducts transacetylase activity (Hoffelder et al., 2010). This unusual domain structure of E1o was also observed in *Mycolicibacterium smegmatis* and occurs in most members belonging to the class of *Actinobacteria* (Fig. 1B) (Wagner et al., 2011, Bruch et al., 2021).
Purification of a Strep-tagged OdhA (E1o) variant from *C. glutamicum* led to the co-purification of E2p (AceF), E1p (AceE), and E3 (Lpd) and, *vice versa*, purification of a Strep-tagged variant of AceE (E1p) showed co-purification with E1o, E2p, and E3, which led to the assumption of a hybrid PDH-ODH complex in *C. glutamicum* (Niebisch et al., 2006). In subsequent studies,

analysis of *C. glutamicum* strains lacking AceF or OdhA and enzyme assays with purified proteins proved that the corynebacterial ODH requires the lipoyl binding domains of AceF (E2p) to enable the transfer of the succinyl group to CoA (Fig. 1C), showing a physiological relevance of the occurrence of a hybrid PDH-ODH complex in *C. glutamicum* (Hoffelder et al., 2010). The presence of the hybrid complex, at the same time being responsible for the carbon flux from glycolysis into the tricarboxylic acid (TCA) cycle as well as in the TCA cycle itself, was recently confirmed by analytical ultracentrifugation experiments (Kinugawa et al., 2020). In addition, this study revealed that the PDH-ODH complex is much smaller than the corresponding dehydrogenase complex of *Escherichia coli* (Kinugawa et al., 2020). This difference in size can be explained by a specific structural feature of the E2 subunit. As described for α-ketoacid dehydrogenase complexes of several species, *C. glutamicum* AceF also forms catalytically active homotrimers, but these trimers cannot form higher oligomeric states (Bruch et al., 2021). The formation of trimer-trimer interactions is mediated by a conserved C-terminal 3_{10}-hydrophobic helix of the E2 protein enabling intermolecular symmetric interactions (Izard et al., 1999). While the overall structure of the *C. glutamicum* E2 protein was similar to those described in the literature for other organisms such as *A. vinelandii* and the active site environment at the interface between the homotrimer subunits appeared conserved, the C-terminal helix, responsible for the trimer-trimer interactions, possessed a phenylalanine-containing insertion of three amino acids. This insertion changes the orientation of the C-terminal helix, leading to intramolecular instead of intermolecular interactions, thereby preventing higher oligomeric states of the E2 subunit (Bruch et al., 2021). Such a phenylalanine-containing insertion was also observed for the E2p ortholog of *M. tuberculosis* and genome analysis revealed that the presence of such an insertion correlated with the existence of an OdhA fusion protein containing a 2-oxoglutarate decarboxylase and a succinyltransferase domain, showing that the lack of higher oligomeric states might be correlated with the necessity of E2p interactions with E1p and E1o to enable PDH as well as ODH activity (Bruch et al., 2021).

This unique architecture of enzyme complexes involved in central carbon metabolism might provide further starting points to improve therapeutic as well as metabolic engineering applications, therefore raising the question of more detailed knowledge on the composition of the entire PDH-ODH complex concerning subunit stoichiometry and interactions sites. A recent study suggests that the complex consists of two AceF trimers, four Lpd dimers, one AceE dimer and one OdhA dimer, but further work is necessary to understand the architecture of the hybrid PDH-ODH complex (Kinugawa et al., 2020).

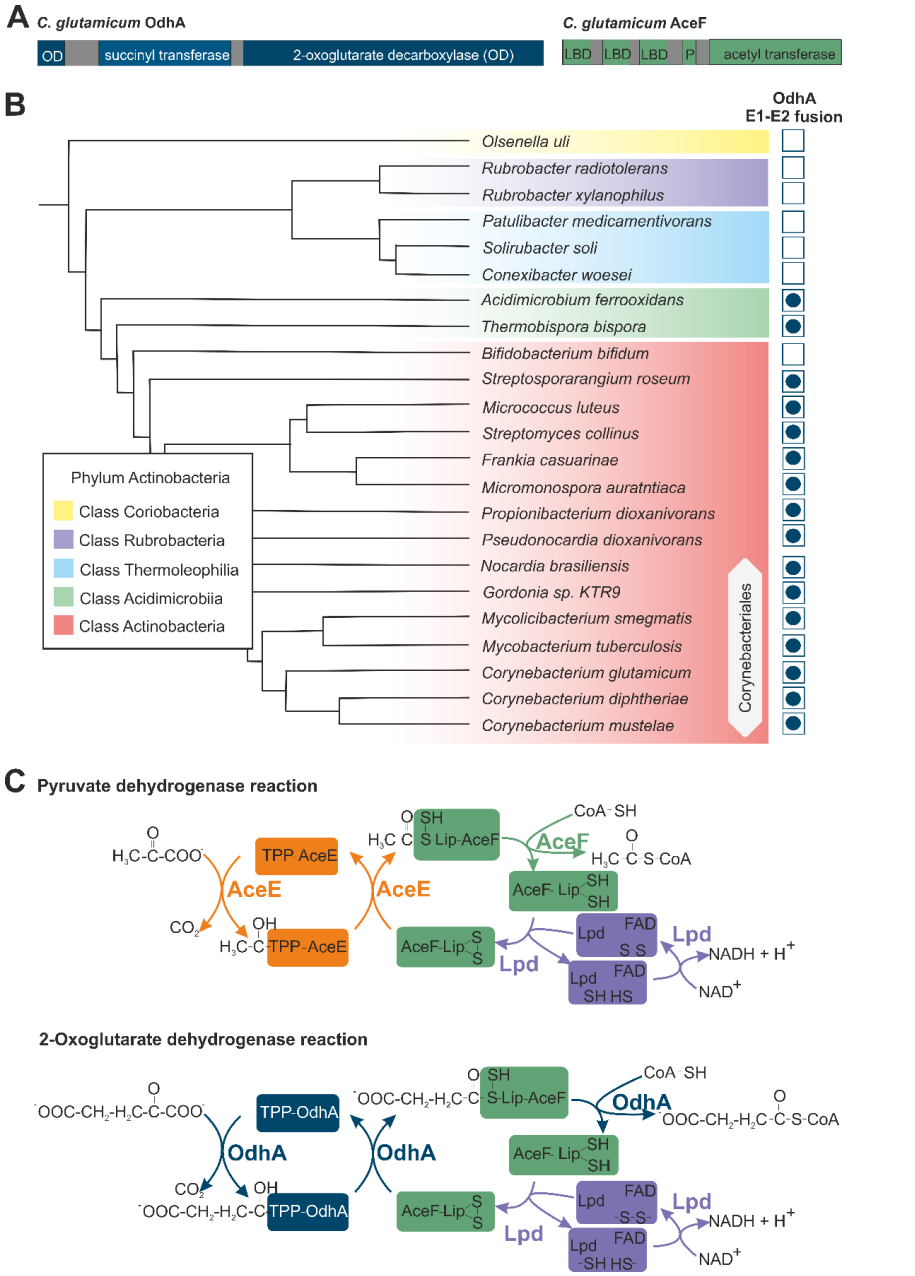

Figure 1: Special features of the actinobacterial 2-oxoglutarate dehydrogenase. (A) Schematic representation of the domain organization of *C. glutamicum* OdhA and AceF. (B) Selection of the actinobacterial phylogenetic tree, showing the existence of an OdhA-like fusion protein possessing 2-oxoglutarate decarboxylase and succinyltransferase domains as shown in A. The figure was adapted from Bruch et al. 2021. (C) Reactions catalyzed by the pyruvate and 2-oxoglutarate dehydrogenase complex subunits in *C. glutamicum*. In case of the PDH, the decarboxylation of pyruvate and the acetylation of the lipoyl group of AceF (E2p) are catalyzed by AceE (E1p) shown in orange. E2p transfers the acyl group to CoA (green).The dihydrolipoyl dehydrogenase Lpd (E3) regenerates the disulfide bridge in the lipoyl group of AceF shown in purple. In case of the ODH complex, OdhA (E1o-E2o) acts as a 2-oxoglutarate decarboxylase and as a succinyltransferase whereby it uses the lipoyl residues of AceF (E2p) indicated by the blue arrows. The regeneration of the disulfide bridge in the lipoyl group is catalyzed by Lpd (purple). Adapted from Bott and Eikmanns 2013.

1.3. Phosphorylation-based signal transduction in bacteria

The adaptation of bacteria to their environment requires precise control of cellular processes, including the regulation of metabolic pathways in response to external nutrient availability. This control takes place on different levels, including transcriptional, translational, and post-translational regulation, all together leading to a variation of protein levels and activities. The post-translational regulation is based on post-translational modifications (PTM) and protein stability, for example, controlled by conditional proteolysis (Jenal and Hengge-Aronis, 2003). Many PTMs are reversible and carried out by specific enzymes, allowing a fast and dynamic response to changing environmental and intracellular conditions. PTMs include, for example, protein phosphorylation, acetylation, succinylation, or glycosylation, with phosphorylation being the most abundant (Macek et al., 2019).

Protein phosphorylation in bacteria was observed for histidine, aspartate, serine, threonine, tyrosine, arginine, and lysine residues and the responsible kinases can be grouped in the five types of bacterial-tyrosine kinases, atypical serine kinases, arginine kinases, Hanks-type serine/threonine protein kinases (STPK), and histidine kinases of two-component signal transduction systems (TCS) (Mijakovic et al., 2016). TCS are the most prominent kinase family and form a linear signal transduction system typically consisting of a membrane-bound sensory kinase and a cytoplasmic response regulator (Zschiedrich et al., 2016). The sensory domain recognizes a specific signal leading to an auto-phosphorylation of a histidine residue followed by a transfer of the phosphoryl group to an aspartate residue of the corresponding response regulator protein, in most cases leading to altered transcription of target genes (Stock et al., 2000, Laub and Goulian, 2007). Thereby, TCSs are usually very specific for a certain stimulus. This specificity is based on the co-evolution of amino acid residues building the interaction site of the histidine kinase domain and the response regulator, which allows differentiation between the cognate response regulator and those response regulators being part of a different TCSs (Skerker et al., 2008). The bifunctionality of many sensory domains further supports the specificity. They prevent crosstalk by resetting the phosphorylation status of the cognate response regulator due to specific dephosphorylation in the absence of the stimulus (Huynh and Stewart, 2011). In *C. glutamicum* TCS are, for example, responsible for the control of the citrate utilization, response to phosphate starvation, osmoregulation or regulation of heme homeostasis (Krüger et al., 2022, Bott and Brocker, 2012, Brocker et al., 2011, Brocker et al., 2009, Schaaf and Bott, 2007).

Phosphorylation of serine and threonine residues in bacterial proteins is often catalyzed by Hanks-type serine/threonine protein kinases. These STPKs were previously called eukaryotic-like STPKs due to the structural and functional homology of their catalytic domain with eukaryotic STPKs (Stancik et al., 2018). Many bacterial STPKs are transmembrane proteins containing cytoplasmic kinase domains and extracellular sensing domains, such as the PASTA

(penicillin-binding protein and serine/threonine kinase-associated) domains. The modular domain organization of bacterial STPKS is highly diverse, most likely representing their different functions in various processes and different organisms (Krupa and Srinivasan, 2005). The overall structure of the catalytic domain of bacterial and eukaryotic STPKs is similar, possessing a characteristic two-lobed catalytic core structure with the active site located in a deep cleft between the two lobes. The N-terminal lobe is involved in binding and orienting of an ATP (adenosine triphosphate) molecule that acts as a phosphate donor, whereas the C-terminal lobe is responsible for binding to the protein substrate and transfer of the phosphate group (Janczarek et al., 2018). Phosphorylation of serine or threonine residues in the activation loop by either auto-phosphorylation or phosphorylation by another kinase introduces conformational changes leading to an active state of the kinase (Durán et al., 2005, Kornev et al., 2006). This activation loop determines substrate specificity and enables protein-protein interactions modulating the kinase activity (Janczarek et al., 2018).

Together with their cognate protein phosphatases, STPKs are often part of complex regulatory networks involved in cellular processes such as stress responses and pathogenicity (Perez et al., 2008, Bellinzoni et al., 2019, Pereira et al., 2011, Burnside and Rajagopal, 2012, Dworkin, 2015). The number of STPKs present varies drastically between different organisms. The first bacterial Hanks-type kinase described in detail by a solved protein structure was PknB from *M. tuberculosis* (Ortiz-Lombardıa et al., 2003, Young et al., 2003). By sequence analysis, 11 STPKs were identified in the *M. tuberculosis* genome in total, while in its relative *C. glutamicum* only four homologs of the mycobacterial STPKs are present (Av-Gay and Everett, 2000, Schultz et al., 2009). A single membrane-bound protein phosphatase, named PstP in *M. tuberculosis* and Ppp in *C. glutamicum*, catalyzes dephosphorylation in both organisms (Molle et al., 2006, Schultz et al., 2009). The domain organization of the corynebacterial STPKs is represented in Fig. 2. *C. glutamicum* PknB and PknL contain a cytoplasmic kinase domain (KD), a transmembrane helix (TM), and C-terminal PASTA domains enabling interaction with the peptidoglycan (Yeats et al., 2002). PknA is membrane-bound as well but does not possess PASTA domains, while PknG is a cytoplasmic enzyme consisting of the kinase domain and a tetratricopeptide repeat (TPR) domain, which is known to mediate protein-protein interactions (Schultz et al., 2009, Lisa et al., 2021, D'Andrea and Regan, 2003, Lisa et al., 2015). PknG homologs are exclusively found in actinobacteria and their modular organization is not present in so far known eukaryotic STPKs (Lisa et al., 2015).

While the histidine kinases of TCSs are usually specific for one response regulator protein, STPKs are known to phosphorylate several protein substrates. PknA and PknB of *M. tuberculosis*, for example, regulate cell growth and peptidoglycan synthesis. The primary substrate of PknB seems to be CwlM, a protein that activates MurA by interaction in its phosphorylated state. MurA is a cytoplasmic enzyme that catalyzes an initial step in

peptidoglycan biosynthesis (Turapov et al., 2018). Furthermore, PknB and PknA were shown to phosphorylate Wag31, a homolog of the cell division protein DivIVA, which regulates polar cell wall synthesis in *M. tuberculosis* (Kang et al., 2008). Moreover, PknA phosphorylates the tubulin homolog FtsZ (Thakur and Chakraborti, 2006). In *C. glutamicum* FtsZ as well as MurC, a protein involved in peptidoglycan synthesis, were also identified as *in vivo* substrates of PknA (Fiuza et al., 2008) and *in vitro* phosphorylation of FtsZ was observed for PknA, PknB and PknL (Schultz et al., 2009). Further, a small forkhead-associated (FHA) domain-containing protein involved in controlling 2-oxoglutarate metabolism was identified as a substrate of PknG and other STPKs in *C. glutamicum* and mycobacteria (Niebisch et al., 2006, O'Hare et al., 2008).

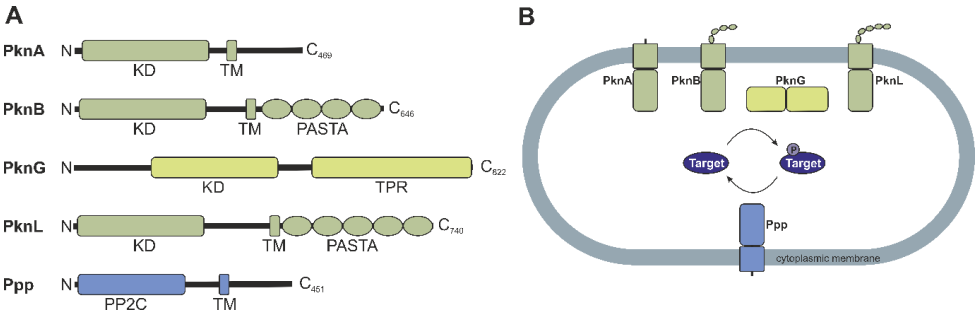

Figure 2: Overview on the four serine/threonine protein kinases and the protein phosphatase in *C. glutamicum*. (A) Domain architecture of the STPKs PknA, PknB, PknG and PknL and the phosphatase Ppp. KD: kinase domain, TM: transmembrane domain, PASTA: penicillin binding protein and serine/threonine-kinase associated domain, TPR: tetratricopeptide repeat domain, PPC2: phosphatase domain. Adapted from Schultz et al 2009 and Lisa et al. 2021. (B) Schematic overview on phosphorylation and dephosphorylation activities of the STPKs and Ppp in *C. glutamicum*.

1.4. Control of the 2-oxoglutarate metabolic branch point in *C. glutamicum*

The utilization of 2-oxoglutarate is an important branch point in central carbon metabolism. It can either be oxidatively decarboxylated to succinyl-CoA in the TCA cycle by the ODH or reductively aminated to L-glutamate by the glutamate dehydrogenase (GDH), and further converted to L-glutamine thereby generating the two major intracellular nitrogen donors in bacteria (Merrick and Edwards, 1995). In addition, glutamate is the precursor for proline and arginine synthesis. In *C. glutamicum* ammonium assimilation is carried out by an NADPH (nicotinamide adenine dinucleotide phosphate)-dependent GDH under nitrogen excess, while under nitrogen limitation ammonium assimilation takes place by conversion of glutamate to glutamine by the glutamine synthetase GlnA. The substrate of this reaction is regenerated by conversion of glutamine and 2-oxoglutarate to two molecules of glutamate by the glutamate 2-oxoglutarate aminotransferase (GOGAT). Glutamine catabolism is carried out by glutaminase K (GlsK) (Fig. 3) (Jakoby et al., 1997, Börmann et al., 1992, Buerger et al., 2016, Shiio et al.,

1982). The formation of glutamate from 2-oxoglutarate, catalyzed by the GDH, is reversible but *C. glutamicum* GDH possesses a low affinity for glutamate (K_m 100 mM) (Shiio and Ozaki, 1970). However, 2-oxoglutarate is generated from glutamate by amino acid transferases, including the aspartate aminotransferase AspT, the alanine aminotransferase AlaT, the branched-chain amino transferase IlvE or the aromatic aminotransferase AroT, which use glutamate as amino donor (Marienhagen et al., 2005). Since the GDH possesses a much lower affinity for the substrate 2-oxoglutarate (K_m 5.7 mM) than the ODH (K_m 0.02–0.13 mM), glutamate production and thus nitrogen assimilation requires regulation of ODH activity (Shiio and Ozaki, 1970, Shiio and Ujigawa-Takeda, 1980, Niebisch et al., 2006, Hoffelder et al., 2010). The relevance of ODH activity for glutamate formation was, for example, observed in a *C. glutamicum* strain which lacks the E1 subunit of the ODH, OdhA, and therefore does not possess ODH activity. This led to an excretion of high levels of glutamate without adding any of the known inducers of glutamate production, such as ethambutol (Asakura et al., 2007, Radmacher et al., 2005).

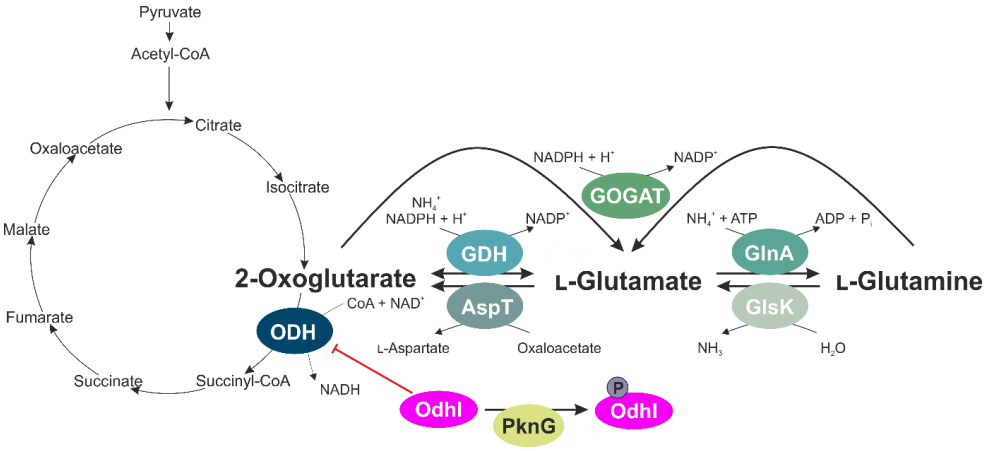

Figure 3: Control of the nitrogen metabolism at the 2-oxoglutarate branch point in *C. glutamicum*. Glutamate dehydrogenase (GDH) and glutamine synthetase (GlnA) enable ammonium assimilation via formation of glutamate and glutamine starting form 2-oxoglutarate. Inhibition of the 2-oxoglutarate dehydrogenase (ODH) by OdhI enables an increased flux toward glutamate. Phosphorylation of OdhI by the serine/threonine protein kinase PknG relieves ODH inhibition and 2-oxoglutarate is primarily used in the TCA cycle. Under nitrogen limitation glutamate is synthesized by the glutamate 2-oxoglutarate aminotransferase (GOGAT). Glutamine catabolism can be catalyzed by the glutaminase K (GlsK) and the aspartate aminotransferase (AspT).

The corynebacterial ODH is activated by acetyl-CoA and inhibited by its product succinyl-CoA as well as by pyruvate, oxaloacetate, NADH, and NADPH (Shiio and Ujigawa-Takeda, 1980) and in addition a regulatory mechanism based on post-translational modification was discovered in actinobacteria. In *C. glutamicum* a small FHA domain-containing protein (15 kDa) was identified, which binds with nM affinity (inhibitor constant K_i of 2.4 nM) to the OdhA

subunit of the ODH and thereby inhibits its activity (Niebisch et al., 2006). Therefore, the protein was named OdhI for ODH inhibitory protein. This small FHA domain-containing protein is highly conserved among actinobacteria and OdhI shares high sequence identity with its mycobacterial homolog GarA (73.5% identity to *M. smegmatis* GarA, 82% identity to *M. tuberculosis* GarA) (Villarino et al., 2005, Raasch et al., 2014, England et al., 2009). Inhibition of the ODH homolog KGD by GarA was also observed, but in addition GarA was shown to interact with two other 2-oxoglutarate utilizing enzymes, GDH and GOGAT, further underlining the importance of this protein for glutamate and nitrogen metabolism. GarA binding leads to an inhibition of GDH activity and activation of GOGAT activity (Nott et al., 2009, O'Hare et al., 2008). It has to be mentioned that GDH of *M. tuberculosis* is an NADH-dependent enzyme, which mainly catalyzes the oxidative deamination of glutamate, thereby acting in glutamate catabolism, which is different from *C. glutamicum* (Gallant et al., 2016). Besides the inhibitory effect of OdhI and GarA on ODH or KGD activity, respectively, the interaction of its FHA domain with the C-terminal decarboxylase domain of OdhA/Kgd was also shown by protein-protein interaction studies for *C. glutamicum* and a solved crystal structure of *M. smegmatis* Kgd/GarA complex (Fig. 4A) (Krawczyk et al., 2010, Raasch et al., 2014, Wagner et al., 2019). The binding interface of GarA and Kgd lies about 30 Å away from the catalytic center of Kgd and does not affect substrate access, but involves a surface exposed α-helix that was shown to move during transition from the resting to the fully-active state of Kgd, meaning that the binding of the FHA domain locks Kgd in its resting state (Wagner et al., 2019, Wagner et al., 2014).

The binding of OdhI to OdhA was shown to be dependent on the phosphorylation status of OdhI. OdhI binding capability is mainly regulated by phosphorylation of an N-terminal threonine residue, Thr14, by the STPK, PknG. However, OdhI can also be phosphorylated by PknB, PknA, and PknL at Thr15, at least *in vitro*, and *in vivo* doubly phosphorylated OdhI was detected in *C. glutamicum* cell extracts by 2D gel electrophoresis and Western blot analysis (Schultz et al., 2009, Niebisch et al., 2006). Phosphorylation of GarA at the corresponding N-terminal threonine residues Thr21 and Thr22 in the conserved ETTS motif is as well catalyzed by STPKs (England et al., 2009, O'Hare et al., 2008). Phosphorylation of these N-terminal threonine residues leads to an intramolecular binding of the phosphorylated N-terminus by the FHA domain, resulting in a conformational change of the protein preventing interaction of the FHA domain with OdhA/Kgd. This conformational change was suggested by biophysical experiments and proven by solved NMR structures of phosphorylated and unphosphorylated OdhI as shown in Fig. 4C and D (Barthe et al., 2009, England et al., 2009). The solved structures of OdhI and GarA not only provide evidence for the intramolecular switch upon phosphorylation and the binding to Kgd but also prove that the protein possesses an unstructured N-terminus and the typical FHA domain β-sandwich structure of 11 β-strands

(Durocher and Jackson, 2002). The binding of phosphorylated threonine residues is a common feature of FHA domains, allowing them to mediate protein-protein interactions (Hammet et al., 2003). While the intramolecular binding of the OdhI/GarA FHA domain to its N-terminus depends on phosphorylated threonine residues, the interaction of the FHA domain with OdhA/Kgd is phospho-independent (Wagner et al., 2019, Raasch et al., 2014). The binding of *M. smegmatis* GarA to Kgd was shown to rely on a phosphomimetic aspartate residue of Kgd, which is located at the interaction surface of the two proteins and occupies the phosphate-binding pocket of the FHA domain. This interaction is stabilized by intermolecular salt bridges and hydrogen bonds build at the interaction surface (Wagner et al., 2019).

Deletion of the *odhI* gene in *C. glutamicum* led to a drastically reduced glutamate production (more than 80%), while internal glutamate levels increased two-fold in a Δ*pknG* mutant (Schultz et al., 2007, Niebisch et al., 2006). These opposite effects on metabolic capabilities were also shown for *pknG* and *garA* deletions in *M. tuberculosis*, once more showing the importance of the regulation of OdhI/GarA by PknG for controlling metabolic fluxes and nitrogen metabolism in actinobacteria (Rieck et al., 2017). The inactivation of OdhI by phosphorylation was shown to be reversible and dephosphorylation is carried out by the protein phosphatase Ppp (PstP in *M. tuberculosis*) (Schultz et al., 2009).

The solved structures of *M. tuberculosis* and *C. glutamicum* PknG (Fig. 4B) enable a better understanding how PknG inactivates OdhI (Lisa et al., 2015, Lisa et al., 2021, Scherr et al., 2007). PknG possesses a unique modular organization, consisting of an unstructured N-terminal region followed by the catalytic domain and a TPR domain that flanks the kinase catalytic core. In the mycobacterial protein and all other actinobacterial PknG homologs an additional rubredoxin-like domain is present, which is missing in *C. glutamicum* PknG (Lisa et al., 2021). Despite this difference, the overall fold and topology of *C. glutamicum* PknG is similar to the mycobacterial one and purified *C. glutamicum* PknG phosphorylated OdhI and GarA to a similar extent. Furthermore, the growth defect observed for *C. glutamicum* Δ*pknG* on agar plates with glutamine as sole carbon and nitrogen source was complemented by plasmid-based expression of corynebacterial as well as mycobacterial *pknG*, showing the high functional similarity of the kinase in both organisms (Niebisch et al., 2006, Lisa et al., 2021). A mutation of the active site of *C. glutamicum* PknG (K205A) did not complement the growth defect of the Δ*pknG* strain, further underlining the importance of PknG-mediated phosphorylation for glutamine utilization (Lisa et al., 2021). Moreover, it was shown that OdhI and GarA are recruited by auto-phosphorylation sites in the N-terminal segment of PknG. These phosphorylated threonine residues are bound by the FHA domain of GarA or OdhI, which allows a more efficient phosphorylation of the specific threonine residues of the FHA domain-containing protein (Lisa et al., 2015, Lisa et al., 2021). In contrast to PknG most other

mycobacterial STPKs possess auto-phosphorylation sites in the activation loop where no auto-phosphorylation sites were found in PknG (Durán et al., 2005, Prisic et al., 2010).

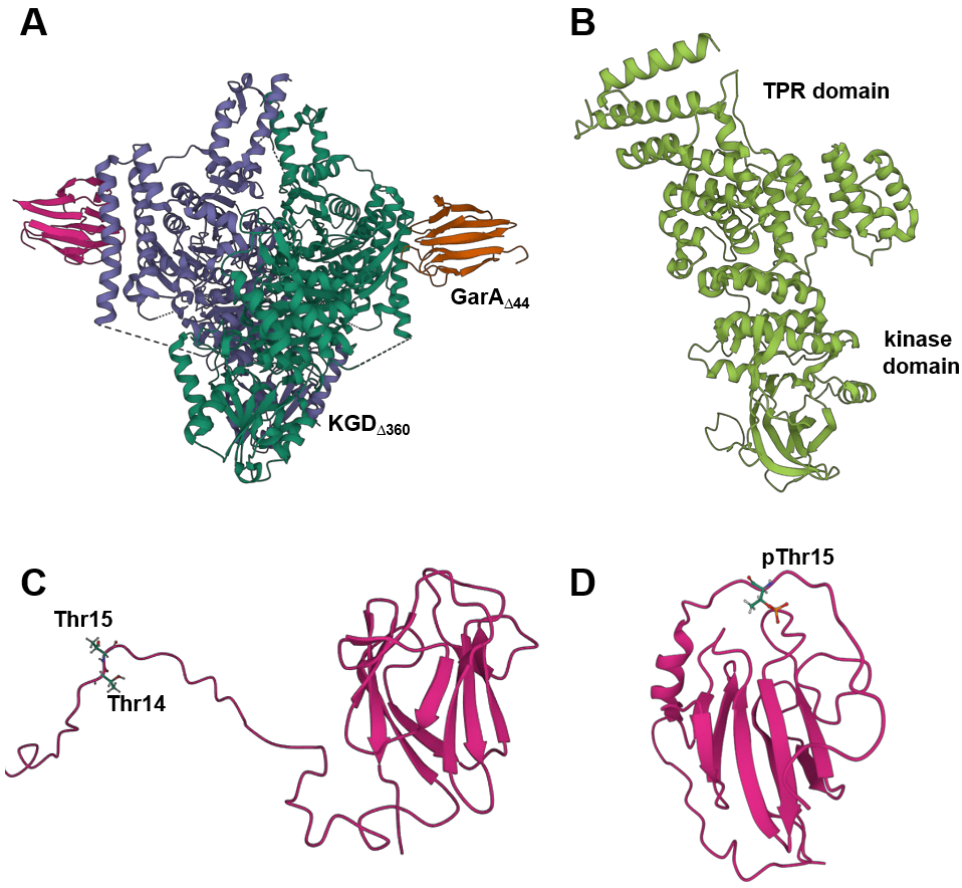

Figure 4: Structural overview on proteins involved in ODH activity control. (A) Crystal structure of the homodimer of the decarboxylase domain of *M. smegmatis* Kgd (KgdΔ360) with the FHA domain of GarA (GarAΔ44). PDB code 6I2Q. (B) Crystal structure of *C. glutamicum* PknG with indication of the kinase domain and the tetratricopeptide repeat (TPR) domain. PDB code 7MXB (C) NMR structure of unphosphorylated OdhI with representation of the N-terminal threonine residues known to be phosphorylated by STPKs. PDB code 2KB4. (D) NMR structure of OdhI phosphorylated at Thr15 (pThr15) by PknB. PDB code 2KB3. Structures were determined by Wagner et al. 2019, Lisa et al. 2021, and Barthe et al. 2009 and visualized using Mol* viewer (Sehnal et al., 2021).

1.5. Regulation of PknG activity

The dependency on PknG for glutamate utilization was shown by the above-mentioned growth defect of a *C. glutamicum pknG* deletion strain when grown on glutamine as sole carbon and nitrogen source as well as in *M. smegmatis*, where the use of glutamate as sole nitrogen source led to reduced growth of a *pknG* deletion mutant (Niebisch et al., 2006, Rieck et al.,

2017). Furthermore, *M. tuberculosis* GarA was shown to be predominantly unphosphorylated when grown under amino acid starvation, and the addition of glutamate caused a rapid increase of phosphorylated GarA in *M. smegmatis* (Rieck et al., 2017). This is in accordance with the observation that OdhI is predominantly unphosphorylated in *C. glutamicum* grown in minimal medium lacking amino acids but mainly phosphorylated in complex medium (Schultz et al., 2007). Together these findings show that phosphorylation of OdhI by PknG is required to relieve the inhibition of ODH activity and shift the flux of 2-oxoglutarate towards energy generation in the TCA cycle, with concomitant reduction of NADPH consumption by the GDH. For efficient control of this metabolic branch point, the activity of PknG itself has to be regulated depending on amino acid availability as well. In contrast to most other STPKs, PknG is a cytoplasmic protein lacking transmembrane or extracellular domains, which could act as sensory domains. But PknG possesses a C-terminal domain with tetratricopeptide repeats (Fig. 4B), which are known for their ability to mediate protein-protein interactions in signal transduction (Blatch and Lässle, 1999, Core and Perego, 2003). This TPR domain was shown to be essential for the response of PknG to extracellular glutamine or glutamate in *C. glutamicum* and *M. smegmatis*, respectively, suggesting its importance for interaction with another protein regulating PknG activity (Lisa et al., 2021, Bhattacharyya et al., 2018).

The *pknG* gene is located in a putative operon with two other genes encoding a putative transmembrane protein (*glnX*) and a putative glutamine binding lipoprotein (*glnH*). This genomic organization of the three genes is conserved among PknG-possessing actinobacteria (Fig. 5A) (Cowley et al., 2004, Niebisch et al., 2006, Bhattacharyya et al., 2018). A deletion of *glnX* and *glnH* in *C. glutamicum* led to the same growth defect on glutamine as sole carbon and nitrogen source as observed for the *pknG* deletion strain (Fig. 5B) (Niebisch et al., 2006). This is also true for a deletion of *glnX* in *M. smegmatis*, which caused the same phenotype as a *pknG* deletion (Bhattacharyya et al., 2018). Furthermore, *M. tuberculosis* GlnH was shown to bind aspartate and glutamate, two amino acids known to stimulate GarA phosphorylation, with high affinity (Rieck et al., 2017, Bhattacharyya et al., 2018). Together this suggests a signal transduction cascade where GlnH acts as an extracellular sensor for external stimuli, most likely amino acids such as glutamine, glutamate, or aspartate, and the information is transferred by protein-protein interaction to the transmembrane protein GlnX, which then activates PknG in the cytoplasm (Fig. 5C). Interaction of GlnX with PknG might be mediated by the TPR domain of PknG. Activated PknG phosphorylates OdhI, which no longer inhibits ODH activity, shifting the metabolic flux at the 2-oxoglutarate node from glutamate formation and ammonium assimilation to succinyl-CoA and energy generation in the TCA cycle.

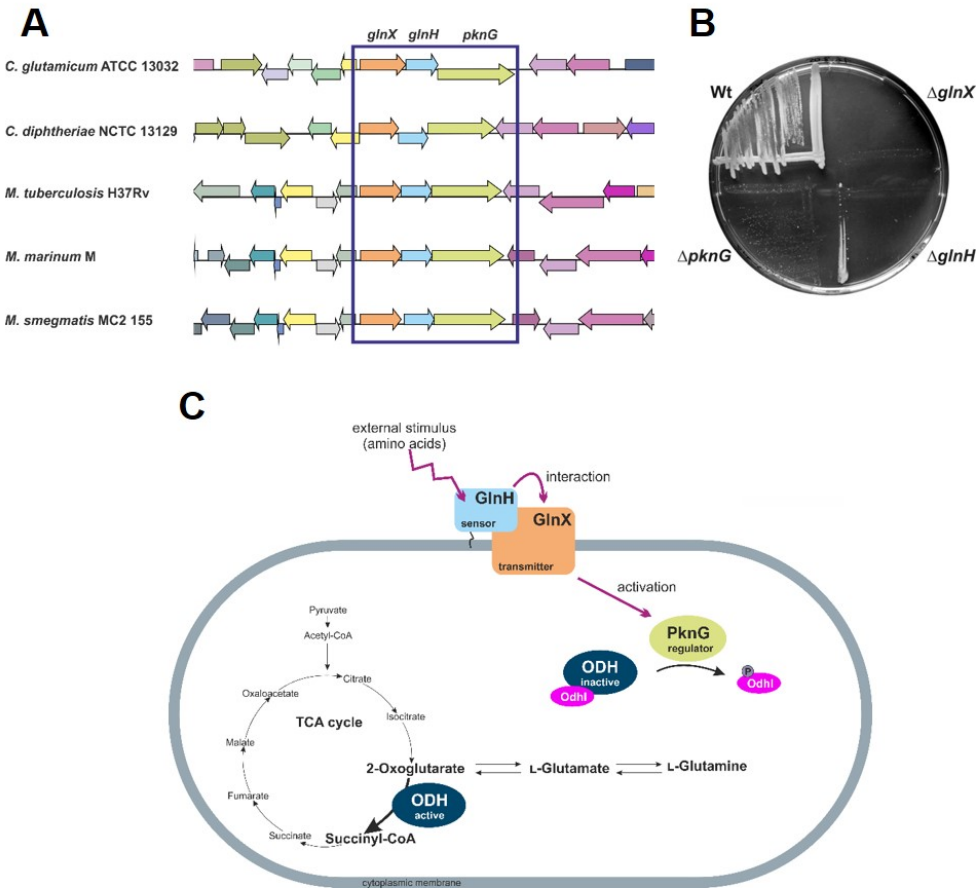

Figure 5: Model of PknG activity regulation. (A) Genomic organization of the putative operon *glnX-glnH-pknG* in different actinobacteria, visualized using Gene Graphics software (Harrison et al., 2018). (B) Growth of *C. glutamicum* wt, and the mutant strains Δ*pknG,* Δ*glnX,* and Δ*glnH* on minimal medium agar plates containing 100 mM glutamine as sole carbon and nitrogen source. The figure was taken from Niebisch et al. 2006. (C) Schematic model of the proposed regulation cascade controlling PknG activity. GlnH senses an external signal, most likely the amino acids aspartate and glutamate, and the information on its loading status is transferred via protein-protein interaction to GlnX, and further to PknG in the cytoplasm. Thereby PknG gets activated and phosphorylates OdhI leading to an active ODH and an increased use of 2-oxoglutarate in the TCA cycle.

1.6. Aim of this work

Since several members of the actinobacteria have a high biotechnological or medical relevance, detailed knowledge of unique features of their metabolism, including regulatory and structural characteristics, is required to further improve or establish industrially relevant production processes and to identify novel drug targets for the pathogenic species such as *M. tuberculosis*. One of these features is a special mechanism that regulates the 2-oxoglutarate dehydrogenase activity and thereby the 2-oxoglutarate flux between the TCA cycle and ammonium assimilation in *Corynebacterium* and *Mycobacterium* species. A major aim of this thesis was the characterization of the GlnH and GlnX proteins involved in the control

of PknG activity. In the case of GlnH, the identification of the ligands and their binding affinities is required to know the signals controlling the PknG activity and thus OdhI phosphorylation and ODH activity. In the case of GlnX, which is assumed to transfer the information sensed by GlnH across the membrane to PknG, the knowledge of its topology is a prerequisite for protein-protein interaction studies. A further aspect to be studied in this thesis was the cellular localization of different proteins involved in the signal transduction cascade by fluorescence microscopy, using fusions to auto-fluorescent proteins. Another aim was to further analyze the composition and function of the hybrid PDH-ODH complex in *C. glutamicum* using co-purification and enzyme activity measurements.

2. Results

2.1 Characteristics of the GlnH and GlnX signal transduction proteins controlling PknG-mediated phosphorylation of OdhI and 2-oxoglutarate dehydrogenase activity in *Corynebacterium glutamicum*

Lea Sundermeyer*, Graziella Bosco*, Srushti Gujar, Melanie Brocker, Meike Baumgart, Dieter Willbold, Oliver H. Weiergräber, Marco Bellinzoni, and Michael Bott (2022). – revised manuscript to be submitted to Microbiology Spectrum (Spectrum02677-22)

*shared first author

Author contributions:

- LS designed and performed the ligand binding experiments with purified GlnH (using ITC and by measuring changes in intrinsic tryptophan fluorescence), the GlnX topology studies, and complementation tests. Figures 6, 7, 8, and 10 resulted from these experiments. LS visualized data obtained by GB, analyzed the data, and participated in manuscript writing.
- GB designed and performed OdhI phosphorylation analysis, characterization of suppressor mutants, and experiments to characterize GlnH as a lipoprotein, analyzed the data and participated in manuscript writing. Figures 1 to 5 resulted from these experiments.
- MBe created the structural model of *C. glutamicum* GlnH using AlphaFold 2, performed the comparison with the *M. tuberculosis* GlnH homolog, and identified amino acid residues potentially responsible for the different binding affinities of the two homologs for L-aspartate and L-glutamate. He wrote the text dealing with these aspects.
- SG and OHW created the structural model of GlnX using AlphaFold 2, performed comparisons with known structures, and wrote the text dealing with these aspects.
- GB was supervised by MBo and MBr, LS was supervised by MBo and MBa, and SG was supervised by OHW and DW.
- MBo developed the overall concept of this study, analyzed the data, and was mainly responsible for writing the manuscript.

Overall contribution LS: 35%

AMERICAN SOCIETY FOR MICROBIOLOGY | Microbiology Spectrum

RESEARCH ARTICLE

Characteristics of the GlnH and GlnX Signal Transduction Proteins Controlling PknG-Mediated Phosphorylation of OdhI and 2-Oxoglutarate Dehydrogenase Activity in *Corynebacterium glutamicum*

Lea Sundermeyer,[a] Graziella Bosco,[a] Srushti Gujar,[a,b,c] Melanie Brocker,[a] Meike Baumgart,[a] Dieter Willbold,[b,c] Oliver H. Weiergräber,[b] Marco Bellinzoni,[d] Michael Bott[a,e]

[a]IBG-1: Biotechnology, Institute of Bio- and Geosciences, Forschungszentrum Jülich, Jülich, Germany
[b]IBI-7: Structural Biochemistry, Institute of Biological Information Processing, Forschungszentrum Jülich, Jülich, Germany
[c]Institut für Physikalische Biologie, Heinrich-Heine-Universität Düsseldorf, Düsseldorf, Germany
[d]Institut Pasteur, Université de Paris Cité, CNRS UMR3528, Unité de Microbiologie Structurale, Paris, France
[e]Bioeconomy Science Center (BioSC), Forschungszentrum Jülich, Jülich, Germany

Lea Sundermeyer and Graziella Bosco contributed equally to this work. Author order was set in order of increasing seniority.

ABSTRACT In *Corynebacterium glutamicum* the protein kinase PknG phosphorylates OdhI and thereby abolishes the inhibition of 2-oxoglutarate dehydrogenase activity by unphosphorylated OdhI. Our previous studies suggested that PknG activity is controlled by the periplasmic binding protein GlnH and the transmembrane protein GlnX, because Δ*glnH* and Δ*glnX* mutants showed a growth defect on glutamine similar to that of a Δ*pknG* mutant. We have now confirmed the involvement of GlnH and GlnX in the control of OdhI phosphorylation by analyzing the OdhI phosphorylation status and glutamate secretion in Δ*glnH* and Δ*glnX* mutants and by characterizing Δ*glnX* suppressor mutants. We provide evidence for GlnH being a lipoprotein and show by isothermal titration calorimetry that it binds L-aspartate and L-glutamate with moderate to low affinity, but not L-glutamine, L-asparagine, or 2-oxoglutarate. Based on a structural comparison with GlnH of *Mycobacterium tuberculosis*, two residues critical for the binding affinity were identified and verified. The predicted GlnX topology with four transmembrane segments and two periplasmic domains was confirmed by PhoA and LacZ fusions. A structural model of GlnX suggested that, with the exception of a poorly ordered N-terminal region, the entire protein is composed of α-helices and small loops or linkers, and it revealed similarities to other bacterial transmembrane receptors. Our results suggest that the GlnH-GlnX-PknG-OdhI-OdhA signal transduction cascade serves to adapt the flux of 2-oxoglutarate between ammonium assimilation via glutamate dehydrogenase and energy generation via the tricarboxylic acid (TCA) cycle to the availability of the amino group donors L-glutamate and L-aspartate in the environment.

IMPORTANCE *Actinobacteria* comprise a large number of species playing important roles in biotechnology and medicine, such as *Corynebacterium glutamicum*, the major industrial amino acid producer, and *Mycobacterium tuberculosis*, the pathogen causing tuberculosis. Many actinobacteria use a signal transduction process in which the phosphorylation status of OdhI (corynebacteria) or GarA (mycobacteria) regulates the carbon flux at the 2-oxoglutarate node. Inhibition of 2-oxoglutarate dehydrogenase by unphosphorylated OdhI shifts the flux of 2-oxoglutarate from the TCA cycle toward glutamate formation and, thus, ammonium assimilation. Phosphorylation of OdhI/GarA is catalyzed by the protein kinase PknG, whose activity was proposed to be controlled by the periplasmic binding protein GlnH and the transmembrane protein GlnX. In this study, we combined genetic, biochemical, and structural modeling

Editor Eric Cascales, Centre national de la recherche scientifique, Aix-Marseille Université

Address correspondence to Michael Bott, m.bott@fz-juelich.de.

The authors declare no conflict of interest.

Received 12 July 2022
Accepted 5 November 2022
Published 29 November 2022

approaches to characterize GlnH and GlnX of *C. glutamicum* and confirm their roles in the GlnH-GlnX-PknG-OdhI-OdhA signal transduction cascade. These findings are relevant also to other *Actinobacteria* employing a similar control process.

KEYWORDS bacterial signaling, *Corynebacterium glutamicum*, 2-oxoglutarate dehydrogenase, protein phosphorylation, periplasmic binding protein, *Actinobacteria*, forkhead-associated domain, four-helix bundle, serine/threonine kinases, signal transduction

Corynebacterium glutamicum is a nonpathogenic Gram-positive soil bacterium that is used in large-scale amino acid production (1–4). It belongs to the order *Corynebacteriales* within the *Actinobacteria*, which includes important human pathogens such as *Corynebacterium diphtheriae* and *Mycobacterium tuberculosis* (5). Due to the importance of *C. glutamicum* in industrial biotechnology, its metabolism and regulatory mechanisms have been extensively studied as a prerequisite for strain development by metabolic engineering. We previously identified a novel type of posttranslational regulation controlling the carbon flux at the 2-oxoglutarate metabolic branching point in *C. glutamicum* (6). At this node, 2-oxoglutarate is either oxidatively decarboxylated to succinyl coenzyme A (succinyl-CoA) by an unusual 2-oxoglutarate dehydrogenase complex (ODH) within the tricarboxylic acid (TCA) cycle (7) or reductively aminated to L-glutamate by glutamate dehydrogenase (GDH). We showed that the activity of ODH is inhibited by the 15-kDa forkhead-associated (FHA) domain-containing protein OdhI. OdhI binds with nM affinity to the OdhA subunit of the ODH and thereby inhibits its activity (6, 8, 9). Phosphorylation of the Thr14 residue of OdhI by the serine/threonine protein kinase PknG leads to a conformational change of OdhI and thereby prevents its binding to OdhA, while the phospho-serine/threonine protein phosphatase Ppp reactivates OdhI by dephosphorylation (6, 8, 10). Not only PknG, but also the serine/threonine protein kinases (STPK) PknA, PknB, and PknL are able to phosphorylate OdhI, at least *in vitro* (10). The conformational change of OdhI upon phosphorylation was demonstrated by structural analysis via nuclear magnetic resonance (NMR) (11). In addition to phosphorylation, succinylation of OdhI at K132 was also reported to diminish the inhibitory effect on ODH (12). The structure of PknG of *C. glutamicum* has also been elucidated recently and revealed features required for interaction with OdhI and signal transduction (13). In a Δ*pknG* mutant, the internal L-glutamate concentration was increased 2-fold, confirming the importance of PknG in glutamate metabolism (6). The inhibition of ODH activity by OdhI enables a shift of the carbon flux from the TCA cycle toward L-glutamate synthesis and thus nitrogen assimilation. Glutamate overproduction by an *odhI* deletion mutant of *C. glutamicum* was drastically impaired, revealing that OdhI is crucial for this process (14). This novel type of posttranslational regulation of ODH was shown to be also present in *Mycobacterium* species, where the OdhI homolog is named GarA (15–19).

For a physiological understanding of the control of the OdhI phosphorylation status and thus of the regulation of carbon flux at the 2-oxoglutarate node, it is crucial to know how the activity of PknG is regulated. In contrast to the other STPKs of *C. glutamicum* (PknA, PknB, PknL), PknG is a cytoplasmic protein lacking extracellular or transmembrane segments which could act as receptors for extracellular nutrients (10, 13). The *pknG* gene is located in a putative operon with *glnH* and *glnX*, which were initially annotated to encode a putative secreted glutamine binding protein and a membrane protein, respectively (6, 20). Deletion of either *glnH* or *glnX* in *C. glutamicum* led to a growth defect comparable to that caused by deletion of *pknG* when the strains were grown on glutamine as the sole nitrogen and carbon source (6). This result suggested that GlnH, GlnX, and PknG are part of a signal transduction cascade in which GlnH serves as an extracellular sensor, presumably for amino acids, whereas GlnX transmits the ligandation status of GlnH to PknG to control its kinase activity. In line with such a model, deletion of *glnX* in *Mycolicibacterium smegmatis* mimicked the growth defect of the *pknG* deletion strain on glutamate, and the GlnH proteins of *Mycobacterium tuberculosis* and *C. glutamicum* were shown to bind L-aspartate and L-glutamate (21).

Remarkably, the affinities of *M. tuberculosis* GlnH for these amino acids were about 100-fold higher than those of *C. glutamicum* GlnH (21).

In this study, we confirmed the involvement of GlnH and GlnX in signal transduction to OdhI and ODH in *C. glutamicum* by analyzing the influence of Δ*glnH* and Δ*glnX* mutants on the OdhI phosphorylation status and glutamate overproduction and by exploring the genetic alterations of Δ*glnX* suppressor mutants that regained the ability to grow on glutamine agar plates. We analyzed whether GlnH is a lipoprotein, determined its ligand binding properties, and identified two residues critical for the ligand binding affinity. Finally, we analyzed the membrane topology of GlnX and predicted its overall architecture and functional properties based on a structural model.

RESULTS

Complementation of the growth defect of the Δ*glnX2* and Δ*glnH* mutants of *C. glutamicum* on glutamine agar plates. In our previous study we reported that Δ*glnX* and Δ*glnH* mutants of *C. glutamicum* show the same growth defect on glutamine agar plates as the Δ*pknG* mutant (6). The growth defect of the Δ*glnH* mutant could be complemented by transformation with the plasmid pAN6-*glnH* expressing *glnH* under the control of the *tac* promoter (see Fig. S1 in the supplemental material). As initial complementation experiments with the Δ*glnX* mutant failed, we constructed another deletion mutant, Δ*glnX2*, in which 59 5′-terminal *glnX* codons and 142 3′-terminal *glnX* codons were retained and the 301 codons in between were deleted and replaced by an artificial 21-bp sequence. The Δ*glnX2* mutant showed the expected growth defect on glutamine agar plates and could be complemented by transformation with the plasmid pJC1-*glnX*Prom expressing *glnX* from its native promoter (Fig. S1). These results show that the growth defect on glutamine agar plates of the Δ*glnX2* and Δ*glnH* mutants is not caused by polar effects on *pknG* expression. The observation that the original Δ*glnX* mutant could not be complemented might be due to the presence of a yet unidentified promoter within the 3′-end of the *glnX* coding region that was retained in the Δ*glnX2* mutant.

Influence of *glnH* and *glnX* deletions on the phosphorylation status of OdhI and glutamate secretion. We previously showed that the lack of PknG resulted in a reduced level of phosphorylated OdhI during growth in BHI medium with glucose (10). To test how the absence of GlnH or GlnX influences the OdhI phosphorylation status under these conditions, the *C. glutamicum* strains wild type (WT), Δ*glnX2*, Δ*glnH*, Δ*pknG*, and Δ*glnX-glnH-pknG* were grown overnight in brain heart infusion (BHI) medium with 4% (wt/vol) glucose, and cell-free protein extracts were then analyzed in Western blots with anti-OdhI antiserum. As shown in Fig. 1, ~40% of OdhI was phosphorylated in the WT, but only between 15% and 20% was phosphorylated in the four mutants. This result indicated that the absence of GlnH and GlnX influences the phosphorylation status of OdhI in a similar manner and extent as the absence of PknG. The simultaneous absence of all three proteins (GlnH, GlnX, and PknG) in the Δ*glnX-glnH-pknG* mutant had the same effect on OdhI phosphorylation as the three individual gene deletions, which is expected if each of the three proteins mediates a distinct and essential step of the same signal transduction cascade.

A reduced phosphorylation of OdhI is expected to cause a strengthened inhibition of ODH activity by unphosphorylated OdhI. In agreement with this assumption, the deletion of *pknG* was previously shown to result in increased glutamate excretion compared to the WT, when cells were cultured in the presence of ethambutol, an inhibitor of cell wall arabinogalactan synthesis causing alterations of the cell wall (14). Ethambutol was shown to trigger glutamate secretion by *C. glutamicum* (22). We now tested the mutants Δ*glnX2* and Δ*glnH* regarding glutamate excretion in the presence of ethambutol and observed a 2-fold-increased glutamate titer in the supernatant compared to the WT (Fig. S2), supporting an increased flux of 2-oxoglutarate to L-glutamate due to an enhanced level of unphosphorylated OdhI. Increased glutamate production could be abolished by plasmid-based expression of *glnX* or *glnH* in the respective deletion mutants (Fig. S2).

Analysis of suppressor mutants selected by growth of strains Δ*glnH* and Δ*glnX2* on glutamine agar plates. Prolonged incubation of the Δ*pknG* strain on glutamine agar plates led to the formation of suppressor mutants that regained the ability

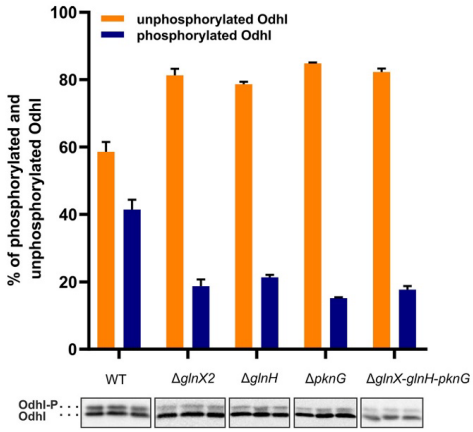

FIG 1 Analysis of the OdhI phosphorylation status in cells grown for 24 h in BHI medium with 4% (wt/vol) glucose. Western blot analysis of cell-free protein extracts (5 μg each) of the indicated *C. glutamicum* strains was performed with polyclonal anti-OdhI antibodies. The experiment was performed in triplicate. The upper band in the Western blot represents singly or doubly phosphorylated OdhI; the lower band represents unphosphorylated OdhI (14). The percentages (mean values with standard deviation) of unphosphorylated OdhI (orange bars) to phosphorylated OdhI (blue bars) were calculated by densitometry.

to grow on glutamine (9). To check for a similar behavior in the case of *glnX* or *glnH* deletions, *C. glutamicum* WT and the mutant strains Δ*glnX2*, Δ*glnH*, Δ*pknG*, and Δ*glnX-glnH-pknG* were cultivated on glutamine agar plates and photographed after 2, 3, 4, and 7 days (Fig. 2). All mutants showed only marginal growth after 2 days, whereas the WT grew well. During further incubation, all mutants formed colonies with a very heterogeneous size, suggesting the occurrence of suppressor mutations enabling growth.

To test whether mutations in *odhI* are responsible for abolishing the growth defect on glutamine, we sequenced the *odhI* gene of 20 Δ*glnX2* suppressor mutants. As shown in Table 1, 16 of the 20 suppressor mutants (named K1 to K20) in fact contained mutations in *odhI*. In five mutants a stop codon was introduced at five different positions (residue 60 in mutant K2, residue 129 in mutant K3, residue 53 in mutant K5, residue 65 in mutant K17, and residue 123 in mutant K20). In three cases, frameshift mutations were found in codon 59 (mutant K11, 1-bp insertion) or in codon 120 (mutants K12 and K19, 1-bp deletion). In seven cases, mutations leading to a single amino acid exchange were identified: R87P in mutants K1 and K4, E91K in mutants K6 and K16, L107V in mutant K8, F137S in mutant K9, and T84I in mutant K10. In the case of mutant K7, two amino acid exchanges were identified, R87P and E91K. In four suppressor mutants (K13, K14, K15, K18) no mutation was found in *odhI*. We therefore also sequenced *odhA* and *pknG* in these four strains but could not find mutations in these genes.

We assumed that the 16 mutated *odhI* genes led to OdhI variants whose ability to inhibit ODH activity was impaired or abolished. To test if the OdhI protein was still formed in the mutant strains, Western blot analysis was performed with an anti-OdhI antiserum. As shown in Fig. 3, in many suppressor mutants OdhI of native size was no longer detectable. This holds true for all three variants with frameshift mutations and the nonsense mutations Q123Stop and Q129Stop. In the case of the mutations Q53Stop and R60Stop, truncated variants were detectable. In the four suppressor mutants without an *odhI* mutation, the OdhI protein was detectable in both the unphosphorylated and phosphorylated forms (lower and upper band, respectively), as in the parental strain. In the case of the OdhI variant with the mutation F137S and in the variant bearing the two mutations, R87P and E91K, OdhI was no longer detectable. The OdhI variants with the single-amino acid exchanges

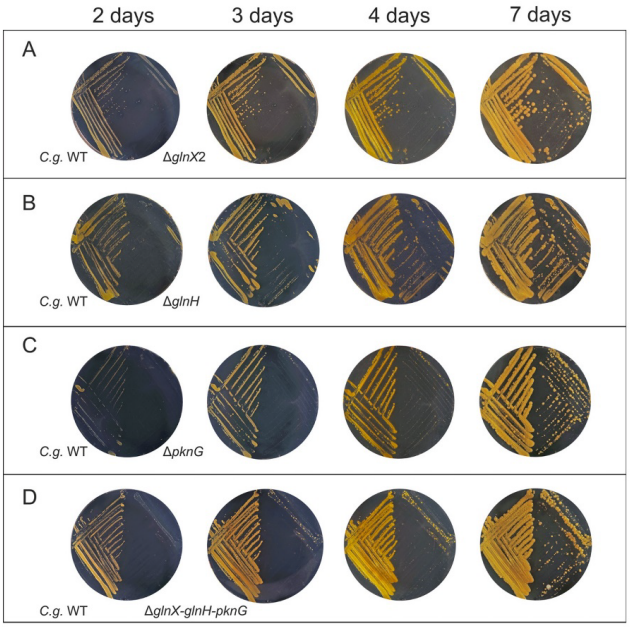

FIG 2 Growth of *C. glutamicum* WT and the indicated mutant strains on agar plates containing 100 mM L-glutamine as the sole carbon and nitrogen source. The plates were incubated at 30°C for 7 days and photographed after 2, 3, 4, and 7 days.

R87P and L107V were easily detectable, whereas for the variants with the single mutations T84I and E91K, only a very weak signal was observed, suggesting that the latter two OdhI variants were instable and largely degraded. The results obtained for the Δ*glnX2* suppressor mutants confirm that GlnX is part of the signal transduction cascade controlling OdhI phosphorylation. Further support was obtained by construction of a Δ*glnX2* Δ*odhI* mutant, which was able to grow on glutamine agar plates (Fig. S3).

Influence of R87P and R87A amino acid exchanges in OdhI on the inhibition of ODH activity. In the suppressor mutants with no or barely detectable OdhI or with a truncated OdhI protein, inhibition of ODH activity is likely no longer possible. In the suppressor mutants, in which mutated OdhI variants were still detectable, the amino acid exchanges might have reduced the binding affinity to OdhA and/or the inhibitory effect of OdhI on ODH activity. As the amino acid exchange R87P occurred more than once in the investigated suppressor mutants, we analyzed the influence of this mutation on the inhibition of ODH activity. For this purpose, the proteins OdhI, OdhI-R87P, and OdhI-R87A were overproduced in *Escherichia coli* and purified (Fig. S4). Their influence on ODH activity was tested with cell-free extracts of *C. glutamicum* Δ*odhI* as previously described (8). As shown in Fig. 4, wild-type OdhI strongly inhibited ODH activity, with a residual activity of only 3% in the presence of 1.9 nM OdhI, which corresponds to previous results (8). OdhI-R87A and OdhI-R87P at equivalent concentrations also led to an inhibition of ODH activity, but it was much weaker. Even at a concentration of 1.9 nM OdhI-R87A or OdhI-R87P, a residual ODH activity of more than 50% was measured. This suggests that OdhI-R87A and OdhI-R87P are still able to interact with OdhA, but the inhibitory effect is strongly reduced, which might be sufficient to enable growth of the suppressor mutants K1 and K4 on glutamine.

We analyzed the residues OdhI-R87 and OdhI-L107 using an AlphaFold2 model of the

TABLE 1 Overview of mutations identified in the *odhI* gene[a]

Mutant	Mutation in *odhI*	Position in *odhI* ORF[b]	Codon exchange	Effect on amino acid sequence
K1	GTTTCACGTCGCCAC	260	CGT → CCT	R87P
K2	GGCGCTCGATTCCTT	178	CGA → TGA	R60Stop
K3	GAGATCCAGATTGGC	385	CAG → TAG	Q129Stop
K4	GTTTCACGTCGCCAC	260	CGT → CCT	R87P
K5	CTGGACCAGCCAACC	195	CAG → TAG	Q53Stop
K6	ATGGAGTCGAGCACC	84	TCG → TCA	Silent (S28)
	CACGCAGAGTTCCGC	271	GAG → AAG	E91K
	GTCATGCAGACCGGT	369	CAG → CAA	Silent (Q123)
	GATGAGATCCAGATT	381	GAG → GAA	Silent (E127)
		387	CAG → CAA	Silent (Q129)
K7	GTTTCACGTCGCCAC	260	CGT → CCT	R87P
	CACGCAGAGTTCCGC	271	GAG → AAG	E91K
K8	GGGTCCCTCAACGGA	319	CTC → GTC	L107V
K9	CTGGTTTTCCTCGCA	410	TTC → TCC	F137S
K10	GATGTCACCGTTTCA	251	ACC → ATC	T84I
K11	GCAGGCGCTCGATTC	176	GCT → GCAT	Frameshift after A59
K12	AACGCTCAGGTCATG		CAG → C-G	Frameshift after A119
K13	No mutation in *odhI*			
K14	No mutation in *odhI*			
K15	No mutation in *odhI*			
K16	CACGCAGAGTTCCGC	271	GAG → AAG	E91K
K17	ATGGAGTCGAGCACC	84	TCG → TCC	Silent (S28)
	GCAGGCGCTCGATTC	176	GCT → GAT	A59D
	CTGGACCAGCCAACC	193	CAG → TAG	Q65Stop
K18	No mutation in *odhI*			
K19	AACGCTCAGGTCATG	359	CAG → C-G	Frameshift after A119
K20	GTCATGCAGACCGGT	367	CAG → TAG	Q123Stop

[a]20 *C. glutamicum* Δ*glnX2* suppressor mutants (K1 to K20) forming colonies on glutamine agar plates.
[b]ORF, open reading frame.

OdhI:OdhA complex (Fig. S5), limited to the OdhA E1o domain (residues 365 to 1221). As expected, the model is consistent with the published structure of the mycobacterial KGD: GarA complex (PDB code 6I2Q), with the apical FHA surface of OdhI involved in a number of interactions with OdhA (Fig. S5A). Among these, the conserved residue S86 (OdhI numbering) is predicted to be at a suitable distance to make a hydrogen bond to OdhA-D795 (Fig. S5B), an interaction observed in the KGD:GarA complex, where KGD-D795 was proposed to mimic a phosphorylated threonine, the usual interaction partner of FHA domains (19). According to the AlphaFold2 model, OdhI-R87 is predicted to make a salt bridge with OdhA-D798 from the same long, outer αE helix (Fig. S5B) shown to be, in mycobacterial KGD, one of the main structural elements interacting with GarA; the lack of movement of this helix, hindered as a consequence of GarA binding, locks the enzyme in the resting state (19). The observed substitutions of OdhI-R87 would therefore be expected to remove the predicted salt bridge, leading to a significant decrease in the OdhI binding affinity. In addition, the model predicts OdhI-L107 to be also situated at the FHA surface, where it would be involved in hydrophobic interactions with the N-terminal side of αE (Fig. S5B), mostly with the side chains of A791 and V792. Substitutions of OdhI-L107 may therefore

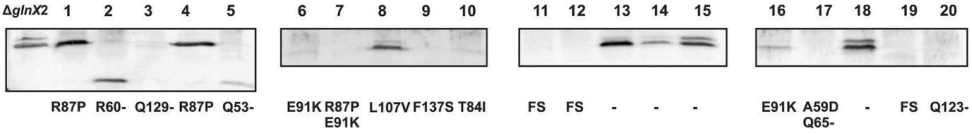

FIG 3 Western blot analysis with anti-OdhI antiserum using crude extracts from *C. glutamicum* Δ*glnX2* as the positive control and 20 different Δ*glnX2* suppressor mutants (K1 to K20) that were able to grow on glutamine agar plates again. The strains were cultivated in BHI medium with 4% (wt/vol) glucose. In each case, 10 μg of protein was separated by SDS-PAGE (15% separating gel) and used for Western blotting. On the bottom line, the OdhI mutations identified in the 20 Δ*glnX2* suppressor mutants are listed (R60-, Q53-, Q65-, Q123-, nonsense mutations; FS, frameshift mutations; –, no mutation found in *odhI*, *odhA*, and *pknG*).

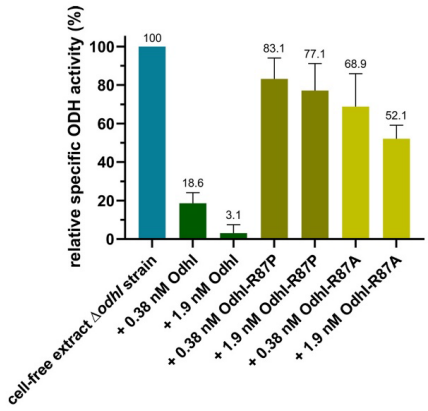

FIG 4 Influence of purified OdhI, OdhI-R87P, and OdhI-R87A on the ODH activity of cell-free extracts of *C. glutamicum* Δ*odhI*. The activity of the cell extract in the absence of added OdhI was 135 ± 12 nmol min^{-1} (mg protein) $^{-1}$, which was set as 100%. Mean values and standard deviations of three replicates are shown.

also have a detrimental effect on the OdhI binding affinity and could therefore contribute to relieve the consequences of the accumulation of unphosphorylated OdhI in the suppressor mutants.

Characterization of GlnH as a lipoprotein. The GlnH protein is predicted to be a lipoprotein based on the presence of the lipobox LLASCT at the end of the signal peptide (MHAFRRPPPLTTRVGAALLAATLLASCTPT) (23). The predicted cleavage site is between amino acid residues S26 and C27. The thiol group of C27 is presumably modified by the prolipoprotein diacylglyceryl transferase Lgt (Cg2292) to form a diacylglyceryl prolipoprotein with a thioether linkage. The signal peptide is then cleaved by the prolipoprotein signal peptidase LspA (Cg2347), thereby liberating the α-amino group of C27. Previous studies with the lipoprotein AmyE (Cg2705) have shown that the α-amino group of the N-terminal cysteine is acylated by apolipoprotein-*N*-acyltransferase Ppm2 (Cg1673) to form triacylated AmyE (24), and a similar process can be envisaged for GlnH.

To confirm that GlnH is a lipoprotein, the cyclic peptide antibiotic globomycin was used, which specifically inhibits the activity of the lipoprotein signal peptidase LspA and thus the cleavage of the signal peptide (25–27). *C. glutamicum* Δ*glnH*/pAN6-*glnH*, which encodes a C-terminally Strep-tagged GlnH, was cultivated in CGXII-glucose medium supplemented with 1 mM IPTG (isopropyl-β-D-thiogalactopyranoside) and 50 μg/mL globomycin to prevent lipoprotein maturation. Crude extracts of samples taken before and hourly after globomycin addition were analyzed by Western blot analysis with StrepTactin-alkaline phosphatase conjugate. As shown in Fig. 5, in the control without globomycin (Fig. 5A), only the mature GlnH protein with an apparent mass of about 45 kDa (predicted mass of about 36 kDa) was visible, whereas in the samples treated with globomycin (Fig. 5B), a GlnH variant with a larger apparent mass became increasingly visible. This enlarged variant presumably represents the diacylglyceryl prolipoprotein form of GlnH still containing the signal peptide. Further support for this interpretation was obtained by Western blot analysis of the strain *C. glutamicum* Δ*glnH*/pAN6-*glnH*-C27A, in which C27 was changed to alanine, thereby preventing thiol modification of C27 and cleavage of the signal peptide. In this case, only the GlnH prolipoprotein was detected (Fig. 5C).

Characterization of the ligand-binding properties of GlnH. Based on the similarity to the glutamine-binding protein GlnH of *E. coli*, which is part of the ABC transporter GlnHPQ (28, 29), the protein encoded by cg3045 in the *C. glutamicum* genome was initially annotated as a putative glutamine binding protein (20). While the

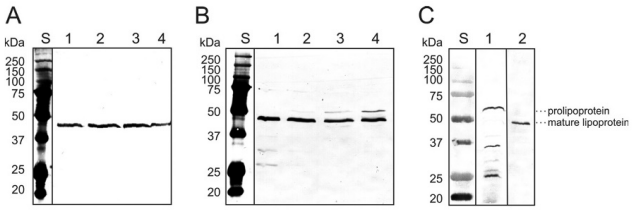

FIG 5 Characterization of GlnH as a lipoprotein. (A to C) Western blot analysis of crude extracts of *C. glutamicum* Δ*glnH*/pAN6-*glnH* (A and B, lanes 1 to 4; C, lane 2) and *C. glutamicum* Δ*glnH*/pAN6-*glnH*-C27A (C, lane 1). The plasmid-encoded GlnH contains a C-terminal StrepTag-II, which was detected by Streptactin-alkaline phosphatase conjugate. Panel A shows the control samples without globomycin, and panel B shows the samples where globomycin was added during exponential growth. Samples were taken immediately before (A and B, lane 1) and 1 h, 2 h, and 3 h after globomycin addition (A and B lanes 2, 3, and 4). In panel C, a comparison of the GlnH-C27A variant (lane 1) and wild-type GlnH (lane 2) is shown. Mutated GlnH-C27A cannot be modified by prolipoprotein diacylglycerol transferase or cleaved by the lipoprotein signal peptidase. In panels A and B, 10 μg protein was applied per lane. In panel C, 50 μg protein of crude extract was applied in lane 1 and 5 μg membrane protein was applied in lane 2. Lane S shows the molecular mass standards. The lanes in panels A, B, and C were derived from a single blot in each case and arranged for better visibility of the relevant features.

phenotype of the Δ*glnH* mutant provided clear evidence for a role of GlnH in the glutamine metabolism of *C. glutamicum*, the glutamine uptake activity of a Δ*glnH* mutant (and a Δ*glnX* mutant) was not strongly affected, suggesting that GlnH might not be involved in glutamine uptake (6). To characterize the ligand binding properties of GlnH, a soluble protein version lacking the N-terminal signal peptide and the lipobox motif was overproduced in *E. coli* BL21(DE3) using the expression plasmid pET-TEV-*glnH*ΔSP and purified by Ni^{2+}-chelate affinity chromatography. The His-tagged protein was used for interaction studies with different potential ligands using isothermal titration calorimetry (ITC). Based on the annotation, L-glutamine was first tested as a ligand, but no binding to His_{10}-GlnHΔSP was observed under the conditions used (40 mM HEPES, pH 7, 100 mM KCl, 10 mM $MgCl_2$). In contrast, L-aspartate and L-glutamate served as ligands for His_{10}-GlnHΔSP, although with moderate affinity. From five independent experiments each, a mean equilibrium dissociation constant (K_D) value of 264 ± 14.6 μM was obtained for L-aspartate, whereas for L-glutamate the affinity was about five times lower with a mean K_D of 1,256 ± 220 μM. In both cases, binding was exothermic with mean observed enthalpy changes of −18.5 ± 4.3 kJ/mol for L-aspartate and −17.5 ± 5.0 kJ/mol for L-glutamate. Besides L-glutamine, L-aspartate, and L-glutamate, L-asparagine and 2-oxoglutarate were also tested as potential ligands, but no interaction with His_{10}-GlnHΔSP was observed. In Fig. 6, representative ITC experiments are shown for the five ligands tested.

Analysis of structural differences between the GlnH proteins of *M. tuberculosis* and *C. glutamicum*. A previous study, focused on the orthologous GlnH protein from *M. tuberculosis*, reported 50- to 135-fold lower K_D values for L-aspartate (4.8 ± 0.6 μM) and L-glutamate (15.2 ± 5.7 μM) compared to *C. glutamicum* GlnH and provided structural evidence of ligand binding to GlnH through the crystal structures of the *M. tuberculosis* protein in complex with either L-aspartate, L-glutamate, or L-asparagine (21). To get insights into GlnH ligand binding specificity and the structural features underlying the different affinities of the two orthologues, we generated a structural model for *C. glutamicum* GlnHΔSP using AlphaFold2 (30). The models superimpose on the experimental structure of *M. tuberculosis* GlnH in complex with L-aspartate (PDB code 6H1U) with a root-mean-square distance (RMSD) of around 0.8 Å (Fig. 7A), indicating that, despite the nonnegligible differences in their amino acid sequences (43% sequence identity), the ligand binding domains of the two orthologues are not expected to show significant differences in their overall fold. The comparison of the ligand binding pockets between the two proteins shows, however, a few subtle differences. Specifically,

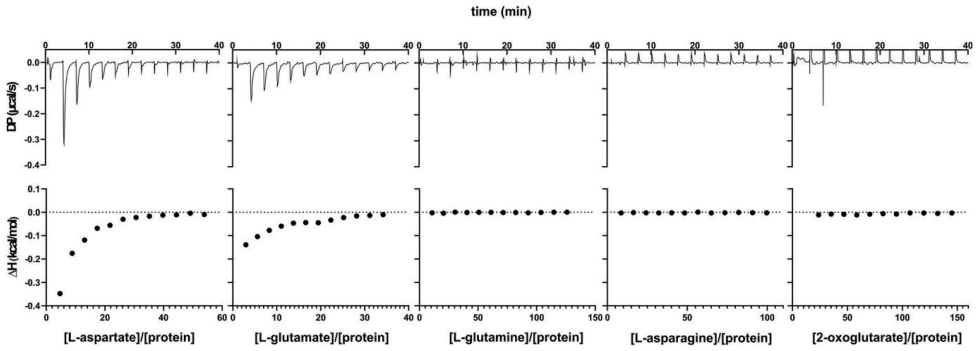

FIG 6 Representative ITC experiments with His_{10}-GlnHΔSP and the indicated ligands. The experiments were performed in 40 mM HEPES buffer, pH 7, with 100 mM KCl and 10 mM $MgCl_2$.

residues in the loop 160 to 166 (*C. glutamicum* GlnH numbering, including signal peptide), which is crucial for ligand binding, are not fully conserved. Most notably, two nearby residues (Thr162 and Ser164 in *M. tuberculosis*), whose hydroxyl groups act as hydrogen bond (H-bond) donors toward the ligand carboxyl groups, have their relative positions swapped in *C. glutamicum*, where they are replaced by Ser163 and Thr165, respectively (Fig. 7B). Also, the Ser163 hydroxyl group potentially falls within H-bond distance from the amide group of Gln103 (Ser102 in *M. tuberculosis*), which, in turn, may contribute to making it unavailable as an H-bond donor to the incoming amino acid ligand (Fig. 7B).

To test the relevance of the amino acid residues S163 and T165 for ligand binding affinity, a GlnH variant (His_{10}-GlnHcore-S163T-T165S) with the amino acid exchanges S163T-T165S was isolated, and its ligand binding properties were compared with the parental protein by measuring the intrinsic tryptophan fluorescence at various ligand concentrations (Fig. 7C and D). For the parental His_{10}-GlnHcore protein, K_D values of 242 μM for L-aspartate and 1,458 μM for L-glutamate were determined, which are comparable to the K_D values determined by ITC. For the His_{10}-GlnHcore-S163T-T165S protein, K_D values of 65 μM for L-aspartate and 243 μM for L-glutamate were measured. The 4- to 6-fold-increased binding affinity caused by a swap of S163 and T165 is remarkable and confirms the relevance of these residues for the ligand binding properties of GlnH.

Analysis of the GlnX topology using PhoA and LacZ fusions. Bioinformatic analysis of the GlnX sequence resulted in the topology shown in Fig. 8A. We based our analyses on a GlnX protein composed of 501 amino acid residues with the N-terminal sequence MIRDGNGEH, assuming a leaderless mRNA formed from the reported transcriptional start site of *glnX* (31), which was confirmed by us via 5′-rapid amplification of cDNA ends (RACE) experiments (data not shown). The GlnX protein is predicted to contain four transmembrane helices (TMHs) and two periplasmic domains comprising approximately 156 and 153 amino acid residues. Three portions of the protein are predicted to face the cytoplasm, which are the N-terminal region comprising about 110 amino acid residues, a small portion of about 11 residues linking TMH-2 and TMH-3, and the C-terminal region of about eight amino acid residues. A search for sequence signatures using the Pfam database matched the second periplasmic region of GlnX to the CHASE3 family, which represents extracellular sensory domains found in various classes of bacterial transmembrane proteins, including histidine kinases and chemoreceptors (32).

To experimentally confirm the predicted topology, seven fusion proteins combining different portions of GlnX with either alkaline phosphatase (PhoA) or β-galactosidase

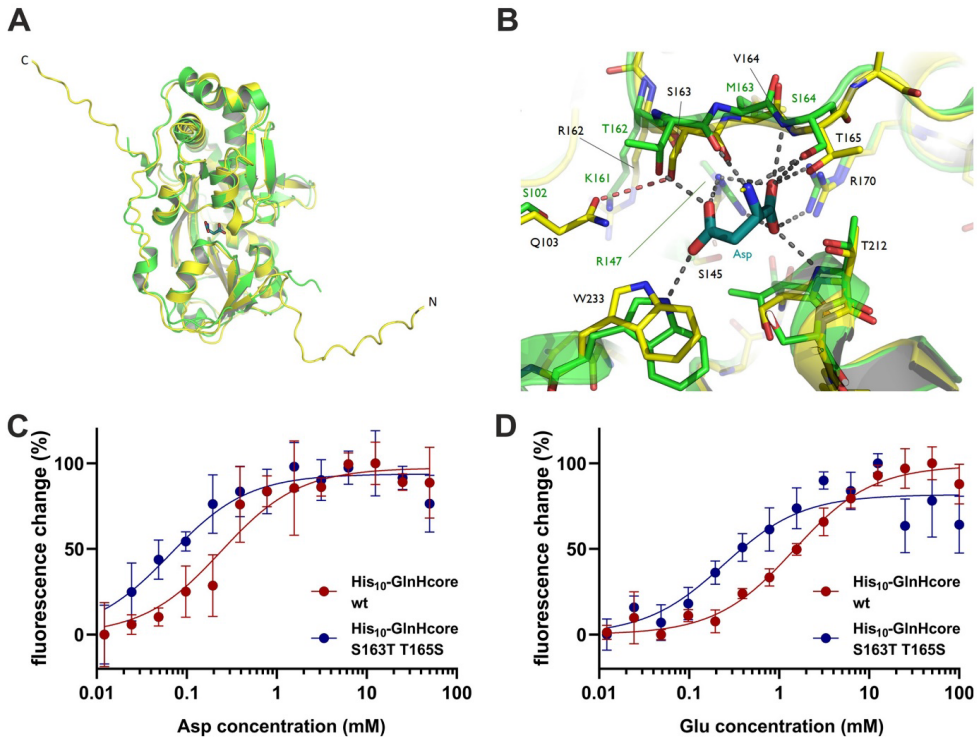

FIG 7 (A) Superimposition of the AlphaFold2 model for GlnHΔSP (yellow) on the crystal structure of *M. tuberculosis* GlnH in complex with aspartate (green; PDB code 6H1U). Both the N- and C-terminal ends of GlnHΔSP are predicted to be unstructured (residues 27 to 50 and 334 to 344, respectively; the N- and C-terminal ends are indicated). (B) Zoomed view of the ligand binding site showing residues involved in ligand binding in the *M. tuberculosis* GlnH-aspartate complex (gray dashed lines represent H-bond interatomic distances) and the equivalent positions in the *C. glutamicum* GlnHΔSP model (yellow; dashed lines in salmon color indicate potential H-bonds specific for *C. glutamicum* GlnH). (C and D) Influence of S163T-T165S swap in *C. glutamicum* GlnH on the ligand binding affinity for L-aspartate and L-glutamate. Ligand binding was analyzed measuring the intrinsic tryptophan fluorescence (excitation 292 nm; emission 340 nm) at different sodium aspartate and sodium glutamate concentrations. Dissociation constants were calculated using a one-site specific binding fit. Shown are mean values of 5 to 6 replicates. Error bars represent the standard deviation.

(LacZ) of *E. coli* were constructed (Fig. 8B). While PhoA is active only if located in the periplasm, LacZ shows activity only when located in the cytoplasm (33, 34). Three fusion sites were positioned in predicted cytoplasmic regions (residues 75, 293, and 501), whereas four fusion sites were located in the two predicted periplasmic regions (residues 132, 247, 335, and 457). The plasmids for expression of the 14 fusion genes were constructed in the vector pPREx2 (35), and *E. coli* TG1 served as the host for the PhoA and LacZ activity measurements. As shown in Fig. 8C, the results confirmed the predicted topology. The fusions at position 75, 293, and 501 showed LacZ, but no PhoA activity, whereas the fusions at positions 132, 247, 335, and 457 possessed PhoA, but no LacZ activity.

Structural model of the GlnX protein. AlphaFold2 was used to predict the structure of the GlnX protein. The *ab initio* prediction was executed using parameters described in Materials and Methods. The run produced five models ranked according to the model confidence level, i.e., the predicted local distance difference test (pLDDT) (Fig. S6). The individual models displayed a similar overall architecture, with high to moderate model confidence in most regions; for description, we will use the top-

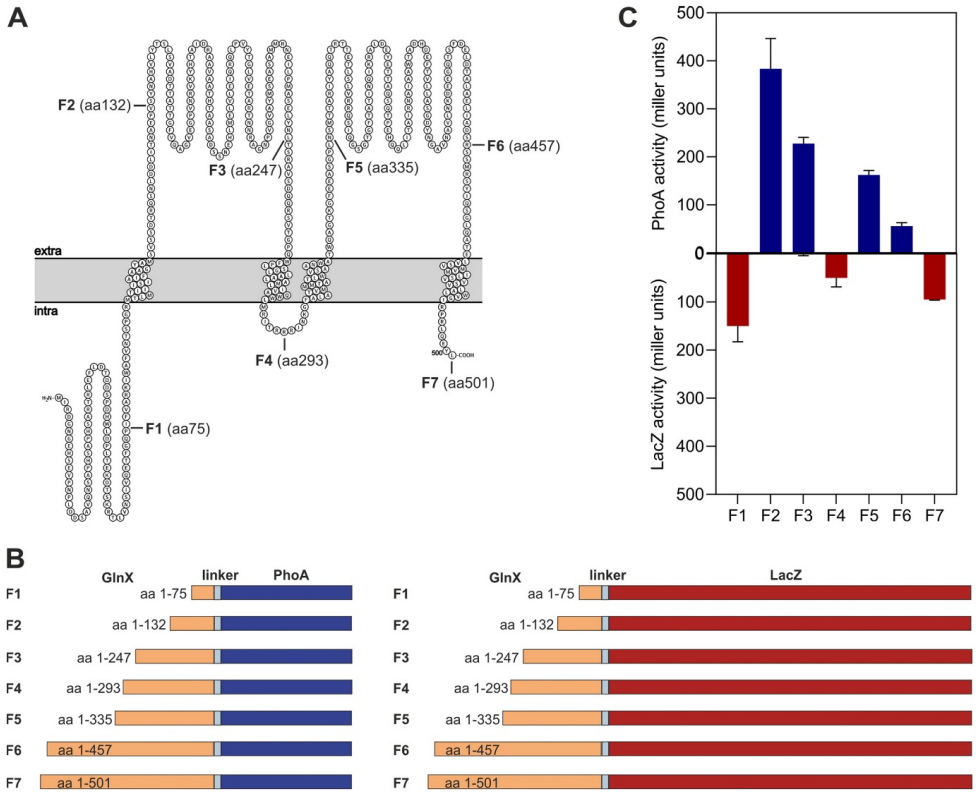

FIG 8 Analysis of the GlnX topology. (A) Predicted topology of GlnX using PROTTER software (37). The seven positions selected for creating PhoA and LacZ fusions are indicated. (B) Scheme of GlnX-PhoA and GlnX-LacZ fusion proteins. (C) PhoA and LacZ activities determined with *E. coli* TG1 cells carrying pPREx2-*glnX-phoA*-F1 to -F7 and pPREx2-*glnX-lacZ*-F1 to -F7 expression plasmids. Cells were cultivated at 30°C in LB medium, and gene expression was induced for 1 h by addition of 1 mM IPTG in the exponential growth phase. Subsequently, cells were permeabilized, and PhoA and LacZ activities were determined using the artificial substrates *p*-nitrophenylphosphate and *o*-nitrophenyl-galactopyranoside, respectively, by measuring the absorbance at 420 nm. Shown are mean values and standard deviation of biological triplicates.

scoring model from the first run (Fig. 9). As anticipated from conventional secondary structure predictions, the AlphaFold2 model of GlnX features a very high α-helical content, and its membrane topology is in accordance with our own prediction and experimental evidence. Specifically, 79% of all residues are involved in either α-helices, 3_{10}-helices, or π-helices as determined by the software DSSP (dictionary of secondary structure of proteins) (36); if the presumably disordered N-terminal 61-residue stretch is excluded, this fraction reaches 90%. The two extracellular segments are suggested to fold into four-helix bundles (with helices H1 to H4 and H1′ to H4′, respectively), which align in parallel to one another and to the membrane normal, intimately interacting with one another. The first and last helices of each bundle are connected to the transmembrane segments of GlnX via linker regions spanning a distance of approximately 15 Å. Intriguingly, for the N-terminal helix of the first bundle and the C-terminal helix of the second, these linkers are all-helical as well, resulting in continuous straight helices spanning almost the entire dimension of the molecule perpendicular to the membrane plane, whereas in the remaining two cases linker helices are kinked and/or

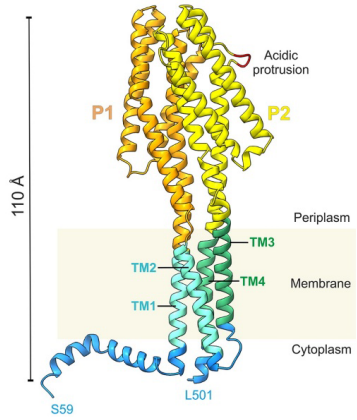

FIG 9 Structural model of GlnX in ribbon representation. The model is colored according to the topology prediction by DeepTMHMM (66) for the periplasmic, cytoplasmic, and transmembrane (TM) segments (orange, P1; yellow, P2; cyan, TM1 and TM2; green, TM3 and TM4; blue, cytoplasmic parts). Residues ^{435}DEE^{437} in the acidic H4′ protrusion (highlighted in red) are hypothesized to be involved in interactions with GlnX ligands (see the text for more details). The helix preceding TM1 displays significant amphipathic character and could be preferentially anchored to the membrane. The N-terminal residues 1 to 58 are not shown in this model, as they were predicted to be disordered.

noncontiguous. Overall, model confidence of the top-ranked GlnX model was higher for the periplasmic portions than for the other parts of the molecule (Fig. S6A). The pLDDT values are consistently below 50 for N-terminal residues 1 to 72 and tend to increase afterwards, exceeding 75 at residue 90. Consistently, DSSP analysis indicates residues 1 to 61 to be disordered, whereas residues 62 to 86 form a helical segment. Note that the N-terminal residues featuring low pLDDT values also have a poorly defined spatial relationship to the remainder of the molecule, as signified by their high predicted aligned error (PAE) values (Fig. S6B). Consequently, excluding residues 1 to 90 from the prediction results in further improvement of PAE for the well-defined parts of the model (not shown).

DISCUSSION

In this study, we analyzed the function and properties of the proteins GlnH and GlnX of *C. glutamicum*, which are encoded together with the gene for the serine/threonine protein kinase PknG in the putative *glnX-glnH-pknG* operon. Deletions of each of these genes individually or of all three genes together led to a strong growth defect when L-glutamine was used as the sole carbon and nitrogen source, and the amount of unphosphorylated OdhI was strongly increased in these strains (Fig. 1). The growth defect can be explained by the inhibition of ODH activity due to binding of unphosphorylated OdhI to the OdhA subunit (6, 8, 9). As a consequence, 2-oxoglutarate generated from glutamine cannot be efficiently oxidized to succinyl-CoA, and carbon flux through the TCA cycle is reduced. Support for this explanation is provided by the finding that the mutants Δ*pknG*, Δ*glnH*, and Δ*glnX* secrete about twice as much L-glutamate as the WT when cultured in the presence of ethambutol, which is known to elicit glutamate overproduction (22). Furthermore, we showed here that the growth defect of the Δ*glnX* mutant can be abolished by the additional deletion of *odhI*. The observation that deletion of the gene cluster *glnX-glnH-pknG* reduced OdhI phosphorylation to a similar extent as the individual deletions of these genes suggests that the three proteins do not have independent, additive effects on the phosphorylation of OdhI but are components of a signal transduction cascade in which GlnH and GlnX regulate the kinase activity of PknG.

Analysis of *C. glutamicum* Δ*glnX2* suppressor mutants that regained the ability to grow on glutamine agar plates further underlined the role of GlnX in the regulation of OdhI activity. Of 20 analyzed suppressor mutants, 16 were found to carry mutations in the *odhI* gene (Table 1), and in most of them OdhI was no longer detectable by Western blotting. Insertion of stop codons or frameshift mutations led to defective OdhI variants that are likely degraded. Also, amino acid exchanges can cause protein misfolding and degradation, which can explain the reduction or absence of detectable OdhI in the variants E91K, T84I, and F137S (Fig. 3). In these cases, the improved growth of the suppressor mutants on glutamine can be explained by the loss of ODH inhibition. For the suppressor mutant carrying OdhI-R87P, OdhI was still detectable, and our studies with purified OdhI-R87P and OdhI-R87A demonstrated that both variants inhibited ODH activity much less than wild-type OdhI, explaining the restored growth on glutamine (Fig. 4). The structural model of the OdhI-OdhA complex suggested that the R87P and R87A exchanges cause the loss of a predicted salt bridge of R87 with OdhA-D798, probably leading to a lowered binding affinity and thus reduced inhibition of ODH activity. In the case of the suppressor variant OdhI-L107V, reduced hydrophobic interactions with the αE-helix of OdhA might cause a lowered binding affinity and ODH inhibition. These suppressor mutations confirmed the importance of individual residues at the OdhI-OdhA interaction surface for the inhibition of ODH activity.

Use of the cyclic peptide antibiotic globomycin, which specifically inhibits the lipoprotein signal peptidase, and use of a GlnH-C27A mutant protein, in which the attachment of the lipid anchor to C27 is prevented, provided experimental evidence that GlnH is an extracytoplasmic protein attached to the membrane by a typical lipoprotein anchor (Fig. 5). In contrast, the original annotation of GlnH as a glutamine binding protein (20) could not be confirmed, as no binding of L-glutamine to a purified soluble GlnH variant was observed in ITC experiments. Rather, L-aspartate and L-glutamate were shown to bind to GlnH with affinities in the high μM to low mM range (Fig. 6). The results from the ITC experiments are in accordance with findings by Bhattacharyya and coworkers, who reported that L-aspartate and L-glutamate increased the thermal stability of GlnH of *C. glutamicum* and caused an increase in intrinsic tryptophan fluorescence (21). The K_D values measured by the change in intrinsic tryptophan fluorescence, as reported by these authors (550 ± 90 μM for L-aspartate, 2,060 ± 390 μM for L-glutamate) were somewhat higher than the K_D values measured in our ITC experiments (264 ± 14.6 μM for L-aspartate, 1,256 ± 220 μM for L-glutamate) but showed a similar ratio for L-aspartate and L-glutamate (21). The roughly 2-fold difference in the K_D values are likely caused by differences in the experimental conditions applied.

For *M. tuberculosis* GlnH, the affinities for L-aspartate and L-glutamate were 50- to 135-fold higher, with K_D values of 4.8 ± 0.6 μM for aspartate and 15.2 ± 5.7 μM for glutamate (21). The strong differences in the ligand binding affinities of the GlnH proteins of these two organisms are surprising and might be explained by the evolutionary adaptation to the different environmental niches of these bacteria. *C. glutamicum* is an apathogenic species originally isolated from soil, whereas *M. tuberculosis* is a pathogen able to survive for long time periods inside human phagocytes. Under these conditions, control of the carbon flux at the 2-oxoglutarate node by GarA, the homolog of OdhI in mycobacteria, might require a response to much lower concentrations of L-aspartate and L-glutamate compared to a soil bacterium. From a structural point of view, these differences might be explained by differences in the architecture of the GlnH ligand binding site. A prominent difference is the exchange of Ser and Thr residues crucial for ligand binding. A mutated variant of the *C. glutamicum* GlnH protein possessing the same arrangement of these residues as that found in the *M. tuberculosis* protein showed a clear increase in the affinities for L-aspartate and L-glutamate (Fig. 7), demonstrating the importance of the position of these two residues for the ligand binding affinity.

Since the membrane protein GlnX is supposed to act as a transmitter between the extracytoplasmic lipoprotein GlnH and the cytoplasmic kinase PknG, knowledge of the

GlnX topology is important to understand its interaction with other proteins. Topology prediction using bioinformatics tools such as Protter (37) and fusion of GlnX variants with commonly used reporters for periplasmic and cytoplasmic localization in bacteria, PhoA and LacZ, provided an experimentally based topology model of GlnX (Fig. 8). According to this model, the large extracytoplasmic segments of GlnX are assumed to be responsible for the proposed interaction with GlnH. Moreover, similarity of the second extracytoplasmic domain with the family of CHASE3 sensor domains found in various classes of transmembrane receptors (32) opens up the possibility that the periplasmic part of GlnX might itself harbor binding sites for small-molecule ligands (38, 39), broadening the sensory capabilities of GlnX beyond the metabolites recognized by GlnH.

The structural model of GlnX created by AlphaFold2 (Fig. 9) not only confirms the conclusions described above but also offers significant new insight into the architecture and functionality of this protein. Schematically, GlnX can be viewed as being composed of three tetra-helical bundles, two constituting the periplasmic portion and the third being inserted into the membrane. The antiparallel arrangement allows for extended helices to be stable despite their significant dipole moment. Indeed, the longest contiguous helix (67 amino acid [aa] residues), comprising the first transmembrane segment, the ensuing linker, and helix H1 of the first bundle, extends over approximately 100 Å. A sequence-based search for related structures in the Protein Data Bank (PDB) using profile hidden Markov models (HMMER [40]) did not yield obvious hits. In contrast, structural comparison via Dali (41) revealed that the periplasmic portion actually represents a well-established fold. Its two four-helix bundles closely resemble the 4HB sensory module originally described for the aspartate receptor Tar of *Salmonella enterica* serotype Typhimurium (42) and later found in a variety of other chemoreceptors and sensory histidine kinases. Indeed, for both periplasmic domains of GlnX, the ligand binding domain of the citrate-sensing chemoreceptor MCP2201 from *Comamonas testosteroni* (PDB code 6ITS) and the periplasmic domain of the transmembrane histidine kinase LytS from *Clostridium beijerinckii* (PDB code 5XSJ) are among the most significant structural matches. In the Pfam database, the 4HB fold is represented by the 4HB_MCP superfamily, comprising four distinct families (4HB_MCP_1, CHASE3, TarH, and HBM). While the second periplasmic domain of GlnX matches CHASE3, albeit with borderline significance (E value, 9.5×10^{-5}), no match was found for the first periplasmic domain, indicating that its sequence has further diverged from the presumed common 4HB ancestor while the characteristic three-dimensional fold was preserved. Indeed, despite insignificant sequence similarity, the two bundles superimpose very well; secondary structure matching (SSM [43]) using segments 128–255 and 330–460 yields an RMSD of 1.9 Å for 117 aligned Cα atoms. Note that the second periplasmic domain is distinguished by an eight-residue insertion into helix H4′, forming a finger-like protrusion with three acidic residues (^{435}DEE^{437}) at its tip (Fig. 9). This portion of GlnX seems poised for interaction with other proteins, an obvious candidate being GlnH (see below).

Periplasmic 4HB domains flanked by transmembrane segments usually occur as a single copy per chain in prokaryotic chemoreceptors and histidine kinases but display a strong tendency to dimerize. These dimers are already found in the apo state but are often stabilized by ligand binding at the interface of the two domains. The helical bimodular (HBM) family represents an exception in that it features two helical domains per chain, with the second being inserted into the first, such that only one retains its connection to membrane-spanning helices. Consequently, receptor dimerization leads to two 4HB dimers in a stacked arrangement. While GlnX is also predicted to contain two periplasmic helical domains, its architecture fundamentally differs from the HBM type. GlnX appears to have evolved by duplication of a canonical 4HB domain, including its flanking membrane anchors; the resulting arrangement closely resembles the noncovalent dimer formed by Tar and similar chemoreceptors, as far as the periplasmic and transmembrane portions are concerned (Fig. S7). Indeed, the two periplasmic helical domains in our GlnX model are related by a rotation of 171°, which is well within the range found for 4HB homodimers in crystal structures if protomers are related by

noncrystallographic symmetry. The interaction involves more than 1,000 Å^2 of surface area on either domain and is stabilized by numerous polar and apolar contacts. To our knowledge, this tandem arrangement of membrane-anchored 4HB domains on a single chain has not been reported for any other protein. In order to distinguish it from the four known 4HB families in Pfam, with which GlnX shares at most borderline sequence similarity (see above), we suggest naming this unique architecture a helical tandem module (HTM).

The actual mechanism by which GlnX receives its input signals and transduces them across the membrane is still under investigation. Importantly, the involvement of an additional protein in the sensing process is not unprecedented in the 4HB family; Tar, e.g., is known to interact with maltose binding protein (MBP), thereby acquiring sensitivity to maltose in addition to aspartic acid, which interacts directly with the 4HB domains. Indeed, both GlnH and MBP belong to the periplasmic binding protein (PBP) superfamily (Pfam families SBP_bac_3 and SBP_bac_1, respectively) and share the same tertiary structure. A potential mode of interaction is indicated by the X-ray structure of the LytS periplasmic domain complexed with its cognate D-xylose sensor XylFII (44). Here, the ligand binding XylFII protein associates with helices H3 and H4 of the LytS 4HB module, with the long axes of both molecules arranged approximately at a right angle. While XylFII and GlnH are at most distantly related, we note that superposition of the LytS-XylFII complex onto our GlnX model positions the periplasmic binding protein in the immediate vicinity of the acidic H4′ finger of GlnX (Fig. S8).

The mode of signal propagation through the membrane used by 4HB sensors is complex and still subject to active research; current evidence points to ligand binding causing (among other changes) a piston-like displacement of helix H4 in the periplasmic sensor module, which may either propagate as such into the transmembrane helix bundle or transform into different modes, such as helical rotation or scissoring (45). Given the architectural similarities of GlnX with the periplasmic and transmembrane portions of a classical dimeric chemoreceptor, it seems reasonable to assume that similar principles apply. On the other hand, the cytoplasmic part of GlnX does not contain any of the domains typically found in bacterial sensors (such as histidine kinase and receiver domains, HAMP domains [present in histidine kinases, adenylyl cyclases, methyl accepting proteins and phosphatases], and kinase control modules), and its mode of interaction with its effector PknG is still elusive.

Taken together, all these findings support a signal transduction model in which the phosphorylation status of OdhI is controlled by a signal transduction cascade consisting of GlnH, GlnX, and PknG (Fig. 10). In this model, the presence of L-glutamate and L-aspartate in the periplasm is sensed by GlnH. GlnH is assumed to interact with the periplasmic domains of GlnX, with the acidic protrusion in helix H4′ being an attractive interaction site. In its ligand-bound state, GlnH is proposed to trigger a conformational change of GlnX, enabling the transfer of the information on the ligandation status of GlnH across the cytoplasmic membrane. The cytoplasmic parts of GlnX are proposed to interact with the tetratricopeptide repeat domain of PknG (13, 21), triggering a conformational change of PknG that activates the kinase activity and causes the dissociation of PknG from GlnX. The phosphorylation of threonine residues in the N-terminal region, which stabilize the interaction with the FHA substrate (13), may play a role in this process. Such a model could explain the observation that PknG was detected both in the membrane fraction and in the cytosolic fraction of *M. tuberculosis* (15) and *C. glutamicum* (our unpublished data). Active PknG then phosphorylates OdhI on T14, thereby abolishing the inhibition of ODH activity by unphosphorylated OdhI. As a consequence, the carbon flux from 2-oxoglutarate is shifted from glutamate synthesis toward the TCA cycle. L-glutamate is the major amino group donor for amino acids in cells and the metabolite with the by far highest concentration (~100 mM) in the cytoplasm of *C. glutamicum* (46). It can be taken up by the ABC transporter GluABCD (47) or the Na^+-coupled secondary transporter GltS (48), thereby reducing the requirement for glutamate synthesis and providing more energy by 2-oxoglutarate catabolism in the TCA cycle. Control of carbon flux at the 2-oxoglutarate node by

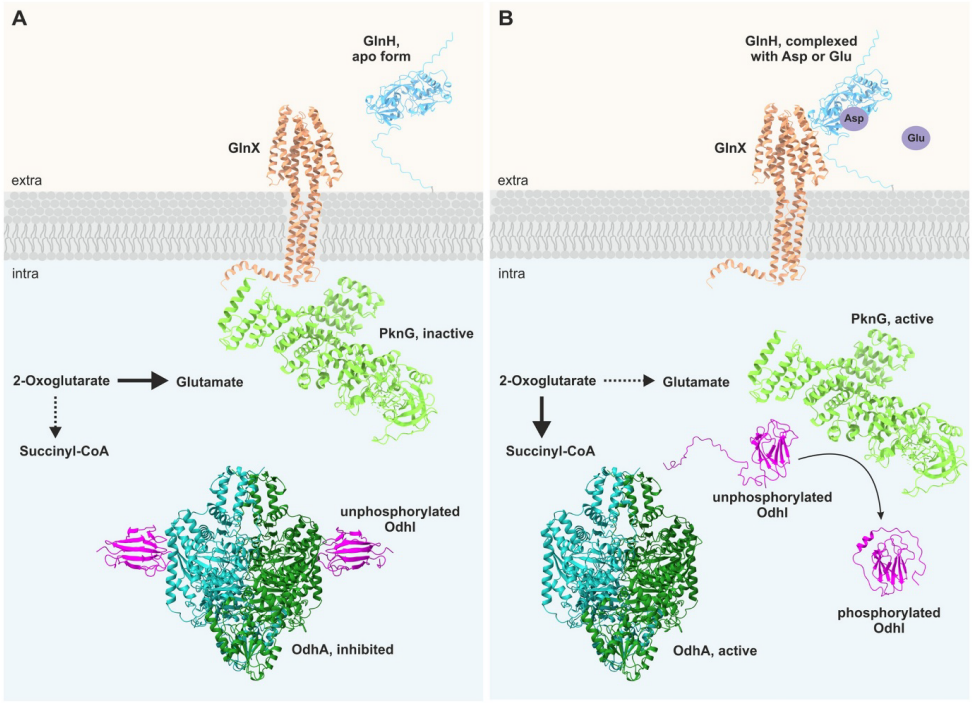

FIG 10 Hypothetical model of the GlnH-GlnX-PknG-OdhI-OdhA signal transduction cascade. Note that the assumed interactions of GlnH with GlnX and of GlnX with PknG have not been demonstrated yet. (A) In the absence of L-aspartate or L-glutamate in the periplasm, PknG forms a complex with the cytoplasmic parts of GlnX and is inactive. OdhI is predominantly unphosphorylated, binds to the OdhA subunit of ODH, and inhibits its activity, shifting the flux of 2-oxoglutarate toward L-glutamate and ammonium assimilation. (B) In the presence of L-aspartate or L-glutamate in the periplasm, GlnH binds these amino acids and interacts with the periplasmic tandem four-helix bundle domain of GlnX. In addition, this domain of GlnX might itself also serve as a receptor to bind yet unknown ligands. These binding events are signaled across the membrane via contiguous α-helices (H1-TMH1 and/or H4′-TMH4) and trigger a conformational change of PknG that causes activation of the kinase activity and dissociation from GlnX. Active PknG phosphorylates OdhI at Thr14, triggering a conformational change of OdhI that abolishes its interaction with OdhA. Consequently, the inhibition of ODH activity is relieved and the flux of 2-oxoglutarate is shifted toward the TCA cycle and energy generation. The structures for GlnH, GlnX, and the OdhI-OdhA complex represent AlphaFold2 models generated in this work. The structure of PknG (PDB code 7MXB [13]) and the structures of unphosphorylated and phosphorylated OdhI (PDB codes 2KB4 and 2KB3, respectively [11]) were determined experimentally.

external glutamate thus appears reasonable. For L-aspartate, no specific uptake system has been described yet in *C. glutamicum*, and its role as nitrogen donor is restricted compared with L-glutamate. Therefore, the reason why L-aspartate may control the OdhI phosphorylation status is not as obvious as for L-glutamate. In summary, the GlnH-GlnX-PknG-OdhI-OdhA signal transduction cascade can be considered a component of the regulatory network controlling the balance between nitrogen assimilation and carbon metabolism in *Corynebacterium* and probably many other members of the *Actinobacteria*, such as *Mycobacterium* species.

MATERIALS AND METHODS

Bacterial strains, media, and culture conditions. All bacterial strains and plasmids used in this work are listed in Table 2. *Escherichia coli* cells were cultivated at 37°C in lysogeny broth (LB) (49) or terrific broth (TB) (12 g L^{-1} tryptone, 24 g L^{-1} yeast extract, 4 mL glycerol, 12.54 g L^{-1} K_2HPO_4, 2.31 g L^{-1} KH_2PO_4; pH 7.0) or on LB agar plates (Carl Roth, Karlsruhe, Germany). *C. glutamicum* strains were cultivated at 30°C in brain heart infusion medium (BHI; Difco Laboratories, Detroit, USA), in CGXII medium with 4% (wt/vol) glucose (50) containing 30 mg L^{-1} 3,4-dihydroxybenzoate as the iron chelator, or in

TABLE 2 Bacterial strains and plasmids used in this study

Strain or plasmid	Description	Reference or source
C. glutamicum strains		
WT	ATCC13032; biotin-auxotrophic WT strain	DSMZ
Δ*pknG*	WT derivative with an in-frame deletion of *pknG* (cg3046)	6
Δ*glnH*	WT derivative with an in-frame deletion of *glnH* (cg3045)	6
Δ*glnX2*	WT derivative with an in-frame deletion of *glnX* (cg3044); 59 codons at the 5′ end and 142 codons at the 3′ end were kept; the 301 codons in between were deleted and replaced by an artificial 21-bp sequence	This work
Δ*glnX-glnH-pknG*	WT derivative with in-frame deletion of *glnX-glnH-pknG* (cg3044-cg3046)	This work
Δ*odhI*	WT derivative with in-frame deletion of *odhI* (cg1630)	6
Δ*glnX2* Δ*odhI*	WT derivative with in-frame deletions of *odhI* (cg1630) and *glnX* (cg3044)	This work
E. coli strains		
DH5α	F- *supE44* Δ*lacU*169 (Φ80*lacZ*Δ*M15*) *hsdR17 recA1 endA1 gyrA96 thi-1 relA1*	53
BL21(DE3)	F- *ompT hsdSB(rB-mB-) gal dcm* (λcIts857) *ind1* Sam7 *nin5 lacUV5*-T7 Gen 1	67
TG1	F- *supE thi*-1 Δ(*lac-proAB*) Δ(*mcrB-hsdSM*)5(rK-mK-)(*traD36 proAB* + *lacI*q *lacZ*Δ*M15*)	Lucigen Corporation
Plasmids		
pK19mobsacB	Kan^R; suicide vector for allelic exchange in *C. glutamicum*; *ori*V_{Ec} *oriT sacB*	68
pK19mobsacB-*glnX*2	Kan^R; pK19mobsacB derivative containing PCR products (primer ΔglnX_1–4) covering the up- and downstream regions of the *glnX* gene	This work
pK19mobsacB-*glnX-glnH-pknG*	Kan^R; pK19mobsacB derivative containing PCR products (primer ΔglnX 1+2 and ΔpknG 3+4) covering the up- and downstream regions of the *glnX and pknG* genes, respectively	This work
pK19mobsacB-*odhI*	Kan^R; pK19mobsacB derivative containing PCR products covering the up- and downstream regions of the *odhI* gene	6
pET-TEV	Kan^R; pET28b derivative for protein overproduction in *E. coli*, contains a His_{10}-tag and a TEV cleavage site	69
pET-TEV-*odhI*	Kan^R; pET-TEV derivative for overproduction of OdhI with an N-terminal His_{10}-tag and TEV cleavage site	8
pET-TEV-*odhI*-R87A	Kan^R; pET-TEV-*odhI* derivative, encodes OdhI-R87A with an N-terminal His_{10}-tag and TEV cleavage site	This work
pET-TEV-*odhI*-R87P	Kan^R; pET-TEV-*odhI* derivative, encodes OdhI-R87P with an N-terminal His_{10}-tag and TEV cleavage site	This work
pET-TEV-*glnH*ΔSP	Kan^R; pET-TEV derivative for overproduction of GlnH lacking the signal peptide and the lipobox motif with an N-terminal His_{10}-tag and TEV cleavage site	This work
pET-TEV-*glnH*core	Kan^R; pET-TEV derivative for overproduction of GlnH lacking flexible N- and C-terminal parts (amino acid residues 48–334 of GlnH) with an N-terminal His_{10}-tag and TEV cleavage site	This work
pET-TEV-*glnH*core-S163T-T165S	Kan^R; pET-TEV-*glnH*core derivative, encodes GlnHcore-S163T-T165S with an N-terminal His_{10}-tag and TEV cleavage site	This work
pJC1	Kan^R; *E. coli-C. glutamicum* shuttle vector	70
pJC1-*glnX*Prom	Kan^R; pJC1 derivative carrying the *glnX* gene, including its native promoter region (383 bp upstream of the transcriptional start site, which is also the translational start site)	This work
pEKEx2	Kan^R, *E. coli*/*C. glutamicum* shuttle vector; P_{tac}; $lacI^q$; ori_{Cg} from pBL1; ori_{Ec} ColE1 from pUC18	71
pEKEx2-*pknG*	Kan^R, pEKEx2 derivative encodes PknG with a C-terminal Strep-tag, contains the native RBS[a] of *pknG*	6
pAN6	Kan^R; *C. glutamicum*/*E. coli* shuttle vector for regulated gene expression	72
pAN6-*glnH*	Kan^R; pAN6 derivative encodes GlnH with a C-terminal Strep-tag	This work
pAN6-*glnH*-C27A	Kan^R; pAN6-glnH derivative, encodes GlnH-C27A with a C-terminal Strep	This work
pPREx2	Kan^R; pPBEx2 derivative (P_{tac}, $lacI^q$, *oriC.g* from pBL1; ori_{Ec} ColE1 from pUC18), with a consensus RBS (AAGGAG) for *C. glutamicum*	35
pPREx2-*glnX*-(F1 to F7)-*phoA*	Kan^R; pPREx2 derivative for expression of GlnX variants of different lengths (F1–F7) fused to the alkaline phosphatase (*phoA*)	This work
pPREx2-*glnX*-(F1 to F7)-*lacZ*	Kan^R; pPREx2 derivative for expression of GlnX variants of different lengths (F1–F7) fused to the β-galactosidase (*lacZ*)	This work
pMA632-Ex	Amp^R; *E. coli* plasmid for topology determination of membrane proteins via *phoA-lacZ* fusions (P_{tac}, $lacI^q$; with RBS) used as template for *phoA* amplification including linker sequence	Provided by Lothar Eggeling, Forschungszentrum Jülich

[a]RBS, ribosomal binding site.

modified CGXII medium lacking glucose, ammonium sulfate, and urea and containing 100 mM L-glutamine as the nitrogen and carbon source. These media were also used for the preparation of solid media by addition of 15 g L^{-1} agar. For induction of glutamate secretion, the CGXII medium with 4% (wt/vol) glucose was supplemented with 500 mg L^{-1} ethambutol and 20 μM IPTG for strains carrying plasmids with an IPTG-inducible promoter. The glutamate concentration in the culture supernatant was measured after 24 h. To maintain plasmid stability, kanamycin was added at concentrations of 25 mg L^{-1} (*C. glutamicum*) or 50 mg L^{-1} (*E. coli*).

Standard recombinant DNA work and construction of deletion mutants. Standard methods such as PCR and plasmid restriction were carried out according to established protocols (51). All oligonucleotides used are listed in Table 3. Plasmids were constructed by ligating DNA fragments obtained by restriction digestion or PCR or by Gibson assembly (52). Oligonucleotide synthesis and DNA sequencing were performed by Eurofins Genomics (Ebersberg, Germany). Site-directed mutagenesis of *odhI* and *glnH* was performed using the QuikChange Lightning site-directed mutagenesis kit (Agilent Technologies, Santa Clara, CA, USA). Transformation of *E. coli* was performed using a standard protocol (53), and *C. glutamicum* transformation was performed by electroporation (54). *C. glutamicum* deletion mutants were constructed by double homologous recombination using pK19mobsacB-based plasmids as described previously (55). Oligonucleotides annealing up- and downstream of the deleted genes were used to confirm genomic deletions by colony-PCR.

Western blot analysis. The phosphorylation status of OdhI in different *C. glutamicum* strains was analyzed by Western blotting. Cell pellets of *C. glutamicum* strains cultivated overnight in BHI medium with 4% (wt/vol) glucose were resuspended in phosphate-buffered saline (PBS) (137 mM NaCl, 2.7 mM KCl, 4.3 mM Na_2HPO_4, 1.4 mM KH_2PO_4) containing cOmplete EDTA-free protease inhibitor (Roche, Basel, Switzerland) and disrupted using 0.1-mm zirconia/silica beads (Roth, Karlsruhe, Germany) in an amalgamator (Silamat S5, Vivadent). Cell lysates were cleared by centrifugation at 13,000 $\times$ *g* and 4°C for 45 min followed by ultracentrifugation at 100,000 $\times$ *g* and 4°C for 1 h. Samples of the supernatants corresponding to 20 μg protein were analyzed using SDS-PAGE and Western blotting as previously described (14). The presence of OdhI in the *C. glutamicum* Δ*glnX2* strain and its suppressor mutants was analyzed with crude cell extract samples (10 μg protein each) using polyclonal rabbit anti-OdhI antiserum in a 1:500 dilution (14). The ECL Advance Western blotting detection kit (GE Healthcare, Chicago, IL, USA) was used for chemiluminescent signal detection using an LAS-3000 image reader (Fujifilm, Minato, Japan). Signal intensity was analyzed using ImageQuant software (GE Healthcare) or AIDA Image Analyzer v. 4.15 (Fujifilm).

To analyze if GlnH is a lipoprotein, the *C. glutamicum* strains Δ*glnH*/pAN6-*glnH* and Δ*glnH*/pAN6-*glnH*-C27A were cultivated in CGXII medium with 4% (wt/vol) glucose and 1 mM IPTG to induce target gene expression. After 4 h of cultivation (optical density at 600 nm [OD_{600}], ~6), 50 mg L^{-1} globomycin (stock solution, 20 g L^{-1} in chloroform) was added, and the culture was further incubated for 3 h at 30°C. In the control culture, no globomycin was added. Crude cell extract samples (10 μg protein) taken prior to addition of globomycin and 1 h, 2 h, and 3 h thereafter were analyzed by Western blotting using a Strep-Tactin-horseradish peroxidase (HRP) conjugate (IBA Lifesciences, Göttingen, Germany) to detect Strep-tagged GlnH.

Determination of glutamate. The concentration of L-glutamate in culture supernatants was determined by reversed-phase high-pressure liquid chromatography as reported previously for L-lysine (56).

Protein production and purification. For measuring their influence on ODH activity, His-tagged OdhI and the mutated derivatives OdhI-R87P and OdhI-R87A were overproduced using the *E. coli* strains BL21(DE3)/pET-TEV-*odhI*, BL21(DE3)/pET-TEV-*odhI*-R87P, and BL21(DE3)/pET-TEV-*odhI*-R87A. The strains were cultivated at 37°C in LB medium, and at an OD_{600} of 0.5, target gene expression was induced with 1 mM IPTG, after which the cultures were incubated for another 4 h at room temperature. His_{10}-GlnHΔSP, His_{10}-GlnHcore, and its mutated derivative His_{10}-GlnHcore-S163T-T165S were overproduced in TB medium using *E. coli* BL21(DE3) containing the plasmids pET-TEV-*glnH*ΔSP, pET-TEV-*glnH*core, and pET-TEV-*glnH*core S163T-T165S. After target gene expression with 500 μM IPTG, the cells were cultivated for 18 h at 18°C. All proteins were purified following the same protocol. Cells were harvested by centrifugation, resuspended in lysis buffer (20 mM Tris-HCl, 500 mM NaCl, 5% [vol/vol] glycerol, 20 mM imidazole, pH 7.9) containing cOmplete EDTA-free protease inhibitor (Roche, Basel, Switzerland), and disrupted by French press treatment. Soluble protein fractions were obtained by centrifugation (5,000 $\times$ *g*, 4°C, 20 min) and subsequent ultracentrifugation of the supernatant (100,000 $\times$ *g*, 4°C, 1 h). Supernatants of the ultracentrifugation were loaded on HisTrap HP (GE Healthcare, Chicago, IL, USA) or gravity flow Ni-NTA columns (Qiagen, Hilden, Germany), and after washing, the His-tagged proteins were eluted using buffer with increasing imidazole concentrations up to 300 mM. In the case of purified OdhI variants, His-tags were cleaved off by addition of His-tagged *Tobacco Etch Virus* (TEV) protease (0.01 mg/mg target protein) and overnight incubation at 4°C followed by a second Ni-NTA purification, in which untagged OdhI was collected in the flowthrough. Untagged OdhI variants and His-tagged GlnH variants were further purified by size exclusion chromatography on a Superdex 200 10/300 GL column (GE Healthcare) equilibrated for the OdhI variants in 0.1 M TES [*N*-tris(hydroxymethyl)methyl-2-aminoethanesulfonic acid] buffer (100 mM TES, pH 7.2, 10 mM $MgCl_2$, 3 mM cysteine, 30% [vol/vol] glycerol), and for GlnH variants in HEPES buffer (40 mM HEPES, pH 7, 100 mM KCl, 10 mM $MgCl_2$). Protein concentrations were determined using the molar extinction coefficient predicted by the ProtParam tool (http://web.expasy.org/protparam/).

Enzyme activity assays. Determination of the ODH activity in the presence of different OdhI variants was carried out using a photometric assay following NADH formation as described previously (6, 8). Native OdhI, OdhI-R87A, or OdhI-R87P at concentrations of 0.38 nM or 1.9 nM were added to cell-free

TABLE 3 Oligonucleotides used in this study

Name	Sequence
Construction of pK19mobsacB-*glnX2* and pK19mobsacB-*glnX-glnH-pknG*	
ΔglnX_1	TATATAGTCGACGCGTTCTGGATCGGCGGGAAAAGG
ΔglnX_2	CCCATCCACTAAACTTAAACAAGAAGTATCCTTCTCCGTTAACGG
ΔglnX_3	TGTTTAAGTTTAGTGGATGGGTCGATTCAGGGCAGTGGCACTGGT
ΔglnX_4	TATATAGGATCCAAAGCAGTCAAGGTTTCTGCCGGT
ΔpknG_3	TGTTTAAGTTTAGTGGATGGGGCGAATGCCGTGCGG
ΔpknG_4	GATTCTAGAGTTAGCTATCGCTAGGTACG
Confirmation of gene deletion by colony-PCR	
ΔglnX_fw	ATTCATCAAGGTAGCCAATACTTTC
ΔglnX_rv	GCTCCTCAGGGGTCAGATCAT
ΔpknG_rv	GATCGATCCAGAGCGTAACGC
Construction of pJC1-*glnX*Prom	
glnXProm-fw	TATAGGATCCGCGTTCTGGATCGGCGGGAAAAG
glnXProm-rev	TATAGTCGACTTATAAGTACTCCTGCAAACGGGGG
Construction of pET-TEV-*odhI*-R87A and pET-TEV-*odhI*-R87P by site-directed mutagenesis	
odhI_R87A fw	CTTGATGATGTCACCGTTTCAGCTCGCCACGCAG
odhI_R87A rv	CTGCGTGGCGAGCTGAAACGGTGACATCATCAAG
odhI_R87P fw	TGTCACCGTTTCACCTCGCCACGCAGAG
odhI_R87P rv	ACAGTGGCAAAGTGGAGCGGTGCGTCTC
Construction of pET-TEV-*glnH*ΔSP	
glnHΔSP fw	TATACATATGACTCCAACACCTGTGGAACCG
glnHΔSP rv	TATACTCGAGTTATCCTTCATCGTTTTCTGT
Construction of pET-TEV-*glnH*core	
glnHcore fw	CCTGTATTTTCAGGGCCATATGCCACTGCCACCGGATTCTTC
glnHcore rv	TGGTGGTGGTGGTGGTGCTCGAGTTATGGCATGTACTGCAGCTGTG
Construction of pET-TEV-*glnH*core-S163T-T165S	
glnH_S163T-T165S fw	ATGTAGATATTGTGATTCGTACGGTCTCCATCACCGACGAACGCGCC
glnH_S163T-T165S rv	GGCGCGTTCGTCGGTGATGGAGACCGTACGAATCACAATATCTACAT
Construction of pAN6-*glnH*	
glnH fw	GACAGTCATATGCACGCTTTTCGACGC
glnH rv	GACGCTAGCTCCTTCATCGTTTTCTGTC
Construction of pAN6-*glnH*-C27A by site-directed mutagenesis	
glnH_C27A fw	AACGCTGCTTGCTTCCGCCACTCCAACACCTGTG
glnH_C27A rv	CACAGGTGTTGGAGTGGCGGAAGCAAGCAGCGTT
Construction of pPREx2-*glnX*-(F1 to F7)-*phoA* and pPREx2-*glnX*-(F1 to F7)-*lacZ*	
glnX fw	TGCAGAAGGAGATATACATATGATCCGGGATGGAAATG
glnX-F1 rv	CGTCTGGCCTCTCGAGGCAGGCTGGCCGAAAGTTTCCTG
glnX-F2 rv	CGTCTGGCCTCTCGAGGCAACAGGCTCCGCATTAGTG
glnX-F3 rv	CGTCTGGCCTCTCGAGGCGTTGTAAAGCTCAGACGCCATC
glnX-F4 rv	CGTCTGGCCTCTCGAGGCCCTGCGCGTAATCCGCATCAAC
glnX-F5 rv	CGTCTGGCCTCTCGAGGCATTCAACGGCCCCGACGCTTC
glnX-F6 rv	CGTCTGGCCTCTCGAGGCGCGAGAATCCGCGATCAG
glnX-F7 rv	CGTCTGGCCTCTCGAGGCTAAGTACTCCTGCAAACG
lacZ fw	GCCTCGAGAGGCCAGACGGGCCAGGCCTTGGGCCCTACCATGATTACGGATTCAC
lacZ rv	GTAAAACGACGGCCAGTGTTATTTTTGACACCAGACCAAC
phoA fw	GCCTCGAGAGGCCAGACG
phoA rv	GTAAAACGACGGCCAGTGTTATTTCAGCCCCAGGGCGGCTTTC
Amplification and sequencing primer for *odhI*, *odhA*, and *pknG*	
odhI-78b-up	CAGGAAATTCTAGGATCTTACGGA
odhI-76b-dwn	GGCATTCTATACACAAAACGGTTG

(Continued on next page)

TABLE 3 (Continued)

Name	Sequence
odhA-up80b-fw	AGCCAACGACCAACGTTACAG
odhA-988b-rv	TGCGCAGGAATTCACCGGA
odhA-862b-fw	TGTCGGTTCCATGGATTACC
odhA-2051b-rv	GTGGTGAAGCCGATCTGGTT
odhA-1982-fw	CCAGAAACCATCAACCTGGC
odhA-dwn75b-rv	GCAGCAAAAAGGGCCGTATGCTGTGT
pknG-up150b-fw	GGTTGATTCGGCAGGTAAACTAC
pknG-1300b-rv	GTTTGCCGTCGCGGACTGCC
pknG-1052b-fw	CGATATTTTCACCATCGGACGC
pknG-dwn150b-rv	CGCAGAAATCACATCAGCCCCAAT

extracts of *C. glutamicum* Δ*odhI* and preincubated for 5 min at room temperature and then for 3 min at 30°C in the spectrophotometer before the reaction was started by addition of 0.2 mM coenzyme A.

For the determination of alkaline phosphatase (PhoA) and β-galactosidase (LacZ) activity of GlnX′-PhoA and GlnX′-LacZ fusion constructs, *E. coli* TG1 cells were transformed with pPREx2 plasmids encoding seven GlnX variants of different lengths fused either to PhoA or to LacZ. The strains (in biological triplicates) were cultivated in LB medium in 96-well deep-well plates at 30°C and 900 rpm for 3 h, and expression of the *glnX-phoA* and *glnX-lacZ* constructs were induced by addition of 1 mM IPTG. After further incubation for 1 h under the same conditions, 100 μL of each culture was harvested. Cells carrying the GlnX-PhoA constructs were resuspended in 300 μL 1 M Tris-HCl, pH 8, while those harboring the GlnX-LacZ constructs were resuspended in 300 μL buffer Z (60 mM Na_2HPO_4, 40 mM NaH_2PO_4, 1 mM $MgSO_4$, 10 mM KCl, 100 mM dithiothreitol [DTT], pH 7) (57). Resuspended cells were permeabilized, and activity assays were carried out as previously described (34, 58). PhoA activity was measured with *p*-nitrophenylphosphate (*p*NPP) (5 g L^{-1} *p*NPP in 1 M Tris-HCl, 5 mM $MgCl_2$, pH 8), while LacZ activity was assayed with *o*-nitrophenol-β-D-galactopyranoside (*o*NPG) (5 g L^{-1} *o*NPG in 100 mM K_2HPO_4, pH 7). The activities were measured by following the changes in the absorbance at 420 nm for up to 2 h at 28°C using a Tecan microplate reader. Prior to the measurement at 420 nm, the absorbance at 550 nm and 600 nm was measured to correct for differences in cell density and light scattering caused by cell debris. The activity in Miller units was calculated according to the equation $MU = 1{,}000 \times ([A_{420} - 1.75 \times A_{550}]/[t \times A_{600}])$, where A_{420} represents the absorbance of the yellow nitrophenolate, A_{550} corrects for light scattering from cell debris, A_{600} represents the cell density, and t is the reaction time.

Isothermal titration calorimetry. Purified His_{10}-GlnHΔSP was dialyzed overnight against a 500-fold excess of dialysis buffer (40 mM HEPES, 100 mM KCl, 10 mM $MgCl_2$, pH 7.0). Stock solutions of the potential ligands L-aspartic acid, L-glutamic acid, L-asparagine, L-glutamine, and 2-oxoglutarate were prepared in dialysis buffer, and the pH was adjusted to pH 7.0 using KOH. ITC measurements were performed with a MicroCal PEAQ-ITC instrument (Malvern Panalytical, Malvern, Great Britain) operated at 25°C. Protein concentrations between 30 μM and 75 μM were used together with ligand concentrations of 7.5 mM to 50 mM. Prior to being filled with 300 μL protein solution, the measuring cell was rinsed with dialysis buffer, while the syringe was filled with 75 μL ligand solution. An ITC run was started with an initial injection of 0.4 μL followed by 12 injections of 3 μL each. In addition, control experiments with ligand solution titrated into the dialysis buffer were performed. The data were analyzed using MicroCal ITC analysis software (Malvern Panalytical), and a fixed 1:1 binding stoichiometry was assumed to determine the binding affinity.

Measurement of the effects of amino acids on intrinsic tryptophan fluorescence of GlnH. Intrinsic fluorescence (excitation at 292 nm, emission at 340 nm) of His_{10}-GlnHcore and His_{10}-GlnHcore-S163T-T165S (0.1 mg/mL) was measured in 40 mM HEPES buffer, pH 7.0, containing 100 mM KCl and 10 mM $MgCl_2$ at various concentrations of sodium aspartate (0.0122 to 50 mM) or sodium glutamate (0.0122 to 100 mM). Fluorescence was measured using 15-μL samples in a Tecan Infinite M1000 PRO plate reader (Tecan, Männedorf, Switzerland) and 384 black shallow-well plates. The dissociation constant of GlnH for amino acids was calculated by fitting fluorescence data to a one-site specific binding equation (GraphPad Prism 8).

Prediction of GlnH and GlnX structures. The recent developments in the field of protein structure prediction, most notably the deep learning systems AlphaFold2 (30, 59) and RoseTTAFold (60), have greatly enhanced the accuracy of the resulting models. In the case of AlphaFold2, structural models of proteins not yet represented in the respective database (https://alphafold.ebi.ac.uk) became more approachable through the availability of the open-source software ColabFold (61), featuring improved speed and resource efficiency. Furthermore, AlphaFold2 has also been reported to be reliable for predicting transmembrane protein structures (62). The monomeric structures of GlnH and GlnX were predicted by AlphaFold2 (30) via the ColabFold interface (30, 59, 63), using the GlnHΔSP sequence (residues 28 to 343) and the full-length GlnX sequence of 501 amino acids, respectively. The pipeline executed for prediction in ColabFold generates a multiple-sequence alignment (MSA) via an MMseqs2 search (64); the MSA was subsequently used as input for the prediction [parameters use_amber: no, template mode: none, msa_mode: MMSeq2 (UniRef+Environmental], num_recycle: 12). The structure was visualized using ChimeraX (65) or PyMol (www.pymol.org) and colored, when appropriate, according to the pLDDT confidence measure annotated in the B-factor field of the PDB file.

SUPPLEMENTAL MATERIAL

Supplemental material is available online only.

SUPPLEMENTAL FILE 1, PDF file, 0.9 MB.

ACKNOWLEDGMENTS

This work was financially supported by the DFG-ANR project MetActino (DFG BO 903/4-1, ANR-18-CE92-0003) and by the Heinrich Heine University Düsseldorf within the framework of the Bio24 graduate school.

We thank Lena Gebel for construction of plasmid pAN6-glnH and Sankyo Chemicals (Tokyo, Japan) for providing globomycin. This work is dedicated to Karl-Erich Jaeger for his pioneering contributions in the field of molecular enzyme technology.

REFERENCES

1. Eggeling L, Bott M (ed). 2005. Handbook of Corynebacterium glutamicum. CRC Press/Taylor & Francis Group, Boca Raton, FL.
2. Eggeling L, Bott M. 2015. A giant market and a powerful metabolism: L-lysine provided by *Corynebacterium glutamicum*. Appl Microbiol Biotechnol 99:3387–3394. https://doi.org/10.1007/s00253-015-6508-2.
3. Becker J, Wittmann C. 2012. Bio-based production of chemicals, materials and fuels: *Corynebacterium glutamicum* as versatile cell factory. Curr Opin Biotechnol 23:631–640. https://doi.org/10.1016/j.copbio.2011.11.012.
4. Wendisch VF, Jorge JMP, Perez-Garcia F, Sgobba E. 2016. Updates on industrial production of amino acids using *Corynebacterium glutamicum*. World J Microbiol Biotechnol 32:105. https://doi.org/10.1007/s11274-016-2060-1.
5. Gao B, Gupta RS. 2012. Phylogenetic framework and molecular signatures for the main clades of the phylum *Actinobacteria*. Microbiol Mol Biol Rev 76:66–112. https://doi.org/10.1128/MMBR.05011-11.
6. Niebisch A, Kabus A, Schultz C, Weil B, Bott M. 2006. Corynebacterial protein kinase G controls 2-oxoglutarate dehydrogenase activity via the phosphorylation status of the OdhI protein. J Biol Chem 281:12300–12307. https://doi.org/10.1074/jbc.M512515200.
7. Bruch EM, Vilela P, Yang L, Boyko A, Lexa-Sapart N, Raynal B, Alzari PM, Bellinzoni M. 2021. Actinobacteria challenge the paradigm: a unique protein architecture for a well-known, central metabolic complex. Proc Natl Acad Sci U S A 118:e2112107118. https://doi.org/10.1073/pnas.2112107118.
8. Krawczyk S, Raasch K, Schultz C, Hoffelder M, Eggeling L, Bott M. 2010. The FHA domain of OdhI interacts with the carboxyterminal 2-oxoglutarate dehydrogenase domain of OdhA in *Corynebacterium glutamicum*. FEBS Lett 584:1463–1468. https://doi.org/10.1016/j.febslet.2010.03.028.
9. Raasch K, Bocola M, Labahn J, Leitner A, Eggeling L, Bott M. 2014. Interaction of 2-oxoglutarate dehydrogenase OdhA with its inhibitor OdhI in *Corynebacterium glutamicum*: mutants and a model. J Biotechnol 191:99–105. https://doi.org/10.1016/j.jbiotec.2014.05.023.
10. Schultz C, Niebisch A, Schwaiger A, Viets U, Metzger S, Bramkamp M, Bott M. 2009. Genetic and biochemical analysis of the serine/threonine protein kinases PknA, PknB, PknG and PknL of *Corynebacterium glutamicum*: evidence for non-essentiality and for phosphorylation of OdhI and FtsZ by multiple kinases. Mol Microbiol 74:724–741. https://doi.org/10.1111/j.1365-2958.2009.06897.x.
11. Barthe P, Roumestand C, Canova MJ, Kremer L, Hurard C, Molle V, Cohen-Gonsaud M. 2009. Dynamic and structural characterization of a bacterial FHA protein reveals a new autoinhibition mechanism. Structure 17:568–578. https://doi.org/10.1016/j.str.2009.02.012.
12. Komine-Abe A, Nagano-Shoji M, Kubo S, Kawasaki H, Yoshida M, Nishiyama M, Kosono S. 2017. Effect of lysine succinylation on the regulation of 2-oxoglutarate dehydrogenase inhibitor, OdhI, involved in glutamate production in *Corynebacterium glutamicum*. Biosci Biotechnol Biochem 81:2130–2138. https://doi.org/10.1080/09168451.2017.1372182.
13. Lisa MN, Sogues A, Barilone N, Baumgart M, Gil M, Grana M, Duran R, Biondi RM, Bellinzoni M, Bott M, Alzari PM. 2021. A tetratricopeptide repeat scaffold couples signal detection to OdhI phosphorylation in metabolic control by the protein kinase PknG. mBio 12:e0171721. https://doi.org/10.1128/mBio.01717-21.
14. Schultz C, Niebisch A, Gebel L, Bott M. 2007. Glutamate production by *Corynebacterium glutamicum*: dependence on the oxoglutarate dehydrogenase inhibitor protein OdhI and protein kinase PknG. Appl Microbiol Biotechnol 76:691–700. https://doi.org/10.1007/s00253-007-0933-9.
15. Cowley S, Ko M, Pick N, Chow R, Downing KJ, Gordhan BG, Betts JC, Mizrahi V, Smith DA, Stokes RW, Av-Gay Y. 2004. The *Mycobacterium tuberculosis* protein serine/threonine kinase PknG is linked to cellular glutamate/glutamine levels and is important for growth *in vivo*. Mol Microbiol 52:1691–1702. https://doi.org/10.1111/j.1365-2958.2004.04085.x.
16. O'Hare HM, Duran R, Cervenansky C, Bellinzoni M, Wehenkel AM, Pritsch O, Obal G, Baumgartner J, Vialaret J, Johnsson K, Alzari PM. 2008. Regulation of glutamate metabolism by protein kinases in mycobacteria. Mol Microbiol 70:1408–1423. https://doi.org/10.1111/j.1365-2958.2008.06489.x.
17. Nott TJ, Kelly G, Stach L, Li J, Westcott S, Patel D, Hunt DM, Howell S, Buxton RS, O'Hare HM, Smerdon SJ. 2009. An intramolecular switch regulates phosphoindependent FHA domain interactions in *Mycobacterium tuberculosis*. Sci Signal 2:ra12.
18. Ventura M, Rieck B, Boldrin F, Degiacomi G, Bellinzoni M, Barilone N, Alzaidi F, Alzari PM, Manganelli R, O'Hare HM. 2013. GarA is an essential regulator of metabolism in *Mycobacterium tuberculosis*. Mol Microbiol 90:356–366.
19. Wagner T, Andre-Leroux G, Hindie V, Barilone N, Lisa MN, Hoos S, Raynal B, Vulliez-Le Normand B, O'Hare HM, Bellinzoni M, Alzari PM. 2019. Structural insights into the functional versatility of an FHA domain protein in mycobacterial signaling. Sci Signal 12:eaav9504. https://doi.org/10.1126/scisignal.aav9504.
20. Kalinowski J, Bathe B, Bartels D, Bischoff N, Bott M, Burkovski A, Dusch N, Eggeling L, Eikmanns BJ, Gaigalat L, Goesmann A, Hartmann M, Huthmacher K, Krämer R, Linke B, McHardy AC, Meyer F, Möckel B, Pfefferle W, Pühler A, Rey DA, Rückert C, Rupp O, Sahm H, Wendisch VF, Wiegrabe I, Tauch A. 2003. The complete *Corynebacterium glutamicum* ATCC 13032 genome sequence and its impact on the production of L-aspartate-derived amino acids and vitamins. J Biotechnol 104:5–25. https://doi.org/10.1016/s0168-1656(03)00154-8.
21. Bhattacharyya N, Nkumama IN, Newland-Smith Z, Lin L-Y, Yin W, Cullen RE, Griffiths JS, Jarvis AR, Price MJ, Chong PY, Wallis R, O'Hare HM. 2018. An aspartate-specific solute-binding protein regulates protein kinase G activity to control glutamate metabolism in mycobacteria. mBio 9:e0093118. https://doi.org/10.1128/mBio.00931-18.
22. Radmacher E, Stansen KC, Besra GS, Alderwick LJ, Maughan WN, Hollweg G, Sahm H, Wendisch VF, Eggeling L. 2005. Ethambutol, a cell wall inhibitor of *Mycobacterium tuberculosis*, elicits L-glutamate efflux of *Corynebacterium glutamicum*. Microbiology (Reading) 151:1359–1368. https://doi.org/10.1099/mic.0.27804-0.
23. Sutcliffe IC, Harrington DJ. 2002. Pattern searches for the identification of putative lipoprotein genes in Gram-positive bacterial genomes. Microbiology (Reading) 148:2065–2077. https://doi.org/10.1099/00221287-148-7-2065.
24. Mohiman N, Argentini M, Batt SM, Cornu D, Masi M, Eggeling L, Besra G, Bayan N. 2012. The ppm operon is essential for acylation and glycosylation of lipoproteins in *Corynebacterium glutamicum*. PLoS One 7:e46225. https://doi.org/10.1371/journal.pone.0046225.
25. Inukai M, Takeuchi M, Shimizu K, Arai M. 1978. Mechanism of action of globomycin. J Antibiot (Tokyo) 31:1203–1205. https://doi.org/10.7164/antibiotics.31.1203.
26. Inukai M, Nakajima M, Osawa M, Haneishi T, Arai M. 1978. Globomycin, a new peptide antibiotic with spheroplast-forming activity. II. Isolation and physico-chemical and biological characterization. J Antibiot (Tokyo) 31:421–425. https://doi.org/10.7164/antibiotics.31.421.
27. Nakajima M, Inukai M, Haneishi T, Terahara A, Arai M, Kinoshita T, Tamura C. 1978. Globomycin, a new peptide antibiotic with spheroplast-forming activity. III. Structural determination of globomycin. J Antibiot (Tokyo) 31:426–432. https://doi.org/10.7164/antibiotics.31.426.

28. Sun YJ, Rose J, Wang BC, Hsiao CD. 1998. The structure of glutamine-binding protein complexed with glutamine at 1.94 A resolution: comparisons with other amino acid binding proteins. J Mol Biol 278:219–229. https://doi.org/10.1006/jmbi.1998.1675.
29. Nohno T, Saito T, Hong J. 1986. Cloning and complete nucleotide sequence of the *Escherichia coli* glutamine permease operon (*glnHPQ*). Mol Gen Genet 205:260–269. https://doi.org/10.1007/BF00430437.
30. Jumper J, Evans R, Pritzel A, Green T, Figurnov M, Ronneberger O, Tunyasuvunakool K, Bates R, Zidek A, Potapenko A, Bridgland A, Meyer C, Kohl SAA, Ballard AJ, Cowie A, Romera-Paredes B, Nikolov S, Jain R, Adler J, Back T, Petersen S, Reiman D, Clancy E, Zielinski M, Steinegger M, Pacholska M, Berghammer T, Bodenstein S, Silver D, Vinyals O, Senior AW, Kavukcuoglu K, Kohli P, Hassabis D. 2021. Highly accurate protein structure prediction with AlphaFold. Nature 596:583–589. https://doi.org/10.1038/s41586-021-03819-2.
31. Pfeifer-Sancar K, Mentz A, Rückert C, Kalinowski J. 2013. Comprehensive analysis of the *Corynebacterium glutamicum* transcriptome using an improved RNAseq technique. BMC Genomics 14:888. https://doi.org/10.1186/1471-2164-14-888.
32. Zhulin IB, Nikolskaya AN, Galperin MY. 2003. Common extracellular sensory domains in transmembrane receptors for diverse signal transduction pathways in bacteria and archaea. J Bacteriol 185:285–294. https://doi.org/10.1128/JB.185.1.285-294.2003.
33. Manoil C, Beckwith J. 1986. A genetic approach to analyzing membrane protein topology. Science 233:1403–1408. https://doi.org/10.1126/science.3529391.
34. Manoil C. 1991. Analysis of membrane protein topology using alkaline phosphatase and beta-galactosidase gene fusions. Methods Cell Biol 34:61–75. https://doi.org/10.1016/s0091-679x(08)61676-3.
35. Bakkes PJ, Ramp P, Bida A, Dohmen-Olma D, Bott M, Freudl R. 2020. Improved pEKEx2-derived expression vectors for tightly controlled production of recombinant proteins in *Corynebacterium glutamicum*. Plasmid 112:102540. https://doi.org/10.1016/j.plasmid.2020.102540.
36. Kabsch W, Sander C. 1983. Dictionary of protein secondary structure: pattern recognition of hydrogen-bonded and geometrical features. Biopolymers 22:2577–2637. https://doi.org/10.1002/bip.360221211.
37. Omasits U, Ahrens CH, Muller S, Wollscheid B. 2014. Protter: interactive protein feature visualization and integration with experimental proteomic data. Bioinformatics 30:884–886. https://doi.org/10.1093/bioinformatics/btt607.
38. Matilla MA, Velando F, Martin-Mora D, Monteagudo-Cascales E, Krell T. 2022. A catalogue of signal molecules that interact with sensor kinases, chemoreceptors and transcriptional regulators. FEMS Microbiol Rev 46:fuab043. https://doi.org/10.1093/femsre/fuab043.
39. Li Y, Liang J, Yang S, Yao J, Chen K, Yang L, Zheng W, Tian Y. 2021. Finding novel chemoreceptors that specifically sense and trigger chemotaxis toward polycyclic aromatic hydrocarbons in *Novosphingobium pentaromativorans* US6-1. J Hazard Mater 416:126246. https://doi.org/10.1016/j.jhazmat.2021.126246.
40. Potter SC, Luciani A, Eddy SR, Park Y, Lopez R, Finn RD. 2018. HMMER web server: 2018 update. Nucleic Acids Res 46:W200–W204. https://doi.org/10.1093/nar/gky448.
41. Holm L. 2020. Using Dali for protein structure comparison. Methods Mol Biol 2112:29–42. https://doi.org/10.1007/978-1-0716-0270-6_3.
42. Milburn MV, Prive GG, Milligan DL, Scott WG, Yeh J, Jancarik J, Koshland DE, Jr, Kim SH. 1991. Three-dimensional structures of the ligand-binding domain of the bacterial aspartate receptor with and without a ligand. Science 254:1342–1347. https://doi.org/10.1126/science.1660187.
43. Krissinel E, Henrick K. 2004. Secondary-structure matching (SSM), a new tool for fast protein structure alignment in three dimensions. Acta Crystallogr D Biol Crystallogr 60:2256–2268. https://doi.org/10.1107/S0907444904026460.
44. Li J, Wang C, Yang G, Sun Z, Guo H, Shao K, Gu Y, Jiang W, Zhang P. 2017. Molecular mechanism of environmental d-xylose perception by a XylFII-LytS complex in bacteria. Proc Natl Acad Sci U S A 114:8235–8240. https://doi.org/10.1073/pnas.1620183114.
45. Gushchin I, Gordeliy V. 2018. Transmembrane signal transduction in two-component systems: piston, scissoring, or helical rotation? Bioessays 40:1700197. https://doi.org/10.1002/bies.201700197.
46. Rehm N, Burkovski A. 2011. Engineering of nitrogen metabolism and its regulation in *Corynebacterium glutamicum*: influence on amino acid pools and production. Appl Microbiol Biotechnol 89:239–248. https://doi.org/10.1007/s00253-010-2922-7.
47. Kronemeyer W, Peekhaus N, Krämer R, Sahm H, Eggeling L. 1995. Structure of the *gluABCD* cluster encoding the glutamate uptake system of *Corynebacterium glutamicum*. J Bacteriol 177:1152–1158. https://doi.org/10.1128/jb.177.5.1152-1158.1995.
48. Trötschel C, Kandirali S, Diaz-Achirica P, Meinhardt A, Morbach S, Krämer R, Burkovski A. 2003. GltS, the sodium-coupled L-glutamate uptake system of *Corynebacterium glutamicum*: identification of the corresponding gene and impact on L-glutamate production. Appl Microbiol Biotechnol 60:738–742. https://doi.org/10.1007/s00253-002-1170-x.
49. Bertani G. 1951. Studies on lysogenesis. I. The mode of phage liberation by lysogenic *Escherichia coli*. J Bacteriol 62:293–300. https://doi.org/10.1128/jb.62.3.293-300.1951.
50. Keilhauer C, Eggeling L, Sahm H. 1993. Isoleucine synthesis in *Corynebacterium glutamicum*: molecular analysis of the *ilvB-ilvN-ilvC* operon. J Bacteriol 175:5595–5603. https://doi.org/10.1128/jb.175.17.5595-5603.1993.
51. Green MR, Sambrook J. 2012. Molecular cloning: a laboratory manual, 3rd ed. Cold Spring Harbor Laboratory Press, Cold Spring Harbor, NY.
52. Gibson DG, Young L, Chuang RY, Venter JC, Hutchison CA, Smith HO. 2009. Enzymatic assembly of DNA molecules up to several hundred kilobases. Nat Methods 6:343–345. https://doi.org/10.1038/nmeth.1318.
53. Hanahan D. 1983. Studies on transformation of *Escherichia coli* with plasmids. J Mol Biol 166:557–580. https://doi.org/10.1016/s0022-2836(83)80284-8.
54. van der Rest ME, Lange C, Molenaar D. 1999. A heat shock following electroporation induces highly efficient transformation of *Corynebacterium glutamicum* with xenogeneic plasmid DNA. Appl Microbiol Biotechnol 52:541–545. https://doi.org/10.1007/s002530051557.
55. Niebisch A, Bott M. 2001. Molecular analysis of the cytochrome bc_1-aa_3 branch of the *Corynebacterium glutamicum* respiratory chain containing an unusual diheme cytochrome c_1. Arch Microbiol 175:282–294. https://doi.org/10.1007/s002030100262.
56. Kabus A, Georgi T, Wendisch VF, Bott M. 2007. Expression of the *Escherichia coli pntAB* genes encoding a membrane-bound transhydrogenase in *Corynebacterium glutamicum* improves L-lysine formation. Appl Microbiol Biotechnol 75:47–53. https://doi.org/10.1007/s00253-006-0804-9.
57. Miller JH. 1992. A short course in bacterial genetics: a laboratory manual and handbook for *Escherichia coli* and related bacteria. Cold Spring Harbor Laboratory Press, Cold Spring Harbor, NY.
58. Keppel M, Davoudi E, Gätgens C, Frunzke J. 2018. Membrane topology and heme binding of the histidine kinases HrrS and ChrS in *Corynebacterium glutamicum*. Front Microbiol 9:183. https://doi.org/10.3389/fmicb.2018.00183.
59. Tunyasuvunakool K, Adler J, Wu Z, Green T, Zielinski M, Žídek A, Bridgland A, Cowie A, Meyer C, Laydon A, Velankar S, Kleywegt GJ, Bateman A, Evans R, Pritzel A, Figurnov M, Ronneberger O, Bates R, Kohl SAA, Potapenko A, Ballard AJ, Romera-Paredes B, Nikolov S, Jain R, Clancy E, Reiman D, Petersen S, Senior AW, Kavukcuoglu K, Birney E, Kohli P, Jumper J, Hassabis D. 2021. Highly accurate protein structure prediction for the human proteome. Nature 596:590–596. https://doi.org/10.1038/s41586-021-03828-1.
60. Baek M, DiMaio F, Anishchenko I, Dauparas J, Ovchinnikov S, Lee GR, Wang J, Cong Q, Kinch LN, Schaeffer RD, Millan C, Park H, Adams C, Glassman CR, DeGiovanni A, Pereira JH, Rodrigues AV, van Dijk AA, Ebrecht AC, Opperman DJ, Sagmeister T, Buhlheller C, Pavkov-Keller T, Rathinaswamy MK, Dalwadi U, Yip CK, Burke JE, Garcia KC, Grishin NV, Adams PD, Read RJ, Baker D. 2021. Accurate prediction of protein structures and interactions using a three-track neural network. Science 373:871–876. https://doi.org/10.1126/science.abj8754.
61. Mirdita M, Schutze K, Moriwaki Y, Heo L, Ovchinnikov S, Steinegger M. 2022. ColabFold: making protein folding accessible to all. Nat Methods 19:679–682. https://doi.org/10.1038/s41592-022-01488-1.
62. Hegedűs T, Geisler M, Lukács GL, Farkas BJC. 2022. Ins and outs of AlphaFold2 transmembrane protein structure predictions. Cell Mol Life Sci 79:73. https://doi.org/10.1007/s00018-021-04112-1.
63. Mirdita M, Schütze K, Moriwaki Y, Heo L, Ovchinnikov S, Steinegger M. 2021. ColabFold: making protein folding accessible to all. bioRxiv. https://doi.org/10.1101/2021.08.15.456425.
64. Steinegger M, Söding J. 2017. MMseqs2 enables sensitive protein sequence searching for the analysis of massive data sets. Nat Biotechnol 35:1026–1028. https://doi.org/10.1038/nbt.3988.
65. Pettersen EF, Goddard TD, Huang CC, Meng EC, Couch GS, Croll TI, Morris JH, Ferrin T. 2021. UCSF ChimeraX: structure visualization for researchers, educators, and developers. Protein Sci 30:70–82. https://doi.org/10.1002/pro.3943.
66. Hallgren J, Tsirigos KD, Pedersen MD, Armenteros JJA, Marcatili P, Nielsen H, Krogh A, Winther O. 2022. DeepTMHMM predicts alpha and beta transmembrane proteins using deep neural networks. bioRxiv. https://doi.org/10.1101/2022.04.08.487609.

67. Studier FW, Moffatt BA. 1986. Use of bacteriophage T7 RNA polymerase to direct selective high-level expression of cloned genes. J Mol Biol 189:113–130. https://doi.org/10.1016/0022-2836(86)90385-2.
68. Schäfer A, Tauch A, Jäger W, Kalinowski J, Thierbach G, Pühler A. 1994. Small mobilizable multi-purpose cloning vectors derived from the *Escherichia coli* plasmids pK18 and pK19: selection of defined deletions in the chromosome of *Corynebacterium glutamicum*. Gene 145:69–73. https://doi.org/10.1016/0378-1119(94)90324-7.
69. Bussmann M, Baumgart M, Bott M. 2010. RosR (Cg1324), a hydrogen peroxide-sensitive MarR-type transcriptional regulator of *Corynebacterium glutamicum*. J Biol Chem 285:29305–29318. https://doi.org/10.1074/jbc.M110.156372.
70. Cremer J, Eggeling L, Sahm H. 1990. Cloning the *dapA dapB* cluster of the lysine-secreting bacterium *Corynebacterium glutamicum*. Mol Gen Genet 220:478–480. https://doi.org/10.1007/BF00391757.
71. Eikmanns BJ, Kleinertz E, Liebl W, Sahm H. 1991. A family of *Corynebacterium glutamicum*/*Escherichia coli* shuttle vectors for cloning, controlled gene expression, and promoter probing. Gene 102:93–98. https://doi.org/10.1016/0378-1119(91)90545-m.
72. Frunzke J, Engels V, Hasenbein S, Gätgens C, Bott M. 2008. Co-ordinated regulation of gluconate catabolism and glucose uptake in *Corynebacterium glutamicum* by two functionally equivalent transcriptional regulators, GntR1 and GntR2. Mol Microbiol 67:305–322. https://doi.org/10.1111/j.1365-2958.2007.06020.x.

Supplementary information

Characteristics of the GlnH and GlnX signal transduction proteins controlling PknG-mediated phosphorylation of OdhI and 2-oxoglutarate dehydrogenase activity in *Corynebacterium glutamicum*

Lea Sundermeyer[1#], Graziella Bosco[1#], Srushti Gujar[1,2,3], Melanie Brocker[1], Meike Baumgart[1], Dieter Willbold[2,3], Oliver H. Weiergräber[2], Marco Bellinzoni[4], and Michael Bott[1,5]*

[#]Lea Sundermeyer and Graziella Bosco contributed equally to this work.

[1]IBG-1: Biotechnology, Institute of Bio- and Geosciences, Forschungszentrum Jülich, 52425 Jülich, Germany

[2]IBI-7: Structural Biochemistry, Institute of Biological Information Processing, Forschungszentrum Jülich, 52425 Jülich, Germany

[3]Institut für Physikalische Biologie, Heinrich-Heine-Universität Düsseldorf, 40225 Düsseldorf, Germany

[4]Unité de Microbiologie Structurale, Institut Pasteur, CNRS UMR 3528, Université de Paris, Paris, France

[5]Bioeconomy Science Center (BioSC), Forschungszentrum Jülich, 52425 Jülich, Germany

*Corresponding author: email m.bott@fz-juelich.de; phone +49 2461 613294

Running title: GlnH-GlnX-PknG-OdhI-OdhA signal transduction cascade

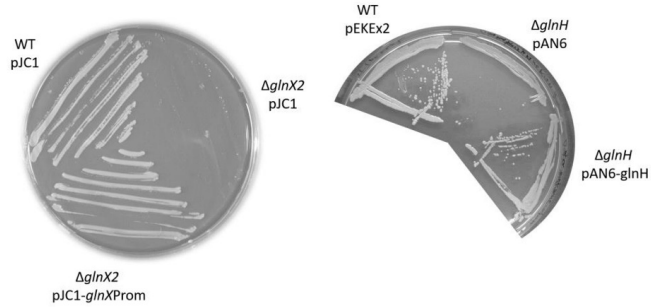

Fig. S1. Complementation of the growth defect on glutamine agar plates of the *C. glutamicum* mutants Δ*glnX2* and Δ*glnH* by plasmid-based expression of *glnX* or *glnH*, respectively.

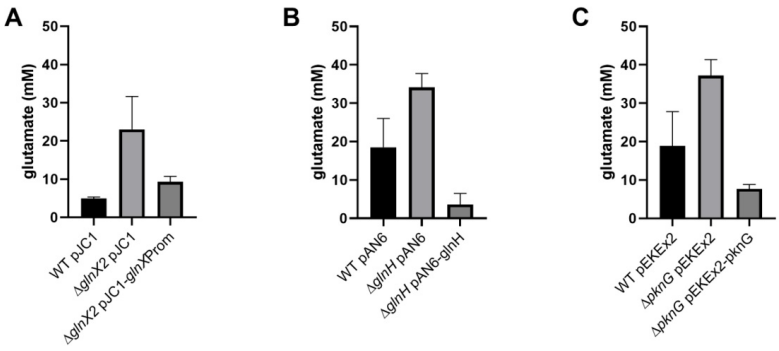

Fig. S2. Glutamate excretion triggered by ethambutol in *C. glutamicum* WT and the mutant strains Δ*pknG*, Δ*glnH*, and Δ*glnX2*. The strains were cultivated in CGXII medium with 4% (w/v) glucose supplemented with 500 mg/l ethambutol and 25 mg/l kanamycin. In experiments B and C, the medium contained 20 µM IPTG in addition. The glutamate concentration in the culture supernatants was measured after 24 h of cultivation. Shown are average values and standard deviations of at least three independent cultivations.

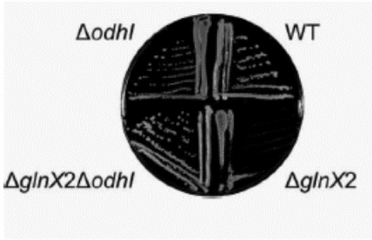

Fig. S3. Growth of the indicated *C. glutamicum* strains on agar plates with L-glutamine as sole carbon and nitrogen source.

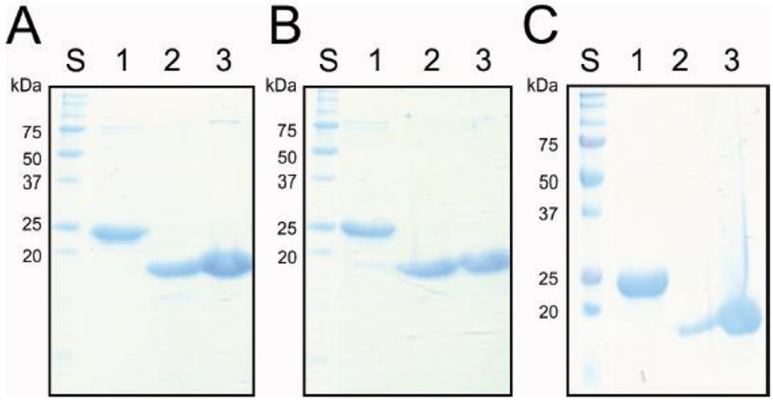

Fig. S4. Purification of OdhI (A), OdhI-R87A (B) and OdhI-R87P (C). The proteins were overproduced in *E. coli* BL21(DE3) using the expression plasmids pET-TEV-odhI, pET-TEV-odhI-R87P und pET-TEV-odhI-R87A and purified by Ni-NTA affinity chromatography (lane 1). Subsequently, the N-terminal His-tag was cleaved off by TEV protease (lane 2) and the buffer was exchanged (lane 3) against buffer B (0.1 M TES/NaOH, pH 7.2; 10 mM $MgCl_2$; 3 mM cysteine; 30% (w/v) glycerol) using PD10 columns for subsequent ODH activity assays. The protein samples were mixed with 6 x SDS loading buffer and analyzed by SDS-PAGE and Coomassie staining.

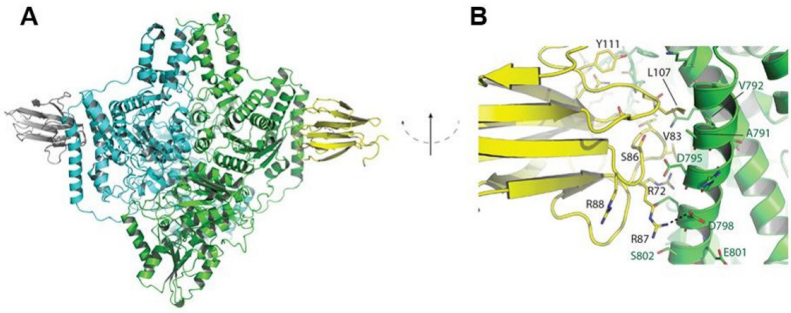

Fig. S5. (a) Cartoon representation of the AlphaFold2 model for the OdhA:OdhI complex, limited to the OdhA E1o domain. The model was generated as a 1:1 complex, and the OdhA E1o dimer was reconstructed by superimposition to the dimeric $KGD_{\Delta 360}$:GarA 2:2 complex (PDB 6I2Q). (b) Zoomed view of the OdhA:OdhI interaction, focusing on the OdhA αE helix.

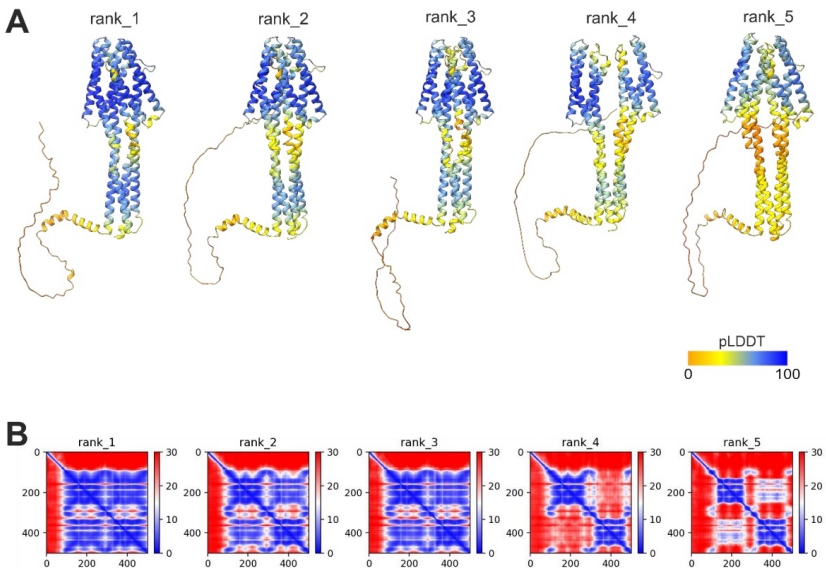

Fig. S6. Individual GlnX models predicted by ColabFold, powered by AlphaFold2. A. The five predicted models for GlnX are coloured according to their respective pLDDT scores. B. Heat maps of PAE (predicted aligned error) values for each model depicting the per-residue position confidence (adopted from ColabFold run output). The overall confidence of the models is based on both pLDDT and PAE values.

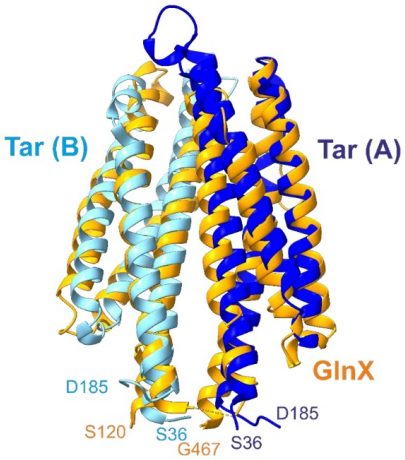

Fig. S7. Superimposition of GlnX with the Tar chemoreceptor. The predicted GlnX periplasmic tandem 4HB (orange) and the dimeric periplasmic domain of Tar from *Escherichia coli* (chain A, blue; chain B, cyan; PDB code 4Z9J) share a similar overall architecture.

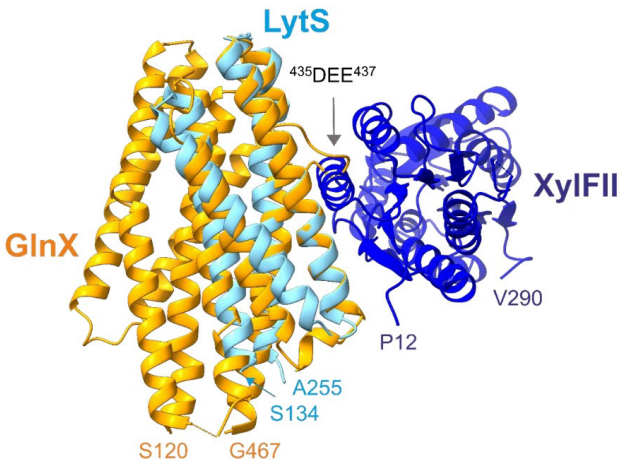

Fig. S8. Superimposition of GlnX with the LytS-XylFII complex (PDB code 5XSJ). Alignment of LytS (cyan) with the second 4HB module of GlnX (orange) places the periplasmic binding protein XylFII (blue) close to the acidic protrusion of GlnX helix H4'.

2.2 Polar localization of regulatory proteins and TCA cycle components in an actinobacterium

Lea Sundermeyer, Jan-Gerrit Folkerts, Benita Lückel, Bastian Wollenhaupt, Christina Mack, Meike Baumgart, Dietrich Kohlheyer, and Michael Bott (2022). – to be submitted

Author contributions:

- LS constructed deletion and integration strains, designed and performed microscopy and microfluidic experiments, analyzed the data, prepared all figures and drafted an initial version of the manuscript.
- JGF performed the microscopy experiments analyzing the OdhI localization in different strain backgrounds and analyzed the data. Figures 1, 3, 4, and 5 resulted from these experiments.
- BL performed the microscopy experiments analyzing the localization of PDH-ODH complex components and analyzed the data. Figures 5, 6, and 7 resulted from these experiments.
- BW designed and performed microfluidics experiments. Figure 2 resulted from these experiments.
- CM constructed integration strains.
- JGF, BL, and CM were supervised by LS, LS was supervised by MBa and MBo, BW was supervised by DK.
- MBo developed the overall concept of this study, analyzed the data, and was responsible for writing the final version of the manuscript.

Overall contribution LS: 50%

Polar localization of regulatory proteins and TCA cycle components in an actinobacterium

Lea Sundermeyer[1], Jan-Gerrit Folkerts[1], Benita Lückel[1], Bastian Wollenhaupt[1], Christina Mack[1], Meike Baumgart[1], Dietrich Kohlheyer[1] and Michael Bott[1,2*]

[1]IBG-1: Biotechnology, Institute of Bio- and Geosciences, Forschungszentrum Jülich, 52425 Jülich, Germany
[2]Bioeconomy Science Center (BioSC), Forschungszentrum Jülich, 52425 Jülich, Germany

*Corresponding author
Email m.bott@fz-juelich.de
Phone +49 2461 613294

ABSTRACT

The 2-oxoglutarate dehydrogenase (ODH) is a key enzyme of the TCA cycle. In several actinobacteria such as *Corynebacterium glutamicum*, it is not present as an independent dehydrogenase but part of a PDH-ODH hybrid complex. The activity of the ODH is regulated by binding of the small FHA domain containing protein OdhI. In its unphosphorylated state OdhI binds to the OdhA subunit thereby inhibiting ODH activity. To get further insights into the cellular function of OdhI we analyzed the intracellular localization of OdhI and other proteins. Here we observed a polar localization of an OdhI-mVenus fusion protein in *C. glutamicum* and this localization was also true for the *M. tuberculosis* OdhI homolog GarA expressed in *C. glutamicum*. We analyzed the influence of different OdhI interaction partners using respective deletion strains and found that the polar localization of OdhI is caused by interaction of the unphosphorylated OdhI with OdhA. We further showed that not only OdhA but also the entire PDH-ODH hybrid complex localizes at the cell poles. In addition, a positive correlation between cell size and number of fluorescent spots per cell and the localization at the cell poles and the division sites indicates a possible connection of the PDH-ODH complex to cell division processes.

KEYWORDS

Corynebacterium glutamicum, 2-oxoglutarate dehydrogenase, pyruvate dehydrogenase, ODH inhibitory protein

INTRODUCTION

Actinobacteria form a large and diverse bacterial phylum (1) including human pathogens such as *Mycobacterium tuberculosis* and *Corynebacterium diphtheriae* as well as biotechnologically important members such as antibiotics-producing *Streptomyces* species (2) or the amino acid producer *Corynebacterium glutamicum* (3-5). Therefore, actinobacterial metabolism and its regulation are subjects of ongoing research to identify novel targets for the treatment of the pathogens and new features to improve the biotechnological producer strains and production processes. The central carbon metabolism provides energy and precursors for biomass formation and is in principle highly conserved, but previous studies have uncovered some unique features in the regulation and structural organization of the pyruvate and 2-oxoglutarate dehydrogenase complexes (PDH and ODH) in actinobacteria.

PDH and ODH are key enzymes in central carbon metabolism catalyzing the oxidative decarboxylation of the 2-ketoacids pyruvate and 2-oxoglutarate to acetyl-CoA and succinyl-CoA, respectively, with concomitant reduction of NAD^+ to NADH. They typically consist of three different subunits each, the pyruvate decarboxylase (E1p) and the 2-oxoglutarate decarboxylase (E1o), a dihydrolipoyl transacetylase (E2p) or transsuccinylase (E2o), and the shared dihydrolipoyl dehydrogenase (E3). In the native state, PDH and ODH form very large complexes (~10 MDa) with a core made of the E2 component. *C. glutamicum* and other actinobacteria do not possess a separate E2o subunit. Rather, the succinyl transferase domain of E2o is fused to the E1o subunit (6, 7). Since this unusual E1o component only possesses the succinyl transferase domain but lacks the lipoyl-binding domains of E2o, an interaction of corynebacterial E1o with E2p is necessary, because the transfer of the succinyl group to coenzyme A (CoA) requires the lipoic acid residues. In fact, purification of a Strep-tagged variant of E1o from *C. glutamicum* revealed co-purification with E2p (AceF), E1p (AceE), and E3 (Lpd) and, vice versa, purification of a Strep-tagged variant of E1p showed co-purification with E1o, E2p, and E3 (8). Subsequent studies confirmed that the succinyl transferase domain of E1o uses the lipoyl groups of E2p to transfer the succinyl group to CoA (9). The existence of a PDH-ODH hybrid complex was also observed in a recent study showing that the PDH and ODH complexes of *C. glutamicum* are much smaller in size than the corresponding *Escherichia coli* complexes (10). This difference in size is presumably caused by a structural feature of the E2 subunit (11). The E2 subunits of most species form homo-trimers that further oligomerize by intermolecular trimer-trimer interactions mediated by a conserved C-terminal 3_{10}-hydrophobic helix, leading to the assembly of eight or even 20 trimers, depending on the

species. The E2p protein of *C. glutamicum* also forms trimers, but a unique C-terminal helix bearing an actinobacteria-specific insertion precludes larger protein oligomerization (11).

The ODH activity of *C. glutamicum* is regulated by post-translational modification of the small forkhead-associated (FHA) domain-containing protein OdhI (8). OdhI binds with nM affinity to the C-terminal 2-oxoglutarate decarboxylase domain of the E1o subunit and inhibits ODH activity with an apparent K_i of 2.4 nM (8, 12, 13). The importance of OdhI for shifting carbon flux at the 2-oxoglutarate node towards L-glutamate synthesis and thus nitrogen assimilation by the NADPH-dependent glutamate dehydrogenase was demonstrated by the fact that an *odhI* deletion mutant of *C. glutamicum* almost completely lost its ability for L-glutamate production (14). Inhibition of ODH activity by OdhI is reversible and controlled by covalent modification of OdhI (8, 12, 13). Phosphorylation of the N-terminal Thr-14 residue of OdhI by the serine/threonine protein kinase PknG leads to a conformational change of OdhI and thereby prevents its binding to OdhA (15). Dephosphorylation by the phospho-serine/threonine protein phosphatase Ppp leads to a reactivation of OdhI (14). OdhI can also be phosphorylated by the three other serine/threonine protein kinases (STPK) present in *C. glutamicum*, PknA, PknB and PknL, at least *in vitro* (16). *In vivo*, besides unphosphorylated and monophosphorylated OdhI, also diphosphorylated OdhI was detected (8, 16) and PknB was shown to phosphorylate OdhI on Thr-15 (15).

The mycobacterial OdhI homolog GarA has not only an inhibitory effect on ODH, but also on the NADH-dependent glutamate dehydrogenase (GDH), while glutamate synthase (GS) was activated by GarA binding in *in vitro* assays (17-19). Mutant studies suggest that the NADH-dependent GDH is required for the utilization of L-glutamate as nitrogen and carbon source (20). These and further studies underline the importance of the regulation of carbon flux at the 2-oxoglutarate node by GarA in *Mycobacterium.*

As the function of OdhI and GarA is determined by their phosphorylation status, it is important to understand the signals that control phosphorylation and dephosphorylation of these proteins. Whereas the control of the phosphatase (Ppp in *Corynebacterium*, PstP in *Mycobacterium*) is still unknown, PknB has been implicated in the regulation of peptidoglycan biosynthesis (reviewed by (21)). Initial experiments on a *pknG* deletion mutant of *M. tuberculosis* revealed the accumulation of glutamate and glutamine, leading to the proposal that PknG mediates the transfer of signals sensing nutritional stress in *M. tuberculosis* and translates them into metabolic adaptation (22). Studies of a *pknG* deletion mutant of *C. glutamicum* revealed a two-fold increased cellular L-glutamate level and a growth defect on agar plates containing L-glutamine as sole carbon and nitrogen source, which is caused by the

inhibition of ODH activity by unphosphorylated OdhI (8). Interestingly, the defect in glutamine utilization was observed not only for the Δ*pknG* mutant, but also for Δ*glnX* and Δ*glnH* mutants. The genes *glnX* and *glnH* are located immediately upstream of the *pknG* gene and encode an integral membrane protein and periplasmic binding protein. The same phenotype of the three mutants clearly suggested that GlnH and GlnX are part of a signal transduction cascade controlling PknG activity in dependence of extracellular amino acids (8). Studies with the GlnH protein of *M. tuberculosis*, including crystal structures, revealed that it binds L-aspartate and L-glutamate with high affinity (K_D of 5 µM and 15 µM, respectively), whereas the GlnH protein of *C. glutamicum* has an about 100-fold lower affinity for these amino acids (23). The involvement of GlnH and GlnX in the control of OdhI phosphorylation was recently confirmed in *C. glutamicum* by showing an increased OdhI phosphorylation level and increased glutamate secretion in Δ*glnH* and Δ*glnX* mutants and by characterizing Δ*glnX* suppressor mutants (24). Studies on the GlnX protein confirmed the predicted topology with four transmembrane helices, two large periplasmic domains, and N- and C-terminus in the cytoplasm. A structural model of GlnX suggested that both periplasmic domains form four-helix bundles and represent a new type of four-helix bundle proteins with a tandem arrangement (24).

To gain further insights into the cellular function of OdhI we analyzed its intracellular localization in this study and elucidated a novel exciting feature related to OdhI and the ODH complex. When analyzing the cellular distribution of an OdhI-mVenus fusion protein by fluorescence microscopy, we discovered strongly fluorescent spots at the cell poles and, when present, at division sites. This localization was only observed for unphosphorylated OdhI, as a Δ*ppp* mutant lacking the phosphatase and containing only phosphorylated OdhI showed an equal distribution of OdhI-mVenus fluorescence throughout the cytoplasm. Further experiments revealed that the fluorescent spots were dependent on the presence of OdhA and that an OdhA-mCherry fusion protein co-localized with OdhI-mVenus. The same localization was also observed for fluorescent versions of the other subunits of the PDH-ODH hybrid complex, AceE, AceF, and Lpd. Thus, we observed for the first time in bacteria a polar localization of a TCA cycle enzyme. The physiological relevance of this localization will be discussed.

RESULTS

Localization of plasmid-encoded OdhI-mVenus in *C. glutamicum* Δ*odhI*. To test the cellular localization of OdhI, we constructed the expression plasmid pPREx2-*odhI-mVenus* coding for a C-terminal fusion protein of OdhI with the yellow fluorescent protein mVenus and

analyzed the localization of the fusion protein in *C. glutamicum* Δ*odhI* by fluorescence microscopy. The *odhI* deletion strain was chosen to prevent competing effects between native OdhI and the OdhI-mVenus fusion protein. The cell membranes were stained using the fluorescent dye Nile red to allow a better differentiation between the individual cells. Surprisingly, cells expressing *odhI-mVenus* showed bright fluorescent spots located at the cell poles and in some cells at the division site in addition to a weak fluorescence that was equally distributed within the entire cytoplasm (Fig. 1A). As controls, we also analyzed the fluorescence of *C. glutamicum* Δ*odhI* carrying the empty plasmid pPREx2 as well as expression plasmid pPREx2-*mVenus* to exclude *C. glutamicum* autofluorescence or artefacts caused by the fluorescent protein itself. As expected, no yellow fluorescence signal was detected for *C. glutamicum* Δ*odhI* pPREx2 cells and expression of *mVenus* alone led to a strong, evenly distributed fluorescence in the entire cell (Fig. 1A), showing that the fluorescent spots observed in *C. glutamicum* Δ*odhI* pPREx2-*odhI-mVenus* are indeed caused by the tagged OdhI protein. A statistical analysis of 100 *C. glutamicum* Δ*odhI* pPREx2-*odhI-mVenus* cells revealed that the majority of the cells (61%) possessed two fluorescent spots, mostly located at the cell poles, while in 22% of the cells only one spot was visible and 17% showed a third fluorescent spot, which was often located at the division site (Fig. 1B). The cells showed the typical rod-shape morphology of *C. glutamicum* and possessed a mean length of 1.84 ± 0.38 µm. The number of OdhI-mVenus fluorescent spots positively correlated with the cell length, with longer cells possessing more fluorescent spots (Fig. 1C). This clear formation of OdhI-mVenus spots at the cell poles was rather unexpected and in the following, we tried to find out what causes this localization.

Localization of genomically encoded OdhI-mVenus. In the first experiments, we used plasmid-based expression of *odhI-mVenus* to analyze the intracellular localization. This approach has the benefit that it allows relatively fast tests for OdhI-mVenus localization in different strain backgrounds. However, as expression is driven from the P_{tac} promoter of the pPREx2 plasmid (25), the number of OdhI-mVenus proteins can strongly differ from the physiological OdhI numbers due to the copy number of the plasmid and the promotor strength. To exclude that the observed spot formation of OdhI-mVenus is an artifact of the plasmid-based expression, we constructed a *C. glutamicum::odhI-mVenus* integration strain allowing the expression of *odhI-mVenus* at the native level. As in the case of plasmid-based expression, intense OdhI-mVenus fluorescent spots were observed at the cell poles and division sites of the integration strain (Fig. 1D).

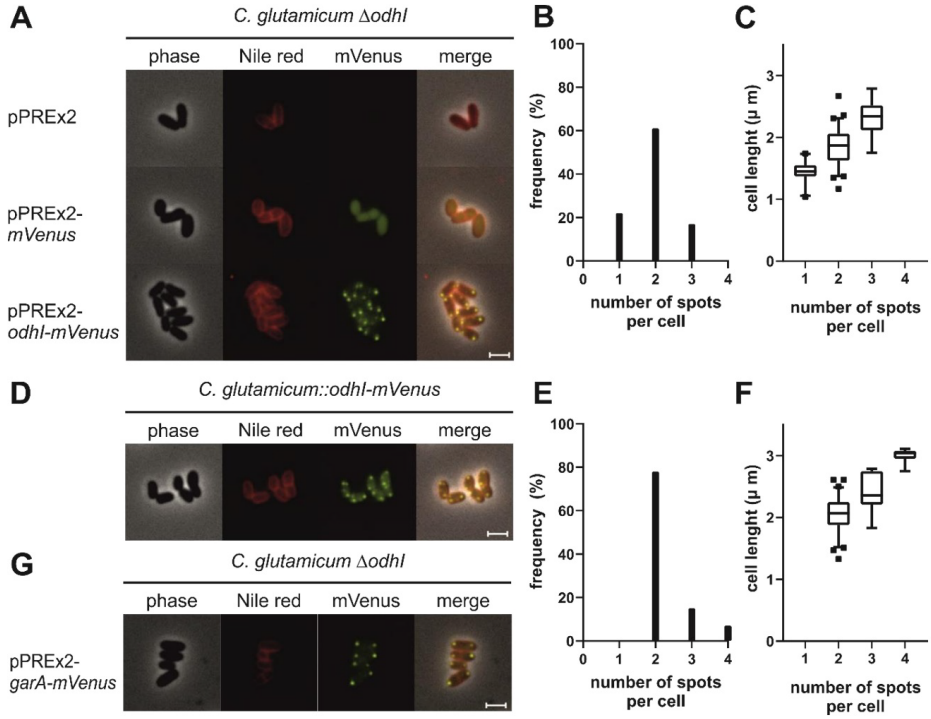

Fig. 1 Intracellular localization of OdhI-mVenus in *C. glutamicum*. (A) Exemplary images of *C. glutamicum* Δ*odhI* cells carrying the plasmids pPREx2-*odhI-mVenus*, pPREx2-*mVenus* and pPREx2. (B) Frequency of number of fluorescent spots per cell detected in *C. glutamicum* Δ*odhI* pPREx2-*odhI-mVenus*. (C) Correlation between the number of spots per cell from B and the length of the respective cell. (D) Exemplary images of OdhI-mVenus localization in a *C. glutamicum::odhI-mVenus* integration strain. (E) Frequency of number of fluorescent spots per cell detected in *C. glutamicum::odhI-mVenus*. (F) Correlation between the number of spots per cell from E and the length of the respective cell. (G) Exemplary images showing the localization of the OdhI homolog GarA in *C. glutamicum* Δ*odhI* pPREx2-*garA-mVenus*. The *C. glutamicum* strains were grown in CGXII medium with 2 % (w/v) glucose. Cell membranes were stained using Nile red and images were taken using an Axio imager M2 microscope. Scale bars in A, D and G represent 2 µm. The line shown in C and F represents the median and the box the 25 to 75 percentile. The whiskers reach from 5 to 95 percentile. The results are obtained by analysis of one hundred cells.

Remarkably, the fluorescence intensity of these spots appeared even stronger compared to the uninduced plasmid-based expression (Fig. 1D), suggesting that the native *odhI* promoter is rather strong. A statistical analysis showed again that the majority of the cells contained two fluorescent spots (78 %) and the residual cells possessed three or four spots. The lack of cells with a single spot might be due to the different expression levels. The number of spots per cell again correlated positively with the cell length (Fig. 1E and F). The increase in mean cell length of 2.17 ± 0.38 compared to *C. glutamicum* Δ*odhI* pPREx2-*odhI-mVenus* (1.84 ± 0.38 µm) might be caused by the differences in expression and the presence of antibiotic kanamycin in the

plasmid-carrying strain. Taken together, these experiments confirmed the formation of fluorescent OdhI-mVenus spots at the cell poles and at the division site at physiological expression levels and showed that pPREx2-based expression is a suitable approach to study the localization of OdhI-mVenus in different strain backgrounds.

Localization of the OdhI ortholog GarA in *C. glutamicum*. As outlined in the introduction, OdhI and its mycobacterial ortholog GarA share strong functional similarities (7). Therefore, we were interested to test if GarA behaves like OdhI with respect to its intracellular localization. When analyzing strain *C. glutamicum* Δ*odhI* transformed with the expression plasmid pPREx2-*garA-mVenus* by fluorescence microcopy, also the GarA-mVenus fusion protein formed fluorescent spots at cell poles (Fig. 1G), suggesting that the interaction partner responsible for the specific localization of OdhI also interacts with GarA.

Localization of OdhI-mVenus throughout the entire cell cycle. In order to test whether OdhI localization is static or dynamic, a microfluidics experiment was performed enabling to follow the localization of the OdhI-mVenus fluorescent spots throughout the cell cycle (26). The microfluidics cultivation of *C. glutamicum::odhI-mVenus* took place in a mother machine cultivation device which allows only linear, one-dimensional growth if the cells are located correctly inside the growth channels (27). Unfortunately, only very few cells entered the channel and in most cases these cells did not grow, therefore the behavior of OdhI-mVenus spots during the cell cycle was analyzed for a few cells trapped close to the entrance of a cultivation channel. As shown in Fig. 2, new OdhI-mVenus spots seem to occur at the future division site and localize at the new cell poles after cell division. The intensity of the polar fluorescent spots changes during cell cycle, but further analysis is necessary to conclude if this is caused by localization of different amounts of fluorescent protein at different cell cycle steps or if it is just an artifact of an altered orientation of the cell in the cultivation channel.

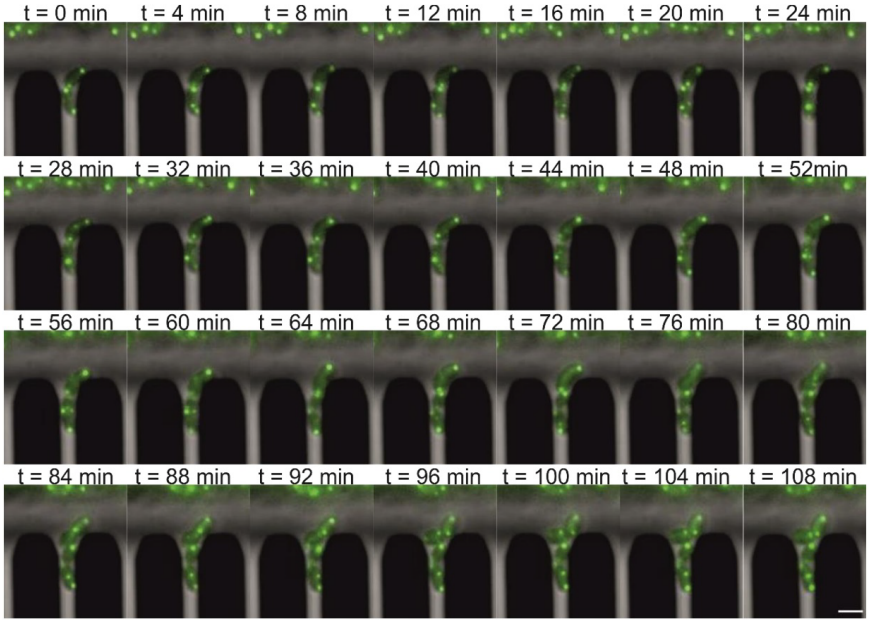

Fig. 2 Analysis of OdhI-mVenus localization during cell cycle using microfluidic cultivation. *C. glutamicum::odhI-mVenus* was cultivated in CGXII medium with 2% (w/v) glucose in a microfluidic mother machine cultivation device. Time-lapse images of every 4 min are shown. Scale bar represents 2 µm.

Influence of PknG on OdhI-mVenus spot formation. Since the phosphorylation status of OdhI is essential for its regulatory function on ODH activity we analyzed if the observed localization depends on the phosphorylation. As PknG is known to be the most important kinase responsible for OdhI phosphorylation (16), we tested if the absence of PknG influences OdhI localization. Plasmid-based expression of *odhI-mVenus* in the double deletion strain *C. glutamicum* Δ*pknG*Δ*odhI* led to the formation of fluorescent spots (Fig. 3A) as observed for the expression of the same fusion protein in the *odhI* deletion strain (Fig. 1A). With 58% of the analyzed cells containing two fluorescent spots and 24% and 15% containing one or three spots (data not shown), respectively, the number of spots was also very similar to the result obtained for the Δ*odhI* strain (Fig. 1B). In addition, a positive correlation between the number of spots per cell and the cell length was observed again and the median cell length was also almost the same for the double deletion strain (1.87 ± 0.41 µm) as for the Δ*odhI* strain (1.84 ± 0.38 µm). These results indicate that PknG is not required for the formation of OdhI-mVenus spots.

Influence of other STPKs on OdhI-mVenus spot formation. The striking localization of OdhI at the cell poles and the division site suggested the responsible interaction partner might

be involved in the cell division process. The STPKs PknA and PknB, which are able to phosphorylate OdhI (15, 16), are membrane-bound enzymes and involved in the regulation of peptidoglycan synthesis (28, 29). In *C. glutamicum*, peptidoglycan synthesis takes place at the cell poles and the septum (30), making the membrane-bound STPKs interesting candidates for triggering localization of OdhI at these sites. We therefore investigated the localization of plasmid-encoded OdhI-mVenus in the deletion strains *C. glutamicum* Δ*pknA*Δ*pknL*Δ*pknG* (Δ*pknALG*) and *C. glutamicum* Δ*pknB*Δ*pknL*Δ*pknG* (Δ*pknBLG*). A simultaneous deletion of *pknA* and *pknB* in *C. glutamicum* seems to be lethal (16). As the triple deletion strains still possess the genomic *odhI* gene, we used *C. glutamicum* wt pPREx2-*odhI-mVenus* as a control. Expression of *odhI-mVenus* led to formation of fluorescent spots both in the mutant strains and in the wt (Fig. 3B). While the wt possessed mainly two spots per cell (57%) and showed a mean cell length of 1.83 ± 0.40 µm, comparable with the results obtained with the Δ*odhI* mutant, strain Δ*pknALG* showed a shift towards a prolonged cell length (2.15 ± 0.44 µm) and an increased number of spots per cell. These effects were even more prominent in the Δ*pknBLG* strain (2.30 ± 0.55 µm) (Fig. 3C and D). Again, a positive correlation between cell length and number of spots per cell was observed (Fig. 3E and F). Although at least one kinase is still present in the triple deletion mutants, the results suggest that the STPKs are not the interaction partner required for the spot formation of OdhI-mVenus.

Influence of the phosphatase Ppp on OdhI-mVenus spot formation. Since the absence of the STPKs did not prevent the fluorescent spot formation by OdhI-mVenus, we then tested the influence of the absence of the membrane bound serine-threonine protein phosphatase Ppp. This enzyme is known to dephosphorylate OdhI (16), meaning that in a *C. glutamicum* Δ*ppp* strain almost only phosphorylated OdhI is present. The deletion of *ppp* causes a strong alteration of the cell morphology with rounded as well as prolonged cells (16). In the majority of cells analyzed here, expression of *odhI-mVenus* led to an equally distributed fluorescence signal and brighter fluorescent spots were only visible in ~14% of the cells. In this cell fraction, the number of spots per cell varied between one and four and no specific localization was visible (Fig. 3G). These findings strongly suggest the fluorescent spots are formed by unphosphorylated OdhI, but not by phosphorylated OdhI.

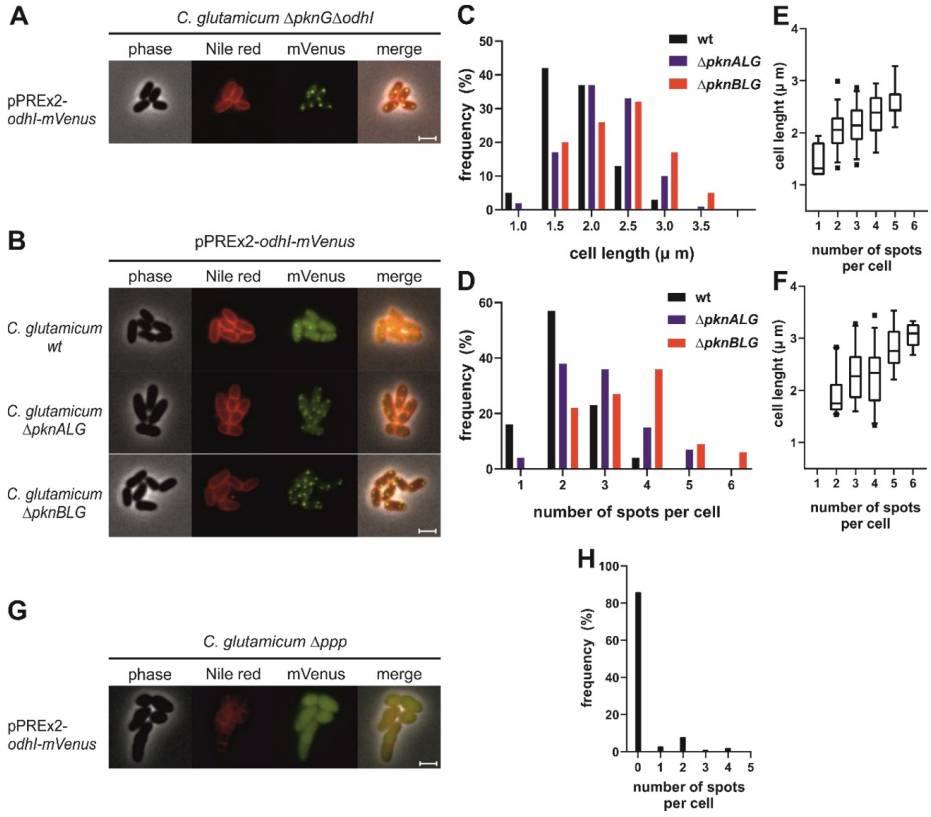

Fig. 3 Influence of Ser/Thr protein kinases and of the phosphatase Ppp on the intracellular localization of OdhI-mVenus in *C. glutamicum*. (A) Exemplary images of *C. glutamicum* Δ*pknG*Δ*odhI* pPREx2-*odhI-mVenus*. (B) Exemplary images of *C. glutamicum* wt, Δ*pknALG* and Δ*pknBLG* carrying the expression plasmid pPREx2-*odhI-mVenus*. (C) Overview on the altered cell length of *C. glutamicum* Δ*pknALG* and Δ*pknBLG* compared to the wt. (D) Frequency of number of fluorescent spots per cell detected in *C. glutamicum* wt, Δ*pknALG* and Δ*pknBLG*. (E) and (F) Correlation between the number of spots per cell and the length of the respective cell. Results of in *C. glutamicum* Δ*pknALG* are shown in E and results of *C. glutamicum* Δ*pknBLG* are shown in F. (G) Exemplary images of *C. glutamicum* Δ*ppp* pPREx2-*odhI-mVenus*. (H) Frequency of number of fluorescent spots per cell in *C. glutamicum* Δ*ppp* pPREx2-*odhI-mVenus*. All strains were grown in CGXII medium with 2 % (w/v) glucose. Cell membranes were stained using Nile red and images were taken using an Axio imager M2 microscope. Scale bars in A, B and G represent 2 µm. The line shown in E and F represents the median and the box the 25 to 75 percentile. The whiskers reach from 5 to 95 percentile. The results were obtained by analysis of one hundred cells per strain.

Influence of OdhA on OdhI-mVenus spot formation. The results described above suggested that none of the STPKs is responsible for the polar localization of OdhI and that unphosphorylated OdhI causes the spots. Therefore, the only known candidate that binds unphosphorylated OdhI remained OdhA. OdhA is a component of the PDH-ODH hybrid complex, which we initially considered unlikely to be located at the poles, as it seems to be the

first time that a specific localization in the bacterial cell has been reported for enzymes of the central metabolism. However, when analyzing a *C. glutamicum* Δ*odhA* pPREx2-*odhI-mVenus* strain, the cells showed an equally distributed fluorescence signal without formation of fluorescent spots at the poles or at the division site (Fig. 4). This surprising result suggested that indeed OdhA is required for the observed specific localization of OdhI.

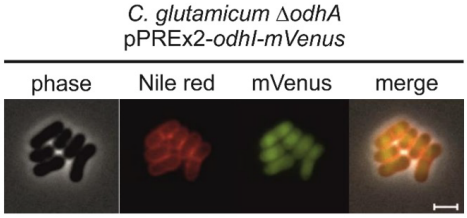

Fig. 4 Localization of OdhI-mVenus in *C. glutamicum* Δ*odhA*. Exemplary images of *C. glutamicum* Δ*odhA* cells carrying the pPREx2-*odhI-mVenus* plasmid grown in CGXII medium with 2 % (w/v) glucose. Cell membranes were stained using Nile red and images were taken using an Axio imager M2 microscope. Scale bar represents 2 µm.

Localization of OdhA and co-localization with OdhI. To confirm that the interaction with OdhA is required for the formation of the OdhI-mVenus fluorescent spots at the cell poles and the division sites, we analyzed the localization of OdhA. We constructed the expression plasmid pPREx2-*odhA-mCherry* coding for OdhA with C-terminal fusion to the red fluorescent protein mCherry and analyzed the localization of the fusion protein in *C. glutamicum* Δ*odhA* by fluorescence microscopy. Due to the use of a red fluorescent protein, membrane staining using Nile red was not possible in this experiment, but the cells could still be distinguished from each other. Similar to the results obtained for OdhI-mVenus, cells expressing *odhA-mCherry* showed bright fluorescent spots located at the cell poles (Fig. 5A). As controls, we also analyzed the fluorescence of *C. glutamicum* Δ*odhA* carrying the expression plasmid pPREx2-*mCherry* to exclude artefacts caused by the fluorescent protein itself. As expected, expression of *mCherry* alone led to a strong, evenly distributed fluorescence in the entire cell (Fig. 5A), showing that the fluorescent spots observed in *C. glutamicum* Δ*odhA* pPREx2-*odhA-mCherry* are indeed caused by the tagged OdhA protein.

Furthermore, we analyzed the co-localization of OdhI and OdhA. For this purpose we constructed a *C. glutamicum::odhA-mVenus* integration strain and a pPREx2-based plasmid coding for an OdhI-mCherry fusion protein and analyzed the localization of OdhI and OdhA in *C. glutamicum::odhA-mVenus* pPREx2-*odhI-mCherry* and *C. glutamicum::odhI-mVenus* pPREx2-*odhA-mCherry* using fluorescence microscopy. Both strains possessed mCherry and

mVenus fluorescent spots, which showed co-localization and were mostly located at the cell poles (Fig. 5B and C). This result suggested that OdhI is located at the cell poles due to its interaction with OdhA.

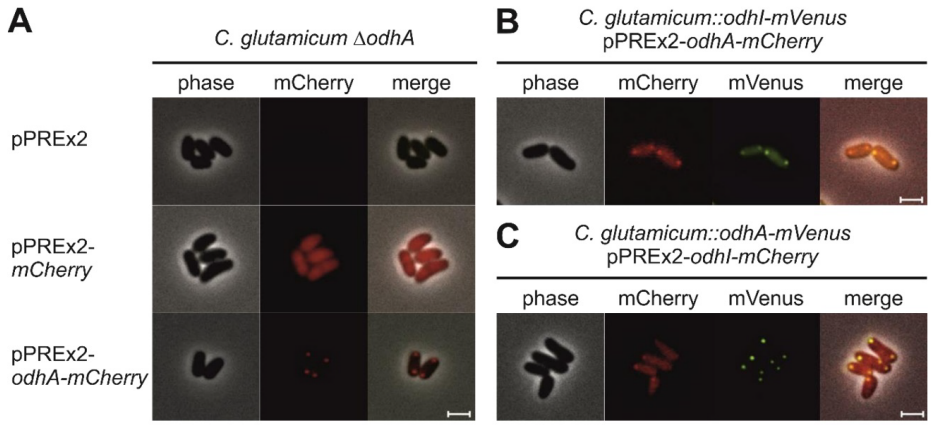

Fig. 5 Localization of OdhA-mCherry and co-localization of OdhI and OdhA. (A) Exemplary images of *C. glutamicum* Δ*odhA* cells carrying the plasmids pPREx2-*odhA-mCherry*, pPREx2-*mCherry* and pPREx2. (B) Exemplary images of *C. glutamicum::odhI-mVenus* pPREx2-*odhA-mCherry*. (C) Exemplary images of *C. glutamicum::odhA-mVenus* pPREx2-*odhI-mCherry*. The *C. glutamicum* strains were grown in CGXII medium with 2 % (w/v) glucose and images were taken using an Axio imager M2 microscope. Scale bars represent 2 µm.

Localization of other interaction partners of OdhA. As OdhA is part of the PDH-ODH hybrid complex, we next studied if the other proteins of this complex, AceE, AceF, and Lpd also show a polar localization or if the OdhA spots are due to excess OdhA interacting with a so far unknown protein. Construction of pPREx2-based expression plasmids coding for C-terminal fusions of AceE and AceF with mVenus and an N-terminal fusion of Lpd with mVenus enabled the analysis of the localization of these proteins by fluorescence microscopy. As shown in Fig. 6A all three fusion proteins led to the formation of fluorescent spots in *C. glutamicum* wt, which mostly localized at the cell poles or at the division site as it was the case for OdhA and OdhI. Notably, the fluorescence signal in general was very heterogeneous and many cells did not show a fluorescence signal at all, suggesting that the fusion constructs might be harmful for the cells under the tested conditions and the fluorescent proteins might affect correct assembly of a functional PDH-ODH complex.

To further prove the localization of the entire PDH-ODH complex at the cell poles we analyzed their co-localization using *C. glutamicum::odhA-mVenus* pPREx2-*aceE-mCherry* and *C. glutamicum::odhA-mVenus* pPREx2-*aceF-mCherry*. As shown in Fig. 6B, the OdhA-mVenus spots co-localized with both the AceE-mCherry and the AceF-mCherry spots. In

addition, we investigated if either OdhA or AceE are responsible for the polar localization of the complex and tested the localization of AceF and AceE or AceF and OdhA in *C. glutamicum* Δ*odhA* or Δ*aceE* deletion strains, respectively. The deletion of neither *odhA* nor *aceE* prevented the formation of fluorescent spots by the fluorescence-tagged proteins (Fig. 6C and D), indicating that their localization is not dependent on OdhA or AceE.

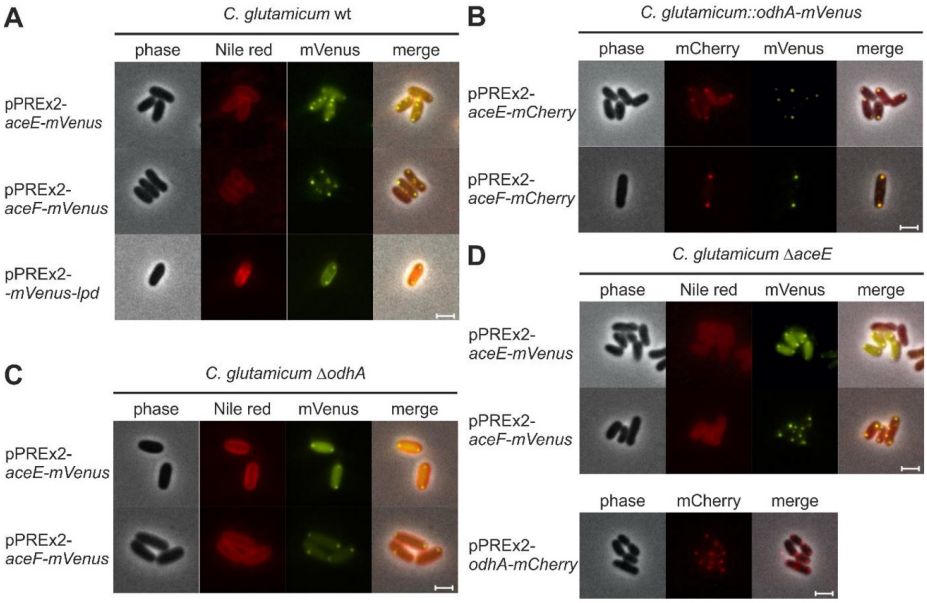

Fig. 6 Localization of the PDH-ODH complex components in *C. glutamicum*. (A) Exemplary images of *C. glutamicum* wt cells carrying the expression plasmids pPREx2-*aceE-mVenus*, pPREx2-*aceF-mVenus* and pPREx2-*mVenus-lpd*. (B) Exemplary images of *C. glutamicum*::*odhA-mVenus* pPREx2-*aceF-mcherry* and *C. glutamicum*::*odhA-mVenus* pPREx2-*aceE-mcherry*. (C) Exemplary images of *C. glutamicum* Δ*odhA* cells carrying the plasmids pPREx2-*aceF-mVenus* and pPREx2-*aceE-mVenus*. (D) Exemplary images of *C. glutamicum* Δ*aceE* cells carrying the plasmids pPREx2-*aceF-mVenus*, pPREx2-*aceE-mVenus* and pPREx2-*odhA-mCherry*. All were grown in CGXII medium with 2 % (w/v) glucose. In case of *C. glutamicum* Δ*aceE* the medium was supplemented with 2 g L^{-1} acetate. If indicated membranes were stained using Nile red and images were taken using an Axio imager M2 microscope. Scale bars represent 2 µm.

Localization of isocitrate dehydrogenase and glutamate dehydrogenase. The specific intracellular localization for the PDH-ODH hybrid complex triggered the question whether an even larger assembly of TCA cycle and ammonium assimilation enzymes exists. The enzymes catalyzing the synthesis of 2-oxoglutarate and its reductive amination to L-glutamate, isocitrate dehydrogenase (Icd) and glutamate dehydrogenase (GDH), were selected to get a first suggestion if other enzymes involved in these processes also show a specific localization. Therefore, we constructed the expression plasmids pPREx2-*mVenus-icd* and pPREx2-*mVenus-*

gdh, coding for N-terminal fusions of Icd or GDH with mVenus, and analyzed the intracellular localization in *C. glutamicum* wt and, in case of the GDH construct, additionally in a *gdh* deletion strain. As shown in Fig. 7, both mVenus-Icd and mVenus-GDH produced uniform fluorescence signals in the cytoplasm, suggesting that the localization at the poles and at the division site is a specific characteristic of the PDH-ODH hybrid complex.

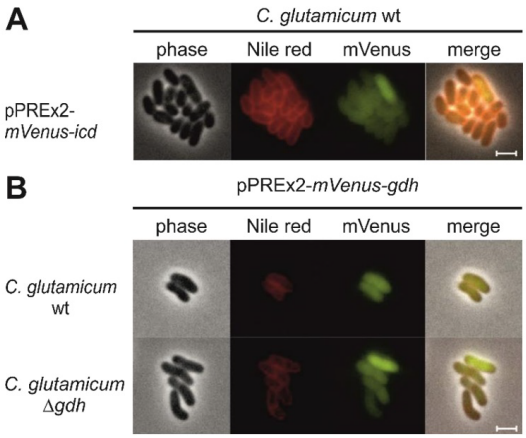

Fig. 7 Localization of isocitrate dehydrogenase and glutamate dehydrogenase in *C. glutamicum*. (A) Exemplary images of *C. glutamicum* pPREx2-*mVenus-icd*. (B) Exemplary images of *C. glutamicum* pPREx2-*mVenus-gdh* and *C. glutamicum* Δ*gdh* pPREx2-*mVenus-gdh*. Cells were grown in CGXII medium with 2 % (w/v) glucose. Cell membranes were stained using Nile red and images were taken using an Axio imager M2 microscope. Scale bars represent 2 µm.

DISCUSSION

Here we analyzed the intracellular localization of the OdhI protein, which is responsible for the regulation of the ODH activity in *C. glutamicum*, and observed a surprising formation of bright fluorescent spots at the cell poles and sometimes also at the division site. This spot formation was visible for plasmid-based expression as well as in a *C. glutamicum::odhI-mVenus* integration strain (Fig. 1), showing that the spots are not caused by inclusion body formation due to overexpression or as an artefact of the plasmid based expression. Besides the bright fluorescent spots, cells expressing *odhI-mVenus* possessed a weak fluorescence signal evenly distributed in the cell (Fig. 1). This suggests that maybe only a portion of the OdhI-mVenus protein builds the fluorescent spots while the other portion of the small protein is spread throughout the cytosol, which supports the idea that the observed localization is not an independent feature of OdhI but more likely caused by interaction with another protein. The observation that the mycobacterial OdhI homolog GarA possessed the same localization in *C. glutamicum* Δ*odhI* pPREx2-*garA-mVenus* (Fig. 1C) shows that this interaction partner

interacts with OdhI and GarA and it could be speculated that GarA itself also shows a specific intracellular localization at native conditions in mycobacterial species.

The specific localization at the cell poles and the division sites and the positive correlation of the observed number of spots per cell and the cell length suggested a connection to cell growth and the cell division process, since a polar localization was already observed for several proteins involved in these processes. A similar intracellular localization in *C. glutamicum* was for example shown for DivIVA, a protein essential for cell elongation (31) or ParB, a protein which binds specific DNA motifs close to the chromosome origin and is important for nucleoid segregation (32). Many other examples for a polar subcellular localization are known for membrane proteins. In some cases, this localization can be explained by their involvement in cell growth. For example, the STPK PknB of *Mycolicibacterium smegmatis* is associated with polar peptidoglycan synthesis in *Mycobacterium*, as is its homolog in *C. glutamicum* (33). Polar localization was also found for histidine kinases controlling asymmetric cell division processes in *Pseudomonas* and *Caulobacter* (34, 35). For other proteins such as chemotaxis receptor proteins (36, 37) or the sensor kinases DcuS and CitA of *E. coli*, that regulate fumarate respiration and citrate fermentation (38, 39). The cause of this specific localization is still under discussion, since no specific localization is expected for sensors and regulators of metabolic processes (38).

Analysis of the fluorescent OdhI-mVenus spots during the cell cycle in a microfluidic experiment suggests that new spots localize at the future division site prior to cell division. Additional experiments are necessary to confirm this observation for multiple cells and division processes and experimental optimization is needed to enable analysis of growing cells properly located inside the cultivation channels to completely restrict the growth to a linear, one-dimensional manner and improve images due to reduced movement of the cells. Furthermore, simultaneous observation of cell division processes such as nucleoid segregation could be interesting to analyze if the localization of the OdhI-mVenus fluorescent spots is connected to a specific state of the cell cycle. Fluorescently-labeled proteins involved in cell division could be used together with OdhI-mVenus for this purpose. A good marker for the early state of the division process would be FtsZ, which is the first protein moving to the future division site and acting as a scaffold for other cell division proteins (40, 41). DNA staining could be included in analysis of fixed cells.

We analyzed the localization of OdhI in deletion strains of different known interaction partners to find out if an interaction with another protein is responsible for the observed polar localization. With respect to their importance for the regulation of OdhI activity and their

relation to cell division processes, we first analyzed the influence of PknG and the other STPKs on the localization of OdhI-mVenus. Neither the absence of PknG nor the absence of either PknA or PknB in combination with PknL and PknG caused a loss of OdhI-mVenus fluorescent spots (Fig. 3), showing that none of the STPKs is the interaction partner responsible for the localization of OdhI at the cell poles. The observed increase in fluorescent spots detected in the triple deletion strains is most likely caused by the altered morphology (16).

Analysis of almost completely phosphorylated OdhI-mVenus in a *ppp* deletion strain (16) led to a uniform cytosolic fluorescence while only a few distinct fluorescent spots were formed (Fig. 3G), suggesting that the polar localization of OdhI is caused by an interaction of the FHA domain of the unphosphorylated protein with another protein. The interaction with Ppp itself as reason for spot formation is unlikely because there were still some spots detected in the *ppp* deletion strain. The residual fluorescent spots detected in the absence of Ppp might be explained by synthesis of new OdhI with the FHA domain capable of interaction until the protein gets phosphorylated by one of the STPKs. These findings are in line with the observation that an exchange of the known phosphorylation sites Thr14 and Thr15 to alanine (8) did not influence OdhI-mVenus spot formation (data not shown), showing that phosphorylation of OdhI is not necessary for the specific localization of OdhI.

The inhibition of the ODH by binding of the OdhI FHA domain to the OdhA subunit was studied previously (8, 12, 13), and expression of *odhI-mVenus* in an *odhA* deletion strain led to a complete loss of OdhI-mVenus fluorescent spot formation (Fig. 4), meaning that the spots are indeed caused by interaction of unphosphorylated OdhI with OdhA. This was underlined by the formation of OdhA-mCherry fluorescent spots at the cell poles of *C. glutamicum* Δ*odhA* and co-localization of fluorescently-tagged OdhA and OdhI (Fig. 5).

Since OdhA was shown here to localize specifically at the cell poles and division sites it was analyzed if this is true only for OdhA alone or also for the entire PDH-ODH complex. Fusion constructs of AceE, AceE and Lpd with mVenus also formed fluorescent spots at the cell poles when expressed in *C. glutamicum* (Fig. 6A) and in case of AceE and AceF, a mCherry fusion construct showed co-localization with OdhA in *C. glutamicum::*o*dhA-mVenus* (Fig. 6B). While this proofs the polar localization of the PDH-ODH hybrid complex in *C. glutamicum,* the reason for this specific localization is still elusive. Expression of all tested ODH and PDH components as fusions with a fluorescent protein in either an *odhA* or *aceE* deletion strain still led to formation of distinct fluorescent spots (Fig. 6C and D), meaning that none of the E1 subunits of ODH or PDH is responsible for the polar localization. Therefore, Lpd and AceF remain as potential causes for the polar localization of the entire complex. AceF is the most

promising candidate, since it is known to build the core of the PDH-ODH hybrid complex interacting with all other components (11). In addition, a C-terminal fusion of Lpd to mCherry did not form fluorescent spots in *C. glutamicum* (data not shown), while the N-terminal fusion with mVenus led to the polar fluorescence signals, suggesting that the C-terminal fusion of Lpd to mCherry prevents interaction with AceF and this interaction with AceF might be necessary for the polar localization of Lpd. This needs to be further analyzed using *aceF* and *lpd* deletion strains. If AceF is indeed the cause of the observed polar localization, an *aceF* deletion is expected to cause loss of fluorescent spot formation at the cell poles for all other tagged PDH-ODH complex components since the complex cannot be formed without the core building AceF. If the remaining proteins still form distinct fluorescence signals in the cell or are distributed equally has to be tested. Furthermore, it would be interesting to analyze if the interaction of OdhA and OdhI, which is independent of AceF, can still be observed by distinct co-localization signals.

The specific localization seems to be unique for the PDH-ODH hybrid complex, since under the analyzed conditions neither for the ICD as another TCA cycle component, nor for the GDH also taking part at the 2-oxoglutartate node, a distinct localization was observed under the used conditions (Fig. 7). Even if it cannot completely be excluded that the fusion with the fluorescent protein impaired the functionality and possible interactions.

The localization of the PDH-ODH complex in *C. glutamicum* at the cell poles and division sites seems to be the first example that such a specific subcellular localization was observed for a cytoplasmic protein complex involved in central carbon central metabolism and not directly linked to cell growth, and leads to some additional questions. So far, it remains unclear what causes the specific localization and formation of the distinct fluorescence signals. One explanation would be an interaction of one of the subunits, most likely AceF, with a protein showing a polar localization itself, for example, a protein involved in cell division processes, as discussed above. Another explanation might be nucleoid exclusion. Whereby the localization at the cell poles would be caused by repression of the large PDH-ODH complex from the cell center by the nucleoid due to the high molecular crowding and diffusion hindrance in this region (42, 43).

When working with fluorescently labeled proteins it always has to be considered that the fluorescent protein itself might cause aggregation and lead to false localization results. Here we used the monomeric fluorescent proteins mVenus and mCherry to reduce the risk of aggregates caused by the fluorescent protein, and showed that the fluorescent protein alone does not show a specific localization. Furthermore, the observed localization of OdhI was

independent from the used fluorescent protein since fusion proteins of OdhI with mVenus and mCherry both showed the formation of polar fluorescent spots. Moreover, the localization was also observed at native expression levels in the *odhA-mVenus* and *odhI-mVenus* integration strains. The clear reduction of OdhI-mVenus fluorescent spots in *C. glutamicum* Δ*ppp* and the complete lack of fluorescent spot formation in the *C. glutamicum* Δ*odhA* proves that the polar localization of OdhI is caused by interaction with OdhA and not caused by an artificial behavior of the protein due to the fusion with the fluorescent protein.

From literature it is known that an aggregation of fluorescent-tagged proteins can also be dependent on high oligomeric states of the fused protein, where the close proximity of the fluorescent proteins in the target protein complex causes aggregation, which is not the case for the isolated fluorescent proteins or monomeric fusion proteins. If this occurs, unipolar as well as bipolar localization can be caused by a combination of aggregation and nucleoid occlusion (44-46). To exclude such a behavior as reason for the observed polar localization of the PDH-ODH hybrid complex, an immunofluorescence staining using specific antibodies against one or several components of the PDH-ODH complex could be used as an alternative to the fusion with fluorescent proteins. The fusion proteins have the advantage that they can be used to monitor the localization of the fused protein in growing cells while immunofluorescence staining requires fixed cells. However, as a control experiment immunofluorescence staining enables the exclusion of artificial localization caused by the fluorescent protein. In case of FtsZ localization studies, immunostaining was already successfully used to analyze the intracellular localization in *C. glutamicum* (41).

Besides the reason for the polar localization, also the composition of the supercomplex and the number of PDH-ODH hybrid complexes forming one fluorescent spot is of large interest. Recent studies focused on the exact composition of the complex showing that the corynebacterial AceF only forms trimers (11) in contrast to the much larger E2 cores reported previously (47). In addition, analytical ultracentrifugation and size-exclusion chromatography experiments showed that PDH and ODH activities in *C. glutamicum* are found for complexes smaller than in *E. coli* and might possess a core of hexameric AceF (10). If nucleoid occlusion due to the large size of the complex causes the polar localization this effect could also be discussed for ODH or PDH complexes of other organisms such as *E. coli*, since these protein complexes are known to form even larger complexes (~10 MDa) than observed for the *C. glutamicum* hybrid complex.

Taken together, the polar localisation of the PDH-ODH complex is of large interest for the

research on corynebacterial and actinobacterial dehydrogenase characteristics in general and leads to many interesting follow up questions and experiments.

MATERIALS AND METHODS

Bacterial strains, media and culture conditions. All bacterial strains and plasmids used in this work are listed in Table 1. *Escherichia coli* cells were cultivated at 37 °C in lysogeny broth (LB) (48) or on LB agar plates (Carl Roth, Karlsruhe, Germany). *C. glutamicum* strains were cultivated at 30 °C in brain heart infusion medium (BHI; Difco Laboratories, Detroit, USA) or in CGXII medium with 2 % (w/v) glucose (49) containing 30 mg L^{-1} 3,4-dihydroxybenzoate as iron chelator. 15 g L^{-1} agar was added to prepare the respective solid media. Kanamycin was added at concentrations of 25 mg L^{-1} (*C. glutamicum*) or 50 mg L^{-1} (*E. coli*) to maintain plasmid stability. In case of the *C. glutamicum* Δ*aceE* strain, the culture medium was supplemented with 2 g L^{-1} acetate.

Table 1. Bacterial strains and plasmids used in this study

Strain or plasmid	Description	Reference or source
***C. glutamicum* strains**		
ATCC13032	Biotin-auxotrophic wild type strain	DSMZ
Δ*odhI*	Wild type derivative with in-frame deletion of *odhI* (cg1630)	(8)
Δ*pknG*Δ*odhI*	Wild type derivative with in-frame deletion of *pknG* (cg3046) and *odhI* (cg1630)	(8)
Δ*pknA*Δ*pknL*Δ*pknG*	Wild type derivative with in-frame deletion of *pknA* (cg0059), *pknL* (cg2388), and *pknG* (cg3046)	(16)
Δ*pknB*Δ*pknL*Δ*pknG*	Wild type derivative with in-frame deletion of *pknB* (cg0057), *pknL* (cg2388), and *pknG* (cg3046)	(16)
Δ*ppp*	Wild type derivative with in-frame deletion of *ppp* (cg0062)	(14)
Δ*odhA*	Wild type derivative with in-frame deletion of *odhA* (cg1280)	This work
Δ*aceE*	Wild type derivative with in-frame deletion of *aceE* (cg2466)	(50)
Δ*gdh*	Wild type derivative with in-frame deletion of *gdh* (cg2280)	(51)
::*odhI-mVenus*	Wild type derivative with in-frame insertion of a linker sequence (GGTACCGCAGCG) and *mVenus* encoding for a C-terminal fusion of OdhI(Cg1630)-mVenus	This work
::*odhA-mVenus*	Wild type derivative with in-frame insertion of a linker sequence (GGTACCGCAGCG) and *mVenus* encoding for a C-terminal fusion of OdhA(Cg1280)-mVenus	This work
***M. tuberculosis* strains**		
H37Rv	Chromosomal DNA was used as template for amplification of *garA* (rv1827)	DSMZ
***E. coli* strains**		

DH5α	F- *supE44* Δ*lacU*169 (Φ80*lacZ*Δ*M15*) *hsdR17 recA1 endA1 gyrA96 thi-1 relA1*	(52)
Plasmids		
pK19mobsacB	Kan^R; suicide vector for allelic exchange in *C. glutamicum*; $oriV_{E. coli}$ *oriT sacB*	(53)
pK19mobsacB-Δ*odhA*	Kan^R; pK19mobsacB derivative containing PCR products covering the up- and downstream regions of the *odhA* (cg1280) gene	This work
pK19mobsacB-*odhI-mVenus*	Kan^R; pK19mobsacB derivative containing PCR products covering the up- and downstream regions of the *odhI* (cg1630) stop codon and the mVenus encoding sequence	This work
pK19mobsacB-*odhA-mVenus*	Kan^R; pK19mobsacB derivative containing PCR products covering the up- and downstream regions of the *odhA* (cg1280) stop codon and the mVenus encoding sequence	This work
pDHL-*mVenus*	Kan^R , pDHL1029 derivative, used for amplification of mVenus encoding sequence	(54)
pPREx2	Kan^R; pPBEx2 derivative (P*tacI*, *lacI*q, *oriC.g* from pBL1; *oriE.c.* ColE1 from pUC18), with a consensus RBS (AAGGAG) for *C. glutamicum*	(25)
pPREx2-*mVenus*	Kan^R; pPREx2 derivative carrying the mVenus encoding sequence	This work
pPREx2-*odhI-mVenus*	Kan^R; pPREx2 derivative carrying the OdhI (Cg1630) and mVenus encoding sequences fused by a linker sequence (GGTACCGCAGCG)	This work
pPREx2-*garA-mVenus*	Kan^R; pPREx2 derivative carrying the GarA (Rv1827) and mVenus encoding sequences fused by a linker sequence (GGTACCGCAGCG)	This work
pPREx2-*target-mVenus*	Kan^R; pPREx2 derivative carrying a linker sequence (GGTACCGCAGCG) and the mVenus encoding sequence to enable C-terminal mVenus fusions to different targets	This work
pPREx2-*mVenus-target*	Kan^R; pPREx2 derivative carrying the mVenus encoding sequence and a linker sequence (GGTACCGCAGCG) to enable N-terminal mVenus fusions to different targets	This work
pPREx2-*aceE-mVenus*	Kan^R; pPREx2-*target-mVenus* derivative carrying the AceE (Cg2466) encoding sequence	This work
pPREx2-*aceF-mVenus*	Kan^R; pPREx2-*target-mVenus* derivative carrying the AceF (Cg2421) encoding sequence	This work
pPREx2-*mVenus-lpd*	Kan^R; pPREx2-*mVenus-target* derivative carrying the Lpd (Cg0441) encoding sequence	This work
pPREx2-*mVenus-icd*	Kan^R; pPREx2-*mVenus-target* derivative carrying the Icd (Cg0766) encoding sequence	This work
pPREx2-*mVenus-gdh*	Kan^R; pPREx2-*mVenus-target* derivative carrying the GDH (Cg2280) encoding sequence	This work
pPREx2-*odhI-mCherry*	Kan^R; pPREx2 derivative carrying the OdhI (Cg1630) and mCherry encoding sequence fused by a linker sequence (GGTACCGCAGCG)	This work
pPREx2-*odhA-mCherry*	Kan^R; pPREx2 derivative carrying the OdhA (Cg1280) and mCherry encoding sequence fused by a linker sequence (GGTACCGCAGCG)	This work

pPREx2-*aceE-mCherry*	Kan^R; pPREx2-*odhI-mCherry* derivative carrying the AceE (Cg2466) encoding sequence, *odhI* was removed by restriction digestion using NdeI and KpnI	This work
pPREx2-*aceF-mCherry*	Kan^R; pPREx2-*odhI-mCherry* derivative carrying the AceF (Cg2421) encoding sequence, *odhI* was removed by restriction digestion using NdeI and KpnI	This work

Standard recombinant DNA work and construction of deletion mutants. Standard methods such as PCR and plasmid restriction were carried out according to established protocols (55) and all oligonucleotides used are listed in Table 2. Plasmids were constructed by Gibson assembly (56). Oligonucleotides were ordered from and DNA sequencing was performed by Eurofins Genomics (Ebersberg, Germany). Transformation of *E. coli* was performed following a standard protocol (52) and *C. glutamicum* transformation was performed by electroporation (57). *C. glutamicum* deletion or integration mutants were constructed by double homologous recombination using pK19mobsacB-based plasmids as described previously (58). Oligonucleotides annealing up- and downstream of the target genes were used to confirm genomic deletions or integrations by colony-PCR.

Table 2. Oligonucleotides used in this study

Name	Sequence
Construction of pK19mobsacB-Δ*odhA*	
ΔodhA_1	CAGGTCGACTCTAGAGGAAACATTGGCTACGGATGC
ΔodhA_2	GGCAGGTACTCGCCTCTTTTC
ΔodhA_3	AAGAGGCGAGTACCTGCCTAAGTCTTTATAGTCCTGCACTAGC
ΔodhA_4	AAAACGACGGCCAGTGAATTATCGGCTGGGTGGATTTC
Construction of pK19mobsacB-*odhI-mVenus*	
odhI-mVenus_I1	CGACGTTGTAAAACGACGGCCAGTGGACAACCCACTTGCGGG
odhI-mVenus_I2	CTCCTTTGCTAGCCGCTGCGGTACCCTCAGCAGGGCCTGCG
odhI-mVenus_I3	GGTACCGCAGCGGCTAGCAAAGGAGAAGAACTTTTCACTG
odhI-mVenus_I4	TAGGAAGTGTTTTTATTTGTAGAGCTCATCCATGCCATG
odhI-mVenus_I5	GCTCTACAAATAAAAACACTTCCTAGGAAAGTTCTTTGCAG
odhI-mVenus_I6	GCATGCCTGCAGGTCGACTCTAGAGCCAAAGGCTCCGAGGAGG
Construction of pK19mobsacB-*odhA-mVenus*	
odhA-mVenus_I1	TTATTTGTAGAGCTCATCCATGC
odhA-mVenus_I2	GACGAGGCTTTCGAGGCTGGTACCGCAGCGGCTAGCAAAGGAGAAGAAC
odhA-mVenus_I3	CAGGTCGACTCTAGAGGAATCGGCTGGGTGGATTTC
odhA-mVenus_I4	GATGAGCTCTACAAATAAGTCTTTATAGTCCTGCACTAGC
odhA-mVenus_I5	AGCCTCGAAAGCCTCGTC
odhA-mVenus_I6	AAAACGACGGCCAGTGAATTCGTCCACTGGTTATCTTC
Construction of pPREx2-*mVenus*	
mVenus fw	AGAAGGAGATATACATATGGCTAGCAAAGGAGAAGAAC
mVenus rv	AAACGACGGCCAGTGAATTCTTATTTGTAGAGCTCATCCATGC
Construction of pPREx2-*odhI-mVenus*	
pPREx2_odhI fw	AGAAGGAGATATACATATGAGCGACAACAACGGCACCC

odhI rv	CTCAGCAGGGCCTGCGAG
odhI-mVenus fw	GCAGGCCCTGCTGAGGGTACCGCAGCGGCTAGCAAAGGAGAAGAAC
mVenus_pPREx2 rv	AAACGACGGCCAGTGAATTCTTATTTGTAGAGCTCATCCATGC
Construction of pPREx2-*garA-mVenus*	
pPREx2_garA fw	TGCAGAAGGAGATATACATATGACGGACATGAACCCGGATATTG
garA rv	GCTAGCCGCTGCGGTACCCGGGCCCCCGGTACTCCCGTC
garA-mVenus fw	GGTACCGCAGCGGCTAGCAAAGGAGAAGAAC
mVenus_pPREx2 rv	AAACGACGGCCAGTGAATTCTTATTTGTAGAGCTCATCCATGC
Construction of pPREx2-*target-mVenus*	
linker-mVenus fw	ATATACATATGACCTGAGGGTACCGCAGCGGTGAGCAAGGGCGAGGAGC TTTTCACTGGAGTTGTC
mVenus rv	AAACGACGGCCAGTGAATTCTTATTTGTAGAGCTCATCCATGC
Construction of pPREx2 *-mVenus-target*	
mVenus fw	AGAAGGAGATATACATATGGCTAGCAAAGGAGAAGAAC
mVenus-linker rv	AAACGACGGCCAGTGAATTCCGCTGCGGTACCTTTGTAGAGCTCATCCAT GC
Construction of pPREx2-*aceF-mVenus* and pPREx2-*aceF-mCherry*	
aceF fw	TGCAGAAGGAGATATACATATGGCGTTCTCCGTAGAGATG
aceF rv	TGCTCACCGCTGCGGTACCGAGCTGCAGATCGCCTTCG
Construction of pPREx2-*aceE-mVenus* and pPREx2-*aceE-mCherry*	
aceE fw	TGCAGAAGGAGATATACATATGGCCGATCAAGCAAAACTTGGTGG
aceE rv	TGCTCACCGCTGCGGTACCTTCCTCAGGAGCGTTTGG
Construction of pPREx2-*mVenus-lpd*	
lpd fw	TGAGCTCTACAAAGGTACCGCAGCGGTGACTGAACATTATGACGTAG
lpd rv	AAACGACGGCCAGTGAATTCCTAGAAGTTGATCATGTGTCCAGAG
Construction of pPREx2-*mVenus-icd*	
icd fw	TGAGCTCTACAAAGGTACCGCAGCGATGGCTAAGATCATCTGGAC
icd rv	AAACGACGGCCAGTGAATTCTTACTTCTTCAGTGCGTCAAC
Construction of pPREx2-*mVenus-lpd*	
gdh fw	TGAGCTCTACAAAGGTACCGCAGCGACAGTTGATGAGCAGGTC
gdh rv	AAACGACGGCCAGTGAATTCTTAGATGACGCCCTGTGC
Construction of pPREx2-*odhI-mCherry*	
pPREx2_odhI fw	AGAAGGAGATATACATATGAGCGACAACAACGGCACCC
odhI-mCherry rv	TCCTCCTCGCCCTTGCTCACCGCTGCGGTACCCTCAGCAGGGCCTGCGAG
mCherry fw	GTGAGCAAGGGCGAGGAG
mCherry_pPREx2 rv	AAACGACGGCCAGTGAATTCTTACTTGTACAGCTCGTC
Construction of pPREx2-*odhA-mCherry*	
pPREx2_odhA fw	GCATGCCTGCAGAAGGAGATATACATGTGAGCAGCGCTAGTACTTTCGG
odhA rv	AGCCTCGAAAGCCTCGTC
odhA-mCherry fw	GCTTATCGACGAGGCTTTCGAGGCTGGTACCGCAGCGG
mCherry_pPREx2 rv	AAACGACGGCCAGTGAATTCTTACTTGTACAGCTCGTC
Confirmation of gene deletion by colony-PCR	
DodhA_fw	AGGACGCCCAAACAACAG
DodhA_rv	AATGAAGGTGCCGTGAAAG

Fluorescence microscopy. Prior to analysis by fluorescence microscopy, the different *C. glutamicum* strains were grown over night at 30 °C and 170 rpm in BHI medium, diluted 1:50 to inoculate a main culture in CCXII medium with 2 % (w/v) glucose and incubated for 3-4 h under the same conditions. For membrane staining, cells were harvested by centrifugation (5 min, 4000 *g*) and resuspended in phosphate buffered saline (PBS; 137 mM NaCl, 2.7 mM KCl, 10 mM Na_2HPO_4, 1.8 mM KH_2PO_4, pH 7.4) containing 250 ng ml^{-1} Nile red followed by 10 min incubation in the dark. Afterwards, cells were immobilized on glass slides with agar pads (0.9 % (w/v) NaCl, 1.5 % (w/v) agarose) and analyzed using an Axio imager M2 microscope equipped with AxioCam ICc 3 and an Zeiss Plan-Apochromat 100x / 1.4 oil Ph3 objective and an HXP 120 C lightning unit (Carl Zeiss). For detection of mVenus fluorescence the filter 46 HE (λex 500/25 nm, λem 535/30 nm) and in case of mCherry or Nile red the filter 43 HE (λex 545/25 nm, λem 605/70 nm) was used. Image processing took place using the AxioVision SE64 Rel. software v. 4.8.2 (Carl Zeiss).

Microfluidic cultivation. Growth of *C. glutamicum*::*odhI-mVenus* was analyzed in microfluidic experiments using a mother machine cultivation channel chip with a channel width of 1.25 µm. The mother machine growth channels restricts the cell-division to a linear direction (27). The growth channels are arranged between parallel medium supply channels which are filled with fresh medium continuously in the perfusion mode, to enable constant cultivation conditions. Prior to the microfluidics cultivation cells were grown overnight in BHI medium, followed by two pre-cultures in CGXII medium with 2% (w/v) glucose. A main culture in CGXII medium with 2% (w/v)glucose was inoculated to a starting OD_{600} of 0.1 and diluted with fresh medium to an OD of 0.5, before loading the chip, to ensure that only single cells would enter the cultivation channel (mother machine). Afterwards fresh medium was applied at a flow rate of 200 nl min^{-1} for 20 h at 30 °C. Time-lapse images were carried out using an automated inverted Nikon Ti Eclipse microscope (Nikon Corporation, Japan)) equipped with a temperature incubator (TempController 2000-2, PeCon, Germany), a 100x oil immersion objective (Plan Apo λ 100x Oil Ph3 DM, Nikon, Japan), and an Andor Zyla VSC-01418 camera (Oxford Instruments Technology, Shanghai). mVenus fluorescence was detected using an YFPhq filter with an exposure time of 100 ms. Selected chambers were monitored using the NIS-Elements Imaging Software (Nikon NIS Elements AR software package, Nikon GmbH, Germany). Time-lapse images were recorded every 2 min and image sequences were analyzed using the open source software Fiji (59).

Statistics. For statistical analysis of the fluorescent spots and the cell size at least 100 cells were analyzed of each strain. Cell size was measured using the AxioVision SE64 Rel. software v. 4.8.2 (Carl Zeiss) and fluorescent spots were counted manually. Dividing cells were counted as individual cells if the Nile red staining showed a new membrane at the division site. Data analysis was carried out using Graphpad Prism 9 (Graphpad, San Diego, USA). The frequency of different cell length was calculated using Graphpad Prism 9 frequency analysis with a bin width of 0.5.

ACKNOWLEDGEMENTS
This work was financially supported by the DFG-ANR project MetActino (DFG BO 903/4-1, ANR-18-CE92-0003). The authors thank Andreas Burkovski (Erlangen, Germany) and Bernhard Eikmanns (Ulm, Germany) for providing *C. glutamicum gdh* or *aceE* deletion strains, respectively.

References

1. Barka, E.A., P. Vatsa, L. Sanchez, N. Gaveau-Vaillant, C. Jacquard, H.-P. Klenk, C. Clément, Y. Ouhdouch and G.P.v. Wezel, Taxonomy, Physiology, and Natural Products of *Actinobacteria*. Microbiology and Molecular Biology Reviews, 2016. 80: 1-43.
2. Hopwood, D.A., *Streptomyces* in nature and medicine: the antibiotic makers. 2007 Oxford University Press, USA.
3. Eggeling, L. and M. Bott, A giant market and a powerful metabolism: L-lysine provided by *Corynebacterium glutamicum*. Applied Microbiology and Biotechnology., 2015. 99: 3387-3394.
4. Wendisch, V.F., J.M.P. Jorge, F. Perez-Garcia and E. Sgobba, Updates on industrial production of amino acids using *Corynebacterium glutamicum*. World Journal of Microbiology and Biotechnology., 2016. 32: 105.
5. Becker, J. and C. Wittmann, Bio-based production of chemicals, materials and fuels – *Corynebacterium glutamicum* as versatile cell factory. Current Opinion in Biotechnology, 2012. 23: 631-640.
6. Usuda, Y., N. Tujimoto, C. Abe, Y. Asakura, E. Kimura, Y. Kawahara, O. Kurahashi and H. Matsui, Molecular cloning of the *Corynebacterium glutamicum* (‘*Brevibacterium lactofermentum*’AJ12036) *odhA* gene encoding a novel type of 2-oxoglutarate dehydrogenase. Microbiology, 1996. 142: 3347-3354.
7. Wagner, T., M. Bellinzoni, A. Wehenkel, H.M. O'Hare and P.M. Alzari, Functional plasticity and allosteric regulation of α-ketoglutarate decarboxylase in central mycobacterial metabolism. Chemistry & biology, 2011. 18: 1011-1020.
8. Niebisch, A., A. Kabus, C. Schultz, B. Weil and M. Bott, Corynebacterial protein kinase G controls 2-oxoglutarate dehydrogenase activity via the phosphorylation status of the OdhI protein. Journal of Biological Chemistry, 2006. 281: 12300-12307.
9. Hoffelder, M., K. Raasch, J. van Ooyen and L. Eggeling, The E2 domain of OdhA of *Corynebacterium glutamicum* has succinyltransferase activity dependent on lipoyl residues of the acetyltransferase AceF. Journal of bacteriology, 2010. 192: 5203-5211.
10. Kinugawa, H., N. Kondo, A. Komine-Abe, T. Tomita, M. Nishiyama and S. Kosono, *In vitro* reconstitution and characterization of pyruvate dehydrogenase and 2-oxoglutarate dehydrogenase hybrid complex from *Corynebacterium glutamicum*. Microbiologyopen, 2020. 9: e1113.
11. Bruch, E.M., P. Vilela, L. Yang, A. Boyko, N. Lexa-Sapart, B. Raynal, P.M. Alzari and M. Bellinzoni, *Actinobacteria* challenge the paradigm: A unique protein architecture for a well-known, central metabolic complex. Proceedings of the National Academy of Sciences, 2021. 118: e2112107118.
12. Krawczyk, S., K. Raasch, C. Schultz, M. Hoffelder, L. Eggeling and M. Bott, The FHA domain of OdhI interacts with the carboxyterminal 2-oxoglutarate dehydrogenase domain of OdhA in *Corynebacterium glutamicum*. FEBS Letters, 2010. 584: 1463-1468.
13. Raasch, K., M. Bocola, J. Labahn, A. Leitner, L. Eggeling and M. Bott, Interaction of 2-oxoglutarate dehydrogenase OdhA with its inhibitor OdhI in *Corynebacterium glutamicum*: Mutants and a model. Journal of Biotechnology, 2014. 191: 99-105.
14. Schultz, C., A. Niebisch, L. Gebel and M. Bott, Glutamate production by *Corynebacterium glutamicum*: dependence on the oxoglutarate dehydrogenase inhibitor protein OdhI and protein kinase PknG. Applied Microbiology and Biotechnology, 2007. 76: 691-700.

15. Barthe, P., C. Roumestand, M.J. Canova, L. Kremer, C. Hurard, V. Molle and M. Cohen-Gonsaud, Dynamic and structural characterization of a bacterial FHA protein reveals a new autoinhibition mechanism. Structure, 2009. 17: 568-578.
16. Schultz, C., A. Niebisch, A. Schwaiger, U. Viets, S. Metzger, M. Bramkamp and M. Bott, Genetic and biochemical analysis of the serine/threonine protein kinases PknA, PknB, PknG and PknL of *Corynebacterium glutamicum*: evidence for non-essentiality and for phosphorylation of OdhI and FtsZ by multiple kinases. Molecular Microbiology, 2009. 74: 724-741.
17. Nott, T.J., G. Kelly, L. Stach, J. Li, S. Westcott, D. Patel, D.M. Hunt, S. Howell, R.S. Buxton and H.M.J.S.S. O'Hare, An intramolecular switch regulates phosphoindependent FHA domain interactions in *Mycobacterium tuberculosis*. Science Signaling, 2009. 2: ra12-ra12.
18. O'Hare, H.M., R. Durán, C. Cerveñansky, M. Bellinzoni, A.M. Wehenkel, O. Pritsch, G. Obal, J. Baumgartner, J. Vialaret and K. Johnsson, Regulation of glutamate metabolism by protein kinases in mycobacteria. Molecular microbiology, 2008. 70: 1408-1423.
19. England, P., A. Wehenkel, S. Martins, S. Hoos, G. André-Leroux, A. Villarino and P.M. Alzari, The FHA-containing protein GarA acts as a phosphorylation-dependent molecular switch in mycobacterial signaling. FEBS Letters, 2009. 583: 301-307.
20. Gallant, J.L., A.J. Viljoen, P.D. van Helden and I.J.F. Wiid, Glutamate Dehydrogenase Is Required by *Mycobacterium bovis* BCG for Resistance to Cellular Stress. PLOS ONE, 2016. 11: e0147706.
21. Bellinzoni, M., A.M. Wehenkel, R. Duran and P.M. Alzari, Novel mechanistic insights into physiological signaling pathways mediated by mycobacterial Ser/Thr protein kinases. Genes and immunity, 2019. 20: 383-393.
22. Cowley, S., M. Ko, N. Pick, R. Chow, K.J. Downing, B.G. Gordhan, J.C. Betts, V. Mizrahi, D.A. Smith and R.W. Stokes, The *Mycobacterium tuberculosis* protein serine/threonine kinase PknG is linked to cellular glutamate/glutamine levels and is important for growth *in vivo*. Molecular microbiology, 2004. 52: 1691-1702.
23. Bhattacharyya, N., I.N. Nkumama, Z. Newland-Smith, L.-Y. Lin, W. Yin, R.E. Cullen, J.S. Griffiths, A.R. Jarvis, M.J. Price, P.Y. Chong, R. Wallis and H.M. O'Hare, An Aspartate-Specific Solute-Binding Protein Regulates Protein Kinase G Activity To Control Glutamate Metabolism in *Mycobacteria*. mBio, 2018. 9: e00931-18.
24. Sundermeyer, L., G. Bosco, S. Gujar, M. Brocker, M. Baumgart, D. Willbold, O.H. Weiergräber, M. Bellinzoni and M. Bott, Characteristics of the GlnH and GlnX signal transduction proteins controlling PknG-mediated phosphorylation of OdhI and 2-oxoglutarate dehydrogenase activity in *Corynebacterium glutamicum* Microbiology Spectrum, under peer review, 2022.
25. Bakkes, P.J., P. Ramp, A. Bida, D. Dohmen-Olma, M. Bott and R. Freudl, Improved pEKEx2-derived expression vectors for tightly controlled production of recombinant proteins in *Corynebacterium glutamicum*. Plasmid, 2020. 112: 102540.
26. Grünberger, A., W. Wiechert and D. Kohlheyer, Single-cell microfluidics: opportunity for bioprocess development. Current Opinion in Biotechnology, 2014. 29: 15-23.
27. Lindemann, D., C. Westerwalbesloh, D. Kohlheyer, A. Grünberger and E. von Lieres, Microbial single-cell growth response at defined carbon limiting conditions. RSC advances, 2019. 9: 14040-14050.
28. Fiuza, M., M.J. Canova, D. Patin, M. Letek, I. Zanella-Cléon, M. Becchi, L.M. Mateos, D. Mengin-Lecreulx, V. Molle and J. Gil, The MurC ligase essential for peptidoglycan biosynthesis is regulated by the serine/threonine protein kinase PknA in *Corynebacterium glutamicum*. Journal of Biological Chemistry, 2008. 283: 36553-36563.
29. Fiuza, M., M.J. Canova, I. Zanella-Cléon, M. Becchi, A.J. Cozzone, L.M. Mateos, L. Kremer, J.A. Gil and V. Molle, From the characterization of the four serine/threonine protein kinases (PknA/B/G/L) of *Corynebacterium glutamicum* toward the role of PknA and PknB in cell division. Journal of Biological Chemistry, 2008. 283: 18099-18112.
30. Daniel, R.A. and J. Errington, Control of cell morphogenesis in bacteria: two distinct ways to make a rod-shaped cell. Cellular microbiology, 2003. 113: 767-776.
31. Letek, M., M. Fiuza, E. Ordóñez, A.F. Villadangos, A. Ramos, L.M. Mateos and J.A. Gil, Cell growth and cell division in the rod-shaped actinomycete *Corynebacterium glutamicum*. Antonie van Leeuwenhoek, 2008. 94: 99-109.
32. Donovan, C., A. Schwaiger, R. Krämer and M. Bramkamp, Subcellular localization and characterization of the ParAB system from *Corynebacterium glutamicum*. Journal of bacteriology, 2010. 192: 3441-51.
33. Mir, M., J. Asong, X. Li, J. Cardot, G.J. Boons and R.N. Husson, The extracytoplasmic domain of the *Mycobacterium tuberculosis* Ser/Thr kinase PknB binds specific muropeptides and is required for PknB localization. PLOS Pathogens, 2011. 7: e1002182.
34. Boyd, J.M., Localization of the histidine kinase PilS to the poles of *Pseudomonas aeruginosa* and identification of a localization domain. Molecular Microbiology, 2000. 36: 153-62.

35. Shapiro, L., H.H. McAdams and R. Losick, Generating and exploiting polarity in bacteria. Science, 2002. 298: 1942-1946.
36. Kentner, D., S. Thiem, M. Hildenbeutel and V. Sourjik, Determinants of chemoreceptor cluster formation in *Escherichia coli*. Molecular Microbiology, 2006. 61: 407-417.
37. Sourjik, V. and H.C. Berg, Localization of components of the chemotaxis machinery of *Escherichia coli* using fluorescent protein fusions. Molecular Microbiology, 2000. 37: 740-751.
38. Scheu, P., S. Sdorra, Y.-F. Liao, M. Wegner, T. Basché, G. Unden and W. Erker, Polar accumulation of the metabolic sensory histidine kinases DcuS and CitA in *Escherichia coli*. Microbiology(Reading) 2008. 154: 2463-2472.
39. Scheu, P.D., P.A. Steinmetz, F. Dempwolff, P.L. Graumann and G. Unden, Polar Localization of a Tripartite Complex of the Two-Component System DcuS/DcuR and the Transporter DctA in *Escherichia coli* Depends on the Sensor Kinase DcuS. PLOS ONE, 2015. 9: e115534.
40. Ortiz, C., P. Natale, L. Cueto and M. Vicente, The keepers of the ring: regulators of FtsZ assembly. FEMS Microbiology Reviews, 2016. 40: 57-67.
41. Ramos, A., M. Letek, A.B. Campelo, J. Vaquera, L.M. Mateos and J.A. Gil, Altered morphology produced by *ftsZ* expression in *Corynebacterium glutamicum* ATCC 13869. Microbiology 2005. 151: 2563-2572.
42. Wu, L.J. and J. Errington, Nucleoid occlusion and bacterial cell division. Nature Reviews Microbiology, 2012. 10: 8-12.
43. Coquel, A.-S., J.-P. Jacob, M. Primet, A. Demarez, M. Dimiccoli, T. Julou, L. Moisan, A.B. Lindner and H. Berry, Localization of Protein Aggregation in *Escherichia coli* Is Governed by Diffusion and Nucleoid Macromolecular Crowding Effect. PLOS Computational Biology, 2013. 9: e1003038.
44. Landgraf, D., B. Okumus, P. Chien, T.A. Baker and J. Paulsson, Segregation of molecules at cell division reveals native protein localization. Nature Methods, 2012. 9: 480-482.
45. Scheu, K., R. Gill, S. Saberi, P. Meyer and E. Emberly, Localization of aggregating proteins in bacteria depends on the rate of addition. Frontiers in Microbiology, 2014. 5: 418.
46. Saberi, S. and E. Emberly, Non-Equilibrium Polar Localization of Proteins in Bacterial Cells. PLOS ONE, 2013. 8: e64075.
47. Izard, T., A. Ævarsson, M.D. Allen, A.H. Westphal, R.N. Perham, A. de Kok and W.G. Hol, Principles of quasi-equivalence and Euclidean geometry govern the assembly of cubic and dodecahedral cores of pyruvate dehydrogenase complexes. Proceedings of the National Academy of Sciences, 1999. 96: 1240-1245.
48. Bertani, G., Studies on lysogenesis I: the mode of phage liberation by lysogenic *Escherichia coli*. Journal of bacteriology, 1951. 62: 293-300.
49. Keilhauer, C., L. Eggeling and H. Sahm, Isoleucine synthesis in *Corynebacterium glutamicum*: molecular analysis of the *ilvB-ilvN-ilvC* operon. Journal of bacteriology, 1993. 175: 5595-5603.
50. Schreiner, M.E., D. Fiur, J. Holátko, M. Pátek and B.J. Eikmanns, E1 Enzyme of the Pyruvate Dehydrogenase Complex in *Corynebacterium glutamicum*: Molecular Analysis of the Gene and Phylogenetic Aspects. Journal of bacteriology, 2005. 187: 6005-6018.
51. Müller, T., J. Strösser, S. Buchinger, L. Nolden, A. Wirtz, R. Krämer and A. Burkovski, Mutation-induced metabolite pool alterations in *Corynebacterium glutamicum*: towards the identification of nitrogen control signals. Journal of biotechnology, 2006. 126: 440-453.
52. Hanahan, D., Studies on transformation of *Escherichia coli* with plasmids. Journal of molecular biology, 1983. 166: 557-580.
53. Schäfer, A., A. Tauch, W. Jäger, J. Kalinowski, G. Thierbach and A. Pühler, Small mobilizable multi-purpose cloning vectors derived from the *Escherichia coli* plasmids pK18 and pK19: selection of defined deletions in the chromosome of *Corynebacterium glutamicum*. Gene, 1994. 145: 69-73.
54. Govers, S.K., J. Mortier, A. Adam and A. Aertsen, Protein aggregates encode epigenetic memory of stressful encounters in individual *Escherichia coli* cells. PLOS Biology, 2018. 16: e2003853.
55. Green, M.R. and J. Sambrook, Molecular Cloning. A Laboratory Manual. 3rd ed. 2012, Cold Spring Harbor, New York: Cold Spring Harbor Laboratory Press.
56. Gibson, D.G., L. Young, R.Y. Chuang, J.C. Venter, C.A. Hutchison and H.O. Smith, Enzymatic assembly of DNA molecules up to several hundred kilobases. Nature Methods, 2009. 6: 343-345.
57. van der Rest, M.E., C. Lange and D. Molenaar, A heat shock following electroporation induces highly efficient transformation of *Corynebacterium glutamicum* with xenogeneic plasmid DNA. Applied Microbiology and Biotechnology, 1999. 52: 541-545.
58. Niebisch, A. and M. Bott, Molecular analysis of the cytochrome bc_1-aa_3 branch of the *Corynebacterium glutamicum* respiratory chain containing an unusual diheme cytochrome c_1. Archives of microbiology, 2001. 175: 282-294.
59. Schindelin, J., I. Arganda-Carreras, E. Frise, V. Kaynig, M. Longair, T. Pietzsch, S. Preibisch, C. Rueden, S. Saalfeld, B. Schmid, J.-Y. Tinevez, D.J. White, V. Hartenstein, K. Eliceiri, P. Tomancak and A. Cardona, Fiji: an open-source platform for biological-image analysis. Nature Methods, 2012. 9: 676-682.

3. Discussion

3.1 GlnH, GlnX, and PknG are part of the same signal transduction cascade

Previous studies identified a novel type of post-translational regulation responsible for the distribution of 2-oxoglutarate, an important metabolite of central carbon metabolism, between energy generation in the TCA cycle and ammonium assimilation by glutamate synthesis in *C. glutamicum* and other actinobacteria (Niebisch et al., 2006, O'Hare et al., 2008). In these organisms, the ODH activity is inhibited by binding of the small inhibitor protein OdhI or its mycobacterial homolog GarA in its unphosphorylated state. The phosphorylation status of OdhI depends on the activity of the serine/threonine protein kinase PknG and the phospho-serine/threonine protein phosphatase Ppp (Niebisch et al., 2006, Schultz et al., 2009). In this thesis, the putative glutamine-binding lipoprotein GlnH and the membrane protein GlnX as members of the signal transduction cascade regulating PknG activity were characterized.

The conserved genomic organization of *pknG* in a putative *glnX-glnH-pknG* operon, together with the growth defect on glutamine as sole carbon and nitrogen source caused by deletion of each of the three genes in *C. glutamicum*, suggested a role of all three proteins in the control of glutamine catabolism (Niebisch et al., 2006). Analysis of the OdhI phosphorylation status showed that the absence of each of the three proteins led to an increased amount of unphosphorylated OdhI (Sundermeyer et al., 2022a). The extent of this increase was similar for the three single deletion strains as well as for the triple deletion strain *C. glutamicum* Δ*glnX-glnH-pknG*, showing that GlnX, GlnH, and PknG do not possess individual functions on glutamine utilization, which would sum up in the triple deletion strain, but are part of the same signal transduction cascade (Sundermeyer et al., 2022a). The increased ODH inhibition caused by a reduced phosphorylation of OdhI in the absence of the three proteins was supported by an increased glutamate production observed for *C. glutamicum* strains Δ*pknG,* Δ*glnX* and Δ*glnH* (Sundermeyer et al., 2022a), showing that the 2-oxoglutarate flux is shifted toward glutamate synthesis in these strains, since the use for succinyl-CoA generation is prevented by binding of unphosphorylated OdhI to the ODH subunit OdhA. The increased glutamate production by the mutants could be abolished by introducing the deleted genes on a plasmid, confirming the causal relationship of the deletions and increased glutamate production (Sundermeyer et al., 2022a). The prevention of the growth defect on glutamine and the loss of increased glutamate production upon simultaneous deletion of *odhI* and *pknG* or *glnX*, respectively, in *C. glutamicum* Δ*pknG*Δ*odhI* or *C. glutamicum* Δ*glnX*Δ*odhI* proved that the influence on glutamate synthesis and glutamine utilization is based on the control of the OdhI phosphorylation status in both cases (Schultz et al., 2007, Sundermeyer et al., 2022a).

Moreover, the occurrence of suppressor mutants of the *C. glutamicum* strains Δ*pknG* and Δ*glnX*, which had regained the ability to grow on glutamine as sole carbon and nitrogen source

(Raasch et al., 2014, Sundermeyer et al., 2022a) and mainly possessed mutations in OdhI and in case of Δ*pknG* also in OdhA, underlined the role of PknG and GlnX in the control of the OdhI phosphorylation status. Insertion of stop codons and frameshift mutations in the *odhI* gene led to degraded OdhI variants and therefore mimicked the effect of an *odhI* deletion, leading to an active ODH and enabling glutamine utilization. This effect is also possible for amino acid exchanges in OdhI, which might impair correct protein folding and stability, especially if the mutations occur at conserved residues in structural elements, as for example, the mutations E91K or F137S (Sundermeyer et al., 2022a), which localize in the β-sheets 5 and 11 of the FHA domain of OdhI (Barthe et al., 2009), and led to no or very weak signals for OdhI in Western blot analysis (Sundermeyer et al., 2022a). A few amino acid exchanges apparently did not lead to OdhI degradation, but showed an influence on the inhibition of OdhA by OdhI. These mutations do not necessarily prevent the interaction of OdhI and OdhA in general, but might reduce the binding affinity due to missing interaction features such as specific salt bridges, as it was observed in case of the variant OdhI-R87P, where the inhibitory effect on ODH activity was reduced (Sundermeyer et al., 2022a). This shows that the individual residues at the interaction surface are important for the high affinity binding of OdhA and OdhI.

We focused on the PknG-mediated phosphorylation of OdhI at Thr14, which was reported to be the most abundant phosphorylation in *C. glutamicum* (Schultz et al., 2009), but it is known that OdhI can also be phosphorylated at Thr15 by other STPKs (PknA, PknB, PknL) and 2D gel electrophoresis demonstrated the presence of mono- as well as doubly-phosphorylated OdhI in *C. glutamicum* (Niebisch et al., 2006). Furthermore, the deletion of *pknG, glnX* and *glnH* increased the amount of unphosphorylated OdhI protein in Western blot analysis, but phosphorylated OdhI was still detected (Sundermeyer et al., 2022a), confirming that OdhI gets phosphorylated by another kinase in these strains. The regulation of ODH activity due to the influence of other kinases on the OdhI phosphorylation status might be an important subject of further research, since the 2-oxoglutarate metabolic branch point needs not only to be regulated depending on extracellular L-aspartate and L-glutamate availability. For instance, it was observed that the amount of phosphorylated OdhI was higher in the stationary phase than during exponential growth (Bosco, 2011, Schultz, 2008), which might reflect the requirement of active ODH to allow an increased flux through the TCA cycle and energy generation in the stationary phase, where the demand for ammonia assimilation is almost completely missing. The regulation of ammonium assimilation by controlling ODH activity on the post-translational level is special for actinobacteria, but recently a post-transcriptional mechanism to control nitrogen assimilation in *E. coli* was reported. There it is assumed that the flux of 2-oxoglutarate is shifted from TCA cycle toward ammonium assimilation, due to a repression of *sucA* mRNA (encoding the E1o subunit in *E. coli*) translation by binding of the sRNA GlnZ, which is produced from the glutamine synthetase mRNA (Miyakoshi et al., 2022).

3.2 The lipoprotein GlnH senses extracellular L-aspartate and L-glutamate

GlnH was originally annotated as a putative glutamine-binding lipoprotein (Kalinowski et al., 2003). While no glutamine binding was observed for GlnH, inhibition of the lipoprotein signal peptidase using the cyclic peptide antibiotic globomycin and experiments with the protein variant GlnH-C27A, which cannot attach the lipid anchor, showed that GlnH is indeed an extracytoplasmic protein attached to the membrane by a lipoprotein anchor (Sundermeyer et al., 2022a). The annotation as a glutamine-binding protein was based on the homology to the *E. coli* protein, with a sequence identity of 24%. GlnH of *E. coli* is part of an ABC-transporter responsible for glutamine uptake, while deletion of *glnH* in *C. glutamicum* did not have a strong effect on glutamine uptake (Niebisch et al., 2006). In combination with the observation that lack of GlnH reduces the fraction of phosphorylated OdhI (Sundermeyer et al., 2022a), we suggest that the *C. glutamicum* protein is not part of a transporter, but of a signal transduction cascade tuning the OdhI phosphorylation status. The extracytoplasmic localization of GlnH and the solved structure of the mycobacterial homolog (Bhattacharyya et al., 2018), suggests that GlnH functions as a sensor for extracytoplasmic stimuli.

Isothermal titration calorimetry (ITC) experiments revealed that purified GlnH binds L-aspartate and L-glutamate with affinities in the high µM to low mM range. With a K_D value of 264 ± 14.6 µM, the affinity for aspartate was clearly higher than the one for glutamate (1256 ± 220 µM) (Sundermeyer et al., 2022a). These results are in accordance with the ligand binding specificity of *C. glutamicum* GlnH determined using thermal stability measurements and analysis of changes in the intrinsic tryptophan fluorescence (Bhattacharyya et al., 2018). The approximately two-fold higher K_D values, reported by Bhattacharyya et al., are most likely caused by a different experimental set up including a different buffer composition and pH. More interesting was the finding, that *M. tuberculosis* also preferentially binds aspartate and glutamate but with much higher affinity, reflected by K_D values of 4.8 ± 0.6 µM for aspartate and 15.2 ± 5.7 µM for glutamate (Bhattacharyya et al., 2018). This differences in the ligand binding affinity might be connected to the evolutionary adaptation of the bacteria to the different environmental niches. The non-pathogenic *C. glutamicum* was originally isolated from soil, whereas the pathogen *M. tuberculosis* has to survive for long time periods inside human phagocytes, where the control of the carbon flux at the 2-oxoglutarate node by GarA, the homolog of OdhI in mycobacteria, might require a response to much lower concentrations of L-aspartate and L-glutamate.

Nevertheless, the huge difference in the affinities was surprising and it was interesting to analyze if this is reflected by structural differences of the two proteins. Unfortunately, crystallization trials using a GlnH variant lacking the N-terminal signal peptide and the lipobox motive (GlnHΔSP, also used in ITC experiments) as well as a variant lacking the predicted flexible N- and C-terminal segments (GlnHcore, comprises amino acid residues 48-334) failed.

However, comparison of an AlphaFold 2 model of *C. glutamicum* GlnH with the solved structure of *M. tuberculosis* GlnH showed that the overall structure of the ligand-binding domain of both proteins is similar, which is to be expected for two proteins showing 43% sequence identity (Sundermeyer et al., 2022a). A detailed analysis revealed that despite the overall similarity the ligand binding sites display a number of differences, which might be responsible for the different affinities. Especially, the residues in the loop 160-166 of *C. glutamicum* GlnH, differ from those in the *M. tuberculosis* protein, where this loop was shown to be crucial for ligand binding (Bhattacharyya et al., 2018). A striking difference concerns the residues Thr162 and Ser164 in *M. tuberculosis* GlnH, whose hydroxyl groups act as hydrogen bond donors towards the ligand carboxyl groups. In *C. glutamicum* GlnH, they are replaced by Ser163 and Thr165, respectively. Furthermore, the Ser163 hydroxyl group potentially builds a hydrogen bond to the amide group of Gln103 in *C. glutamicum* GlnH (Ser102 in *M. tuberculosis*), which might impair its availability as a hydrogen bond donor to the amino acid ligand. The relevance of the residues Ser163 and Thr165 for ligand binding affinity was tested using a GlnH variant with the amino acid exchanges S163T and T165S by measuring changes in intrinsic tryptophan fluorescence (Sundermeyer et al., 2022a). In case of an unaltered ligand binding site, this method led to K_D values of 242 µM for aspartate and 1458 µM for glutamate, which are comparable to the K_D values determined by ITC. For the GlnH-S163T-T165S variant, K_D values of 65 µM for aspartate and 243 µM for glutamate were measured (Sundermeyer et al., 2022a). This strong increase in binding affinity caused by a swap of Ser163 and Thr165 to the arrangement found in *M. tuberculosis* GlnH is remarkable and demonstrates the importance of these residues for the ligand binding affinity.

Despite their different binding affinities, L-aspartate and L-glutamate were identified as ligands recognized by GlnH in *C. glutamicum* and *M. tuberculosis* leading to a phosphorylation of OdhI via the GlnH-GlnX-PknG signal transduction cascade, which allows an increased flux through the TCA cycle due to an active ODH. In line with the ligand-binding affinity of GlnH, the dependency of PknG activation on the presence of amino acids, such as glutamate and aspartate and the related amino acids glutamine and asparagine, was shown *in vivo* in *M. smegmatis* (Rieck et al., 2017). GlnH is a substrate-binding protein, which acts as a sensor protein to control PknG mediated phosphorylation, while substrate-binding proteins were previously mainly described as part of ABC-transporters, sensor-histidine kinases, ion-channels, G-protein coupled receptors or transcriptional regulators (Berntsson et al., 2010). The solved structure of the *M. tuberculosis* GlnH protein is related to the fold of amino acid-binding proteins belonging to the substrate-binding protein cluster F-IV (Bhattacharyya et al., 2018, Berntsson et al., 2010).

3.3 Characteristics of GlnX enabling signal transduction

In the postulated signal transduction cascade the transmembrane protein GlnX is assumed to be responsible for the transfer of the information about the loading status of the extracytoplasmic sensor protein GlnH to the cytoplasmic STPK PknG to activate the kinase activity. Besides its functional link to PknG and its influence on OdhI/GarA phosphorylation (Bhattacharyya et al., 2018, Niebisch et al., 2006, Sundermeyer et al., 2022a), not much is known about GlnX so far. To gain better insights into possible protein-protein interactions, which might mediate the signal transduction, we analyzed the protein topology using bioinformatic predictions and the common experimental markers for cytoplasmic and periplasmic localization, β-galactosidase and alkaline phosphatase, respectively (Sundermeyer et al., 2022a). The GlnX protein is predicted to contain four transmembrane helices and two large periplasmic domains comprising approximately 150 amino acid residues each. The N-terminal region, comprising about 110 amino acid residues, a small portion of about 11 residues linking the second and third transmembrane helices, and the C-terminal region of about eight amino acid residues are predicted to be located in the cytoplasm. The second periplasmic region of GlnX shows similarities with CHASE3 family proteins, which represent extracellular sensory domains of transmembrane proteins including histidine kinases and chemoreceptors (Zhulin et al., 2003). This might be a hint for an additional binding of small-molecule ligands by GlnX itself. Based on the sequence signature search using Pfam, no other domains could be identified in GlnX, but structure-based comparisons using an AlphaFold 2 model of GlnX revealed that the periplasmic domains represent a well-established fold (Sundermeyer et al., 2022a). The AlphaFold 2 model predicts the two periplasmic domains to form four-helix bundles, which closely resemble the four helix-bundle sensory module described for chemoreceptors and sensory histidine kinases, such as the ligand-binding domain of the aspartate receptor Tar from *Salmonella typhimurium*, or the ligand-binding domain of the citrate-sensing chemoreceptor MCP2201 from *Comamonas testosteroni*, or the xylose-sensing domain of the transmembrane histidine kinase LytS from *Clostridium beijerinckii* (Milburn et al., 1991, Hong et al., 2019, Li et al., 2017). Furthermore, the AlphaFold 2 model, predicts an eight amino acid residue insertion in the fourth helix of the second periplasmic domain, which forms a finger-like protrusion with three acidic residues (^{435}DEE^{437}) at its tip, which might be involved in interactions with other proteins, such as GlnH (Sundermeyer et al., 2022a).

The cytoplasmic parts of GlnX are potential interaction partners for PknG, whereby especially the cytoplasmic loop linking the second and third transmembrane helices, which contains many acidic amino acid residues, and the C-terminus are conserved among GlnX-possessing actinobacteria (Bosco, 2011). This conservation might indicate their function in protein-protein interactions. In accordance with this assumption it was observed that C-terminal GlnX fusion

proteins do not complement the growth defect of *C. glutamicum* Δ*glnX2* on glutamine as sole carbon and nitrogen source, even if only a short amino acid sequence such as a Strep-tag was added, while the insertion into the membrane was not affected by these C-terminal fusions (supplementary Fig. S1). In order to test if the C-terminus or the cytoplasmic loop are bound by the TPR domain of PknG (Lisa et al., 2021), co-crystallization of PknG with the C-terminal peptide or a peptide corresponding to the cytoplasmic loop could be tested. Such an approach, was successfully applied for an artificial TPR domain and the C-terminal peptide of the heat-shock protein Hsp90 (Cortajarena et al., 2010). As an alternative, the binding could be tested using methods like ITC, microscale thermophoresis (MST) or surface plasmon resonance (SPR). Interaction of GlnX with PknG might also occur via the comparably large cytoplasmic N-terminus of GlnX, even though its amino acid sequence is less conserved and fusion constructs including the fluorescent protein mVenus and an affinity tag did not affect complementation ability (supplementary Fig. S1). Since the N-terminal part of GlnX is predicted to be partially unstructured, purification of the isolated domain could be difficult and truncation variants of the N-terminal segment might be an option to analyze its importance for GlnX functionality *in vivo*.

To analyze if GlnX indeed possesses a unique helical tandem module architecture as postulated based on the AlphaFold 2 structural model (Sundermeyer et al., 2022a), the protein structure needs to be solved. As the purification of the membrane protein GlnX can be challenging, we also tried to purify the periplasmic domains separately, an approach which was successfully used, for example, to analyze ligand binding and structure of the periplasmic domain of the histidine kinase CitA (Kaspar et al., 1999, Sevvana et al., 2008, Reinelt et al., 2003) or to analyze the structure of the periplasmic domain of histidine kinase EnvZ of the EnvZ-OmpR two-component system (Hwang et al., 2017). The first periplasmic domain of GlnX was successfully purified and the elution volume obtained by size exclusion chromatography indicated a trimeric state of the purified domain (supplementary Fig. S2). If this oligomerization status is an artefact of the isolated purification of the domain or reflects a higher oligomeric state of GlnX in general needs to be further analyzed and is an interesting aspect, since the predicted arrangement of the two four-helix bundles of GlnX closely resembles the non-covalent dimer formed by Tar and similar chemoreceptors (Sundermeyer et al., 2022a).

In contrast the second periplasmic domain, which contains the acidic protrusion, so far always aggregated during purification. Since the AlphaFold 2 model predicts a large interaction surface between both periplasmic domains (Sundermeyer et al., 2022a), the first periplasmic domain might be necessary to stabilize the second domain and fusion constructs of both domains might be an option to improve purification. In addition the use of different affinity tags which are known to improve protein solubility, such as MBP (maltose binding protein), GST

(glutathione-S-transferase), or SUMO (small ubiquitin-related modifier) could be tested. Purified periplasmic domains would enable *in vitro* interaction studies with GlnH, for example by size exclusion chromatography of mixed protein samples or SPR experiments. *In vivo* interaction studies using a GlnX mutant lacking the acidic protrusion might be used to test if this mimics the effect of *glnX* or *glnH* deletion, which would be expected if this structural feature is necessary for interaction and signal transfer. Furthermore random mutagenesis of GlnX could be performed to create a mutant library that is transferred into the Δ*glnX2* mutant and analyzed with respect to the ability for growth on glutamine. GlnX variants failing to complement could enable the identification of interaction sides as well as residues crucial for the signal transfer. Such an approach was used, for example to identify interactions of MBP and the Tar receptor of *E. coli* (Kossmann et al., 1988, Manson and Kossmann, 1986). In addition, structural modelling of the GlnH-GlnX, GlnX-PknG, or GlnH-GlnX-PknG complexes can be used to predict amino acid residues involved in protein-protein interactions, which can subsequently be mutagenized and tested.

The mode of signal transfer over the membrane used by four-helix bundles of classical dimeric chemoreceptors is also still under discussion, with indications for a piston-like displacement of the fourth helix in the sensor modules upon ligand binding, which may either propagate into the transmembrane helix bundle or transform into different modes including helical rotation or scissoring (Gushchin and Gordeliy, 2018). The similarities of the predicted GlnX structure with the periplasmic and transmembrane portions of these classical dimeric chemoreceptors, support the idea that a similar mechanism enables the signal transduction from GlnH to PknG via GlnX, even if the cytoplasmic part of GlnX does not contain any of the domains typically found in bacterial sensors, such as histidine kinases or receiver domains (Sundermeyer et al., 2022a).

3.4 Intracellular localization of OdhI

The question how the proposed interaction of GlnX with PknG activates the kinase activity of this protein can currently not be answered. One possibility is that inactive PknG is bound to GlnX and gets activated and released from GlnX after a conformational change of GlnX triggered by binding liganded GlnH in the periplasm (Sundermeyer et al., 2022a). Such a model is based on the observation that PknG is found both in cytoplasmic and in the membrane fraction in *C. glutamicum* and mycobacterial species (Bosco, 2011, Cowley et al., 2004). To further analyze the intracellular localization of PknG in *C. glutamicum*, fusion constructs of PknG with fluorescent proteins such as mVenus were constructed. Plasmid-based expression of these constructs led to a fluorescent signal that was equally distributed in the cytoplasm and not affected by the absence of GlnX or different growth conditions (Folkerts, 2022). The

plasmid-based expression of *pknG-mVenus* enabled complementation of the growth defect of *C. glutamicum* Δ*pknG* on glutamine as sole carbon and nitrogen source (Folkerts, 2022), suggesting that the fusion protein is functional. *C. glutamicum* transcriptome analysis suggests a very weak transcription of *pknG* (personal communication, Jörn Kalinowski, Bielefeld University), and plasmid-based overexpression strongly differs from the native situation. Therefore, a *C. glutamicum::pknG-mVenus* integration strain was constructed, which can be used in future experiments to analyze the intracellular localization of PknG at different growth conditions. However, initial experiments with this strain in glucose minimal medium did not show a specific intracellular localization (data not shown).

Together with the localization of PknG we investigated the intracellular localization of OdhI in *C. glutamicum*, using an OdhI-mVenus fusion protein and surprisingly observed bright fluorescent spots mainly localized at the cell poles and sometimes also at the division site (Sundermeyer et al., 2022b). This spot formation was visible for plasmid-based expression of *odhI-mVenus* in a Δ*odhI* mutant as well as in an a *C. glutamicum::odhI-mVenus* integration strain, suggesting that the spots are not caused by inclusion body formation due to overexpression or as an artefact of the plasmid-based expression. Interestingly, the OdhI-mVenus fluorescence signal in the integration strain was stronger than in the strain with plasmid-encoded OdhI-mVenus under uninduced conditions (Sundermeyer et al., 2022b), suggesting that the native promotor of *odhI* is rather strong and OdhI is a highly abundant protein in *C. glutamicum*. This observation is in line with transcriptome analysis data, which indicate the *odhI* promotor being a strong one (personal communication, Jörn Kalinowski, Bielefeld University). The functionality of C-terminal fusions of OdhI with fluorescent proteins was shown by expression of *odhI-mVenus* and *odhI-mCherry* in *C. glutamicum* Δ*pknG*Δ*odhI,* where it prevented the growth on glutamine (Folkerts, 2022), thereby mimicking the growth defect of the *pknG* single deletion strain.

Since phosphorylation is crucial for controlling the inhibitory effect of OdhI on ODH activity, it was tested if the specific localization observed for OdhI-mVenus also depends on the phosphorylation status and if interaction with proteins involved in OdhI phosphorylation and dephosphorylation is required for its polar localization. Neither the absence of PknG nor the absence of either PknA or PknB in combination with PknL and PknG caused a loss of OdhI-mVenus fluorescent spots, suggesting that none of the STPKs is the interaction partner responsible for the localization of OdhI at the cell poles (Sundermeyer et al., 2022b). But analysis of almost completely phosphorylated OdhI-mVenus in a deletion strain of the phosphatase Ppp (Schultz et al., 2009) led to an almost uniform cytosolic fluorescence with only very few distinct fluorescent spots formed (Sundermeyer et al., 2022b). This observation clearly suggested that the polar localization of OdhI is caused by the unphosphorylated OdhI protein. The interaction with Ppp itself is unlikely to cause the distinct localization since in the

ppp deletion strain, a few OdhI-mVenus spots were still formed. Newly synthesized OdhI might cause the residual fluorescent spots detected in the absence of Ppp before it gets phosphorylated by one of the STPKs. In addition, *C. glutamicum* might possess additional phosphatases, which dephosphorylate OdhI with low activity. Further support for unphosphorylated OdhI being responsible for OdhI-mVenus fluorescent spot formation comes from the experiments with OdhI variants in which the known phosphorylation sites Thr14 and Thr15 have been exchanged to alanine (Niebisch et al., 2006). These variants also showed OdhI-mVenus spot formation (Folkerts, 2022), confirming that unphosphorylated OdhI is responsible for the polar localization.

An approach to further confirm that phosphorylated OdhI does not form fluorescent spots is the use of an OdhI variant in which the threonine phosphorylation sites are replaced by the charged amino acids aspartate or glutamate to mimic permanent phosphorylation (Dissmeyer and Schnittger, 2011). While the substitution of threonine by glutamate was, for example, able to mimic a phosphorylated and thereby active form of a mammalian guanylyl cyclase-A (Otto et al., 2017), a T14E substitution in OdhI did not efficiently mimic the phosphorylated threonine residue. This was shown by the growth defect of *C. glutamicum* Δ*pknG*Δ*odhI* with pPREx2-*odhI*-T14E-*mVenus* on glutamine (Folkerts, 2022). Efficient binding of the glutamate residue by the FHA domain should lead to a closed conformation of the OdhI protein, which would prevent inhibition of ODH activity and therefore allow growth on glutamine as observed for *C. glutamicum* Δ*pknG*Δ*odhI* (Niebisch et al., 2006). Other studies also observed that substituting serine and threonine residues with aspartate and glutamate is not always suitable to mimic phosphorylated residues. For example, phosphomimetic substitutions in the hydrophobic motif site of human AGC kinases led to a constitutive activation, while substitutions in the activation loop failed to successfully mimic phosphorylation sites since they do not reconstruct essential structural features as the formation of salt bridges with other residues (Somale et al., 2020).

3.5 Polar localization of the hybrid PDH-ODH complex in *C. glutamicum*

The findings that the polar fluorescent spots of OdhI-mVenus represent unphosphorylated OdhI and that none of the STPKs causes this localization obviously suggested that OdhA is responsible for this specific localization, as it is the only known interaction partner of unphosphorylated OdhI. This was confirmed by the observations that expression of *odhI-mVenus* in an *odhA* deletion strain led to a complete loss of OdhI-mVenus fluorescent spots and that OdhA-mCherry also formed fluorescent spots at the cell poles in *C. glutamicum* Δ*odhA* with pPREx2-*odhA-mCherry* (Sundermeyer et al., 2022b). Furthermore, the co-localization of fluorescently tagged OdhI and OdhA proteins was shown (Sundermeyer et al., 2022b). As

OdhA is part of the hybrid PDH-ODH complex, the question was raised whether the polar localization is specific for OdhA and might be connected to a so far unknown additional function of OdhA or if the entire PDH-ODH complex possesses a polar localization. Therefore the intracellular localization was analyzed for the other proteins of the hybrid complex, AceE, AceF, and Lpd. Fusion constructs of AceE, AceF, and Lpd with mVenus also formed fluorescent spots at the cell poles when expressed in *C. glutamicum*, and a co-localization of AceE-mCherry and AceF-mCherry with OdhA-mVenus was observed for the plasmid-based synthesis of the AceE and AceF fusion constructs in a *C. glutamicum*::*odhA-mVenus* integration strain (Sundermeyer et al., 2022b).

The observation of a polar localization of the hybrid PDH-ODH complex of *C. glutamicum* is an interesting new feature of this unusual complex and it seems to be the first time that such a specific subcellular localization was observed for a cytoplasmic protein complex of the central carbon metabolism. This finding led to the question if *C. glutamicum* possesses an even larger assembly of enzymes involved in the TCA cycle and ammonium assimilation that localizes at the cell poles. However, the analysis of the intracellular localization of isocitrate dehydrogenase and glutamate dehydrogenase as representatives for other enzymes involved in these processes did not show a specific localization but were equally distributed in the cytoplasm (Sundermeyer et al., 2022b).
Examples of cytoplasmic proteins that process a polar localization in *C. glutamicum* are DivIVA and ParB (Letek et al., 2008a, Donovan et al., 2010). DivIVA is a polar scaffold protein that forms large oligomers at the cell poles and at a late state of the cell cycle also at the division site due to its ability to recognize negative membrane curvature (Lenarcic et al., 2009). *C. glutamicum* DivIVA possesses interaction sites for proteins involved in cell elongation and chromosome segregation, thereby being involved in the spatio-temporal control of these cellular processes (Sieger and Bramkamp, 2015). One example of a DivIVA interaction partner involved in chromosome segregation is ParB (Donovan et al., 2012), which binds specific DNA motifs close to the chromosome origin and is important for nucleoid segregation (Donovan and Bramkamp, 2014). Another example of a protein possessing a polar localization in actinobacteria is the membrane-bound STPK PknB, which is associated with peptidoglycan synthesis in mycobacteria (Bellinzoni et al., 2019), but was also identified as a kinase responsible for the phosphorylation of OdhI (Schultz et al., 2009, Barthe et al., 2009).

In contrast to the examples mentioned above, the observed specific localization of the PDH-ODH complex cannot be connected to its function on the first view. Its localization could be caused by interaction with another protein possessing a polar localization or by effects such as nucleoid exclusion. In the latter case, the localization at the cell poles would be caused by the exclusion of the large PDH-ODH complex from the cell center by the nucleoid due to the high molecular crowding and diffusion hindrance in this area (Wu and Errington, 2012, Coquel

et al., 2013).

To find out if one of the PDH-ODH complex proteins possesses an additional interaction partner responsible for the polar localization, the localization of AceE, AceF, and OdhA fusion constructs with the fluorescent proteins mVenus or mCherry were analyzed in *odhA* and *aceE* deletion strains. Since the absence of the E1 subunits of ODH and PDH did not affect the formation of fluorescent spots formed by the other dehydrogenase components, it can be assumed that neither OdhA nor AceE are responsible for the polar localization (Sundermeyer et al., 2022b). Therefore, analysis of the localization of the PDH-ODH complex proteins in *lpd* and *aceF* deletion strains would be very interesting. In a *C. glutamicum* Δ*aceF* strain, it might be the case that no specific localization is detected for the other proteins of the hybrid complex, even if AceF does not interact with an unknown polarly localized protein, since AceF forms the center of the PDH-ODH complex and connects the other protein components (Bruch et al., 2021, Kinugawa et al., 2020). Therefore it would also be very interesting to analyze the effect of AceF truncation variants lacking the lipoyl binding domains or the peripheral-subunit binding domain on the formation of the PDH-ODH complex and its polar localization, since these domains are required for the acyl group transfer or as interaction sites of AceF with the E1 and E3 subunits, respectively (Kinugawa et al., 2020).

If the polar localization of the hybrid complex is indeed caused by an interaction with another protein, not only the responsible component of the PDH-ODH complex needs to be identified but also the interaction partner. During co-purification experiments no obvious candidate was identified so far (see chapter 5.3). Therefore, cross-linking experiments might be an option to stabilize protein interactions and identify new interaction partners. This analysis should include cytoplasmic as well as membrane proteins since especially membrane-bound proteins might be responsible for a polar localization. *In vivo* cross-linking could be tested using formaldehyde or other membrane-permeable chemical cross-linkers, for example, the lysin-targeted cross-linker DSP (di-thiobis(succinimidyl propionate)) or cystein-targeted TMAE (tris(2-maleimidoethyl)amine) (Studdert and Parkinson, 2007). As an alternative, photo-reactive amino acids such as L-photo-leucine or L-photo-methionine, which are added as supplements to the culture medium during growth and later on activated by UV light, could be tested for cross-linking (Suchanek et al., 2005). Another cross-linking approach, based on incorporating photo-reactive amino acids into proteins, is the use of an orthogonal aminoacyl-tRNA synthetase/tRNA pair, which was developed for incorporation of *p*-benzoyl-L-phenylalanine into proteins in *E. coli*. In this method, an amber codon (UAG) is introduced in the DNA sequence encoding for the protein of interest and plasmid-based expression of the target gene as well as the orthogonal aminoacyl-tRNA synthetase gene and the tRNA, specific for *p*-benzoyl-L-phenylalanine and the amber codon, leads to site-specific incorporation of the photo-reactive amino acid into the target protein when *p*-benzoyl-L-phenylalanine is present in the

growth medium (Chin et al., 2002). However, *p*-benzoyl-L-phenylalanine is also incorporated during the translation of mRNAs that natively contain amber codons. It could be tested if this approach is also suitable for *C. glutamicum*.

The use of fluorescently labeled proteins allows the analysis of the intracellular localization in living cells, but although it is a good approach applicable in different growth conditions and due to plasmid-based expression also in different strain backgrounds, it also has some bottlenecks. One aspect is that the N- or C-terminal fusion of a target protein with a fluorescent protein might affect its enzymatic activity or protein-protein interaction properties. Especially in large complexes such as the PDH-ODH complex of *C. glutamicum*, the fluorescent proteins might be hindering efficient complex formation. Therefore, it would be interesting to compare the growth behavior of integration strains such as *C. glutamicum::odhA-mVenus* to a *C. glutamicum* wt strain and to measure ODH and PDH activities in cell lysates of the integration strains. Furthermore, it has to be considered that the fluorescent protein itself might cause aggregation and lead to false localization results. The use of monomeric fluorescent proteins, such as mVenus and mCherry, in our study reduces the risk of aggregates caused by the fluorescent protein. In addition, control experiments analyzing the cellular localization of the fluorescent proteins alone without target protein fusion and strains enabling physiological expression levels, such as *C. glutamicum::odhI-mVenus* or *C. glutamicum::odhA-mVenus* (Sundermeyer et al., 2022b), reduce the risk of artifacts caused by the fused fluorescent protein.

Control experiments analyzing the intracellular localization of native proteins in fixed cells by immunostaining are a good option to validate the specific localization observed in our studies since especially for large complexes aggregation of fluorescently tagged proteins could occur due to the proximity of the fluorescent proteins in such a complex. Such aggregates were shown to possess unipolar as well as bipolar localization caused by a combination of aggregation and nucleoid occlusion (Landgraf et al., 2012, Scheu et al., 2014, Saberi and Emberly, 2013). Therefore the polar localization of the hybrid PDH-ODH complex could be analyzed in an immunostaining experiment to prove its polar localization. Such an immunostaining experiment requires primary antibodies against components of the hybrid PDH-ODH complex, for example, OdhA. As controls, primary antibodies for *C. glutamicum* proteins, which are either known to possess a specific localization, such as FtsZ, or are expected to be evenly distributed in the cytoplasm, such as isocitrate dehydrogenase or aconitase could be used. Besides the suitable fluorescent-labeled secondary antibodies, an efficient permeabilization procedure is necessary to allow antibody detection of intracellular proteins despite the thick corynebacterial cell envelope. Permeabilization using lysozyme could be an option, as it was successfully applied in *C. glutamicum* for FtsZ localization studies by immunostaining (Ramos et al., 2005).

Furthermore, additional microfluidics experiments with *C. glutamicum::odhA-mVenus* or integration strains of other fluorescently labeled PDH-ODH complex components could reveal how their localization changes during the cell cycle. In our initial experiments with *C. glutamicum::odhI-mVenus,* new OdhI-mVenus fluorescent spots seemed to be formed at the division site (Sundermeyer et al., 2022b). Parallel observation of fluorescently labeled proteins known for their localization at an early or late state of the division process, such as FtsZ or DivIVA (Margolin, 2005, Letek et al., 2008b), respectively, might be interesting.
DNA staining could be included in future microscopy experiments to analyze if nucleoid occlusion is responsible for the polar localization of the hybrid PDH-ODH complex. If nucleoid occlusion due to the size of the complex, turns out to be responsible for its localization, it would be interesting to analyze the intracellular localization of ODH and PDH complexes in other organisms, such as *E. coli,* since these dehydrogenase complexes are known to form complexes of ~10 MDa, which are presumably much larger than the hybrid PDH-ODH complex of *C. glutamicum* (Kinugawa et al., 2020).

3.6 Composition of the hybrid PDH-ODH complex

The observation of a polar localization of the hybrid PDH-ODH complex is an interesting new feature of this unusual dehydrogenase complex and improvement of knowledge on the stoichiometry of its components, protein-protein interactions, and protein structure was the major aim of our cooperation partners at the Institute Pasteur in Paris (Dr. Marco Bellinzoni). The use of a *C. glutamicum* strain with a genomically encoded AceF-Strep protein was assumed to improve co-purification of the hybrid complex by providing a more balanced ratio of AceE and OdhA than observed for co-purification using OdhA-Strep or AceE-Strep in previous experiments (Niebisch et al., 2006) since AceF is required for both PDH and ODH activity and interacts with all three other proteins of the complex (Hoffelder et al., 2010). However, SDS-PAGE analysis of samples purified via AceF-Strep revealed a similar protein composition as observed for OdhA-Strep samples, with comparably low amounts of co-purified AceE (supplementary Fig. S5). The less efficient co-purification of AceE was also reflected by the lower PDH than ODH activities determined for the AceF-Strep-purified samples, suggesting that the binding of AceF to AceE is weaker than the binding to OdhA. The lower affinity of AceE and AceF was also observed in analytical ultracentrifugation and size exclusion chromatography experiments in a recent study (Kinugawa et al., 2020). In general, the determined PDH activities were lower than the ODH activities in the AceE-Strep sample as well, which might be caused by an impaired formation of the PDH complex since decarboxylase activity measurements in the AceE-Strep purified sample revealed about ten-fold higher values for AceE than for OdhA in these sample (supplementary Fig. S6). The decarboxylase activity measures only the activity of the E1 subunit and its higher AceE than

OdhA activity correlated with the high amounts of AceE protein identified by SDS-PAGE analysis in these samples. However this was not reflected by the ratio of PDH to ODH dehydrogenase activities, which require the assembly of all dehydrogenase components. Additional aspects, such as an insufficient removal of potential allosteric inhibitors, might play a role as well.

Strong variations in the ODH activities of different AceF-Strep-purified samples (supplementary Fig. S5) suggest that already slight changes during cell disruption and protein purification might affect the co-purification success. The strong dependency of successful complex assembly on the environment was also supported by the observation that heterologous production and purification of the four protein components in *E. coli* only enabled formation of an active PDH-ODH complex when the purification buffer contained 10% (v/v) glycerol (personal communication, Lu Yang, Institute Pasteur, Paris), as initially described by Niebisch et al. 2006. In this thesis it was shown that the positive effect of high glycerol concentrations during cell disruption and protein purification can be taken over by *myo*-inositol as buffer additive (supplementary Fig. S7), which was previously reported to stabilize the pyruvate carboxylase of *M. smegmatis* (Mukhopadhyay and Purwantini, 2000). It is assumed that high glycerol or *myo*-inositol concentrations mimic intracellular molecular crowding important for efficient PDH-ODH complex assembly.

Samples of the PDH-ODH complex co-purified using either Strep-tagged OdhA, Strep-tagged AceE, or Strep-tagged AceF were provided to our cooperation partners for cryogenic electron microscopy (cryo-EM) experiments, but unfortunately the interactions of the different protein components were too flexible to allow structure determination (personal communication, Marco Bellinzoni and Lu Yang, Institute Pasteur, Paris). Cross-linking and the use of nanobodies were discussed to reduce flexibility and movement of the different protein components, but so far the studies focused more on the structure elucidation of the individual protein components and their potential interaction sites. For this purpose, our cooperation partners performed *in vitro* interaction studies with purified proteins to gain a better understanding of the interacting protein regions within the hybrid PDH-ODH complex. A part of the OdhA protein that is assumed to be responsible for interaction with AceF is the N-terminus (Hoffelder et al., 2010). To analyze if it is indeed necessary for interaction with AceF, we analyzed the complementation ability of different N-terminally truncated variants of OdhA in a *C. glutamicum* Δ*odhA* strain (supplementary Fig. S8). Deletion of the *odhA* gene prevents ODH formation and thereby interrupts the TCA cycle, which leads to a strong growth defect and an accumulation of 2-oxoglutarate and acetate in the growth medium (Hoffelder et al., 2010). To prevent fast acidification of the culture medium and thereby impaired growth of the analyzed *C. glutamicum* strains, the complementation tests were carried out in a medium composed of the unbuffered complex medium BHI and buffered defined salt medium CGXII with 2% (w/v) glucose. While

the *odhA* deletion strain carrying the empty plasmid showed reduced growth compared to *C. glutamicum* wt, plasmids encoding either full-length OdhA or the variants OdhAΔ26, OdhAΔ40, and OdhAΔhelix2 enabled complementation to a similar extent and led to a growth behavior comparable to the wt, while the variant OdhAΔ97 enabled only partial complementation (supplementary Fig. S9). When target gene expression was induced by the addition of IPTG, a positive effect was observed for the growth of the strain carrying the expression plasmid encoding OdhAΔ97 (supplementary Fig. S10), indicating that at higher expression levels, the complementation capability of the OdhAΔ97 variant is comparable to the other OdhA variants. This suggests that the assumed lower affinity of OdhAΔ97 to AceF can be overcome by higher protein levels of this variant. Presumably, the N-terminal 97 amino acids of OdhA enhance the interaction with AceF but are not essential for the interaction in general, which is most likely explained by additional protein-protein interactions, for example via the lipoyl-binding domains of AceF, that still enable the interaction of OdhAΔ97 with AceF. Protein interaction studies of OdhA full-length and the OdhAΔ97 mutant with AceF full-length and truncated AceF variants lacking either the lipoyl binding domains or the peripheral subunit binding domain could be performed to verify this hypothesis. In a previous study, a chromosomal deletion of the N-terminal extension of OdhA prevented ODH activity and showed a similar growth defect as a complete deletion of the *odhA* gene (Hoffelder et al., 2010). This difference might be explained by the higher protein levels reached by plasmid-based expression, which could overcome the lower affinity of the truncation variant to AceF. Use of chromosomal deletions to generate the different N-terminal OdhA truncations that were tested here via plasmid-based synthesis might allow to identify which N-terminal structural elements facilitate the interaction with AceF, since in this case lower binding affinities cannot be hidden by higher protein levels. Further *in vitro* as well as *in vivo* interaction studies, for example using AceF truncation variants and an *aceF* deletion strain, might enable further insights into the protein-protein interactions involved in the assembly of the hybrid PDH-ODH complex in *C. glutamicum* and other actinobacteria, even if the overall aim is still to determine the structure of the entire PDH-ODH complex.

3.7 Overview on the post-translational regulation of the 2-oxoglutarate metabolic branch point in *C. glutamicum*

The activity of the corynebacterial ODH is regulated by the small FHA domain-containing protein OdhI. OdhI binds with nM affinity to the E1 subunit OdhA and thereby inhibits ODH activity, enabling an increased flux of 2-oxoglutarate towards L-glutamate synthesis and nitrogen assimilation (Niebisch et al., 2006, Raasch et al., 2014, Krawczyk et al., 2010). Phosphorylation of OdhI by a STPK triggers a conformational change and prevents binding to OdhA (Niebisch et al., 2006, Barthe et al., 2009, Krawczyk et al., 2010). While phosphorylation

by PknG was identified to be mainly responsible for OdhI phosphorylation, the three membrane-bound STPKs PknA, PknB, and PknL were also shown to phosphorylate OdhI (Schultz et al., 2009). This thesis focused on the signal transduction cascade tuning PknG activity, but further studies should also investigate the signals controlling OdhI phosphorylation by the three other kinases.

Here it was shown that the lipoprotein GlnH, the membrane protein GlnX, and the kinase PknG are part of a signal transduction cascade regulating the OdhI phosphorylation status depending on the availability of L-aspartate or L-glutamate in the environment. It is speculated that in the absence of these amino acids in the periplasm, which are sensed by GlnH, PknG forms a complex with the cytoplasmic portion of GlnX and is inactive. At this stage, OdhI is predominantly unphosphorylated, binds to the OdhA subunit of ODH and inhibits its activity, which enables a shift of the 2-oxoglutarate flux from TCA cycle towards L-glutamate synthesis and ammonium assimilation. In the presence of L-aspartate or L-glutamate in the periplasm, GlnH binds these amino acids and interacts with the periplasmic tandem four-helix bundle domain of GlnX. Binding of additional, so far unknown ligands by GlnX might occur in addition. The mode of signal transfer across the membrane by structural changes in GlnX upon GlnH binding has to be elucidated. We assume that these structural changes in GlnX lead to conformational changes in PknG enabling the activation of the kinase activity. Once activated PknG phosphorylates OdhI at Thr14, the interaction of OdhI with OdhA is prevented and consequently the flux of 2-oxoglutarate is shifted towards the TCA cycle and energy generation as represented in Fig. 6 (Sundermeyer et al., 2022a).

Another interesting new feature was observed for the unusual hybrid PDH-ODH complex. Fluorescence microscopy approaches revealed a polar localization of this complex (Sundermeyer et al., 2022b). Such a specific subcellular localization was not expected for an enzyme complex involved in central metabolism. The functional relevance of this localization and its potential connection to cell division processes is subject of ongoing research.

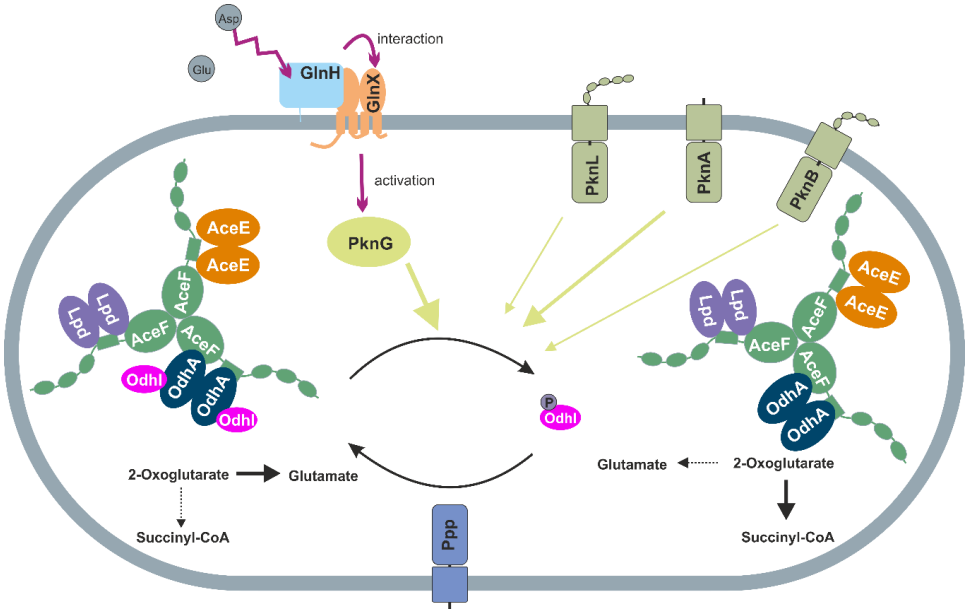

Figure 6: Schematic representation of the post-translational control of the 2-oxoglutarate metabolic branch point in *C. glutamicum*. The distribution of 2-oxoglutarate between the TCA cycle and glutamate synthesis and thus nitrogen assimilation is regulated by control of the ODH activity. The activity of corynebacterial ODH is inhibited by binding of OdhI. Phosphorylation of OdhI by a Ser/Thr protein kinase triggers a conformational change that prevents binding to OdhA. The strength of the green arrows indicates the influence of the four STPKs PknG, PknA, PknB, and PknL on the phosphorylation status of OdhI *in vivo* as determined by Schultz et al. 2009. Dephosphorylation of phosphorylated OdhI is catalyzed by the phospho-Ser/Thr protein phosphatase Ppp. PknG activity is regulated by a signal-transduction cascade consisting of the extracytoplasmic lipoprotein GlnH and the membrane protein GlnX. GlnH senses external L-aspartate and L-glutamate concentrations. The information on the GlnH loading status is transferred across the cytoplasmic membrane via GlnX by protein-protein interactions and leads to an activation of the PknG kinase activity in the cytoplasm. The exact mechanisms and protein-protein interaction sites are subjects of ongoing research. The corynebacterial ODH consists of three subunits OdhA, AceF, and Lpd. AceF and Lpd are shared between ODH and PDH and together with the PDH subunit AceE they form the unusual hybrid PDH-ODH complex in *C. glutamicum*, which showed a polar localization in fluorescence microscopy approaches using fluorescent-tagged protein variants. The reason of the polar localization as well as its functional relevance are interesting aspects of ongoing research. The representation of the PDH-ODH complex reflects the assumed oligomeric states of AceF, AceE, Lpd and OdhA in the complex, but does not represent the overall stoichiometry of the different components in the hybrid PDH-ODH complex. In addition other oligomeric states of the PDH-ODH components such as OdhA hexamers (Kinugawa et al., 2020) could be present in *C. glutamicum*.

4. References

ABE, S., TAKAYAMA, K.-I. & KINOSHITA, S. 1967. Taxonomical studies on glutamic acid-producing bacteria. *The Journal of General Applied Microbiology,* 13**,** 279-301.

ASAKURA, Y., KIMURA, E., USUDA, Y., KAWAHARA, Y., MATSUI, K., OSUMI, T. & NAKAMATSU, T. 2007. Altered metabolic flux due to deletion of *odhA* causes L-glutamate overproduction in *Corynebacterium glutamicum*. *Applied and environmental microbiology,* 73**,** 1308-1319.

AV-GAY, Y. & EVERETT, M. 2000. The eukaryotic-like Ser/Thr protein kinases of *Mycobacterium tuberculosis*. *Trends in microbiology,* 8**,** 238-244.

BAKKES, P. J., RAMP, P., BIDA, A., DOHMEN-OLMA, D., BOTT, M. & FREUDL, R. 2020. Improved pEKEx2-derived expression vectors for tightly controlled production of recombinant proteins in *Corynebacterium glutamicum*. *Plasmid,* 112**,** 102540.

BARKA, E. A., VATSA, P., SANCHEZ, L., GAVEAU-VAILLANT, N., JACQUARD, C., KLENK, H.-P., CLÉMENT, C., OUHDOUCH, Y. & WEZEL, G. P. V. 2016. Taxonomy, physiology, and natural products of *Actinobacteria*. *Microbiology and Molecular Biology Reviews,* 80**,** 1-43.

BARTHE, P., ROUMESTAND, C., CANOVA, M. J., KREMER, L., HURARD, C., MOLLE, V. & COHEN-GONSAUD, M. 2009. Dynamic and structural characterization of a bacterial FHA protein reveals a new autoinhibition mechanism. *Structure,* 17**,** 568-578.

BAYAN, N., HOUSSIN, C., CHAMI, M. & LEBLON, G. 2003. Mycomembrane and S-layer: two important structures of *Corynebacterium glutamicum* cell envelope with promising biotechnology applications. *Journal of Biotechnology,* 104**,** 55-67.

BECKER, J., ROHLES, C. M. & WITTMANN, C. 2018. Metabolically engineered *Corynebacterium glutamicum* for bio-based production of chemicals, fuels, materials, and healthcare products. *Metabolic Engineering,* 50**,** 122-141.

BELLINZONI, M., WEHENKEL, A. M., DURÁN, R. & ALZARI, P. M. 2019. Novel mechanistic insights into physiological signaling pathways mediated by mycobacterial Ser/Thr protein kinases. *Genes & Immunity,* 20**,** 383-393.

BERNTSSON, R. P. A., SMITS, S. H. J., SCHMITT, L., SLOTBOOM, D.-J. & POOLMAN, B. 2010. A structural classification of substrate-binding proteins. *FEBS Letters,* 584**,** 2606-2617.

BERTANI, G. 1951. Studies on lysogenesis I: the mode of phage liberation by lysogenic *Escherichia coli*. *Journal of Bacteriology,* 62**,** 293-300.

BHATTACHARYYA, N., NKUMAMA, I. N., NEWLAND-SMITH, Z., LIN, L.-Y., YIN, W., CULLEN, R. E., GRIFFITHS, J. S., JARVIS, A. R., PRICE, M. J., CHONG, P. Y., WALLIS, R. & O'HARE, H. M. 2018. An aspartate-specific solute-binding protein regulates protein kinase G activity to control glutamate metabolism in mycobacteria. *mBio,* 9**,** e00931-18.

BLATCH, G. L. & LÄSSLE, M. 1999. The tetratricopeptide repeat: a structural motif mediating protein-protein interactions. *BioEssays,* 21**,** 932-939.

BLOMBACH, B., RIESTER, T., WIESCHALKA, S., ZIERT, C., YOUN, J.-W., WENDISCH, V. F. & EIKMANNS, B. J. 2011. *Corynebacterium glutamicum* Tailored for Efficient Isobutanol Production. *Applied and Environmental Microbiology,* 77**,** 3300-3310.

BÖRMANN, E. R., EIKMANNS, B. J. & SAHM, H. 1992. Molecular analysis of the *Corynebacterium glutamicum gdh* gene encoding glutamate dehydrogenase. *Molecular microbiology,* 6**,** 317-326.

BOSCO, G. 2011. Charakterisierung von Proteinen einer neuartigen Signaltransduktionskaskade in *Corynebacterium glutamicum*. *Reihe Gesundheit/Health, Forschungszentrum Jülich GmbH*.

BOTT, M. & BROCKER, M. 2012. Two-component signal transduction in *Corynebacterium glutamicum* and other corynebacteria: on the way towards stimuli and targets. *Applied Microbiology and Biotechnology,* 94**,** 1131-1150.

BOTT, M. & EIKMANNS, B. J. 2013. TCA cycle and glyoxylate shunt of *Corynebacterium glutamicum*. *In: Yukawa H., Inui M. (eds) Corynebacterium glutamicum. Microbiology Monographs, vol. 23.* Springer, Berlin, Heidelberg.

BROCKER, M., MACK, C. & BOTT, M. 2011. Target genes, consensus binding site, and role of phosphorylation for the response regulator MtrA of *Corynebacterium glutamicum*. *Journal of Bacteriology,* 193**,** 1237-1249.

BROCKER, M., SCHAFFER, S., MACK, C. & BOTT, M. 2009. Citrate utilization by *Corynebacterium glutamicum* is controlled by the CitAB two-component system through positive regulation of the citrate transport genes *citH* and *tctCBA*. *Journal of Bacteriology,* 191**,** 3869-3880.

BRUCH, E. M., VILELA, P., YANG, L., BOYKO, A., LEXA-SAPART, N., RAYNAL, B., ALZARI, P. M. & BELLINZONI, M. 2021. Actinobacteria challenge the paradigm: A unique protein architecture for a well-known, central metabolic complex. *Proceedings of the National Academy of Science,* 118**,** e2112107118.

BUERGER, J., REHM, N., GREBENSTEIN, L. & BURKOVSKI, A. 2016. Glutamine metabolism of *Corynebacterium glutamicum*: role of the glutaminase GlsK. *FEMS Microbiology Letters,* 363**,** fnw230.

BURNSIDE, K. & RAJAGOPAL, L. 2012. Regulation of prokaryotic gene expression by eukaryotic-like enzymes. *Current Opinion in Biotechnology,* 15**,** 125-31.

CHIN, J. W., MARTIN, A. B., KING, D. S., WANG, L. & SCHULTZ, P. G. 2002. Addition of a photocrosslinking amino acid to the genetic code of *Escherichia coli*. *Proceedings of the National Academy of Sciences,* 99**,** 11020-11024.

COQUEL, A.-S., JACOB, J.-P., PRIMET, M., DEMAREZ, A., DIMICCOLI, M., JULOU, T., MOISAN, L., LINDNER, A. B. & BERRY, H. 2013. Localization of protein aggregation in *Escherichia coli* is governed by diffusion and nucleoid macromolecular crowding effect. *PLOS Computational Biology,* 9**,** e1003038.

CORE, L. & PEREGO, M. 2003. TPR-mediated interaction of RapC with ComA inhibits response regulator-DNA binding for competence development in *Bacillus subtilis*. *Molecular Microbiology,* 49**,** 1509-1522.

CORTAJARENA, A. L., WANG, J. & REGAN, L. 2010. Crystal structure of a designed tetratricopeptide repeat module in complex with its peptide ligand. *The FEBS Journal,* 277**,** 1058-1066.

COWLEY, S., KO, M., PICK, N., CHOW, R., DOWNING, K. J., GORDHAN, B. G., BETTS, J. C., MIZRAHI, V., SMITH, D. A. & STOKES, R. W. 2004. The *Mycobacterium tuberculosis* protein serine/threonine kinase PknG is linked to cellular glutamate/glutamine levels and is important for growth *in vivo*. *Molecular microbiology,* 52**,** 1691-1702.

D'ANDREA, L. D. & REGAN, L. 2003. TPR proteins: the versatile helix. *Trends in biochemical science,* 28**,** 655-62.

DE LIMA PROCÓPIO, R. E., DA SILVA, I. R., MARTINS, M. K., DE AZEVEDO, J. L. & DE ARAÚJO, J. M. 2012. Antibiotics produced by *Streptomyces*. *The Brazilian Journal of infectious diseases,* 16**,** 466-471.

DISSMEYER, N. & SCHNITTGER, A. 2011. Use of phospho-site substitutions to analyze the biological relevance of phosphorylation events in regulatory networks. *In: Dissmeyer, N., Schnittger, A. (eds) Plant Kinases. Methods in Molecular Biology. Humana, Totowa, NJ.,* 779**,** 93-138.

DONOVAN, C. & BRAMKAMP, M. 2014. Cell division in *Corynebacterineae*. *Frontiers in microbiology,* 5**,** 132.

DONOVAN, C., SCHWAIGER, A., KRÄMER, R. & BRAMKAMP, M. 2010. Subcellular localization and characterization of the ParAB system from *Corynebacterium glutamicum*. *Journal of Bacteriology,* 192**,** 3441-51.

DONOVAN, C., SIEGER, B., KRÄMER, R. & BRAMKAMP, M. 2012. A synthetic *Escherichia coli* system identifies a conserved origin tethering factor in *Actinobacteria*. *Molecular Microbiology,* 84**,** 105-116.

DREW, D., LERCH, M., KUNJI, E., SLOTBOOM, D.-J. & DE GIER, J.-W. 2006. Optimization of membrane protein overexpression and purification using GFP fusions. *Nature Methods,* 3**,** 303-313.

DURÁN, R., VILLARINO, A., BELLINZONI, M., WEHENKEL, A., FERNANDEZ, P., BOITEL, B., COLE, S. T., ALZARI, P. M. & CERVEÑANSKY, C. 2005. Conserved autophosphorylation pattern in activation loops and juxtamembrane regions of *Mycobacterium tuberculosis* Ser/Thr protein kinases. *Biochemical and biophysical research communications,* 333**,** 858-867.

DUROCHER, D. & JACKSON, S. P. 2002. The FHA domain. *FEBS Letters,* 513**,** 58-66.

DWORKIN, J. 2015. Ser/Thr phosphorylation as a regulatory mechanism in bacteria. *Current Opinion in Microbiology,* 24**,** 47-52.

EGGELING, L. & BOTT, M. 2005. *Handbook of Corynebacterium glutamicum*, CRC press. Taylor&Francis, Boca Raton, Florida, USA

EGGELING, L. & BOTT, M. 2015. A giant market and a powerful metabolism: L-lysine provided by *Corynebacterium glutamicum*. *Applied Microbiology and Biotechnology,* 99**,** 3387-3394.

EIKMANNS, B. J., RITTMANN, D. & SAHM, H. 1995. Cloning, sequence analysis, expression, and inactivation of the *Corynebacterium glutamicum icd* gene encoding isocitrate dehydrogenase and biochemical characterization of the enzyme. *Journal of Bacteriology,* 177**,** 774-782.

ENGLAND, P., WEHENKEL, A., MARTINS, S., HOOS, S., ANDRÉ-LEROUX, G., VILLARINO, A. & ALZARI, P. M. 2009. The FHA-containing protein GarA acts as a phosphorylation-dependent molecular switch in mycobacterial signaling. *FEBS Letters,* 583**,** 301-307.

FIUZA, M., CANOVA, M. J., PATIN, D., LETEK, M., ZANELLA-CLÉON, I., BECCHI, M., MATEOS, L. M., MENGIN-LECREULX, D., MOLLE, V. & GIL, J. A. 2008. The MurC ligase essential for peptidoglycan biosynthesis is regulated by the serine/threonine protein kinase PknA in *Corynebacterium glutamicum*. *Journal of Biological Chemistry,* 283**,** 36553-36563.

FOLKERTS, J.-G. 2022. Zelluläre Lokalisation regulatorischer Proteine in *Corynebacterium glutamicum*. *Masterarbeit, Heinrich-Heine-Universität Düsseldorf*.

GALLANT, J. L., VILJOEN, A. J., VAN HELDEN, P. D. & WIID, I. J. F. 2016. Glutamate dehydrogenase is required by *Mycobacterium bovis* BCG for resistance to cellular stress. *PLOS ONE,* 11**,** e0147706.

GAO, B. & GUPTA, R. S. 2012. Phylogenetic framework and molecular signatures for the main clades of the phylum *Actinobacteria*. *Microbiology and Molecular Biology Reviews,* 76**,** 66-112.

GIBSON, D. G., YOUNG, L., CHUANG, R.-Y., VENTER, J. C., HUTCHISON, C. A. & SMITH, H. O. 2009. Enzymatic assembly of DNA molecules up to several hundred kilobases. *Nature Methods,* 6**,** 343-345.

GREEN, M. R. & SAMBROOK, J. 2012. *Molecular cloning: a laboratory manual*. 3rd ed. 2012, *Cold Spring Harbor Laboratory Press;* Cold Spring Habor, New York.

GUSHCHIN, I. & GORDELIY, V. 2018. Transmembrane signal transduction in two-component systems: piston, scissoring, or helical rotation? *Bioessays,* 40**,** 1700197.

HAMMET, A., PIKE, B., MCNEES, C., CONLAN, L., TENIS, N. & HEIERHORST, J. 2003. FHA domains as phospho-threonine binding modules in cell signaling. *IUBMB Life,* 55**,** 23-27.

HANAHAN, D. 1983. Studies on transformation of *Escherichia coli* with plasmids. *Journal of Molecular Biology,* 166**,** 557-580.

HARRISON, K. J., CRÉCY-LAGARD, V. & ZALLOT, R. 2018. Gene Graphics: a genomic neighborhood data visualization web application. *Bioinformatics,* 34**,** 1406-1408.

HOFFELDER, M., RAASCH, K., VAN OOYEN, J. & EGGELING, L. 2010. The E2 domain of OdhA of *Corynebacterium glutamicum* has succinyltransferase activity dependent on lipoyl residues of the acetyltransferase AceF. *Journal of Bacteriology,* 192**,** 5203-5211.

HONG, Y., HUANG, Z., GUO, L., NI, B., JIANG, C.-Y., LI, X.-J., HOU, Y.-J., YANG, W.-S., WANG, D.-C., ZHULIN, I. B., LIU, S.-J. & LI, D.-F. 2019. The ligand-binding domain of

a chemoreceptor from *Comamonas testosteroni* has a previously unknown homotrimeric structure. *Molecular Microbiology,* 112**,** 906-917.

HUYNH, T. N. & STEWART, V. 2011. Negative control in two-component signal transduction by transmitter phosphatase activity. *Molecular Microbiology,* 82**,** 275-286.

HWANG, E., CHEONG, H.-K., KIM, S.-Y., KWON, O., BLAIN, K. Y., CHOE, S., YEO, K. J., JUNG, Y. W., JEON, Y. H. & CHEONG, C. 2017. Crystal structure of the EnvZ periplasmic domain with CHAPS. *FEBS Letters,* 591**,** 1419-1428.

IKEDA, M. & NAKAGAWA, S. 2003. The *Corynebacterium glutamicum* genome: features and impacts on biotechnological processes. *Applied Microbiology and Biotechnology,* 62**,** 99-109.

IZARD, T., ÆVARSSON, A., ALLEN, M. D., WESTPHAL, A. H., PERHAM, R. N., DE KOK, A. & HOL, W. G. J. P. O. T. N. A. O. S. 1999. Principles of quasi-equivalence and Euclidean geometry govern the assembly of cubic and dodecahedral cores of pyruvate dehydrogenase complexes. *Proceedings of the National Academy of Sciences,* 96**,** 1240-1245.

JAKOBY, M., TESCH, M., SAHM, H., KRÄMER, R. & BURKOVSKI, A. 1997. Isolation of the *Corynebacterium glutamicum glnA* gene encoding glutamine synthetase I. *FEMS microbiology letters,* 154**,** 81-88.

JANCZAREK, M., VINARDELL, J.-M., LIPA, P. & KARAŚ, M. 2018. Hanks-type serine/threonine protein kinases and phosphatases in bacteria: roles in signaling and adaptation to various environments. *International Journal of Molecular Sciences,* 19**,** 2872.

JENAL, U. & HENGGE-ARONIS, R. 2003. Regulation by proteolysis in bacterial cells. *Current Opinion in Microbiology,* 6**,** 163-172.

KALINOWSKI, J., BATHE, B., BARTELS, D., BISCHOFF, N., BOTT, M., BURKOVSKI, A., DUSCH, N., EGGELING, L., EIKMANNS, B. J., GAIGALAT, L., GOESMANN, A., HARTMANN, M., HUTHMACHER, K., KRÄMER, R., LINKE, B., MCHARDY, A. C., MEYER, F., MÖCKEL, B., PFEFFERLE, W., PÜHLER, A., REY, D. A., RÜCKERT, C., RUPP, O., SAHM, H., WENDISCH, V. F., WIEGRÄBE, I. & TAUCH, A. 2003. The complete *Corynebacterium glutamicum* ATCC 13032 genome sequence and its impact on the production of L-aspartate-derived amino acids and vitamins. *Journal of Biotechnology,* 104**,** 5-25.

KANG, C. M., NYAYAPATHY, S., LEE, J. Y., SUH, J. W. & HUSSON, R. N. 2008. Wag31, a homologue of the cell division protein DivIVA, regulates growth, morphology and polar cell wall synthesis in mycobacteria. *Microbiology* 154**,** 725-735.

KASPAR, S., PEROZZO, R., REINELT, S., MEYER, M., PFISTER, K., SCAPOZZA, L. & BOTT, M. 1999. The periplasmic domain of the histidine autokinase CitA functions as a highly specific citrate receptor. *Molecular Microbiology,* 33**,** 858-872.

KEILHAUER, C., EGGELING, L. & SAHM, H. 1993. Isoleucine synthesis in *Corynebacterium glutamicum*: molecular analysis of the *ilvB-ilvN-ilvC* operon. *Journal of Bacteriology,* 175**,** 5595-5603.

KIMPLE, M. E., BRILL, A. L. & PASKER, R. L. 2013. Overview of affinity tags for protein purification. *Current Protocols in Protein Science,* 73**,** 9.9.1-9.9.23.

KINOSHITA, S., UDAKA, S. & SHIMONO, M. 1957. Amino acid fermentation. I. Production of L-glutamic acid by various microorganisms. *Journal of General and Applied Microbiology,* 3**,** 193-205.

KINUGAWA, H., KONDO, N., KOMINE-ABE, A., TOMITA, T., NISHIYAMA, M. & KOSONO, S. 2020. *In vitro* reconstitution and characterization of pyruvate dehydrogenase and 2-oxoglutarate dehydrogenase hybrid complex from *Corynebacterium glutamicum*. *Microbiologyopen*, 9**,** e1113.

KOGURE, T. & INUI, M. 2018. Recent advances in metabolic engineering of *Corynebacterium glutamicum* for bioproduction of value-added aromatic chemicals and natural products. *Applied Microbiology and Biotechnology,* 102**,** 8685-8705.

KORNEV, A. P., HASTE, N. M., TAYLOR, S. S. & TEN EYCK, L. F. 2006. Surface comparison of active and inactive protein kinases identifies a conserved activation mechanism. *Proceedings of the National Academy of Sciences,* 103**,** 17783-17788.

KORTMANN, M., BAUMGART, M. & BOTT, M. 2019. Pyruvate carboxylase from *Corynebacterium glutamicum*: purification and characterization. *Applied Microbiology and Biotechnology,* 103**,** 6571-6580.

KORTMANN, M., KUHL, V., KLAFFL, S. & BOTT, M. 2015. A chromosomally encoded T7 RNA polymerase-dependent gene expression system for *Corynebacterium glutamicum*: construction and comparative evaluation at the single-cell level. *Microbial biotechnology,* 8**,** 253-265.

KOSSMANN, M., WOLFF, C. & MANSON, M. D. 1988. Maltose chemoreceptor of *Escherichia coli*: interaction of maltose-binding protein and the tar signal transducer. *Journal of Bacteriology,* 170**,** 4516-4521.

KRAWCZYK, S., RAASCH, K., SCHULTZ, C., HOFFELDER, M., EGGELING, L. & BOTT, M. 2010. The FHA domain of OdhI interacts with the carboxyterminal 2-oxoglutarate dehydrogenase domain of OdhA in *Corynebacterium glutamicum*. *FEBS Letters,* 584**,** 1463-1468.

KRÜGER, A., KEPPEL, M., SHARMA, V. & FRUNZKE, J. 2022. The diversity of heme sensor systems – heme-responsive transcriptional regulation mediated by transient heme protein interactions. *FEMS Microbiology Reviews,* 46**,** fuac002.

KRUPA, A. & SRINIVASAN, N. 2005. Diversity in domain architectures of Ser/Thr kinases and their homologues in prokaryotes. *BMC Genomics,* 6**,** 129.

LACEY, H. J. & RUTLEDGE, P. J. 2022. Recently discovered secondary metabolites from *Streptomyces* species. *Molecules,* 27**,** 887.

LANDGRAF, D., OKUMUS, B., CHIEN, P., BAKER, T. A. & PAULSSON, J. 2012. Segregation of molecules at cell division reveals native protein localization. *Nature Methods,* 9**,** 480-482.

LAUB, M. T. & GOULIAN, M. 2007. Specificity in two-component signal transduction pathways. *Annual Review of Genetics,* 41**,** 121-145.

LENARCIC, R., HALBEDEL, S., VISSER, L., SHAW, M., WU, L. J., ERRINGTON, J., MARENDUZZO, D. & HAMOEN, L. W. 2009. Localisation of DivIVA by targeting to negatively curved membranes. *The EMBO journal,* 28**,** 2272-2282.

LETEK, M., FIUZA, M., ORDÓÑEZ, E., VILLADANGOS, A. F., RAMOS, A., MATEOS, L. M. & GIL, J. A. 2008a. Cell growth and cell division in the rod-shaped actinomycete *Corynebacterium glutamicum*. *Antonie van Leeuwenhoek,* 94**,** 99-109.

LETEK, M., ORDÓÑEZ, E., VAQUERA, J., MARGOLIN, W., FLÄRDH, K., MATEOS LUIS, M. & GIL JOSÉ, A. 2008b. DivIVA is required for polar growth in the MreB-lacking rod-shaped *Actinomycete Corynebacterium glutamicum*. *Journal of Bacteriology,* 190**,** 3283-3292.

LI, J., WANG, C., YANG, G., SUN, Z., GUO, H., SHAO, K., GU, Y., JIANG, W. & ZHANG, P. 2017. Molecular mechanism of environmental D-xylose perception by a XylFII-LytS complex in bacteria. *Proceedings of the National Academy of Sciences,* 114**,** 8235-8240.

LISA, M.-N., GIL, M., ANDRÉ-LEROUX, G., BARILONE, N., DURÁN, R., BIONDI, RICARDO M. & ALZARI, PEDRO M. 2015. Molecular basis of the activity and the regulation of the eukaryotic-like S/T protein kinase PknG from *Mycobacterium tuberculosis*. *Structure,* 23**,** 1039-1048.

LISA, M.-N., SOGUES, A., BARILONE, N., BAUMGART, M., GIL, M., GRAÑA, M., DURÁN, R., BIONDI, R. M., BELLINZONI, M., BOTT, M., ALZARI, P. M. & BRENNAN, R. G. 2021. A tetratricopeptide repeat scaffold couples signal detection to OdhI phosphorylation in metabolic control by the protein Kinase PknG. *mBio,* 12**,** e01717-21.

MACEK, B., FORCHHAMMER, K., HARDOUIN, J., WEBER-BAN, E., GRANGEASSE, C. & MIJAKOVIC, I. 2019. Protein post-translational modifications in bacteria. *Nature Reviews Microbiology,* 17**,** 651-664.

MANSON, M. D. & KOSSMANN, M. 1986. Mutations in *tar* suppress defects in maltose chemotaxis caused by specific *malE* mutations. *Journal of Bacteriology,* 165**,** 34-40.

MARGOLIN, W. 2005. FtsZ and the division of prokaryotic cells and organelles. *Nature Reviews Molecular Cell Biology,* 6**,** 862-871.

MARIENHAGEN, J., KENNERKNECHT, N., SAHM, H. & EGGELING, L. 2005. Functional analysis of all aminotransferase proteins inferred from the genome sequence of *Corynebacterium glutamicum*. *Journal of Bacteriology,* 187**,** 7639-7646.

MATTEVI, A., OBMOLOVA, G., SCHULZE, E., KALK, K. H., WESTPHAL, A. H., DE KOK, A. & HOL, W. G. J. 1992. Atomic structure of the cubic core of the pyruvate dehydrogenase multienzyme complex. *Science,* 255**,** 1544-1550.

MERRICK, M. J. & EDWARDS, R. A. 1995. Nitrogen control in bacteria. *Microbiological reviews,* 59**,** 604-622.

MIJAKOVIC, I., GRANGEASSE, C. & TURGAY, K. 2016. Exploring the diversity of protein modifications: special bacterial phosphorylation systems. *FEMS Microbiology Reviews,* 40**,** 398-417.

MILBURN, M. V., PRIVE, G. G., MILLIGAN, D. L., SCOTT, W. G., YEH, J., JANCARIK, J., KOSHLAND, D. E., JR. & KIM, S. H. 1991. Three-dimensional structures of the ligand-binding domain of the bacterial aspartate receptor with and without a ligand. *Science,* 254**,** 1342-1347.

MILKE, L., MUTZ, M. & MARIENHAGEN, J. 2020. Synthesis of the character impact compound raspberry ketone and additional flavoring phenylbutanoids of biotechnological interest with *Corynebacterium glutamicum*. *Microbial cell factories,* 19**,** 1-12.

MIYAKOSHI, M., MORITA, T., KOBAYASHI, A., BERGER, A., TAKAHASHI, H., GOTOH, Y., HAYASHI, T. & TANAKA, K. 2022. Glutamine synthetase mRNA releases sRNA from its 3'UTR to regulate carbon/nitrogen metabolic balance. *bioRxiv***,** 2022.07.25.501400.

MOLLE, V., BROWN, A. K., BESRA, G. S., COZZONE, A. J. & KREMER, L. 2006. The condensing activities of the *Mycobacterium tuberculosis* type II fatty acid synthase are differentially regulated by phosphorylation. *Journal of Biological Chemistry,* 281**,** 30094-30103.

MUKHOPADHYAY, B. & PURWANTINI, E. 2000. Pyruvate carboxylase from *Mycobacterium smegmatis*: stabilization, rapid purification, molecular and biochemical characterization and regulation of the cellular level. *Biochimica et Biophysica Acta,* 1475**,** 191-206.

NIEBISCH, A., KABUS, A., SCHULTZ, C., WEIL, B. & BOTT, M. 2006. Corynebacterial protein kinase G controls 2-oxoglutarate dehydrogenase activity via the phosphorylation status of the OdhI protein. *Journal of Biological Chemistry,* 281**,** 12300-12307.

NOTT, T. J., KELLY, G., STACH, L., LI, J., WESTCOTT, S., PATEL, D., HUNT, D. M., HOWELL, S., BUXTON, R. S. & O'HARE, H. M. J. S. S. 2009. An intramolecular switch regulates phosphoindependent FHA domain interactions in *Mycobacterium tuberculosis*. *Science Signaling*, 2**,** ra12-ra12.

O'HARE, H. M., DURÁN, R., CERVEÑANSKY, C., BELLINZONI, M., WEHENKEL, A. M., PRITSCH, O., OBAL, G., BAUMGARTNER, J., VIALARET, J. & JOHNSSON, K. 2008. Regulation of glutamate metabolism by protein kinases in mycobacteria. *Molecular microbiology,* 70**,** 1408-1423.

ORTIZ-LOMBARDıA, M., POMPEO, F., BOITEL, B. & ALZARI, P. M. 2003. Crystal structure of the catalytic domain of the PknB serine/threonine kinase from *Mycobacterium tuberculosis*. *Journal of Biological Chemistry,* 278**,** 13094-13100.

OTTO, N. M., MCDOWELL, W. G., DICKEY, D. M. & POTTER, L. R. 2017. A glutamate-substituted mutant mimics the phosphorylated and active form of guanylyl cyclase-A. *Molecular Pharmacology,* 92**,** 67.

PATEL, M. S., NEMERIA, N. S., FUREY, W. & JORDAN, F. 2014. The pyruvate dehydrogenase complexes: structure-based function and regulation. *Journal of Biological Chemistry,* 289**,** 16615-16623.

PEREIRA, S. F. F., GOSS, L. & DWORKIN, J. 2011. Eukaryote-like serine/threonine kinases and phosphatases in bacteria. *Microbiology and Molecular Biology Reviews,* 75**,** 192-212.

PEREZ, J., CASTANEDA-GARCIA, A., JENKE-KODAMA, H., MÜLLER, R. & MUNOZ-DORADO, J. 2008. Eukaryotic-like protein kinases in the prokaryotes and the myxobacterial kinome. *Proceedings of the National Academy of Sciences,* 105**,** 15950-15955.

PERHAM, R. 1991. Domains, motifs, and linkers in 2-oxo acid dehydrogenase multienzyme complexes: a paradigm in the design of a multifunctional protein. *Biochemistry,* 30**,** 8501-8512.

PERHAM, R. N. 2000. Swinging arms and swinging domains in multifunctional enzymes: Catalytic machines for multistep reactions. *Annual review of biochemistry,* 69**,** 961-1004.

PRISIC, S., DANKWA, S., SCHWARTZ, D., CHOU, M. F., LOCASALE, J. W., KANG, C. M., BEMIS, G., CHURCH, G. M., STEEN, H. & HUSSON, R. N. 2010. Extensive phosphorylation with overlapping specificity by *Mycobacterium tuberculosis* serine/threonine protein kinases. *Proceedings of the National Academy of Sciences,* 107**,** 7521-6.

RAASCH, K., BOCOLA, M., LABAHN, J., LEITNER, A., EGGELING, L. & BOTT, M. 2014. Interaction of 2-oxoglutarate dehydrogenase OdhA with its inhibitor OdhI in *Corynebacterium glutamicum*: Mutants and a model. *Journal of Biotechnology,* 191**,** 99-105.

RADMACHER, E., STANSEN, K. C., BESRA, G. S., ALDERWICK, L. J., MAUGHAN, W. N., HOLLWEG, G., SAHM, H., WENDISCH, V. F. & EGGELING, L. 2005. Ethambutol, a cell wall inhibitor of *Mycobacterium tuberculosis*, elicits L-glutamate efflux of *Corynebacterium glutamicum*. *Microbiology,* 151**,** 1359-1368.

RAMOS, A., LETEK, M., CAMPELO, A. B., VAQUERA, J., MATEOS, L. M. & GIL, J. A. 2005. Altered morphology produced by *ftsZ* expression in *Corynebacterium glutamicum* ATCC 13869. *Microbiology* 151**,** 2563-2572.

RAMP, P., LEHNERT, A., MATAMOUROS, S., WIRTZ, A., BAUMGART, M. & BOTT, M. 2021. Metabolic engineering of *Corynebacterium glutamicum* for production of *scyllo*-inositol, a drug candidate against Alzheimer's disease. *Metabolic engineering,* 67**,** 173-185.

RAMP, P., PFLEGER, C., DITTRICH, J., MACK, C., GOHLKE, H. & BOTT, M. 2022. Physiological, biochemical, and structural bioinformatic analysis of the multiple inositol dehydrogenases from *Corynebacterium glutamicum*. *Microbiology Spectrum***,** e01950-22.

REINELT, S., HOFMANN, E., GERHARZ, T., BOTT, M. & MADDEN, D. R. 2003. The structure of the periplasmic ligand-binding domain of the sensor kinase CitA reveals the first extracellular PAS domain. *Journal of Biological Chemistry,* 278**,** 39189-39196.

RIECK, B., DEGIACOMI, G., ZIMMERMANN, M., CASCIOFERRO, A., BOLDRIN, F., LAZAR-ADLER, N. R., BOTTRILL, A. R., LE CHEVALIER, F., FRIGUI, W., BELLINZONI, M., LISA, M.-N., ALZARI, P. M., NGUYEN, L., BROSCH, R., SAUER, U., MANGANELLI, R. & O'HARE, H. M. 2017. PknG senses amino acid availability to control metabolism and virulence of *Mycobacterium tuberculosis*. *PLOS Pathogens,* 13**,** e1006399.

SABERI, S. & EMBERLY, E. 2013. Non-equilibrium polar localization of proteins in bacterial cells. *PLOS ONE,* 8**,** e64075.

SCHAAF, S. & BOTT, M. 2007. Target genes and DNA-binding sites of the response regulator PhoR from *Corynebacterium glutamicum*. *Journal of Bacteriology,* 189**,** 5002-5011.

SCHÄFER, A., TAUCH, A., JÄGER, W., KALINOWSKI, J., THIERBACH, G. & PÜHLER, A. 1994. Small mobilizable multi-purpose cloning vectors derived from the *Escherichia coli* plasmids pK18 and pK19: selection of defined deletions in the chromosome of *Corynebacterium glutamicum*. *Gene,* 145**,** 69-73.

SCHERR, N., HONNAPPA, S., KUNZ, G., MUELLER, P., JAYACHANDRAN, R., WINKLER, F., PIETERS, J. & STEINMETZ, M. O. 2007. Structural basis for the specific inhibition of protein kinase G, a virulence factor of *Mycobacterium tuberculosis*. *Proceedings of the National Academy of Sciences,* 104**,** 12151-6.

SCHEU, K., GILL, R., SABERI, S., MEYER, P. & EMBERLY, E. 2014. Localization of aggregating proteins in bacteria depends on the rate of addition. *Frontiers in Microbiology,* 5**,** 418.

SCHULTZ, C. 2008. Posttranslationale Regulation der 2-Oxoglutarat-Dehydrogenase in *Corynebacterium glutamicum*. *Reihe Gesundheit/Health, Forschungszentrum Jülich GmbH*.

SCHULTZ, C., NIEBISCH, A., GEBEL, L. & BOTT, M. 2007. Glutamate production by *Corynebacterium glutamicum*: dependence on the oxoglutarate dehydrogenase inhibitor protein OdhI and protein kinase PknG. *Applied Microbiology and Biotechnology,* 76**,** 691-700.

SCHULTZ, C., NIEBISCH, A., SCHWAIGER, A., VIETS, U., METZGER, S., BRAMKAMP, M. & BOTT, M. 2009. Genetic and biochemical analysis of the serine/threonine protein kinases PknA, PknB, PknG and PknL of *Corynebacterium glutamicum*: evidence for non-essentiality and for phosphorylation of OdhI and FtsZ by multiple kinases. *Molecular Microbiology,* 74**,** 724-741.

SCHWINDE, J. W., HERTZ, P. F., SAHM, H., EIKMANNS, B. J. & GUYONVARCH, A. 2001. Lipoamide dehydrogenase from *Corynebacterium glutamicum*: molecular and physiological analysis of the *lpd* gene and characterization of the enzyme. *Microbiology* 147**,** 2223-2231.

SEHNAL, D., BITTRICH, S., DESHPANDE, M., SVOBODOVÁ, R., BERKA, K., BAZGIER, V., VELANKAR, S., BURLEY, S. K., KOČA, J. & ROSE, A. S. 2021. Mol* Viewer: modern web app for 3D visualization and analysis of large biomolecular structures. *Nucleic Acids Research,* 49**,** W431-W437.

SEVVANA, M., VIJAYAN, V., ZWECKSTETTER, M., REINELT, S., MADDEN, D. R., HERBST-IRMER, R., SHELDRICK, G. M., BOTT, M., GRIESINGER, C. & BECKER, S. 2008. A ligand-induced switch in the periplasmic domain of sensor histidine kinase CitA. *Journal of Molecular Biology,* 377**,** 512-523.

SHIIO, I. & OZAKI, H. 1970. Regulation of nicotinamide adenine dinucleotide phosphate-specific glutamate dehydrogenase from *Brevibacterium flavum*, a glutamate-producing bacterium. *The Journal of Biochemistry,* 68**,** 633-647.

SHIIO, I., OZAKI, H. & MORI, M. 1982. Glutamate metabolism in a glutamate-producing bacterium, *Brevibacterium flavum*. *Agricultural and Biological Chemistry,* 46**,** 493-500.

SHIIO, I. & UJIGAWA-TAKEDA, K. 1980. Presence and regulation of alpha-ketoglutarate dehydrogenase complex in a glutamate-producing bacterium *Brevibacterium flavum*. *Agricultural and Biological Chemistry,* 44**,** 1897-1904.

SIEGER, B. & BRAMKAMP, M. 2015. Interaction sites of DivIVA and RodA from *Corynebacterium glutamicum*. *Frontiers in Microbiology,* 5**,** 738.

SKERKER, J. M., PERCHUK, B. S., SIRYAPORN, A., LUBIN, E. A., ASHENBERG, O., GOULIAN, M. & LAUB, M. T. 2008. Rewiring the specificity of two-component signal transduction systems. *Cell,* 133**,** 1043-1054.

SMITH, K. M., CHO, K. M. & LIAO, J. C. 2010. Engineering *Corynebacterium glutamicum* for isobutanol production. *Applied Microbiology and Biotechnology,* 87**,** 1045-55.

SOMALE, D., DI NARDO, G., DI BLASIO, L., PULIAFITO, A., VARA-MESSLER, M., CHIAVERINA, G., PALMIERO, M., MONICA, V., GILARDI, G., PRIMO, L. & GAGLIARDI, P. A. 2020. Activation of RSK by phosphomimetic substitution in the activation loop is prevented by structural constraints. *Scientific Reports,* 10**,** 591.

STANCIK, I. A., ŠESTAK, M. S., JI, B., AXELSON-FISK, M., FRANJEVIC, D., JERS, C., DOMAZET-LOŠO, T. & MIJAKOVIC, I. 2018. Serine/threonine protein kinases from bacteria, archaea and eukarya share a common evolutionary origin deeply rooted in the tree of life. *Journal of Molecular Biology,* 430**,** 27-32.

STOCK, A. M., ROBINSON, V. L. & GOUDREAU, P. N. 2000. Two-component signal transduction. *Annual review of biochemistry,* 69**,** 183-215.

STUDDERT, C. A. & PARKINSON, J. S. 2007. [19] - *In Vivo* crosslinking methods for analyzing the assembly and architecture of chemoreceptor arrays. *In:* SIMON, M. I., CRANE, B. R. & CRANE, A. (eds.) *Methods in Enzymology*. Academic Press.

SUCHANEK, M., RADZIKOWSKA, A. & THIELE, C. 2005. Photo-leucine and photo-methionine allow identification of protein-protein interactions in living cells. *Nature Methods,* 2**,** 261-7.

SUNDERMEYER, L., BOSCO, G., GUJAR, S., BROCKER, M., BAUMGART, M., WILLLBOLD, D., WEIERGRÄBER, O. H., BELLINZONI, M. & BOTT, M. 2022a. Characteristics of the GlnH and GlnX signal transduction proteins controlling PknG-mediated

phosphorylation of OdhI and 2-oxoglutarate dehydrogenase activity in *Corynebacterium glutamicum*. *Microbiology Spectrum,* 10**,** e02677-22.

SUNDERMEYER, L., FOLKERTS, J.-G., LÜCKEL, B., WOLLENHAUPT, B., MACK, C., KOHLHEYER, D., BAUMGART, M. & BOTT, M. 2022b. Polar localization of regulatory proteins and TCA cycle components in an actinobacterium. *to be submitted*.

THAKUR, M. & CHAKRABORTI, P. K. 2006. GTPase activity of mycobacterial FtsZ is impaired due to its transphosphorylation by the eukaryotic-type Ser/Thr Kinase, PknA. *Journal of Biological Chemistry,* 281**,** 40107-40113.

TSUGE, Y., HASUNUMA, T. & KONDO, A. 2015. Recent advances in the metabolic engineering of *Corynebacterium glutamicum* for the production of lactate and succinate from renewable resources. *Journal of Industrial Microbiology and Biotechnology,* 42**,** 375-389.

TURAPOV, O., FORTI, F., KADHIM, B., GHISOTTI, D., SASSINE, J., STRAATMAN-IWANOWSKA, A., BOTTRILL, A. R., MOYNIHAN, P. J., WALLIS, R. & BARTHE, P. 2018. Two faces of CwlM, an essential PknB substrate, in *Mycobacterium tuberculosis*. *Cell reports,* 25**,** 57-67.

USUDA, Y., TUJIMOTO, N., ABE, C., ASAKURA, Y., KIMURA, E., KAWAHARA, Y., KURAHASHI, O. & MATSUI, H. 1996. Molecular cloning of the *Corynebacterium glutamicum* (‘*Brevibacterium lactofermentum*’AJ12036) *odhA* gene encoding a novel type of 2-oxoglutarate dehydrogenase. *Microbiology,* 142**,** 3347-3354.

VAN DER REST, M. E., LANGE, C. & MOLENAAR, D. 1999. A heat shock following electroporation induces highly efficient transformation of *Corynebacterium glutamicum* with xenogeneic plasmid DNA. *Applied Microbiology and Biotechnology,* 52**,** 541-545.

VENTURA, M., CANCHAYA, C., TAUCH, A., CHANDRA, G., FITZGERALD GERALD, F., CHATER KEITH, F. & VAN SINDEREN, D. 2007. Genomics of *Actinobacteria*: tracing the evolutionary history of an ancient phylum. *Microbiology and Molecular Biology Reviews,* 71**,** 495-548.

VILLARINO, A., DURAN, R., WEHENKEL, A., FERNANDEZ, P., ENGLAND, P., BRODIN, P., COLE, S. T., ZIMNY-ARNDT, U., JUNGBLUT, P. R., CERVEÑANSKY, C. & ALZARI, P. M. 2005. Proteomic identification of *M. tuberculosis* protein kinase substrates: PknB recruits GarA, a FHA domain-containing protein, through activation loop-mediated interactions. *Journal of Molecular Biology,* 350**,** 953-963.

WAGNER, T., ANDRÉ-LEROUX, G., HINDIE, V., BARILONE, N., LISA, M.-N., HOOS, S., RAYNAL, B., VULLIEZ-LE NORMAND, B., O’HARE, H. M., BELLINZONI, M. & ALZARI, P. M. 2019. Structural insights into the functional versatility of an FHA domain protein in mycobacterial signaling. *Science Signaling,* 12**,** eaav9504.

WAGNER, T., BARILONE, N., ALZARI, PEDRO M. & BELLINZONI, M. 2014. A dual conformation of the post-decarboxylation intermediate is associated with distinct enzyme states in mycobacterial KGD (α-ketoglutarate decarboxylase). *Biochemical Journal,* 457**,** 425-434.

WAGNER, T., BELLINZONI, M., WEHENKEL, A., O'HARE, H. M. & ALZARI, P. M. 2011. Functional plasticity and allosteric regulation of α-ketoglutarate decarboxylase in central mycobacterial metabolism. *Chemistry & Biology,* 18**,** 1011-1020.

WENDISCH, V. F., JORGE, J. M., PÉREZ-GARCÍA, F. & SGOBBA, E. 2016. Updates on industrial production of amino acids using *Corynebacterium glutamicum*. *World Journal of Microbiology and Biotechnology,* 32**,** 1-10.

WOLF, S., BECKER, J., TSUGE, Y., KAWAGUCHI, H., KONDO, A., MARIENHAGEN, J., BOTT, M., WENDISCH, VOLKER F. & WITTMANN, C. 2021. Advances in metabolic engineering of *Corynebacterium glutamicum* to produce high-value active ingredients for food, feed, human health, and well-being. *Essays in Biochemistry,* 65**,** 197-212.

WU, L. J. & ERRINGTON, J. 2012. Nucleoid occlusion and bacterial cell division. *Nature Reviews Microbiology,* 10**,** 8-12.

YEATS, C., FINN, R. D. & BATEMAN, A. 2002. The PASTA domain: a β-lactam-binding domain. *Trends in Biochemical Sciences,* 27**,** 438-440.

YOUNG, T. A., DELAGOUTTE, B., ENDRIZZI, J. A., FALICK, A. M. & ALBER, T. 2003. Structure of *Mycobacterium tuberculosis* PknB supports a universal activation

mechanism for Ser/Thr protein kinases. *Nature Structural & Molecular Biology,* 10**,** 168-74.

ZHULIN, I. B., NIKOLSKAYA, A. N. & GALPERIN, M. Y. 2003. Common extracellular sensory domains in transmembrane receptors for diverse signal transduction pathways in bacteria and archaea. *Journal of Bacteriology,* 185**,** 285-94.

ZSCHIEDRICH, C. P., KEIDEL, V. & SZURMANT, H. 2016. Molecular mechanisms of two-component signal transduction. *Journal of Molecular Biology,* 428**,** 3752-3775.

5. Appendix

5.1. Influence of N- and C-terminal tags on the functionality of GlnX

In vitro protein-protein interaction experiments of GlnX with GlnH and PknG require purified proteins. To optimize the purification of the membrane protein GlnX several different growth conditions including different media, temperature and inducer conditions as well as variation of purification buffer composition and use of different detergents needs to be tested. So far the purification success of GlnX at different conditions was tested using time-consuming Western blot analysis. To control the purification success at various intermediate steps in the overproduction and purification process, a fusion of the membrane protein with a fluorescent reporter protein based on a study by Drew et al. might be a suitable and faster approach (Drew et al., 2006). A combination of mVenus as fluorescent reporter output and a Strep-tag for affinity purification was chosen as an option for purification optimisation of GlnX.

Protein purification using affinity-tags is well-established (Kimple et al., 2013), however, to enable later on interaction tests or activity assay it has to be ensured that these tags do not affect the correct folding and functionality of the target protein or at least can be removed after purification to restore full protein functionality. Therefore, the two expression plasmids pPREx2-*glnX*-TEV-*mVenus*-Strep and pPREx2-Strep-*mVenus*-TEV-*glnX* encoding for either a C- or N-terminal fusion of GlnX with mVenus and a Strep-tag were constructed and the functionality of the resulting fusion proteins was tested by complementation tests in a *glnX* deletion strain. The growth defect of *C. glutamicum* Δ*glnX2* on agar plates containing glutamine as sole carbon and nitrogen source was restored in *C. glutamicum* Δ*glnX2* pPREx2-Strep-*mVenus*-TEV-*glnX*, while the plasmid coding for the C-terminal GlnX fusion protein did not enable growth (Fig. S1A). Fluorescence microscopy analysis of both strains showed that the lack of complementation capability is not due to an impaired insertion into the membrane, since both constructs lead to a fluorescence signal located at the membrane of the *C. glutamicum* cells (Fig. S1B), suggesting that the C-terminus of GlnX might be important for its functionality. The importance of an unaltered C-terminus was further underlined by the observation that already the fusion of the *glnX* gene with a C-terminal Strep-tag coding sequence hindered complementation of the growth defect of *C. glutamicum* Δ*glnX2* (Fig. S1C).

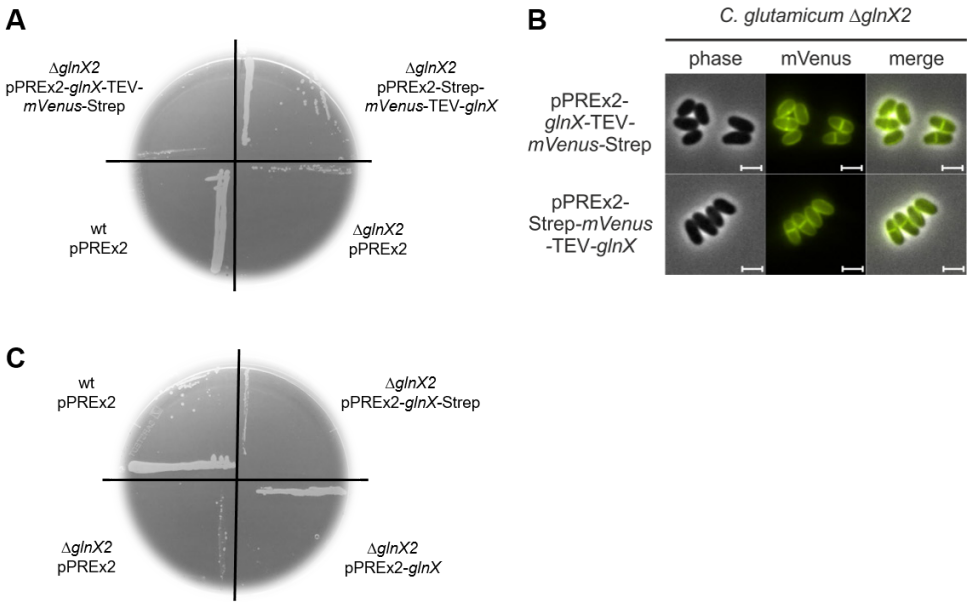

Figure S1: Effect of N- and C-terminal tags on GlnX functionality. (A) Growth of *C. glutamicum* wt pPREx2 and *C. glutamicum* Δ*glnX2* carrying the plasmids pPREx2, pPREx2-*glnX*-TEV-*mVeuns*-Strep and pPREx2-Strep-*mVenus*-TEV-*glnX* on a CGXII agar plate containing glutamine as sole carbon and nitrogen source. (B) Fluorescence microscopy images of *C. glutamicum* Δ*glnX2* pPREx2-*glnX*-TEV-*mVenus*-Strep and *C. glutamicum* Δ*glnX2* pPREx2-Strep-*mVenus*-TEV-*glnX*. Cells were grown in CGXII medium with 2% (w/v) glucose and images were taken 4 h after target gene expression with 100 µM IPTG. Scale bars represent 2 µm. (C) Growth of *C. glutamicum* wt pPREx2 and *C. glutamicum* Δ*glnX2* carrying the plasmids pPREx2, pPREx2-*glnX* and pPREx2-*glnX*-Strep on a CGXII agar plate containing glutamine as sole carbon and nitrogen source.

5.2. Purification of the periplasmic domains of GlnX

The experimental verification of the predicted protein topology and the generation of an AlphaFold 2 model of the membrane protein GlnX (Sundermeyer et al., 2022a) enabled a better understanding of possible protein-protein interaction sites with GlnH and PknG. To experimentally analyze these potential interactions we aimed to perform protein-protein interaction tests using purified proteins. Since the purification of protein in concentrations suitable for interaction tests is still challenging in case of the membrane protein GlnX, we aimed to purify the two large periplasmic domains, identified by topology analysis and structure prediction, separately. These domains could be interaction partners of GlnH and may also sense additional ligands themselves (Sundermeyer et al., 2022a). Construction of the expression plasmids pPREx6-*glnX*-P1-Strep and pPREx6-*glnX*-P2-Strep enabled the T7-RNA polymerase based production of the two periplasmic domains in *C. glutamicum* MB001(DE3). SDS-PAGE analysis showed successful production of GlnX-P1-Strep and GlnX-P2-Strep (Fig. S2). GlnX-P1-Strep samples showed a strong protein band corresponding to the theoretical size of 17.9 kDa, both in the crude cell extract and in the soluble protein fraction. For GlnX-P2-

Strep, an overexpression band was visible in crude cell extract and the soluble protein fraction as well. In this case the size derived from the SDS-PAGE analysis is around 15 kDa while the calculated theoretical protein size is 18 kDa.

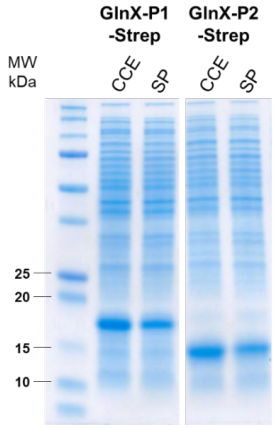

Figure S2: GlnX-P1-Strep and GlnX-P2-Strep production in *C. glutamicum* MB001(DE3). Coomassie-stained SDS-PAGE to control the overexpression of GlnX-P1-Strep and GlnX-P2-Strep. Shown are crude cell extract (CCE) and soluble protein fraction (SP) samples of *C. glutamicum* MB001(DE3) pPREx6-*glnX*-P1-Strep and *C. glutamicum* MB001(DE3) pPREx6-*glnX*-P2-Strep overproduction cultures.

GlnX-P1-Strep and GlnX-P2-Strep were purified by Strep-Tactin affinity chromatography and size exclusion chromatography (SEC) (for material and methods see chapter 5.5.3). The SEC chromatogram of the GlnX-P1-Strep sample showed two peaks. SDS-PAGE analysis showed that both peaks contained the target protein (Fig. S3 A-C). The first peak (elution volume 8 to 9 ml) is most likely caused by aggregated protein while the second one (elution volume 14.81 ml) suggests the purified GlnX-P1-Strep being an oligomer with a size of 52.7 kDa. With a theoretical monomer size of 17.9 kDa this suggests that the isolated periplasmic domain forms trimers (theoretical size 53.7 kDa). It needs to be further analyzed if the oligomerization is an artefact of the isolated periplasmic domain or an indication that the membrane protein GlnX builds oligomers under physiological conditions as well. The SEC chromatogram of the GlnX-P2-Strep purification showed only one peak with an early elution volume (8 to 9 ml) containing aggregated GlnX-P2-Strep protein (Fig. S3 D-F).

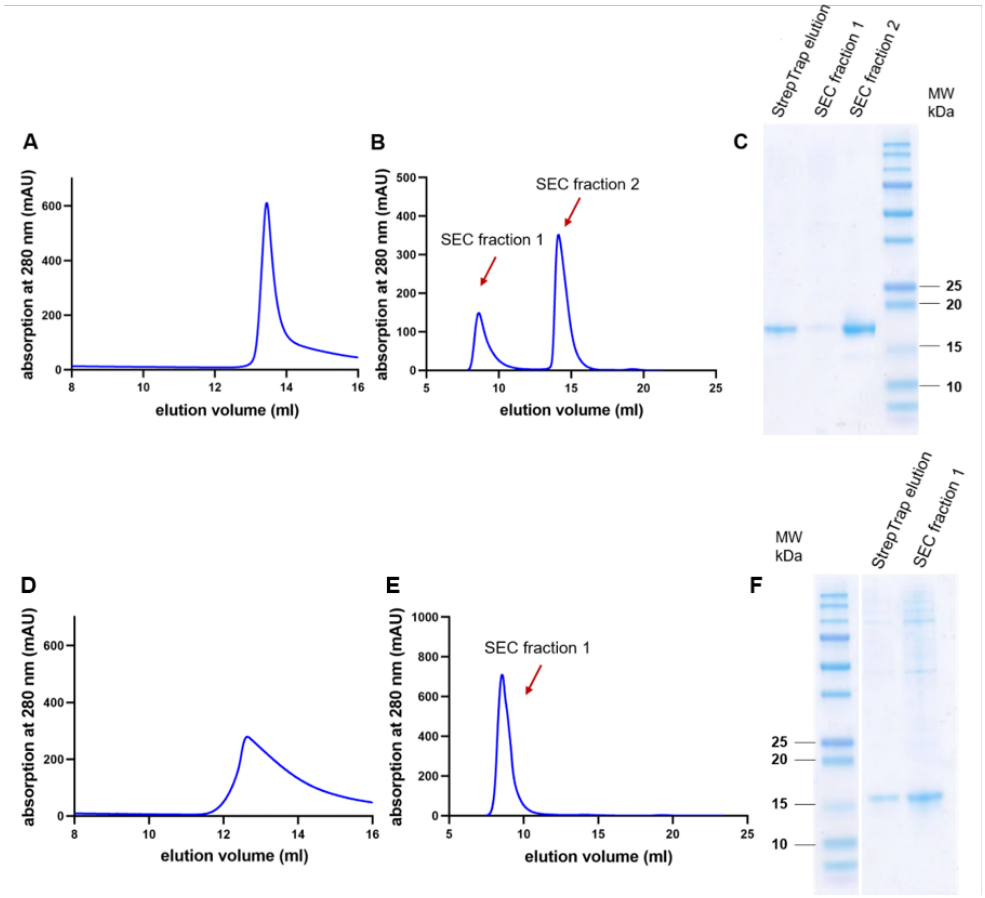

Figure S3: Purification of the periplasmic domains of GlnX. Strep-tagged proteins were produced in *C. glutamicum* MB001(DE3) carrying expression plasmids pPREx6-*glnX*-P1-Strep or pPREx6-*glnX*-P2-Strep. (A) Strep-tactin affinity purification elution profile of GlnX-P1-Strep using a 1 ml StrepTrap HP column and elution buffer containing 2.5 mM desthiobiotin. (B) SEC elution profile of GlnX-P1-Strep using a Superdex 200 Increase 10/300 GL column. (C) Coomassie-stained SDS-PAGE to control the GlnX-P1-Strep purification. (D) Strep-tactin affinity purification elution profile of GlnX-P2-Strep using a 1 ml StrepTrap HP column and elution buffer containing 2.5 mM desthiobiotin (E) SEC elution profile of GlnX-P2-Strep using a Superdex 200 Increase 10/300 GL column. (F) Coomassie-stained SDS-PAGE to control the GlnX-P2-Strep purification.

5.3. Purification of the of the hybrid PDH-ODH complex of *C. glutamicum*

In previous studies, a co-purification of ODH and PDH proteins was observed for purification of Strep-tagged OdhA or AceE (Niebisch et al. 2006). This observation led to the assumption of a hybrid PDH-ODH complex in *C. glutamicum*. One original aim of this thesis was to improve the purification of this hybrid complex to provide the purified proteins for structural biology approaches such as cryo-EM, performed by our cooperation partners at the Institute Pasteur in Paris.

Since AceF is required for both PDH and ODH activity and known to interact with all other components of the hybrid complex (AceE, OdhA and Lpd) (Hoffelder et al., 2010), a tagged version of AceF seemed to be promising for improved co-purification of all components of the hybrid PDH-ODH complex. For this purpose, the integration plasmid pK18mob-*aceF*-Strep was constructed and used to create the strain *C. glutamicum*::pK18mob-*aceF*-Strep (WT-*aceF*$_{St}$), analogous to the *C. glutamicum* strains WT-*odhA*$_{St}$ and WT-*aceE*$_{St}$ constructed by Niebisch et al..

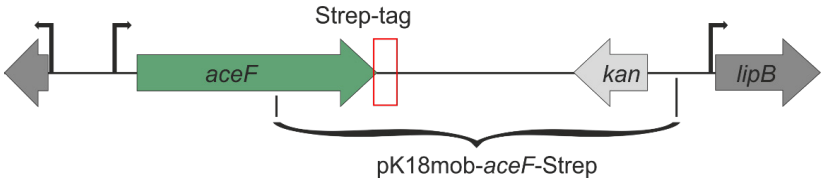

Figure S4: Schematic representation of the genomic organization at the *aceF* locus in *C. glutamicum*::pK18mob-*aceF*-Strep.

To compare the co-purification success of Strep-tagged OdhA and AceE with the new AceF-Strep construct, WT-*odhA*$_{St}$, WT-*aceE*$_{St}$ and WT-*aceF*$_{St}$ were cultivated in BHI medium and the hybrid PDH-ODH complex was purified from all three strains in parallel using Strep-tag affinity purification (see chapter 5.5.3). In all three samples, protein bands of OdhA (136 kDa), Lpd (51 kDa) and biotinylated proteins were identified (Fig. S5A and C). For the AceE-Strep purification, a strong AceE (104 kDa) band was visible, while this was rather weak in the OdhA-Strep and AceF-Strep samples. The protein band observed for AceF corresponds to a higher molecular weight than predicted from the amino acid sequence (72 kDa), which could be caused by effects of bound lipoylic acids. The protein pattern of the AceF-Strep purification was similar to the one of OdhA-Strep. As expected, a ratio increase of purified AceF compared to the other purified proteins was observed. The identity of the protein bands was confirmed by mass spectrometry (MALDI-TOF-MS).

The SDS-PAGE analysis revealed the successful co-purification of all four dehydrogenase complex components. To test whether the proteins form an active hybrid PDH-ODH complex, dehydrogenase activities were measured. ODH catalyzes the conversion of 2-oxoglutarate to succinyl-CoA while PDH converts pyruvate to acetyl-CoA. Both reactions depend on NAD^+ as cofactor. Hence, the enzyme activity of ODH and PDH can be determined in a photometric assay by measuring the increasing NADH concentration. The assay was performed as described by Niebisch et al. (see chapter 5.5.4). For all co-purification samples, the ODH activity was higher than the PDH activity (Fig. S5 B and D). In a first co-purification, no PDH activity was measured for OdhA-Strep, while in a second experiment a low activity of 0.03 U mg^{-1} with pyruvate as substrate was observed. The ODH activity of 1.42 U mg^{-1} and 1.48 U mg^{-1} was similar in both purifications (Fig. S5 B and D). In case of the AceF-Strep

samples, PDH activities of about 0.1 U mg^{-1} were detected, while the ODH activities of the second purification were about three-fold higher compared to the first purification with values of 0.84 U mg^{-1} and 2.76 U mg^{-1}, showing that that co-purification and composition of the protein sample is difficult to reproduce, and that even small experimental differences might affect the formation of the active hybrid complex. For the AceE-Strep sample similar ODH and PDH activities where determined in independent purifications with specific activities of 0.58 U mg^{-1} and 0.69 U mg^{-1} or 0.36 U mg^{-1} and 0.37 U mg^{-1}, respectively (Fig. S5 B and D). The lower PDH activities of the AceE-Strep samples were unexpected, since high amounts of AceE were visible in SDS-PAGE analysis and earlier studies reported higher PDH than ODH activities for AceE-Strep purification samples (Niebisch et al., 2006).

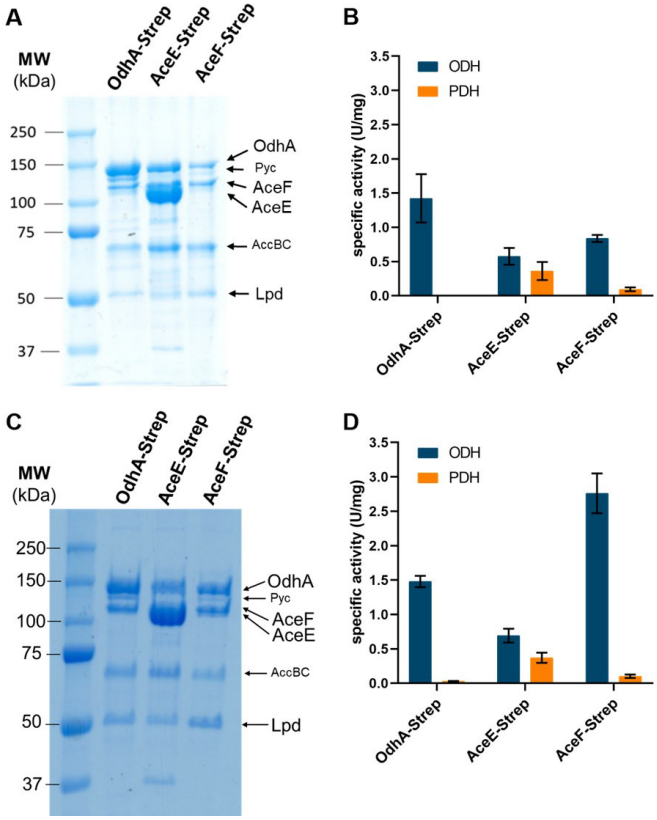

Figure S5: Purification of the hybrid PDH-ODH complex using OdhA-Strep, AceE-Strep, AceF-Strep and subsequent enzyme assays. The protein complexes were purified from *C. glutamicum* strains carrying chromosomally encoded, C-terminal Strep-tags at the given proteins. (A) and (C) Coomassie stained 8 % SDS gel analyzing protein samples of Strep-tag affinity purification followed by PD-10 gel filtration. The arrows indicate the protein bands of four protein components of ODH and PDH (OdhA, AceE, AceF and Lpd) and the biotinylated proteins Pyc and AccBC. (B and D) Specific ODH (blue) and PDH (orange) activities in U/mg total protein for OdhA-Strep, AceE-Strep and AceF-Strep purification samples. ODH and PDH activities were determined using an NAD^+ dependent activity assay with 1.5 mM 2-oxoglutarate and 1.5 mM pyruvate (B) or 15 mM pyruvate (D) as substrates. Shown are mean values of technical triplicates with error bars representing standard deviations. ODH and PDH activities shown in B were obtained for samples analyzed in A and activities shown in D were obtained for samples analyzed in C.

One reason for the low PDH activities might be an insufficient removal of allosteric inhibitors by the gel filtration on PD-10 columns and it could be tested to remove potential allosteric inhibitors more efficiently by dialysis. In case of OdhA-Strep and AceF-Strep purifications, the low PDH activities might be caused by the low amount of co-purified AceE. In contrast, in the AceE-Strep samples high amounts of AceE were purified but this did not increase PDH activity significantly. To analyze if the lower PDH than ODH activities in this case are caused by an inactive AceE protein or by an insufficient formation of the PDH complex, we had a closer look on the dehydrogenase activities of the WT-*aceE*$_{St}$ strain. Besides ODH and PDH activity, the isocitrate dehydrogenase activity was analyzed to include an enzyme, which should not be affected by the tagged PDH component. The PDH activity (0.05 U mg^{-1}) in WT-*aceE*$_{St}$ cell extract was slightly lower than the ODH activity (0.07 U mg^{-1}) (Fig. S6 A), while literature reports similar PDH and ODH activities of around 0.1 U mg^{-1} in *C. glutamicum* cell extracts (Hoffelder et al., 2010). The observed Icd activity of about 0.8 U mg^{-1} is similar to those reported in literature (0.9 to 1.1 U mg^{-1}) (Eikmanns et al., 1995), showing that the applied cell disruption procedure is suitable to maintain dehydrogenase activities. In addition, ODH and PDH activities were measured in AceE-Strep samples after affinity purification, and again lower PDH than ODH activities were observed, even if the values were much lower in general (Fig. S6 B). Furthermore, the specific activities of the E1 subunits OdhA and AceE were determined in a DCPIP (2,6-dichlorophenolindophenol) assay and showed an about ten-fold higher activity for AceE than for OdhA, which correlates with the much higher amount of AceE in AceE-Strep samples observed in SDS-PAGE analysis (see Fig. S5 A and C). Taken together, these results suggest that the low PDH activities observed in AceE-Strep samples are caused by an impaired formation of the PDH complex and not due to the purification of inactive AceE. It has to be analyzed further if this impaired formation of the PDH complex is at least partially caused by the C-terminal Strep-tag or if the affinity between AceE and AceF is lower than between OdhA and AceF, which would explain why the AceF-Strep sample contains less AceE than OdhA (see Fig. S5 A and C).

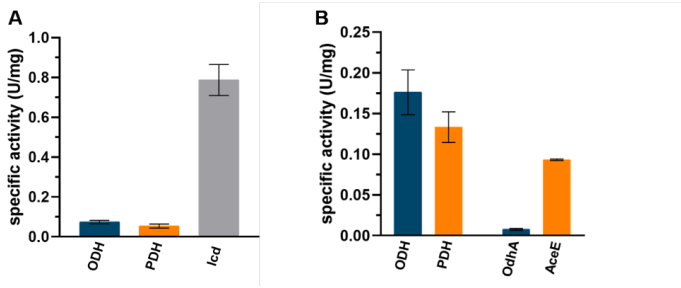

Figure S6: Dehydrogenase activities in WT-*aceE*$_{St}$ cell extracts and AceE-Strep purified protein samples. (A) Shown are the specific ODH, PDH and Icd activities in U/mg total protein determined for WT-*aceE*$_{St}$ cell extracts in NAD^+ (ODH and PDH) or $NADP^+$ (Icd) dependent assays using 1.5 mM 2-oxoglutarate, 15 mM pyruvate and 0.8 mM isocitrate as substrates. (B) The protein complexes were co-purified from WT-*aceE*$_{St}$ using Strep-Tactin affinity chromatography. Shown are specific ODH and PDH activities in U/mg protein determined using an NAD^+ dependent activity assay with 1.5 mM 2-oxoglutarate and 15 mM pyruvate as substrates as well as the specific OdhA and AceE activities determined using a DCPIP-dependent assay with 1 mM 2-oxoglutarate or pyruvate as substrates. Shown are mean values of technical triplicates and error bars represent standard deviation.

Besides the construction of the WT-*aceF*$_{St}$ strain, another idea to optimize the purification of the hybrid PDH-ODH complex was to test different purification buffers, for example using high KCl concentrations (1 M) or *myo*-inositol as buffer additives, which improved protein purification in case of the pyruvate carboxylase of *C. glutamicum* (Kortmann et al., 2019). To compare the effect of the buffer additives 5% (w/v) *myo*-inositol or 1 M KCl to the so far used glycerol on the purification success WT-*aceF*$_{St}$ cell pellets were split equally, and dissolved in the previously used buffer either containing glycerol or 5% (w/v) *myo*-inositol. The protein composition of the *myo*-inositol and glycerol elution fractions, analyzed by SDS-PAGE (Fig. 7A), showed a successful purification of all hybrid PDH-ODH complex components which was confirmed by the PDH and ODH activities determined for both samples. As it was the case for glycerol, *myo*-inositol enabled the co-purification of all PDH-ODH complex components, showing comparable PDH activities of 0.15 U mg^{-1} and 0.14 U mg^{-1}, respectively (Fig. S7 B). Although the ODH activity of the sample containing 5% (w/v) *myo*-inositol as buffer additive was lower than in the sample containing 10% (v/v) glycerol as buffer additive (0.86 U mg^{-1} and 1.31 U mg^{-1}), *myo*-inositol appears to be a suitable alternative. In contrast, the use of 1 M KCl did not enable purification of active PDH-ODH complexes (data not shown). An inhibition of enzyme activity due to a high KCl concentrations has been reported in other studies (Mukhopadhyay and Purwantini, 2000) and restoration of activity by removal of KCl could be tested.

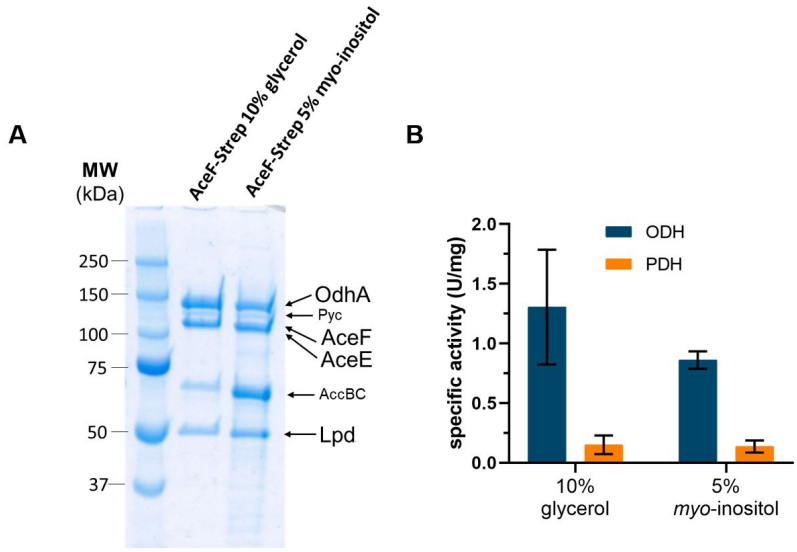

Figure S7: Purification of the hybrid PDH-ODH complex using AceF-Strep and 10% glycerol or 5% *myo*-inositol as buffer additives. (A) Coomassie stained 8 % SDS gel of AceF-Strep elution fraction of Strep-tag affinity purification in 50 mM TES-NaOH, 1 mM $MgCl_2$, pH 7.7 with either 10 % (w/v) glycerol or 5 % (w/v) *myo*-inositol as buffer additive. (B) Specific ODH (blue) and PDH (orange) activities in U/mg protein for AceF-Strep samples purified with glycerol or *myo*-inositol as buffer additives. ODH and PDH activities were determined using an NAD^+ dependent activity assay with 2-oxoglutarate or pyruvate as substrates. Shown are mean values of technical triplicates with error bars representing standard deviations.

Since the altered buffer composition did not lead to clear improvement in the obtained protein concentrations or higher specific activities, glycerol was kept as buffer additive for hybrid PDH-ODH complex purification and samples were provided for cryo-EM experiments. Unfortunately, structure determination was neither possible with samples purified from *C. glutamicum* nor for the complex build of the protein components heterologously produced in *E. coli* (experiments performed by our project partners at Institute Pasteur), due to the high flexibility of the protein interactions in the hybrid complex. Therefore, our project partners focused on the determination of the individual protein structures and the protein-protein interactions enabling the formation of the hybrid PDH-ODH complex.

5.4. Relevance of the N-terminal extension of OdhA *in vivo*

In *C. glutamicum* and other actinobacteria the ODH E1 domain OdhA, harbors the 2-oxoglutarate decarboxylase as well as the succinyltransferase domain of E2, while an independent E2o subunit is missing (Usuda et al., 1996). Since ODH lacks a lipoyl-binding domain of E2, an interaction of OdhA with AceF, the E2 subunit of the PDH, is necessary, to ensure the transfer of the succinyl group to CoA (Hoffelder et al., 2010).

Our project partners at the Institute Pasteur in Paris solved the structures of the *C. glutamicum*

PDH and ODH components and performed interaction studies of OdhA with AceF to gain a better understanding of the interacting protein regions within the hybrid PDH-ODH complex. One part of the OdhA protein that is assumed to be responsible for interaction with AceF is an N-terminal extension. They constructed pPREx2-based expression plasmids encoding for OdhA variants lacking different N-terminal segments (Fig.S8). To analyze the importance of these different N-terminal parts for the functionality of OdhA and thereby draw conclusions about the interaction of OdhA and AceF *in vivo*, we constructed a *C. glutamicum* Δ*odhA* strain and performed a complementation assay with the different N-terminally truncated OdhA variants.

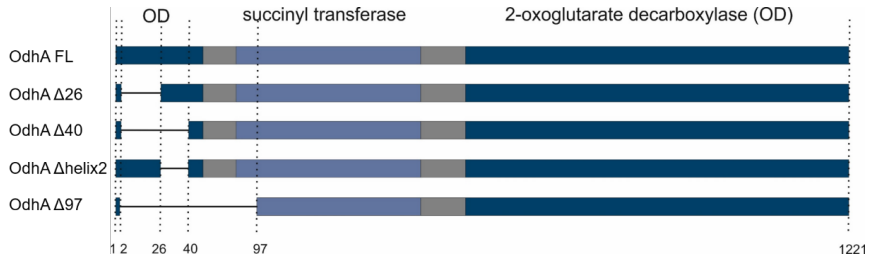

Figure S8: Schematic representation of the N-terminally truncated OdhA variants. Shown is the organization of 2-oxoglutarate decarboxylase (OD, dark blue) and succinyltransferase (light blue) domains of OdhA, linker regions are marked in grey (following Hoffelder et al. 2010). Besides the full length protein, four truncated OdhA variants are shown. OdhA Δ26 lacks the first predicted α-helix, OdhA Δ40 lacks two N-terminal alpha helices, OdhA Δhelix2 lacks residues Ser27 to Gly40 and OdhA Δ97 lacks the whole N-terminal segment.

Deletion of the *odhA* gene prevents formation of the ODH and thereby interrupts the TCA cycle, which leads to a strong growth defect as well as an accumulation of 2-oxoglutarate and acetate in the growth medium of the *odhA* deletion strain (Hoffelder et al., 2010). In accordance with this we observed a reduced growth of the deletion strain in BHI medium with 2 % (w/v) glucose and an acidification of culture medium which was not observed for the wt strain (data not shown). Since a strong acidification of the culture medium impairs *C. glutamicum* growth, a combination of BHI and CGXII medium with 2% (w/v) glucose was used in the complementation experiments with the OdhA truncation variants to prevent fast pH changes. The growth of *C. glutamicum* Δ*odhA* carrying the empty plasmid pPREx2, and the pPREx2 derivatives encoding for an OdhA full-length (FL) protein or different N-terminal truncation variants was monitored in a BioLector cultivation. The deletion strain carrying the empty plasmid showed slower growth and reduced final backscatter value compared to *C. glutamicum* wt pPREx2 (Fig.S9). Strains carrying plasmids encoding for full length OdhA as well as the Δ26, Δ40 and Δhelix2 variants complemented to a similar extend and led to a growth

behavior similar to the wt while the OdhA Δ97 variant enabled only partial complementation (intermediate growth rate but final backscatter like the wt).

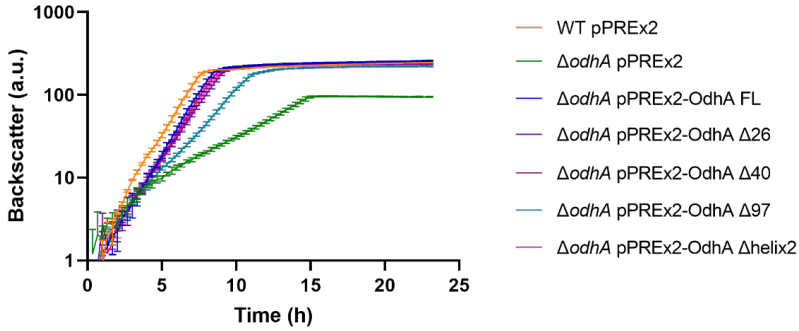

Figure S9: Complementation of *C. glutamicum* Δ*odhA* growth with OdhA variants of different length. *C. glutamicum* wt carrying the empty plasmid and *C. glutamicum* Δ*odhA* carrying the empty plasmid pPREx2 or pPREx2-based expression plasmids for different truncated OdhA variants were cultivated in a BioLector at 30 °C and 1200 rpm. Cultivation took place in BHI/CGXII + 2 % (w/v) glucose (25 µg/ml kanamycin). Shown are mean values and error bars representing the standard deviation of technical triplicates.

Already without induction of gene expression by addition of IPTG, the basal plasmid-based expression showed strong complementation effects for the different OdhA variants. In addition to the above mentioned experiment, a second cultivation with the same strains was performed to analyze the influence of different induction levels on the complementation effect. The different *C. glutamicum* strains were again cultivated in BHI/CGXII with 2% (w/v) glucose and 25 µg/ml kanamycin, this time containing 0 µM, 1 µM or 5 µM IPTG. While the expression of the full length protein and the OdhA Δ26, Δ40 and Δhelix2 variants showed almost wt growth behavior already without IPTG (Fig. S9), a positive effect was observed for the strain carrying the OdhA Δ97 expression plasmid with increasing IPTG concentrations (Fig. S10), which shows that at higher expression levels the OdhAΔ97 truncation variant complements the growth defect comparable to the other OdhA variants. This could mean that the lower affinity between AceF and this OdhA variant with the large N-terminal truncation gets bypassed by higher OdhA levels present in the cell.

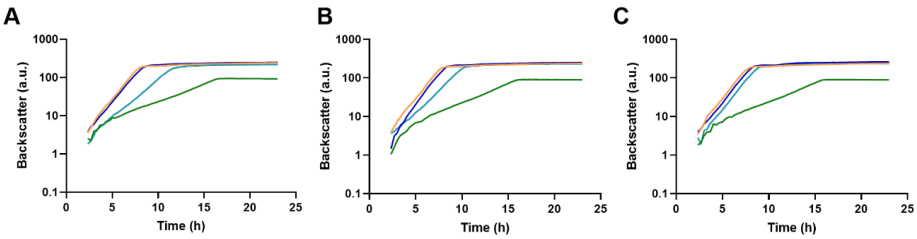

Figure S10: Complementation of *C. glutamicum* Δ*odhA* growth at different inducer concentrations. *C. glutamicum wt* carrying the empty plasmid pPREx2 (orange) and *C. glutamicum* Δ*odhA* carrying the empty plasmid (green) or pPREx2 based expression plasmids for different OdhA full length (dark blue), and OdhA Δ97 (cyan) were cultivated in a BioLector at 30 °C and 1200 rpm. Cultivation took place in BHI/CGXII + 2 % (w/v) glucose (25 µg/ml kanamycin) with 0 µM (A), 1 µM (B) or 5 µM IPTG (C). Shown are mean values of biological duplicates.

5.5. Material and methods of supplementary experiments

5.5.1 Bacterial strains and cultivation conditions

All bacterial strains and plasmids used in experiments shown in the appendix are listed in Table S1. *E. coli* cells were cultivated at 37 °C in lysogeny broth (LB) (Bertani, 1951) or on LB agar plates (Carl Roth, Karlsruhe, Germany). *C. glutamicum* strains were cultivated at 30 °C in brain heart infusion medium (BHI; Difco Laboratories, Detroit, USA) or in CGXII medium with 2% (w/v) glucose (Keilhauer et al., 1993) containing 30 mg L^{-1} 3,4-dihydroxybenzoate as iron chelator or in a mixture of both media. These media were also used for the preparation of solid media by addition of 15 g L^{-1} agar. Complementation tests were performed on agar plates containing modified CGXII medium lacking glucose, ammonium sulfate and urea and containing 100 mM L-glutamine as sole carbon and nitrogen source. To maintain plasmid stability, kanamycin was added at concentrations of 25 mg L^{-1} (*C. glutamicum*) or 50 mg L^{-1} (*E. coli*).

For BioLector cultivations, single colonies of *C. glutamicum* strains were used to inoculate overnight pre-cultures in BHI medium with 2 % (w/v) glucose in shake flasks. Cells corresponding to an OD_{600} of 8 were resuspended in 1 ml BHI/CGXII + 2 % (w/v) glucose and used to inoculate the flower plate wells to a starting OD_{600} of 0.5. Cultivation took place at 30 °C and 1200 rpm in a BioLector system (m2p-labs, Baesweiler, Germany).

Table S1: Bacterial strains and plasmids used in experiments described in the appendix.

Strain or plasmid	Description	Reference or source
***C. glutamicum* strains**		
ATCC13032	Biotin-auxotrophic wild type strain	DSMZ
Δ*glnX2*	Wild type derivative with in-frame deletion of *glnX* (cg3044)	(Sundermeyer et al., 2022a)
WT-*odhA*$_{St}$	Wild type derivative with plasmid pK18mob-*odhA*-Strep integrated into the chromosomal	(Niebisch et al., 2006)

	odhA gene (cg1280) adding a Strep-tag to the OdhA C-terminus	
WT-*aceE*$_{St}$	Wild type derivative with plasmid pK18mob-*aceE*-Strep integrated into the chromosomal *aceE* gene (cg2466) adding a Strep-tag to the AceE C-terminus	(Niebisch et al., 2006)
WT-*aceF*$_{St}$	Wild type derivative with plasmid pK18mob-*aceF*-Strep integrated into the chromosomal *aceF* gene (cg2421) adding a Strep-tag to the AceF C-terminus	This work
MB001(DE3)	MB001 derivative with chromosomally encoded T7 gene *1* (cg1122-P$_{lacI}$-*lacI*P$_{lacUV5}$-*lacZ*α-T7 gene *1*-cg1121)	(Kortmann et al., 2015)
***E. coli* strains**		
DH5α	F- *supE44* Δ*lacU*169 (Φ80*lacZ*Δ*M15*) *hsdR17 recA1 endA1 gyrA96 thi-1 relA1*	(Hanahan, 1983)
Plasmids		
pK18mob	Kan^R; *E. coli* vector unable to replicate in *C. glutamicum* (*oriV E.c.*, *sacB*, *lacZα*)	(Schäfer et al., 1994)
pK18mob-*aceF*-Strep	Kan^R; pK18mobsacB derivative containing a 691-bp PCR product covering the 3'-terminal end of the *aceF* gene elongated with a Strep-tag coding sequence before the stop codon	This work
pPREx2	Kan^R; pPBEx2 derivative (P$_{tacI}$, *lacI*^{q}, *ori*$_{C.g}$ from pBL1; *ori*$_{E.c.}$ ColE1 from pUC18), with a consensus RBS (AAGGAG) for *C. glutamicum*	(Bakkes et al., 2020)
pPREx2-*glnX*	Kan^R; pPREx2 derivative for expression of *glnX* (cg3044)	This work
pPREx2-*glnX*-Strep	Kan^R; pPREx2 derivative for expression of *glnX* (cg3044) with a with C-terminal Strep-tag	This work
pPREx2-*glnX*-TEV-*mVenus*-Strep	Kan^R; pPREx2 derivative coding for a GlnX (cg3044) fusion protein with a C-terminal TEV protease cleavage site followed by mVenus and a Strep-tag	This work
pPREx2-Strep-*mVenus*-TEV-*glnX*	Kan^R; pPREx2 derivative coding for a GlnX (cg3044) fusion protein with an N-terminal Strep-tag followed by mVenus and a TEV protease cleavage site	This work
pPREx2-OdhA-FL	Kan^R; pPREx2 derivative for expression of *odhA* (cg1280)	Provided by Lu Yang (Institute Pasteur, Paris)
pPREx2-OdhA-Δ26	Kan^R; pPREx2 derivative encoding for an OdhA (cg1280) truncation variant lacking the first predicted α-helix	Provided by Lu Yang (Institute Pasteur, Paris)
pPREx2-OdhA-Δ40	Kan^R; pPREx2 derivative encoding for an OdhA (cg1280) truncation variant lacking two N-terminal α-helices	Provided by Lu Yang (Institute Pasteur, Paris)
pPREx2-OdhA-Δhelix2	Kan^R; pPREx2 derivative encoding for an OdhA (cg1280) truncation variant lacking residues Ser27 to Gly40	Provided by Lu Yang (Institute Pasteur, Paris)
pPREx2-OdhA-Δ97	Kan^R; pPREx2 derivative encoding for an OdhA (cg1280) truncation variant lacking the entire N-terminal segment	Provided by Lu Yang (Institute Pasteur, Paris)
pPREx6	Kan^R; pPREx2 derivative with P$_{tac}$ exchanged for P$_{T7}$	(Ramp et al., 2022)
pPREx6-*glnX*-P1-Strep	Kan^R; pPREx6 derivative encoding the first periplasmic domain of GlnX (amino acid residues 111-266) (cg3044) with C-terminal Strep-tag	This work
pPREx6-*glnX*-P2-Strep	Kan^R; pPREx6 derivative encoding the second periplasmic domain of GlnX (amino acid residues 320-472) (cg3044) with C-terminal Strep-tag	This work

5.5.2 Standard recombinant DNA work and construction of deletion mutants

Standard methods such as PCR and plasmid restriction were carried out according to established protocols (Green and Sambrook, 2012). Plasmids were constructed by Gibson assembly (Gibson et al., 2009). The oligonucleotides listed in Table S2 were obtained from and DNA sequencing was performed by Eurofins Genomics (Ebersberg, Germany). Transformation of *E. coli* was performed using a standard protocol (Hanahan, 1983) and *C. glutamicum* transformation was performed by electroporation (van der Rest et al., 1999). The *C. glutamicum* strain WT-*aceF*$_{St}$ was obtained by a single homologous recombination event in the *C. glutamicum* genome and recombinant strains were selected on agar plates containing kanamycin.

Table S2 Oligonucleotides used in experiments shown in the appendix.

Name	Sequence
Construction of pK18mob-*aceF*-Strep	
aceF-Strep fw	GCTTGCATGCCTGCAAGCTGCACGAGGTCGATATG
aceF-Strep rv	ATGACCATGATTACGATTTACTTCTCGAACTGTGGGTGGGACCAAGCAGAGAGCTGC AGATCGCCTTC
Construction of pPREx2-*glnX* and pPREx2-*glnX*-Strep	
glnX fw	TGCAGAAGGAGATATACATATGATCCGGGATGGAAATG
glnX rv	AAACGACGGCCAGTGAATTCTTATAAGTACTCCTGCAAACG
glnX-Strep rv	GAACTGTGGGTGGGACCAGCTAGCTAAGTACTCCTGCAAACG
Construction of pPREx2-*glnX*-TEV-mVenus-Strep	
glnX fw	TGCAGAAGGAGATATACATATGATCCGGGATGGAAATG
glnX-TEV rv	AATACAGGTTCTCGGATCCTAAGTACTCCTGCAAACG
TEV-mVenus fw	GGATCCGAGAACCTGTATTTTCAGGGCCAATTCGtTAGCAAAGGAGAAGAAC
mVenus-Strep rv	GAACTGTGGGTGGGACCAGCTAGCAAGCTTTTTGTAGAGCTCATCCATGC
Construction of pPREx2-Strep-*mVenus*-TEV-*glnX*	
Strep-mVenus fw	TGCAGAAGGAGATATACATatgGCTAGCTGGTCCCACCCACAGTTCGAGAAGGGATC CGCTAGCAAAGGAGAAGAAC
mVenus-TEV rv	GCCCTGAAAATACAGGTTCTCGGATCCTTTGTAGAGCTCATCCATGC
TEV-glnX fw	AACCTGTATTTTCAGGGCATGATCCGGGATGGAAATG
glnX rv	AAACGACGGCCAGTGAATTCTTATAAGTACTCCTGCAAACG
Construction of pPREx6-*glnX*-P1-Strep	
glnX-P1 fw	TTTAAGAAGGAGATATACAtATGTCGGTGTCTTCGGATAC
glnX-P1 rv	GAACTGTGGGTGGGACCAGCTAGCCTGCGGACCCGTCACCGAAC
Construction of pPREx6-*glnX*-P2-Strep	
glnX-P2 fw	TTTAAGAAGGAGATATACATATGACGTGGCAGGCTGGCACGAAG
glnX-P2 rv	GAACTGTGGGTGGGACCAGCTAGCCTCCGTGGCCTGCAGGCC

5.5.3 Protein production and purification

The periplasmic domains of GlnX were produced using *C. glutamicum* strains MB001(DE3) pPREx6-*glnX*-P1-Strep and MB001(DE3) pPREx6-*glnX*-P2-Strep. The strains were cultivated at 30 °C in BHI medium with 2% (w/v) glucose with a starting OD_{600} of 0.5 and target gene expression was induced after 3 h by addition of 250 µM IPTG. After overnight cultivation cells were harvested by centrifugation. Cell pellets were suspended in buffer A (100 mM Tris-HCl, 150 mM NaCl, 1 mM EDTA, pH 8) and disrupted by French press treatment. Soluble protein fractions were obtained by centrifugation (5000*g*, 4 °C, 20 min) and subsequent ultracentrifugation of the supernatant (100000*g*, 4 °C, 1 h). The supernatant was filtered and manually applied to a 1 ml StrepTrap HP (GE Healthcare, Chicago, IL, USA) column. The column was inserted into an Äkta pure system and unspecifically bound proteins were removed by a washing step with buffer A. Specifically bound protein was eluted in a one-step elution using buffer A with 2.5 mM desthiobiotin. The eluted proteins were further purified by size exclusion chromatography on a Superdex Increase 200 10/300 GL column (GE Healthcare, Chicago, IL, USA) equilibrated with buffer A. To estimate the oligomeric state of GlnX-P1-Strep, a calibration curve for the used Superdex 200 Increase 10/300 GL column was prepared, using cytochrome c (12.4 kDa), carbonic anhydrase (29 kDa), bovine serum albumin (66 kDa), alcohol dehydrogenase (150 kDa) and β-amylase (200 kDa) (Gel filtration molecular weight markers, Sigma-Aldrich) at the same settings as applied for GlnX-P1-Strep. The void volume was determined using dextran blue. This revealed a calibration function of y = -3.218x + 3.068 with y being the logarithm of the relative molecular weight ($\log(M_r)$) and x the = partition coefficient (K_{av}). Protein concentrations were determined using the molar extinction coefficient predicted by the ProtParam tool (http://web.expasy.org/protparam/).

For purification and subsequent enzyme assays of the hybrid PDH-ODH complex *C. glutamicum* strains WT-*odhA*$_{St}$, WT-*aceE*$_{St}$ and WT-*aceF*$_{St}$ were cultivated at 30 °C in BHI medium until an OD_{600} of 8 to 10 was reached. Subsequently, cells were harvested by centrifugation and the pellet was suspended in buffer B (50 mM TES-NaOH, 1 mM $MgCl_2$, pH 7.7) containing 30 % (w/v) glycerol and cOmplete EDTA-free protease inhibitor (Roche, Basel, Switzerland) as described by Niebisch et al. and disrupted by French press treatment. Cell debris was removed by centrifugation (10 min, 4 °C, 18000*g*). The supernatant was diluted with the same volume of buffer B to reduce the glycerol concentration and subsequently transferred to a Strep-Tactin gravity flow column (1 ml bed volume, Strep-Tactin sepharose, IBA) equilibrated with buffer B containing 10 % (w/v) glycerol. Unspecifically bound protein was removed in a wash step and elution of specifically bound protein was carried out using buffer B containing 10 % (w/v) glycerol and 2.5 mM desthiobiotin. The elution fraction was concentrated and further purified by gel filtration on PD-10 columns to remove possible allosteric inhibitors. The PD-10 elution fraction was concentrated to a volume of 1 ml. The

protein concentration was determined using BCA assay (Interchim, Montlucon, France). The protein composition of these samples was analyzed by SDS-PAGE and the protein samples were used in enzyme activity assays or provided for structure determination experiments. In case of experiments testing alternative buffer additives, glycerol was replaced by 5% (w/v) *myo*-inositol or 1 M KCl. In contrast to glycerol, these concentrations were kept constant in all buffers during the purification steps.

5.5.4 Enzyme activity assays

Determination of ODH and PDH activities was carried out in a photometric assay following the initial increase in concentration of NADH at 340 nm as described by Niebisch et al 2006. The assay buffer contained 3 mM L-cysteine, 0.9 mM TPP, 2 mM NAD^+, 50 µM chlorpromazine, 25–100 µl of cell extract or purified PDH-ODH complexes and the reaction was started by addition of 2-oxoglutarate (1.5 mM) or pyruvate (1.5 mM or 15 mM) and 0.2 mM coenzyme A in an assay volume of 1 ml. Measurements were performed at 30 °C and an activity of 1 U refers to 1 µmol of NADH formed per min. The Icd activity was measured in an $NADP^+$ dependent assay at 340 nm. The reaction buffer contained 50 mM TES-NaOH pH 7.7, 0.8 mM $MnSO_4$, 0.5 mM $NADP^+$ and 0.8 mM isocitrate as substrate following the assay composition described by Eikmanns et al. 1995. The decarboxylase activities of the E1 subunits OdhA and AceE in an AceE-Strep purified sample were analyzed measuring the reduction of the alternative electron acceptor DCPIP at 600 nm in buffer containing 80 mM potassium phosphate (pH 7.5), 3 mM KCN, 0.23 mM DCPIP, 2.2 mM phenazine methosulfate, 1 mM MgCl2, 0.2 mM TPP, and 1 mM 2-oxoglutarate or pyruvate as described by Hoffelder et al. 2010.

Danksagung

Ein besonderer Dank gilt Prof. Dr. Michael Bott für die Überlassung des spannenden Themas, das stetige Interesse am Fortgang meines Projektes, die Unterstützung und die hilfreichen Diskussionen.

Bei Prof. Dr. Lutz Schmitt bedanke ich mich für die freundliche Übernahme des Zweitgutachtens meiner Arbeit.

Bei Dr. Meike Baumgart bedanke ich mich herzlich für ihre Unterstützung, die vielen hilfreichen Diskussionen und die zahlreichen Ratschläge zu Experimenten, Auswertungen und Texten.

Besonderer Dank gilt auch unseren Kooperationspartnern Marco Bellinzoni und Lu Yang für die hilfreichen und interessanten Diskussionen, die gute Zusammenarbeit und die interessanten Projekttreffen.

Ich bedanke mich herzlich bei meinen Masterstudenten Jan-Gerrit Folkerts und Benita Lückel für ihre Arbeit und die große Motivation, mit der sie dieses Projekt unterstützt haben.

Ein großes Dankeschön geht an alle Mitarbeiter des IBG-1 für die freundliche Arbeitsatmosphäre und die Hilfsbereitschaft und Unterstützung in allen Belangen. Besonders bedanken möchte ich mich bei allen Mitgliedern der AG Regulation. Herzlichen Dank an Alexander, Angela, Astrid, Benita, Brita, Claudia, Daniel, Friederike, Helga, Jan-Gerrit, Johanna, Johanna, Karen, Kiki, Lea Zola, Lingfeng, Marielle, Monica, Natalie, Paul, Philipp, Rico, Srushti, Susana und Tina für eure Unterstützung, die schöne gemeinsame Zeit im Labor, die interessanten Gespräche und die schönen gemeinsamen Abende.

Bei meiner Familie und meinen Freunden bedanke ich mich für die Unterstützung während meines Studiums, der Arbeit an dieser Dissertation und in jeder anderen Situation. Danke Niklas, dass du immer für mich da bist und es immer wieder schaffst meine Stimmung zu verbessern und mich zu motivieren.

Eidesstattliche Erklärung

Ich versichere an Eides Statt, dass die vorgelegte Dissertation von mir selbständig und ohne unzulässige fremde Hilfe unter Beachtung der „Grundsätze zur Sicherung guter wissenschaftlicher Praxis an der Heinrich-Heine-Universität Düsseldorf“ erstellt worden ist. Die Dissertation wurde in der vorgelegten oder in ähnlicher Form noch bei keiner anderen Institution eingereicht. Ich habe bisher keine erfolglosen Promotionsversuche unternommen.

Solingen, den 28.09.2022

Band / Volume 260
Crystal and Magnetic Structure of CrAs under Extreme Conditions
A. Eich (2022), viii, 235 pp
ISBN: 978-3-95806-655-7

Band / Volume 261
Applications of transcription factor-based biosensors for strain development and evolutionary engineering
R. G. Stella (2022), x, 128 pp
ISBN: 978-3-95806-657-1

Band / Volume 262
Strömungsmechanische Simulation und experimentelle Validierung des kryogenen Wasserstoff-Moderators für die Europäische Spallationsneutronenquelle ESS
Y. Beßler (2022), XXIV, 154, xxxiii pp
ISBN: 978-3-95806-660-1

Band / Volume 263
9th Georgian-German School and Workshop in Basic Science September 12 – 16, 2022 | Kutaisi, Tbilisi | Georgia
A. Kacharava, E. Portius, N. J. Shah, H. Ströher (2022)
ISBN: 978-3-95806-664-9

Band / Volume 264
Self-assembly of Au-Fe_3O_4 dumbbell nanoparticles
N. Nandakumaran (2022), xiv, 234 pp
ISBN: 978-3-95806-666-3

Band / Volume 265
Time-resolved and three-dimensional characterisation of magnetic states in nanoscale materials in the transmission electron microscope
T. Weßels (2023), xx, 211 pp
ISBN: 978-3-95806-685-4

Band / Volume 266
Dissecting iron and heme regulatory networks and adaptation to heme stress in *Corynebacterium glutamicum*
A. Krüger (2023), IV, 274 pp
ISBN: 978-3-95806-686-1

Band / Volume 267
Morphological and functional characterization of layer 5 neurons in rat medial prefrontal cortex, their synaptic microcircuitry and serotonin modulation
R. Rama (2023), 116 pp
ISBN: 978-3-95806-688-5

Band / Volume 268
Magnetic and transport studies of the parent and Fe doped Hexagonal-Mn_3Ge Weyl semimetal
V. Rai (2023), xviii, 156 pp
ISBN: 978-3-95806-695-3

Band / Volume 269
The complex inositol metabolism of *Corynebacterium glutamicum* and its application for the production of rare inositols
P. Ramp (2023), VI, 161 pp
ISBN: 978-3-95806-699-1

Band / Volume 270
Spin- and orbital-dependent band structure of unconventional topological semimetals
K. Hagiwara (2023), v, 115 pp
ISBN: 978-3-95806-701-1

Band / Volume 271
Neutron scattering
Experimental Manuals of the JCNS Laboratory Course held at Forschungszentrum Jülich and at the Heinz-Maier-Leibnitz Zentrum Garching edited by T. Brückel, S. Förster, K. Friese, M. Kruteva, M. Zobel and R. Zorn (2023), ca 150 pp
ISBN: 978-3-95806-705-9

Band / Volume 272
Ab-initio investigation of the interplay between the hyperfine interaction and complex magnetism at the nanoscale
S. R. S. Shehada (2023), ix, xi, 119 pp
ISBN: 978-3-95806-718-9

Band / Volume 273
Analysis of the signal transduction cascade tuning the 2-oxoglutarate dehydrogenase activity in *Corynebacterium glutamicum*
L. Sundermeyer (2023), VI, 119 pp
ISBN: 978-3-95806-722-6

Weitere ***Schriften des Verlags im Forschungszentrum Jülich*** unter
http://wwwzb1.fz-juelich.de/verlagextern1/index.asp

Schlüsseltechnologien / Key Technologies
Band / Volume 273
ISBN 978-3-95806-722-6

Mitglied der Helmholtz-Gemeinschaft

JÜLICH
Forschungszentrum